UNIVERSITÄT ZU LÜBECK

From the Institute of Human Genetics
of the University of Lübeck
Director: Prof. Dr. med. Malte Spielmann

Ruling the regulator: Fat depot-specific epigenetic regulation of quantitative leptin gene expression depends on adipocyte size and is reprogrammed in obesity

Dissertation
for Fulfillment of
Requirements
for the Doctoral Degree
of the University of Lübeck

from the Department of Natural Sciences

Submitted by

Natalie Barbara Taege
from Wiesbaden

Lübeck, 2024

First referee: Prof. Dr. rer. nat. Henriette Kirchner
Second referee: Prof. Dr. rer. nat. Kristina Kusche-Vihrog
Date of oral examination: 02.09.2024
Approved for printing. Lübeck, 06.09.2024

Declaration

Herewith, I confirm that I have written the present PhD thesis independently and with no other sources and aids than quoted.

Lübeck, April 2024
Natalie Taege

Abstract

Leptin is a hormone involved in energy homeostasis and is secreted from adipocytes in proportion to fat mass. In obesity, one of the leading health problems worldwide, the anorexigenic response to leptin is impaired due to leptin resistance caused by high circulating leptin levels. Reduction of circulating leptin levels in obesity leads to leptin resensitization with concomitant weight loss. However, the precise mechanism that enables the organism to adapt leptin gene expression to environmental and nutritional stimuli remains unknown. Gene expression influenced through the environment is regulated by epigenetic mechanisms such as DNA methylation in enhancer sites and long non-coding RNAs. Therefore, this thesis hypothesizes that adipocyte-specific epigenetic modifications are pivotal in regulating quantitative leptin gene expression and contribute to leptin overexpression in obesity.

This work identified DNA methylation-sensitive enhancer sites of the leptin gene. Along with the long non-coding RNA *lncOb*, the DNA methylation in these leptin enhancer sites was investigated during obesity progression over 12 weeks in a male C57/B6 mouse model of diet-induced obesity in epididymal and inguinal adipose tissue. During the progression of obesity, a fat depot-specific DNA methylation and *lncOb* expression pattern were observed. The hypermethylation in leptin enhancer sites in obesity was confirmed in human visceral adipose tissue. Sorting epididymal mouse adipocytes by size revealed that DNA methylation in leptin enhancer sites decreased in hypertrophic adipocytes of lean mice. However, in obesity, the size-dependent DNA methylation pattern was reprogrammed. This reprogramming was independent of central leptin feedback signaling, as tested in ob/ob mice, and independent of nuclear stretching, as tested by stretching differentiating and mature 3T3-L1 adipocytes. Furthermore, regulation of leptin gene expression by DNA methylation of leptin enhancer sites was validated using a dead Cas9 system and methylation-sensitive luciferase assays. Methylation-sensitive transcription factors of the leptin gene were identified by mass spectrometry. Short- and long-term dietary interventions showed impaired epigenetic pattern reversibility during weight loss in epididymal adipose tissue. In additional acute fasting, in contrast to DNA methylation, *lncOb* showed normal responsiveness. Weight loss induced by vertical sleeve gastrectomy showed recoupling of the DNA methylation pattern and *lncOb* with leptin gene expression, while oral metformin treatment did not affect fat mass, leptin levels, or DNA methylation.

Overall, this work identified two novel epigenetic mechanisms that regulate quantitative, fat depot-specific leptin gene expression in relation to fat mass, which are reprogrammed in hypertrophic adipocytes in obesity. It provides the fundamentals for understanding the unregulated overshooting of leptin in obesity and could pave the way for novel therapeutic strategies targeting leptin resensitization and avoiding the adverse metabolic consequences of leptin resistance.

Zusammenfassung

Leptin ist ein Hormon, das an der Energiehomöostase beteiligt ist und von Adipozyten im Verhältnis zur Fettmasse ausgeschüttet wird. Bei Adipositas, einem der weltweit führenden Gesundheitsprobleme, ist die anorexigene Reaktion auf Leptin aufgrund einer Leptinresistenz, die durch hohe zirkulierende Leptinspiegel entsteht, vermindert. Die Senkung der zirkulierenden Leptinspiegel bei Adipositas führt zu einer Resensibilisierung für Leptin bei gleichzeitigem Gewichtsverlust. Der genaue Mechanismus, der es dem Organismus ermöglicht, die Leptin-Genexpression an Umwelt- und Ernährungsreize anzupassen, ist jedoch noch unbekannt. Die durch die Umwelt beeinflusste Genexpression wird durch epigenetische Mechanismen wie die DNA-Methylierung in Enhancerstellen und lange nicht-kodierende RNAs reguliert. Daher wird in dieser Arbeit die Hypothese aufgestellt, dass adipozytenspezifische epigenetische Modifikationen, insbesondere die DNA-Methylierung in Enhancerstellen, eine zentrale Rolle bei der Regulation der quantitativen Leptin-Genexpression spielen und zur Leptinüberexpression bei Adipositas beitragen.

In dieser Arbeit wurden DNA-methylierungssensitive Enhancerstellen des Leptingens identifiziert. Zusammen mit der langen nicht-kodierenden RNA *lncOb* wurde die DNA-Methylierung in diesen Leptin-Enhancerstellen über einen 12-wöchigen Zeitraum der Adipositasentwicklung in epididymalen und inguinalen Fettgewebe von männlichen C57/B6-Mäusen eines ernährungsbedingten Adipositasmodells untersucht. Während der Adipositasentwicklung wurde ein fettdepotspezifisches DNA-Methylierungs- und *lncOb*-Expressionsmuster beobachtet. Die Hypermethylierung in Leptin-Enhancerstellen bei Adipositas wurde im humanen viszeralen Fettgewebe bestätigt. Die Größensortierung epididymaler Adipozyten von Mäusen ergab eine Abnahme der DNA-Methylierung in Leptin-Enhancerstellen in hypertrophen Adipozyten von schlanken Mäusen. Bei Adipositas hingegen wurde das größenabhängige DNA-Methylierungsmuster reprogrammiert. Diese Reprogrammierung war unabhängig von der zentralen Leptin-Rückkopplung, wie bei ob/ob-Mäusen getestet, und unabhängig von der Dehnung des Nukleus, wie bei der Dehnung differenzierender und reifer 3T3-L1-Adipozyten getestet. Zusätzlich wurde die Regulierung der Leptinexpression durch DNA-Methylierung von Leptin-Enhancerstellen mit einem dead-Cas9-System und methylierungssensitiven Luciferase-Assays validiert. Methylierungssensitive Transkriptionsfaktoren des Leptingens wurden durch Massenspektrometrie identifiziert. Die Gewichtsabnahme durch kurz- und langfristige Ernährungstherapien zeigte eine beeinträchtigte Reversibilität der epigenetischen Muster im epididymalen Fettgewebe. Im Gegensatz zur DNA-Methylierung zeigte *lncOb* eine normale Reaktionsfähigkeit auf zusätzliches akutes Fasten. Die Gewichtsabnahme durch eine Sleeve-Gastrektomie führte zu einer erneuten Kopplung der Leptin-Genexpression mit den DNA-Methylierungsmustern und mit *lncOb*, während eine orale Metforminbehandlung keine Auswirkung auf die Fettmasse, die Leptinspiegel oder die DNA-Methylier-

ung hatte.

Zusammenfassend wurden in dieser Arbeit zwei neuartige epigenetische Mechanismen identifiziert, die die quantitative, fettdepotspezifische Leptin-Genexpression in Abhängigkeit von der Fettmasse regulieren und in hypertrophen Adipozyten bei Adipositas reprogrammiert werden. Sie liefert die Grundlagen für das Verständnis der unregulierten Leptinüberexpression bei Adipositas und könnte den Weg für neue therapeutische Strategien ebnen, die auf die Resensibilisierung für Leptin abzielen und die nachteiligen metabolischen Konsequenzen der Leptinresistenz vermeiden.

Contents

List of abbreviations

℃	degree Celsius
ABCG1	ATP-binding Cassette Sub-family G Member 1
Adrb1	β1-adrenergic receptor gene
AgRP	Agouti-related Peptide
AKT	V-akt Murine Thymoma Viral Oncogene Homolog 1
AMPK	AMP-activated Protein Kinase
ANOVA	analysis of variance
AP2A	Ap-2 Alpha
AP2β	Transcription Factor AP-2 Beta
ARC	arcuate nucleus of the hypothalamus
Arg1	Arginase 1 gene
ATP	adenosine triphosphate
AUC	area under the curve
bisPCR	bisulfite polymerase chain reaction
BSA	bovine serum albumin
BMI	body mass index
C/EBPα	CCAAT/enhancer binding protein alpha
cAMP	cyclic adenosine monophosphate
CART	Cocaine And Amphetamine Regulated Transcript
Cas9	CRIPSPR associated protein 9
cDNA	complementary DNA
CMV	cytomegalovirus
CO_2	carbon dioxide
CR	calorie restricted chow diet
CREB	cAMP Response Element-binding Protein
CRISPR	Clustered Regularly Interspaced Short Palindromic Repeats
db	diabetes = *LepR* gene
dCas9	dead Cas9
DEPC	diethylpyrocarbonat
DF	degrees of freedom
DIO	diet-induced obesity
dL	deciliter
DNA	deoxyribonucleic acid

DNMT*#	DNA methyltransferases
e.g.	exempli gratia
EBF1	Early B Cell Factor 1
EDTA	ethylenediaminetetraacetic acid
EGR1	Early Growth Response 1
ELISA	enzyme-linked immunosorbent assay
ERK1/2	Extracellular-signal Regulated Kinases 1/2
eWAT	epididymal white adipose tissue
F	F-statistic
FBS	fetal bovine serum
FDR	false discovery rate
FOSL2	FOS like 2
FoxO1	Forkhead Box Protein O1
g	gram
GIP	Glucose-dependent Insulinotropic Peptide
GLP-1	Glucagon-like Peptide-1 Receptor
GnRH	Gonadotropin-releasing hormone
gPCR	genomic polymerase chain reaction
h	hour
HAT	histone acetyl transferase
HC	HFD to chow diet switch
HDAC	histone deacetyltransferases
HFD	high fat diet
Hprt	Hypoxanthine-guanine phosphoribosyltransferase gene
HSO_3^-	bisulfite
IL	Interleukin
ipGTT	intraperitoneal glucose tolerance test
IRS1/2	Insulin-receptor substrates 1/2
Itgax	Integrin Subunit Alpha X gene, CD11c
iWAT	inguinal white adipose tissue
JAK2	Janus kinases 2
JUND	AP-1 Transcription Factor Subunit
kg	kilogram
KRAB	Krüppel associated box
KEGG	Kyoto Encyclopedia of Genes and Genomes
L	liter
*Lep**#	leptin gene
LEPR*	leptin receptor (gene)
Lipe	Lipase E gene
lncRNA	long non-coding RNA

µ	micro
m	meter
M	molar=mol/liter
mm	millimeter
MAFG	MAF BZIP transcription factor G
MAFK	MAF BZIP transcription factor K
MBD	Methyl-CpG Binding Domain Protein
MECP	Methyl-CpG binding Proteins
mg	milligram
miRNA	microRNA
mL	milli liter
mRNA	messenger RNA
mTOR	Mammalian Target Of Rapamycin
n	nano
NaOH	sodium hydroxide
NFI	Nuclear Factor I
NF-Y	Nuclear Factor Y
NH_4^+	ammonium
NPY	Neuropeptide Y
ob	obesity = *Lep* gene
OH^-	hydroxide
PCA	principal component analysis
PCR	polymerase chain reaction
PI3K	Phosphatidylinositol-4,5-trisphosphate kinase
pmol	picomol
Pnpla2	Patatin Like Phospholipase Domain Containing 2 gene
POMC	Proopiomelanocortin
PPARγ	Peroxisome Proliferator Activated Receptor Gamma
PPi	pyrophosphate
pSTAT3	phosphorylated STAT3
PTPB1	Protein tyrosine phosphatase 1B
qPCR	quantitative real-time polymerase chain reaction
RISC	RNA-induced Silencing Complex
RNA	ribonucleic acid
Rplp0	ribosomal protein lateral stalk subunit P0 gene
RPL37A	ribosomal protein L37a gene
rpm	rounds per minute
RS	*Lep* regulatory enhancer site
RXRα	Retinoid X Receptor Alpha
SAT	subcutaneous adipose tissue

SD	standard deviation of the mean
sgRNA	single guide RNA
SH2	Src homology 2
SHP2	SH2-containing Protein Tyrosine Phosphatase 2
SOCS3	Suppressor of Cytokine Signaling 3
SP1	Transcription factor SP1
SREBP1	Sterol Regulatory Element Binding Transcription Factor 1
STAT	Signal Transducer And Activator Of Transcription
TDG	thymine DNA glycosylase
TET*#	ten-eleven translocation methylcytosine deoxygenase
TFs	transcription factors
TIAR	intracellular antigen 1-restricted T cell proteins
TNFα	Tumor-necrosis-factor-alpha
TOF	time of flight
Tyr	tyrosine
TYY1	transcriptional repressor protein ying-yang 1
UHRF1	Ubiquitin Like With PHD And Ring Finger Domains 1
V	volume
VAT	visceral adipose tissue
vs	versus
VSG	vertical sleeve gastrectomy
WAT	white adipose tissue
xg	times gravity

*marked abbreviations are used for both genes/mRNA (italic) and proteins (non-italic)
abbreviations are used for human genes (capital, italic) or mouse genes (non-capital, italic)

1. Introduction

This chapter provides a comprehensive background on leptin, elucidating its signaling and regulation, and its significant implications in obesity. It offers a detailed overview of epigenetic mechanisms, in particular deoxyribonucleic acid (DNA) methylation, and examines their incompletely understood impact on obesity and leptin expression. Finally, this chapter will outline the motivation, hypothesis, and objectives of this thesis.

1.1. Leptin

The discovery of leptin 30 years ago fundamentally advanced our knowledge of the regulation of energy homeostasis and paved the way for the acceptance of adipose tissue as an endocrine organ. Leptin is a 146 amino acid peptide hormone that is produced primarily by adipocytes, making it the first acknowledged adipokine. It is secreted in proportion to fat mass and energy status, and acts on central circuits to promote an anorexigenic response, playing a key role in energy homeostasis [1]–[3]. However, in obesity, overshooting levels of leptin lead to leptin resistance, confounding attempts to restore energy balance [4, 5].

1.1.1. Functions of leptin and leptin signaling

Leptin is regulated and stimulated by several factors, including nutritional status, amount of fat, glucocorticoids, and catecholamines, as described in more detail in section 1.1.3. Leptin exerts its anorexigenic effects on energy homeostasis centrally by binding to the leptin receptor (LEPR) in the arcuate nucleus of the hypothalamus (ARC). The ARC contains the two functional antagonistic neuronal groups Proopiomelanocortin/Cocaine And Amphetamine Regulated Transcript (POMC/CART) neurons and Neuropeptide Y/Agouti-related Peptide (NPY/AgRP) neurons. POMC/CART neurons, which promote satiety, reduce food intake and increase energy expenditure, are activated by leptin. In contrast, leptin inhibits NPY/AgRP neurons [6, 7]. These effects are primarily mediated by the Melanocortin Receptors 3 and 4 (MC3/4R) [8]. Other central regulations by leptin include the hedonic regulation of feeding, neuroendocrine function, memory, and learning. An overview of the central and peripheral functions of leptin is given in Figure 1.1.

Furthermore, leptin affects the periphery mainly through the central nervous system [9]. This includes reduced glucose production and insulin secretion in the liver [10, 11], increased glucose uptake and fatty acid production in muscles [9, 12], and decreased glucagon and insulin secretion from the pancreas [10, 11]. Leptin signaling is required for functional reproduction and

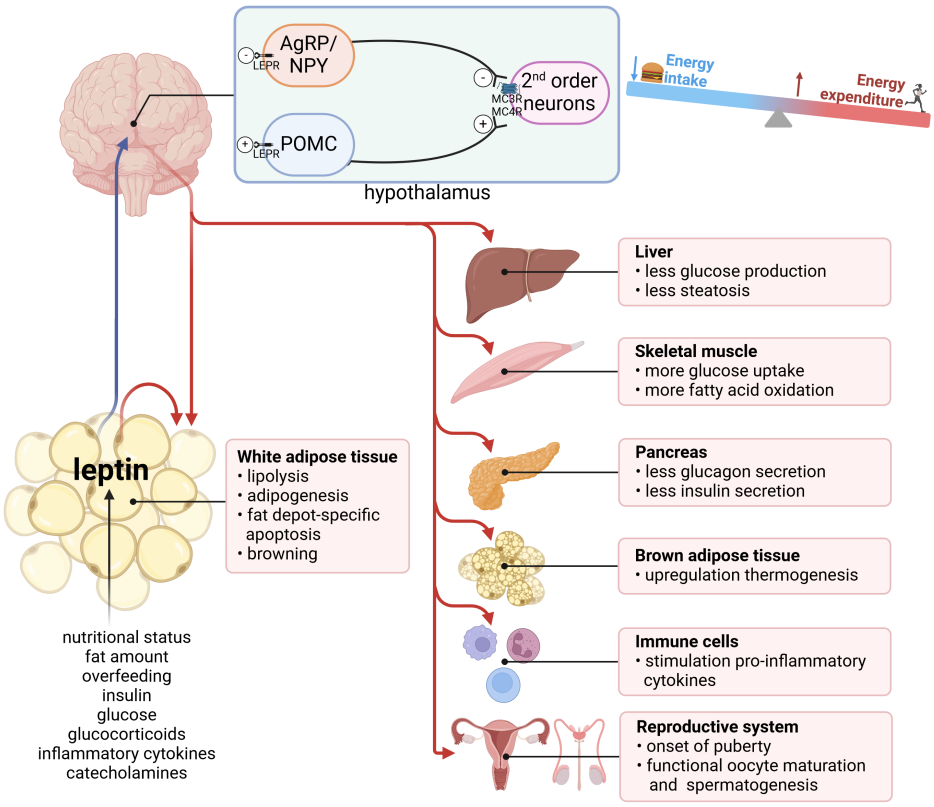

Figure 1.1.: Central and peripheral effects of leptin. AgRP–Agouti-related Peptide neurons; MC3/4R–Melanocortin Receptors 3 and 4; NPY–Neuropeptide Y neurons; POMC–Proopiomelanocortin neurons

the onset of puberty by activating neurons in the ventral premammillary nucleus. These neurons signal through the hypothalamic-pituitary-gonadal axis, stimulating Kiss1 neurons that, in turn, activate Gonadotropin-Releasing Hormone (GnRH) neurons [13]. Furthermore, during fasting, reproduction is suppressed by stimulation of AgRP neurons [14]. Additionally, leptin directly affects gonadotropes in the pituitary and the ovaries/testes, promoting oocyte maturation and spermatogenesis when in a healthy physiological range [13, 15]. In brown adipose tissue, leptin stimulates thermogenesis and therefore energy expenditure through sympathetic activation [16]. Furthermore, sympathetic stimulation by leptin and its direct paracrine and autocrine action affect white adipose tissue [17]: Lipolysis, adipogenesis, and fat depot-specific apoptosis are promoted [18]–[23] and browning of white adipose tissue is induced [24]. In addition, leptin directly targets immune cells, leading to an increase in pro-inflammatory cytokines such as Interleukin (IL)-12, IL-6 and Tumor-necrosis-factor alpha (TNFα) [25]–[27]. Many of these effects depend on the levels of circulating leptin and only function properly in lean, healthy humans and mice. In obesity, leptin function is altered due to the development of leptin resistance as described in section 1.1.5.

At the molecular level, leptin exerts its effects by binding to the LEPRs [28, 29]. The LEPR is part of the cytokine class 1 family and has six isoforms, which possess the leptin binding domain. In addition to the leptin binding domain, four short isoforms (LEPRa, c, d, f) contain a transmembrane and shorter c-terminal cytoplasmatic domain, whereas the soluble form LEPRe

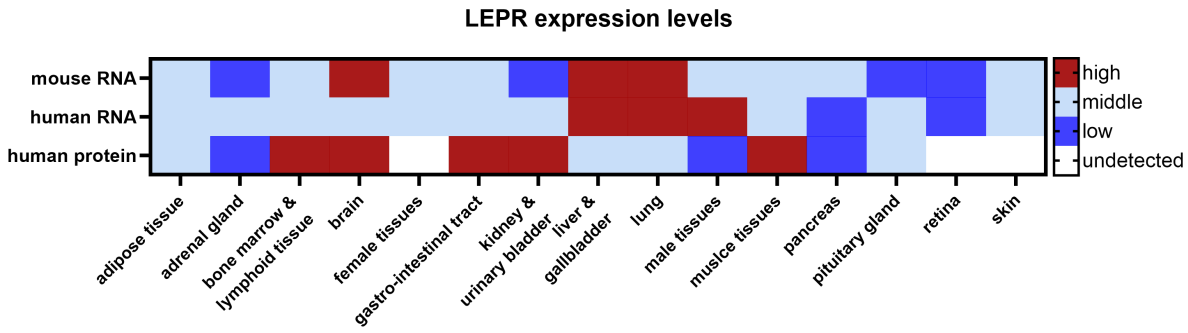

Figure 1.2.: Relative expression levels of LEPR in mice (ms) and human (hu). Data are presented as relative levels within the data sets. Data sets for mouse were retrieved from the Mouse Genome Informatics repository (*www.informatics.jax.org*, accessed 08/04/2024), European Bioinformatics Institute expression atlas (EDI; *www.ebi.ac.uk*, accessed 08/04/2024; [31]) and for human from the human protein atlas (*www.proteinatlas.org*, accessed 08/04/2024, [32] and EDI. Maximum values of the data sets are displayed.

lacks these domains. LEPRe binds leptin in the circulation, likely leading to modulation of leptin binding to other LEPRs. The full-length isoform LEPRb features the transmembrane domain and a longer c-terminal cytoplasmic domain, enabling its full activation [5, 30]. The impact on energy expenditure can be explained by the expression profiles of the LEPR, since *LEPRb* is highly expressed in the brain and to a lesser extent in other peripheral tissues such as adipose tissue, liver, immune cells, reproductive tissues, muscle, pancreas, and pituitary [28, 29] as indicated in the total LEPR expression data, retrieved from various data repositories shown in Figure 1.2.

The functional signaling pathways downstream of LEPRb are illustrated in Figure 1.3. Upon binding of leptin, Janus Kinases 2 (JAK2s) are activated, autophosphorylate, and phosphorylate tyrosines Tyr^{985}, Tyr^{1077} and Tyr^{1138}. Phosphorylation of Tyr^{1138} recruits Src Homology 2 (SH2) domain of Signal Transducer And Activator Of Transcription (STAT) 3 [33]. Activated phosphorylated STAT3 (pSTAT3) dimers translocate to the nucleus, where they modulate target gene expression. This induces changes in energy homeostasis through activation of POMC neurons and stimulation of locomotion through AgRP neurons [34]. Additionally, STAT3 induces the expression of the Suppressor Of Cytokine Signaling 3 (SOCS3), which inhibits leptin signaling via a negative feedback loop [35]. Similarly, Protein Tyrosine Phosphatase 1B (PTPB1) inhibits leptin signaling by inhibiting JAK2 [36, 37].

Tyr^{1077} phosphorylation activates the transcription factor STAT5, which is involved in the regulation of weight and food consumption [38, 39]. Another signaling pathway involves the phosphorylation of Insulin Receptor Substrates 1/2 (IRS1/2) by JAK2, leading to the activation of Phosphatidylinositol-4,5-trisphosphate kinase (PI3K) and, subsequently, V-akt Murine Thymoma Viral Oncogene Homolog 1 (AKT) [40]. AKT signaling through Mammalian Target Of Rapamycin (mTOR), cAMP Response Element-binding Protein (CREB) and Forkhead Box Protein O1 (FoxO1) modulates energy expenditure and food intake [41]–[43]. AMP-activated Protein Kinase (AMPK) activity influences appetite and sympathetic nerve activity [44, 45], while thermogenesis and anorexigenic effects are mediated by Tyr^{985} phosphorylation, activat-

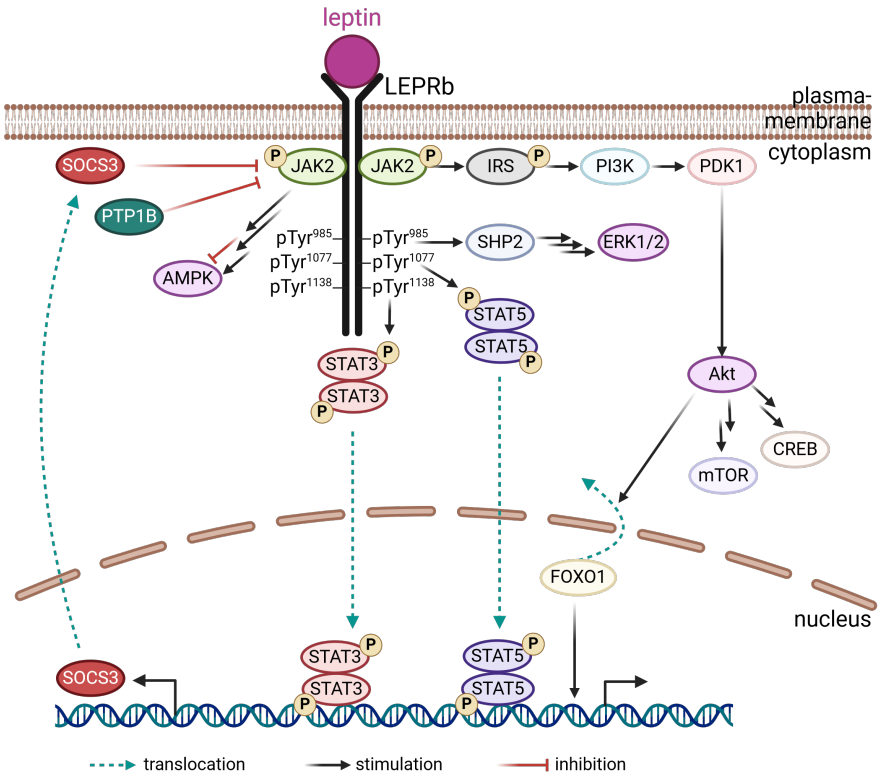

Figure 1.3.: Leptin signaling pathways. After activation of LEPRb by leptin binding, several signalling cascades are activated leading to (auto-)phosphorylation, indicated by the letter p. AMPK–AMP-activated Protein Kinase; AKT–V-akt Murine Thymoma Viral Oncogene Homolog 1; CREB–cAMP Response Element-binding Protein; ERK1/2–Extracellular-signal Regulated Kinases; FOXO1–Forkhead Box Protein O1; IRS1/2–Insulin-Receptor Substrates 1/2; JAK2–Janus Kinase 2; mTOR–Mammalian Target Of Rapamycin; PI3K–Phosphatidylinositol-4,5-trisphosphate kinase; PTPB1–Protein Tyrosine Phosphatase 1B; SHP2–SH2-containing Protein Tyrosine Phosphatase 2; STAT–signal Transducer And Activator Of Transcription; Tyr–tyrosine

ing SH2-containing Protein Tyrosine Phosphatase 2 (SHP2) and Extracellular-signal Regulated Kinases 1/2 (ERK1/2) signaling [46].

1.1.2. White adipose tissue as source for leptin

Adipose tissue is a highly plastic, endocrine, energy-storing organ and consists of adipocyte progenitor cells, immune cells, hematopoietic cells, endothelial cells, and adipocytes. Beige and brown adipose tissues are important for thermogenesis, while white adipose tissue (WAT) is important for lipid storage and endocrine function. This work focuses on WAT, the most abundant type of adipose tissue and the predominant site of leptin production [47]. In addition to leptin, WAT secretes various adipokines, including adiponectin, which have a major impact on energy homeostasis and signaling throughout the body. WAT stores energy in lipid droplets through lipogenesis, using glucose, amino acids, and fatty acids. It releases energy through lipolysis, breaking down stored triacylglycerol and releasing free fatty acids. Therefore, WAT exhibits impressive plasticity, which depends on energy availability, with approximately 10 % adipocyte turnover per year in humans [47]–[49]. This plasticity includes the expansion of the WAT.

WAT expansion occurs through differentiation of adipocyte progenitors into mature adipocytes, leading to an increased number of adipocytes (hyperplasia) and through enlargement of lipid droplets, leading to an increase in adipocyte size (hypertrophy) [47]. The expandability of WAT differs between its two major depots, visceral adipose tissue (VAT, human)/epididymal adipose tissue (eWAT, mice) and subcutaneous adipose tissue (SAT, human)/inguinal adipose tissue (iWAT, mouse) [50, 51]. VAT, located in the peritoneal cavity, is more prone to inflammation and hypertrophic expansion in obesity, often associated with metabolic dysfunction [47, 49]–[52]. Additionally, VAT and SAT differ in their pool of adipocyte progenitors, differentiation capability, and general plasticity of adipocytes [47, 50, 53]. Mechanobiological cues play a significant role in adipocyte function and gene expression during hypertrophic expansion in obesity. As lipids accumulate in hypertrophic expansion, adipocytes undergo drastic actin remodeling, lipid droplet enlargement, and cell and tissue stiffening [54]–[57]. These changes lead to nucleus deformation and subsequent chromatin remodeling alters gene expression [55]. Interestingly, large adipocytes display higher leptin gene (*Lep*) expression than small adipocytes [58], and leptin production shifts from VAT/eWAT to SAT/iWAT in obesity [59]–[63].

1.1.3. Regulation of *Lep* expression

Leptin is secreted proportionally to fat mass and *Lep* is exclusively expressed by adipocytes. Basal and acute changes in leptin levels depend on the metabolic and nutritional status. Several factors influence leptin secretion, leptin translation, and *Lep* transcription in adipocytes: Leptin secretion is stimulated directly and indirectly by oxytocin [64], glucose, and insulin [65], but diurnal variations, including acute sleep restriction, also reduce leptin secretion [66]. Catecholamines reduce leptin levels post-translationally, while insulin leads to an increase in leptin levels [67, 68]. Furthermore, catecholamines, insulin, pro-inflammatory cytokines, and glucocorticoids affect *Lep* transcription, as depicted in Figure 1.4: Catecholamines, stimulated by cold exposure, lead to a reduction in *Lep* expression through sympathetic activation of β3-adrenergic receptors. This activation stimulates the formation of cyclic adenosine monophosphate (cAMP), which ultimately reduces *Lep* expression [69]–[72]. Insulin increases *Lep* messenger ribonucleic acid (mRNA) levels [73, 74]. Long-term exposure to TNFα decreases *Lep* expression, whereas it has an acute stimulatory effect when interacting with the synthetic glucocorticoid dexamethasone, similar to IL-6 [75]–[77]. In addition to dexamethasone, cortisol also stimulates *Lep* expression [78]–[81].

In general, several leptin stimulating factors are described, but the underlying molecular and genetic factors influencing quantitative *Lep* expression specific to adipose tissue are not fully understood. The core leptin promoter of 762 base pairs upstream of the leptin gene was identified by DNA sequence analysis and cloning experiments [82, 83] and confers basal *Lep* expression, if it is accessible for its transcription factors and machinery. The ubiquitous transcription factors (TFs) that bind in the promoter region include CCAAT/enhancer Binding Protein Alpha (C/EBPα), Sterol Regulatory Element Binding Transcription Factor 1 (SREBP1), Transcription Factor SP1 (SP1) and Early Growth Response 1 (EGR1) [31, 84]–[88]. The Transcription Factor

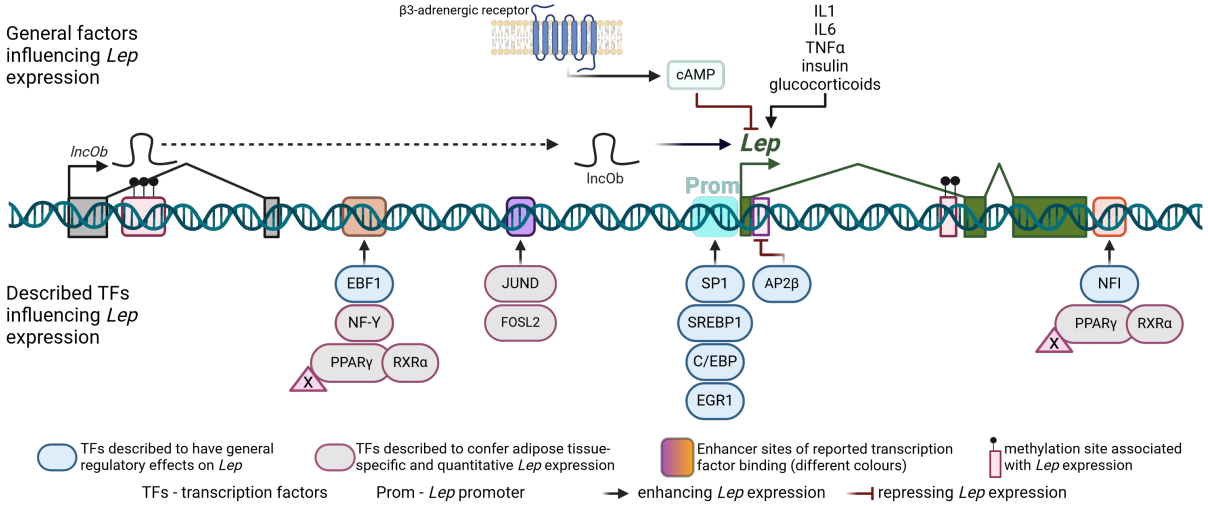

Figure 1.4.: Factors influencing *Lep* transcription. The general factors influencing *Lep* expression are shown in the upper half of the image. In the lower half, transcription factors (TFs) influencing *Lep* expression are shown. The arrows indicate whether transcription factors have a stimulating or inhibiting effect on *Lep* expression, pointing to the binding sites on the DNA relative to the *Lep* (in green). The gene boxes indicate exons. AP2β–Transcription Factor AP-2 Beta; C/EBPα–CCAAT/enhancer binding protein alpha; EBF1–Early B Cell Factor 1; EGR1–Early Growth Response 1; FOSL2–FOS Like 2; JUND–AP-1 Transcription Factor Subunit; NFI–Nuclear Ffactor I; NF-Y–Nuclear Factor Y; PPARγ–Peroxisome Proliferator Activated Receptor Gamma; RXRα–Retinoid X Receptor Alpha; SP1–Transcription factor SP1; SREBP1–Sterol Regulatory Element Binding Transcription Factor 1

AP-2 Beta (AP2β) binds proximal to the *Lep* promoter and inhibits its activity [89]. However, the promoter is not sufficient to confer quantitative responses of *Lep* expression to nutritional status [90, 91]. This suggests that regulatory enhancer sites and other TFs are responsible for adipose-tissue-specific, quantitative *Lep* expression. TFs that adhere to enhancer sites and stimulate *Lep* expression include ubiquitously occurring Early B Cell Factor 1 (EBF1) and Nuclear Factor I (NFI) proteins [92, 93]. TFs that were specifically shown to initiate *Lep* expression at the beginning or during adipogenesis leading to basal leptin levels and to contribute to the adipose tissue-specific *Lep* expression include Nuclear Factor Y (NF-Y), AP-1 Transcription Factor Subunit (JUND), and FOS Like 2 (FOSL2) [94, 95]. The latter is stimulated by dexamethasone, possibly providing a link to the glucocorticoid effect on *Lep* expression. The TFs Peroxisome Proliferator Activated Receptor Gamma/Retinoid X Receptor Alpha (PPARγ/RXRα), together with an additional unknown cofactor, appear to regulate quantitative *Lep* expression by binding to two non-canonical enhancer sites [92]. In summary, as illustrated in Figure 1.4, several transcription factors and enhancer sites that influence *Lep* expression have already been identified. However, it is not understood how these factors are orchestrated to regulate the specific and quantitative expression of *Lep* in adipocytes. For example, although the PPARγ/RXRα complex promotes *Lep* expression, systemic administration of PPARγ decreases *Lep* expression by antagonizing C/EBPα [96]. Furthermore, recent studies suggest the involvement of epigenetic factors, which play a vital role in quantitative, adipose tissue-specific *Lep* expression, as discussed in more detail in section 1.3.

1.1.4. Genetic leptin deficiency in mice and humans

Two commonly used mouse models in the investigation of obesity and type 2 diabetes are the ob/ob and db/db mice. In ob/ob mice, a mutation in *Lep*, previously known as *ob*, results in the synthesis of a nonfunctional truncated protein on the C57BL/6J background [1]. The resulting leptin deficiency causes severe hyperphagia, decreased body temperature and energy expenditure, impaired immune function, and infertility [97, 98]. This phenotype, paired with more severe insulin resistance and hyperglycemia induced by pancreatic hypertrophy, is observed in db/db mice, which lack functional LEPRs [97]–[99]. The underlying reasons for the difference in the phenotypes of ob/ob and db/db mice, albeit mutations affecting the same leptin signaling pathway, remain unclear, although speculation revolves around variances in microbiome composition and genetic background [100, 101].

In humans, congenital leptin deficiency, caused by missense or nonsense mutations in *LEP* or *LEPR*, manifests early in life with severe hyperphagia and obesity, accompanied by metabolic, immune and neuroendocrine dysfunctions [102, 103]. Likewise, metabolic phenotypes, along with growth retardation, are observed in patients with genetic or acquired lipodystrophy, who suffer from leptin deficiency due to the lack or maldistribution of adipose tissue [104]–[109].

1.1.5. Obesity and leptin resistance

Obesity is defined by a body mass index (BMI) $\geqslant 30\,\mathrm{kg/m^2}$ and is accompanied by severe comorbidities such as cardiovascular disease, type 2 diabetes, and liver diseases [110]. In addition to lifestyle factors and the overavailability of energy in the form of calories, several genetic mutations, such as the above described *LEP* or *LEPR* deficiency, but also genetic and epigenetic predispositions, can favor the development of obesity. In obesity, the overavailability of energy is stored in WAT, which increases in mass, leading to an unregulated overproduction of leptin [1, 5]. The overproduction of leptin results in the development of systemic leptin resistance (compare Figure 1.5).

Leptin resistance is characterized by a reduced tissue response to leptin, which plays a crucial role in the pathophysiology of obesity and related metabolic disorders. Leptin resistance is associated with chronic low-grade inflammation, insulin resistance, and altered energy expenditure [4, 5]. However, the underlying molecular mechanisms remain incompletely understood. The proposed mechanisms include impaired leptin transport across the blood-brain barrier [111], although more recent tracing studies suggest intact leptin transport in this context [112, 113]. Emerging insights indicate a potential role for dysfunctional tanycytes in mediating resistance to leptin [114, 115]. Additionally, reduced *LEPR* expression and subsequent attenuated leptin signaling have been implicated as contributing factors [116]. Other proposed contributors to impaired leptin signaling include elevated expression and activation of leptin signaling inhibitors, such as SOCS3 and PTB1B (also refer to Figure 1.3) [117]–[119].

Together, leptin resistance is a multilayered pathology that leads to a compromised leptin-mediated anorexigenic response, worsening obesity. Although the very effective dual Glucose-

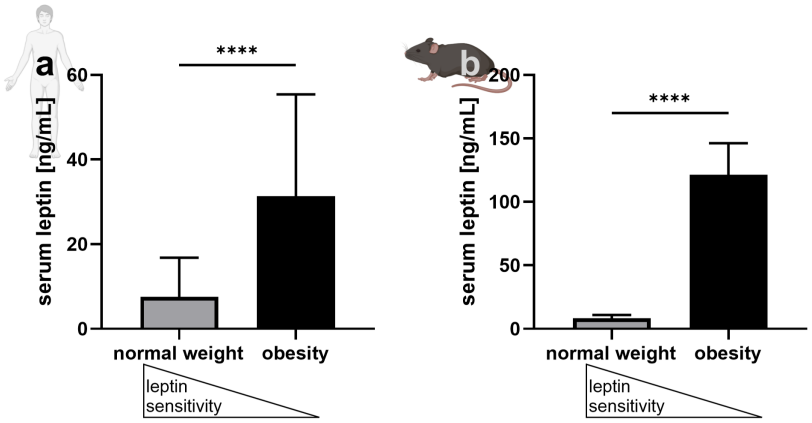

Figure 1.5.: Circulating leptin levels in mice and humans rise with obesity, while leptin sensitivity is reduced. a) Serum leptin levels in normal weight (BMI = $23.0 kg/m^2 \pm 2.5$) and obese subjects (BMI = $35.1 kg/m^2 \pm 7.2$), data from [2]. b) Serum leptin levels in normal weight (body weight = $32.7g \pm 2.7$) and diet-induced obese mice (body weight = $53.1g \pm 2.5$), unpublished data.

dependent Insulinotropic Peptide/Glucagon-like Peptide-1 Receptor (GIP/GLP-1) agonist was approved for obesity treatment [120], understanding the quantitative *Lep* expression leading to over-surge of leptin and leptin resistance is pivotal to prevent obesity development and maintain weight loss, as explained in the next section.

1.1.6. Leptin as treatment and the concept of leptin resensitization

After its discovery, leptin was initially thought to be a potential remedy for obesity owing to its anorexigenic properties. In particular, patients suffering from leptin deficiency, caused by mutations or lipodystrophy (see section 1.1.4), benefit significantly from leptin replacement therapy. This intervention leads to body weight loss, amelioration of insulin resistance and improvement in hyperglycemia, liver steatosis, immune function and fertility [102]–[109]. However, leptin therapy has not been proven efficacious in treating obesity in subjects without leptin deficiency due to the insensitivity of target tissues to leptin caused by leptin resistance. Studies revealed only modest effects, likely caused by conditions of hypersensitivity to leptin, such as fasting [104, 121]. This hypersensitivity to leptin appears to be the key to the efficacy of leptin treatment in obesity. Leptin sensitizers, such as amylin or exendin-4, demonstrated the ability to mitigate leptin resistance. Amylin achieves leptin resensitization by activating pSTAT3 signaling and stimulating the ERK-signaling pathway in POMC neurons. Co-administration of leptin sensitizers with leptin induces gradual weight loss in mice and rats [122, 123].

Moreover, the extent of early reduction in leptin levels during dietary interventions is a predictor of the degree of weight loss in human subjects [124, 125]. Recent investigations have targeted circulating leptin directly as an approach to induce weight loss by leptin resensitization, and to protect from diet-induced obesity. In two mouse models with a genetic partial reduction in leptin, mice of both sexes fed a high-fat diet gained less weight with reduced fat mass and displayed improved glucose tolerance, insulin sensitivity, and reduced inflammation compared to their littermate controls. These findings show that leptin reduction in an obesogenic environment can protect against weight gain [126]. Genetic downregulation of leptin in

mature adipocytes using inducible Clustered Regularly Interspaced Short Palindromic Repeats and CRISPR-associated protein 9 (CRISPR-Cas9)-based and Cre-loxP approaches resulted in reduced body weight gain and improved glucose tolerance compared to littermate controls when fed a high-fat diet [127]. Pharmacological downregulation of leptin in obese mice with neutralizing leptin antibodies stopped weight gain and led to metabolic improvement [127]. Importantly, this reduction in leptin levels resulted in a sustained resensitization to endogenous leptin in the hypothalamus, which improved the anorexigenic response of leptin by overcoming leptin resistance in obesity [127].

The approach of leptin resensitization is not only relevant for weight reduction in obesity, but also underscores the importance of preventing a rise in leptin levels early in obesity development to maintain sensitivity to endogenous leptin and prevent further weight gain. Additionally, targeting leptin could be beneficial in maintaining weight loss after weight loss interventions. A persistent challenge after weight loss interventions, including the newly approved dual agonist, is weight regain after discontinuation of the intervention [128]. As weight decreases, a disproportionate reduction in leptin levels is observed, even exceeding those of lean individuals when adjusted for overall fat mass. The resulting sustained signaling of hunger to the brain hinders the maintenance of weight loss. This probably represents a counterregulatory mechanism against evolutionary unfavorable weight loss, contributing to the phenomenon of yo-yo dieting, in which people regain weight, often exceeding their initial weight [5, 129, 130]. Preventing this leptin deficit after leptin resensitization could offer a promising therapeutic approach to sustained weight loss.

1.2. Epigenetics

Epigenetics refers to heritable or *de novo* changes in gene expression patterns that occur without alterations in the DNA sequence itself. Epigenetic modifications include histone modifications, noncoding RNAs, RNA modifications, and DNA methylation. These epigenetic modifications play a fundamental role in the regulation of various processes. They orchestrate chromatin remodeling, control gene transcription, and mRNA translation, allowing genetically identical cells to function differently [131]–[135]. Therefore, epigenetic mechanisms are pivotal for development and can be altered through environmental factors such as diet, toxin exposure, and stress. In addition to cell differentiation, epigenetic processes are critical for physiological functions such as X-chromosome inactivation in women, memory formation, aging-related changes in gene expression, and metabolic regulation. Dysregulation of epigenetic mechanisms is involved in the pathogenesis of numerous diseases, including obesity, metabolic syndromes, and cancer [136]–[138]. An overview over the most prominent epigenetic modifications is given in Figure 1.6 and will be described in more detail in the following.

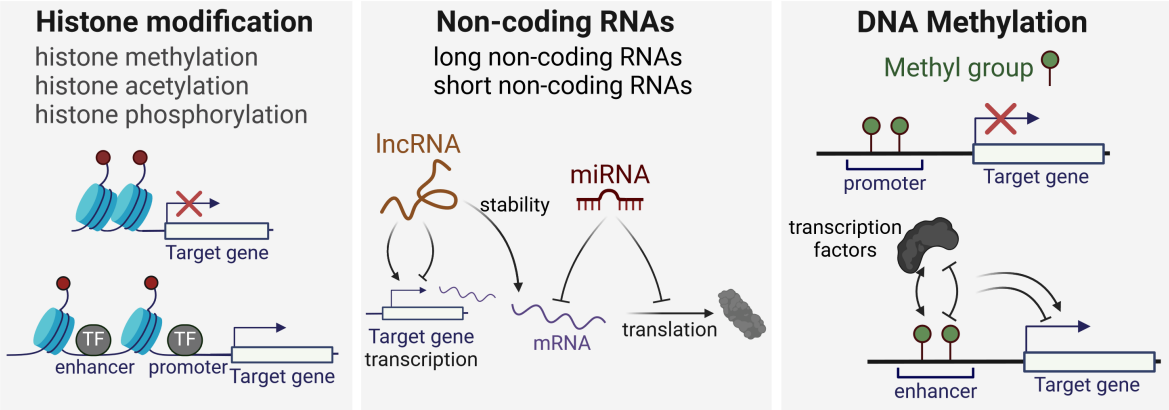

Figure 1.6.: Overview of the most prominent epigenetic modifications leading to alteration of gene expression. lncRNA–long non-coding RNA; miRNA–microRNA

1.2.1. Histones

Histones are proteins with structural functions that assemble into octamer units known as nucleosomes. These nucleosomes serve as the basic building blocks around which DNA is coiled, forming chromatin [132, 139]. The chromatin structure plays a crucial role in packaging DNA, which regulates accessibility and thus gene expression. The regulation is achieved through the opening or closing of chromatin through modifications of histones, including methylation, phosphorylation, and acetylation. Acetylation of the lysine side chains leads to loss of charge, weakening the interaction with the negatively charged DNA [132, 139]. The DNA becomes more accessible to the transcription machinery. Acetylation and deacetylation of histones is catalyzed by histone acetyltransferases (HATs) and histone deacetyltransferases (HDACs). Histone phosphorylation occurs predominantly at the N-terminal tails of tyrosines, threonines, and serines and is catalyzed by kinases and phosphatases. Histone methylation occurs as mono-, di-, or tri-methylation on lysines and asymmetrically or symmetrically at arginine side chains. Specific methylation patterns are associated with the silencing or activation of associated genes [132, 140].

1.2.2. Non-coding RNA

Non-coding RNAs encompass long non-coding RNAs (lncRNAs) and short non-coding RNAs. The lncRNAs are more than 200 nucleotides long and often colocalize with their target gene. They are transcribed by the machinery responsible for general gene expression. Similarly to mRNAs, transcription is regulated through chromatin structure, alternative splicing sites, and by transcription factors. Once transcribed, they control gene expression through various mechanisms, including stabilization of the transcription machinery at the target gene promoter, direct interaction with transcriptional proteins or enhancers, stabilization of mRNAs, or sponging of microRNAs (miRNAs) [133, 134]. Short non-coding RNAs include the transfer RNAs (tRNAs), which deliver amino acids to the ribosome during translation, and ribosomal RNAs (rRNAs), which encode ribosomal protein synthesis. Other short non-coding RNAs are epigenetically

active mainly in gene silencing and include PIWI-interacting RNAs (piRNAs), small nuclear RNAs (snRNAs), and circular RNAs (circRNAs) [133]. The most prominent epigenetic short non-coding RNAs are the small interfering RNAs (siRNAs) and miRNAs. MiRNAs are 18–22 base–long nucleotides that are transcribed from their genes as pri-miRNAs, subsequently processed into pre-miRNA and finally mature miRNAs. The mature miRNAs are loaded into the RNA-induced silencing complex (RISC) that modulates the expression of the target gene [141]. The 6–8 nucleotide seed sequence of miRNA is complementary to its target mRNA, guiding the RISC complex to the mRNA [141]. Typically, miRNAs target multiple genes, inhibiting transcription, leading to mRNA degradation or mRNA cleavage [142]. SiRNAs function similarly to miRNA through the RISC complex, but are of viral origin and have a specific target mRNA [133].

1.2.3. DNA methylation and methods of detection

DNA methylation is an epigenetic modification capable of altering gene expression depending on its occurrence on the DNA strand relative to the target gene. DNA methylation occurs mainly on cytosine residues followed by guanine nucleotides at a DNA locus, known as CpG sites. An overview of the structures and enzymes involved in DNA methylation and demethylation is given in Figure 1.7. At the CpG sites, a methyl group at 5-C of the cytosine is covalently attached by DNA methyltransferases (DNMTs). There are two different families of DNMTs: DNMT1 is responsible for maintaining DNA methylation patterns during replication. This ensures the preservation of established methylation profiles across cell generations, which is particularly crucial during embryonic development [143, 144]. The other family includes DNMT3A and DNMT3B, which are responsible for *de novo* DNA methylation of previously unmethylated cytosines [144, 145]. The third familiy member DNMT3L is inactive on its own, as it does not possess residues for DNA methyltransferase activity [146]. DNA methylation can be actively removed by ten-eleven translocation methylcytosine dioxygenases (TETs) that oxidate 5-methylcytosine to 5-hydroxymethylcytosine. Further oxidation leads to the formation of 5-formylcytosine and/or 5-carboxylcytosine, depending on the enzymatic and isoform-specific activity [147, 148]. The final product 5-carboxylcytosine and other derivatives of cytosine can be transformed into cytosines by thymine DNA glycosylase (TDG) of the DNA base-excision repair mechanism [131, 149]–[151].

Influence on gene expression depend on location of DNA methylation

DNA methylation has different effects on gene expression, depending on its location within the DNA sequence relative to the target genes and the cellular context. Approximately 70 % of the gene promoters encompass CpG islands, regions characterized by a high density of CpGs. Hypermethylation of these islands is associated with gene silencing, especially in cancer pathogenesis, gene imprinting, and cell differentiation [151]–[155]. Within promoter regions, DNA methylation predominantly suppresses gene expression by inhibiting transcription factor binding [131, 156]. In contrast, intragenic regions within gene bodies, typically CpG-poor, exhibit

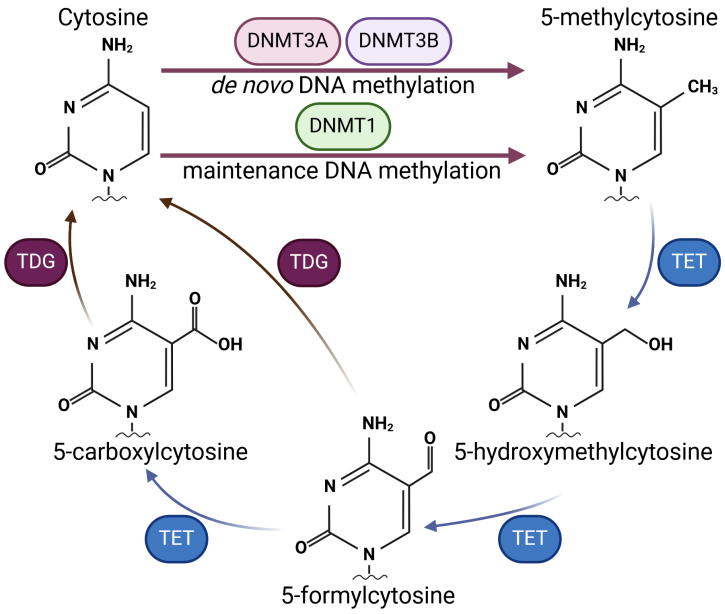

Figure 1.7.: DNA methylation and demethylation processes. DNA methyltransferases (DNMTs) catalyze the methylation of 5-C of a cytosine. Ten-eleven translocation methylcytosine dioxygenases (TET) oxidize the methyl-cytosine through several derivatives. Thymine DNA glycosylase (TDG) transforms the derivatives to cytosines.

high levels of DNA methylation, which can suppress intragenic transcriptional start sites or improve transcription elongation [157]–[159].

Enhancer regions are cis-regulatory DNA sequences, several kilobases up to megabases distal from their target gene [160]. These regions are free of nucleosomes, making the DNA accessible to transcription factors and therefore hypersensitive to digestion with DNase I [160, 161]. Additionally, enhancer sites are flanked by nucleosomes with specific histone modifications. In addition to histone modifications, DNA methylation within enhancer regions modulates gene expression and plays a pivotal role in cell differentiation, cancer development, and metabolic diseases [135, 162]–[164]. Various mechanisms are proposed to underlie these effects, depending on enhancer genomic contexts and tissue-specific occurrence: DNA methylation within an enhancer region inhibits or promotes transcription factor binding [156, 165]–[171]. It recruits methyl-sensitive factors, such as Methyl-CpG Binding domain proteins (MBD) or Methyl-CpG binding proteins (MECP) leading to chromatin closure and transcriptional repression [156, 172, 173], or it recruits factors mediating further alteration in DNA methylation, such as DNMTs or TETs [162, 174].

Methods of detection

In general, three main methods are used to detect DNA methylation, each offering various downstream applications [175]: *Methylation-sensitive restriction enzymes* cleave specific unmethylated DNA sequences, resulting in methylation-dependent DNA fragmentation. However, the resolution of this method is limited and restricted to specific enzyme cleavage sites. *Methylated*

DNA Immunoprecipitation utilizes antibodies to target methylated cytosines or methylation binding proteins like MBD to enrich methylated DNA fragments. The method is constrained by resolution and antibody specificity. *Bisulfite conversion* remains the gold standard for DNA methylation detection, involving the chemical conversion of unmethylated cytosines to uracils. While offering base-pair resolution analysis of CpGs, the harsh reaction conditions in the bisulfite reaction can lead to DNA breakage. These methods can be followed by various downstream applications, such as polymerase chain reaction (PCR) for site-specific analysis and next-generation sequencing techniques. The latter includes whole genome bisulfite sequencing for genome-wide methylation analysis, microarrays for targeted genome-wide sequencing, nanopore sequencing for real-time and long-read sequencing, and pyrosequencing for quantitative methylation analysis [175].

In the here presented work, bisulfite conversion coupled with pyrosequencing was employed, allowing base pair resolution quantification of DNA methylation. Bisulfite sequencing typically involves three major steps [175, 176]: First, bisulfite treatment of genomic DNA converts unmethylated cytosines to uracils, while methylated cytosines remain unchanged (compare Figure 1.8 bisulfite conversion). Unmethylated cytosines are sulfonated by bisulfite (HSO_3^-), reacting to cytosinesulphonate, which reacts to uracilsulfonate by hydrolytic deamination with ammonium (NH_4^+). Desulfonation in a basic (OH^-) environment produces uracil. As a result of a slower reaction with bisulfite, methylated cytosines are protected from the reaction and remain cytosines. The final bisulfite-converted DNA is a non-complementary single-stranded DNA molecule containing mainly adenine, guanine, and uracil bases with fewer cytosines. Second, the region of interest containing the CpG(s) of interest is amplified in a bisulfite PCR (bisPCR). Using a specific assay designed for the upper or lower bisulfite converted DNA strand, bisPCR transforms uracils into thymines (compare Figure 1.8 bisulfite PCR, assay for the upper strand shown in this example). One of the primers contains a 5'-biotin label, which is crucial for subsequent pyrosequencing. In the first PCR cycle, only the reverse primer is able to bind to the forward strand, as no complementary strand exists. The polymerase incorporates adenins complementary to uracils. In the second PCR cycle, both forward and reverse primers can bind, yielding the region of interest for the first time, which is further amplified in the following PCR cycles, with thymines instead of uracils. Third, pyrosequencing, a sequencing-by-synthesis method, is performed to determine the DNA sequence and to quantify DNA methylation by discriminating between thymines and cytosines (compare Figure 1.8 pyrosequencing). Biotin-labeled PCR products are immobilized on streptavidin-coated magnetic beads. Through denaturation of the PCR product, the sequencing primer anneals. The pyrosequencer delivers a defined series of nucleotides. The successful incorporation of the offered nucleotide (here a dTTP) creates a detectable light signal: The polymerase releases a pyrophosphate (PPi) during nucleotide incorporation. PPi is converted to adenosine triphosphate (ATP) by ATP sulfurylase, and ATP drives the luciferase-catalyzed conversion of luciferin to oxyluciferin, resulting in light emission. The intensity of the light signal is proportional to the number of strands that incorporate the nucleotide, allowing the determination of the DNA sequence. This enables the

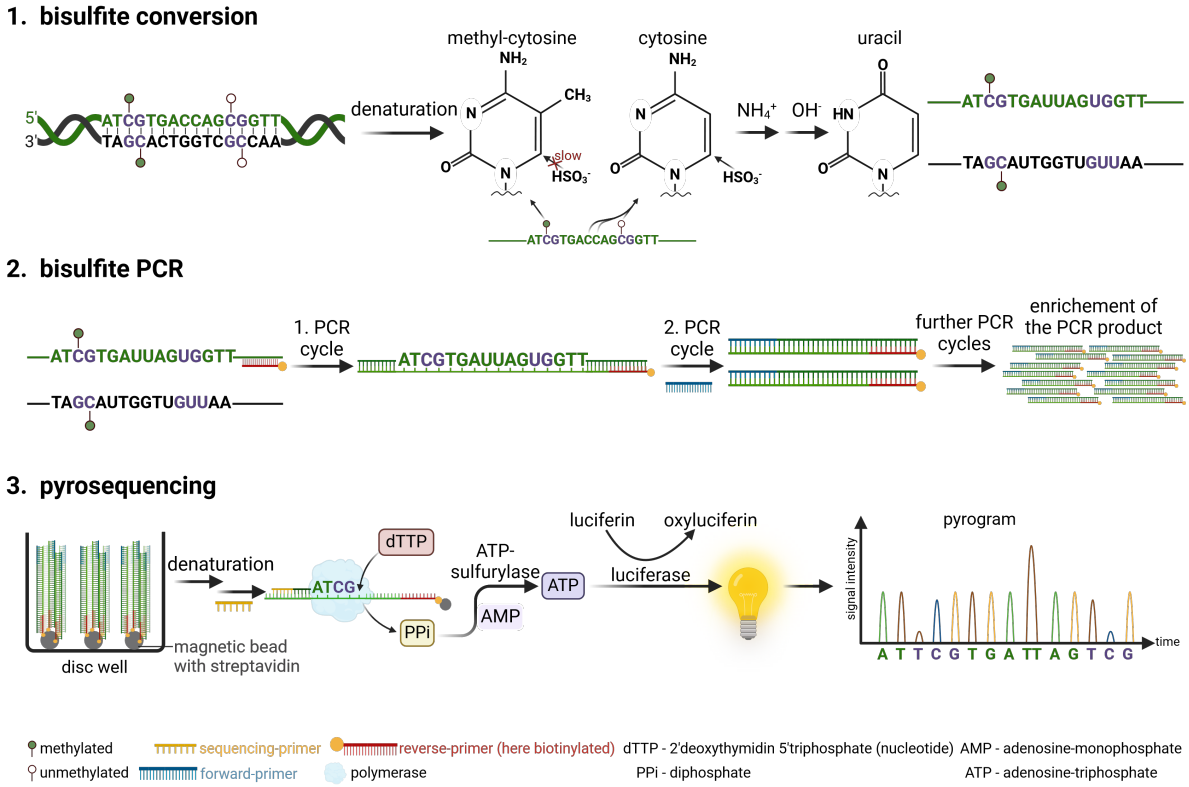

Figure 1.8.: Illustration of the steps performed for the detection of DNA methylation using pyrosequencing.

calculation of the percentage of DNA strands methylated at the CpG site based on the intensity of sequenced thymines vs cytosines.

1.3. Epigenetics in obesity and in the regulation of *Lep* expression

Epigenetics influence gene expression and exert profound effects on cell identity and pathogenesis of various diseases, including metabolic disorders such as obesity [136, 137, 177]. Epigenetic alterations in obesity result from exposure to obesogenics, for instance solvents, bisphenol A [178], lack of physical activity [179]–[181] and sleep deprivation [177, 182]. Furthermore, dietary factors such as high-fat and hypercaloric diets lead to tissue-specific epigenetic alterations associated with obesity, which can be reversed, for example, by calorie restriction [137, 164, 183]–[187]. These epigenetic alterations are heritable across multiple generations through maternal and paternal transmission [136, 138, 188].

The epigenetic alterations observed in obesity include histone modifications of e.g. adipogenesis regulating genes (e.g. C/EBPA and PPARγ) and pro-inflammatory cytokines (e.g. TNFα) [189, 190]. Furthermore, several miRNAs and lncRNAs involved in adipogenesis, triglyceride accumulation, and inflammation are altered in obesity [191]–[193]. In particular, the long non-coding RNA *lncOb* was shown to be required for high *Lep* expression in mature adipocytes, as well as the onset of *Lep* expression during differentiation of adipocytes (see also Figure 1.4) [93, 194, 195]. *LncOb* most likely forms a loop, bringing enhancer sites close to the *Lep* promoter

[93, 194]. However, the results between the two studies describing the *lncOb* are ambiguous regarding the fat depot-specific *lncOb* expression. *LncOb* and *Lep* expression rose in iWAT in diet-induced obesity, while the expression in eWAT remained unchanged, despite an increase in *Lep* expression. However, *lncOb* expression was downregulated in response to fasting in both depots [194]. In contrast, the second study showed obesity-induced changes in *lncOb* expression in both iWAT and eWAT [93].

Additionally, alterations in DNA methylation patterns play an important role in the development and progression of obesity. For example, changes in DNA methylation associated with altered expression profiles of genes involved in glycolysis and lipogenesis have been found in the livers of obese individuals compared to lean [164]. Insulin promoter demethylation was associated with tissue-specific insulin gene expression [196], while DNA methylation of obesity markers ATP-binding Cassette Sub-family G Member 1 (ABCG1) and SREBP1 was positively correlated with BMI [197]. Downregulation of the expression of the Glucosetransporter Typ 4 gene *Slc2a4* accompanied by increased methylation [183] and altered DNA methylation patterns in genes related to adipogenesis [198] further underscore the role of DNA methylation in obesity-related metabolic disturbances. Studies have identified tissue-specific DNA methylation signatures in adipose tissue, revealing novel target genes associated with obesity pathophysiology [199].

DNA methylation appears to regulate *Lep* expression depending on the nutritional status of the organism: In chronic obesity, elevated methylation levels were observed in the *LEP* promoter together with increased *LEP* expression in adipose tissue. This methylation persisted after weight loss with bariatric surgery [200], while *LEP* promoter DNA methylation in blood decreased together with *LEP* expression [201]. On the contrary, a negative correlation was observed between the methylation of the *LEP* promoter in blood and circulating leptin levels [202]. Similarly, adipocytes from diet-induced obese rats showed higher *Lep* promoter methylation linked to lower circulating leptin levels [203]. In human adipocytes and mouse cell culture models of adipogenesis, increased *Lep* expression during maturation coincided with reduced promoter methylation [204, 205]. Furthermore, higher levels of methylation at the *LEP* promoter were associated with a reduced differentiation potential in human preadipocytes and adipose-derived stem cells [206]. However, in conjunction with an increase in weight in diet-induced obese mice, *Lep* promoter DNA methylation was associated with increased *Lep* expression [184, 207].

Interestingly, contradictory results on the relationship between DNA methylation and *Lep* expression in obese versus lean mice were observed [208]. Additionally, the response to low-calorie diets appears to be better correlated with lower *Lep* methylation levels [209]. So far, only one study investigated the effects of an intragenic and a distal *Lep* enhancer site and the associated reduced DNA methylation at these sites observed in offspring from HFD-fed dams with higher *Lep* expression ([188], see also Figure 1.4). Overall, while promoter and enhancer DNA methylation are known to influence obesity-related genes, the specific effects of DNA methylation on *Lep* expression remain ambiguous. This highlights the complexity of epigenetic regulation in obesity and the little understood interaction of transcription factors in

the regulation of quantitative *Lep* expression in adipocytes.

1.4. Motivation, hypothesis and objectives

Obesity as one of the leading health problem worldwide, with estimates expecting that 20 % of the world's population will be obese by 2030 and with a global economic impact of $3.23 trillion [110]. Obesity is accompanied by severe comorbidities such as hypertension and cardiovascular disease, type 2 diabetes, liver and kidney diseases. Leptin plays a pivotal role in the pathophysiology of obesity, particularly its association with leptin resistance, and in the sustainability of weight loss interventions. This highlights the importance of a deeper understanding of how leptin gene expression is regulated in response to current fat mass within the adipocyte. Despite extensive research, the precise mechanism governing the quantitative expression of *Lep* in both lean and obese individuals remains unclear. This includes adipocyte-specific epigenetic mechanisms such as DNA methylation of enhancer sites and mechanobiological stress induced by hypertrophic adipocytes. Therefore, I hypothesize that adipocyte-specific epigenetic modifications, particularly DNA methylation of enhancer regions, play a crucial role in the regulation of quantitative *Lep* expression and contribute to the observed overshooting of leptin during the progression of obesity. This doctoral thesis aimed to address this hypothesis by:

- Identifying obesity-related DNA methylation patterns within enhancer sites proximal and distal to *Lep* in adipose tissue in a time-resolved manner. To this end, DNA methylation-sensitive enhancer sites of *Lep* were investigated in eWAT and iWAT from mice in the progression of diet-induced obesity. Furthermore, the results were translated to human VAT.

- Investigating factors that influence differential DNA methylation within adipose tissue. These factors included leptin feedback signaling, which was investigated in ob/ob mice; mechanobiological stress as studied in a stretching experiment of 3T3-L1 adipocytes; and adipocyte size which was analyzed in size sorted adipocytes of lean and obese mice.

- Elucidating the functional mechanisms by which DNA methylation influences *Lep* expression. For this purpose, methylation-sensitive luciferase assays, mass spectrometry, and CRISPR-dCas9 were used.

- Demonstrating the reversibility of DNA methylation patterns in various obesity intervention studies. To achieve this objective, WAT was examined from mice undergoing dietary short-and longterm, pharmacological, and surgical weight loss interventions.

- Exploring the additional epigenetic factor *lncOb* that can influence *Lep* expression during obesity development and weight loss interventions. To this end, *lncOb* was studied in WAT from the murine models described above.

2. Methods

This chapter describes the experimental settings and procedures. I performed all experiments unless otherwise specified. Details about materials, software and their versions, devices and their manufacturers, buffer and media compositions are provided in section A.1. Some data and procedures are published, and some are part of a submitted manuscript as indicated in the text.

2.1. Mouse models and *in vivo* procedures

All mouse experiments were in accordance with the German Law for Animal Protection, FELASA's guidelines for animal research, EU Directive 2010/63/EU and approved by the ethical committee of the Ministry of Energy Change, Rural Areas & Consumer Protection (MELUR) Schleswig-Holstein, Germany (licenses 4(111-9/16), 4(76-6/17), 4(99-11/18)) or by the State of Bavaria, Germany.

2.1.1. Diet-induced obesity mouse model

For the model of diet-induced obesity (DIO), male C57BL/6N mice (Charles River Laboratories, Sulzfeld, Germany) were group-housed in the animal facility at the Center of Brain, Behaviour and Metabolism (CBBM), University of Lübeck, Germany, in sets of four, at a constant temperature of 22±1 °C, a 12-hour light/dark cycle and unrestricted access to food and water. At 5 weeks of age, mice were randomly divided into two groups, ensuring similar body weights. The control group received a standard chow diet, while the treated group received a 60 % high-fat diet (HFD, D12492). Subgroups of eight mice per group were sacrificed at weeks 1, 2, 4, 5, 6, 7, 8, and 12. The tissues were immediately snap-frozen and stored at −80 °C. Dr. Cathleen Geißler performed the *in vivo* procedures and tissue collection together with Dr. Christin Krause and Prof. Henriette Kirchner. Jan Hendric Britsemmer performed the DNA isolation and part of the RNA isolation from eWAT. Sina Junge performed part of the DNA and RNA isolation, as well as qPCR, bisulfite conversion, bisPCR, and pyrosequencing from iWAT samples under my supervision as part of her bachelor's thesis. The phenotypic characterization is published [185, 210]. A schematic of the study can be found in Figure 2.1.

2.1.2. Metformin treatment study

For a pharmacological intervention of HFD-induced effects, mice were treated with metformin (1,1−dimethylbiguanide hydrochloride). The mice were housed, divided into subgroups, and treated as described in section 2.1.1 for 12 weeks without sacrificing subcohorts. At 12 weeks

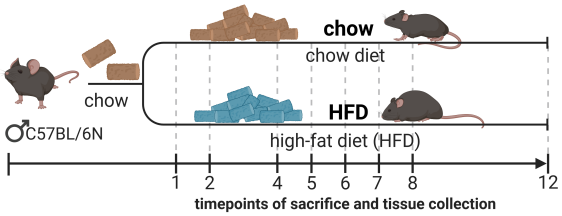

Figure 2.1.: Design of the diet-induced obesity mouse model. The figure is part of the submitted manuscript.

of HFD, the HFD group was randomly divided into 2 subgroups of similar body weight. I treated the mice with metformin orally over the drinking water: One group received metformin at 250 mg/kg body weight per day. The amount of metformin was calculated based on the mean weight of the mice and their water intake within their cage from the day before. The other subgroup received only HFD. The water was changed daily and the mice had *ad libitum* access to water and food. A subcohort of 10 mice from each group (chow, HFD, HFD+metformin) was sacrificed after 14 weeks (2 weeks of metformin treatment), the other after 18 weeks (6 weeks of metformin treatment). For tissue collection, mice were anesthetized with isoflurane and sacrificed by decapitation during the light phase with the help of Jan Hendric Britsemmer, Dr. Christin Krause, Prof. Henriette Kirchner, and Martina Grohs. Whole blood was collected, tissues were immediately snap frozen and stored at −80 °C. The handling of mice and experiments were non-blinded. A comprehensive overview of the metformin treatment study with all procedures performed is provided in Figure 2.2 and the procedures will be described in detail in the next sections. Body weight and liver data from the metformin treatment study are published in [185].

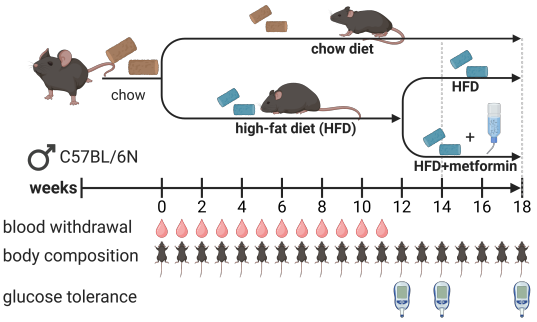

Figure 2.2.: Design of the metformin treatment mouse study. Blood drop icons indicate the timepoints of blood withdrawal, mice icons indicate the timepoints of body composition measurements, and glucometer icons indicate the timepoints of intraperitoneal glucose tolerance test.

Blood withdrawal

Additional experiments in mice from the metformin treatment study included weekly blood withdrawal from the tail vein of 5 chow and 6–7 HFD mice, ensuring that individual mice did not undergo the procedure more than once every 4 weeks. Less than 100 µL blood was withdrawn and collected in tubes coated with Ethylenediaminetetraacetic Acid (EDTA), 10 µL

antiproteolytic cocktail (Table A.1) was added, placed on ice, and plasma was collected after 2000 xg centrifugation for 15 min at 4 °C. Plasma was frozen at −80 °C and used for the ELISA analysis described in section 2.3.20.

Intraperitoneal glucose tolerance test

An intraperitoneal glucose tolerance test (ipGTT) was performed at week 12 for the whole cohort, at week 14 and week 18, respectively, for the group sacrificed one day later. Mice were fasted for 6 h starting in the early light phase from 7 am on. Fasting blood glucose levels were measured using an Accu-Check glucometer with Accu-Check Aviva blood glucose test stripes from the second blood drop from a lateral tail vein puncture. The mice were then injected intraperitoneally with 20 % glucose in 0.9 % BC isotone saline solution at 2 g/kg body weight. Blood glucose levels were measured as described in "Blood withdrawal" after 15, 30, 60 and 120 min. The GTT data of individual mice were omitted from the analysis, when the injection clearly failed, as evidenced by minimal (glucose differences ±20 mg/dL) or no reaction to glucose. In cases where HFD-fed mice exhibited extremely high blood glucose levels exceeding the maximum measurable limit of the Accu-Check device, the blood glucose values for these mice were set to 600 mg/dL, representing the maximum measurable value of the device. The ipGTT was performed with the help of Jan Hendric Britsemmer and Martina Grohs.

Body composition

Body composition was non-invasively assessed using time-domain nuclear magnetic resonance (Minispec LF110). This method discriminates between fat tissue, lean tissue, and free fluid based on their distinct characteristics of water content. To ensure calibration, a check sample containing rape seeds was used. Measurement, analysis and quantification were performed using Minispec Plus NF and Opus 7.0 software. Measurements were carried out by placing the animals in a mouse restrainer within the machine.

2.1.3. Vertical sleeve gastrectomy

Vertical sleeve gastrectomy (VSG) was performed by Dr. Anne-Marie Neumann at the CBBM, Lübeck, Germany. Detailed procedures and additional results are published in [211, 212]. Briefly, C57BL/6JRj mice (Janvier Labs, Le Genest-Saint-Isle, France) were received at 3–4 weeks of age and housed in sets of 3–5 until two weeks before surgery at housing conditions described in section 2.1.1. Mice received *ad libitum* HFD (D12492) upon arrival at the animal facility. Three days pre-surgery, mice were given a liquid diet. The HFD was discontinued two days before surgery and the mice underwent an overnight fast before the procedure. After surgery, mice received a liquid diet for two days, a choice of a liquid diet and HFD on the third day, and only HFD for the rest of the experimental period. Mice weighing at least 35 g before fasting underwent a VSG or a sham operation. In the VSG, around 80 % of the stomach was resected or blocked. Sham mice underwent the same procedures without resection, but with exposure of

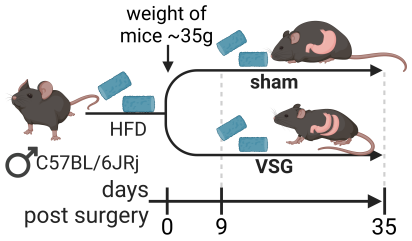

Figure 2.3.: Design of the vertical sleeve gastrectomy study.

the stomach to 15–20 s of mechanical pressure. Mice were repeatedly treated with analgesics (1 mg/kg meloxicam) until four days post-surgery. Mice were sacrificed and tissues were collected and snap frozen on day 9 or day 35 post-surgery (Figure 2.3).

2.1.4. Intervention Studies

The murine studies described in this subsection were performed by Dr. Sonja Schriever in the Neurobiology Research Unit, Institute for Diabetes and Obesity, Helmholtz Center Munich. They were approved by the State of Bavaria, Germany, performed in adult male C57BL/6J mice (Janvier Labs, Saint-Berthevin, Cedex, France), housed on 12 h light/dark cycle with *ad libitum* access to water and chow diet (1314, Altromin, Germany) or 58 %/60 % high fat diet (D12331, Research Diets, US/E15742, Ssniff, Germany).

10-day intervention with additional fasting

The protocol for the acute weight loss intervention has already been published in [112]. Mice received a 60 % HFD for 27 weeks prior to a 10-day weight loss intervention: Two groups of HFD-fed mice were switched to a chow diet (diet switch, HC) or a calorie restricted chow diet (CR, 50% of calories consumed by the HC group), while one group continued on the HFD and an age-matched chow group served as additional control group. A subgroup of each of the four groups underwent a 16 h overnight fast before sacrifice at 9 am. An illustration of the study is given in Figure 2.4a.

Weight cycling study

The weight cycling study has already been published [213]. Mice received a 58 % HFD for 24 weeks prior to the intervention: the first group of mice continued with HFD for another 12 weeks before a diet change to chow for another 12 weeks (HC). The second group switched to chow for 12 weeks and then switched back to HFD for another 12 weeks (Yoyo). The third group continued on the HFD and age-matched chow-fed mice served as an additional control. Before sacrifice and tissue collection, the mice were fasted for three hours. An illustration of the study is given in Figure 2.4b.

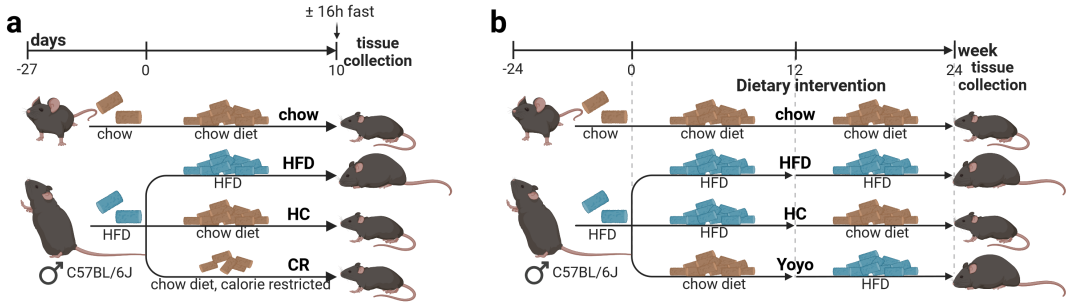

Figure 2.4.: Designs of dietary intervention studies. a) Illustration of the 10-day dietary intervention with additional overnight fasting. b) Illustration of the long-term, weight cycling study intervention. The figures are part of the submitted manuscript.

ob/ob mice

Epididymal adipose tissues (eWAT) of 12 week old male ob/ob mice fed a chow diet were collected.

2.1.5. Human samples

VAT tissue biopsies from subjects with obesity were collected by Dr. med. Oliver Mann and Dr. med. Stefan Wolter. Physiological data of subjects are given in Table 2.1. RNA and DNA isolation, bisulfite conversion, and quantitative real-time PCR were performed by Dr. Christin Krause and Dr. Helen Sievert. The details are published in [214]–[216]. Briefly, VAT biopsies were collected during bariatric surgery in obese individuals at the University Hospital Eppendorf, Hamburg, Germany. Biopsies were obtained from overnight fasted subjects and all participants provided informed consent. The approval of the study was granted by the local ethics committee (Ethik Komission der Ärztekammer Hamburg, PV4889, 2015).

Samples of non-obese subjects were collected and adipocytes isolated at the Institute of Diabetes and Clinical Metabolic Research, University Medical Center Schleswig-Holstein, Campus Kiel, Germany, in collaboration with Prof. Matthias Laudes and Dr. Katharina Heitmann as described in [217]. VAT biopsies of control, overnight fasted patients were collected during elective abdominal surgery. All participants gave their informed consent. Ethical approval was granted by the local ethics committee (Christian-Albrechts University in Kiel, B278/11). In contrast to the samples from patients with obesity, adipocytes were isolated from VAT: VAT was mechanically homogenized and digested with collagenase type II for 1 h at 37 °C in a shaking incubator and filtered through a sieve (355 µm, 280 µm). Subsequently, the samples were centrifuged at 1000 rpm for 5 min, floating adipocytes collected and frozen at −80 °C.

Table 2.1.: Physiological data of human subjects investigated. The table is part of the submitted manuscript.

	obese	control
Number of subjects	92	3
Sex [female/male]	67/25	1/2
BMI [kg/m^2]	52.17 ± 10.11	26.13 ± 0.99
Weight [kg]	152.22 ± 32.00	83.00 ± 8.54
Age [years]	43 ± 12	69 ± 9

2.2. Cell culture

Cell culture experiments help to understand the underlying molecular mechanisms of the processes observed *in vivo*. Cell culture experiments were performed as technical duplicates and biological replicates. The number of biological replicates is stated or shown in the results.

2.2.1. 3T3-L1 experiments

The murine fibroblast cell line 3T3-L1 can differentiate into adipocytes and is frequently used as a cell model for adipocyte differentiation and adipogenesis. Unlike adipocytes *in vivo*, differentiated 3T3 adipocytes contain multiple lipid droplets of different sizes instead of a unilocular one.

Differentiation and Maintenance

3T3-L1 cells were maintained in growth medium in a T75 flask at 37 %, 5 % CO_2. The buffer composition is stated in Table A.2. When reaching 70 % confluency, cells were passaged. For cell seeding or passaging, cells were washed with 1x DPBS and incubated with trypsin for 5 min at 37 °C. Growth medium was added to inactivate trypsin and cells were dissociated from clumps by gentle up and down pipetting. After transfer to a reaction tube, cells were pelleted at 500 xg for 5 min. The medium was discarded and the pellet was resuspended in 37 °C growth medium. For the calculation of the number of cells, 10 µL cell suspension was mixed with 10 µL trypan blue and transferred to a Neubauer counting chamber. Cells were counted and the concentration of cells per mL was calculated. The cells were seeded accordingly.

For differentiation, 3T3-L1 cells were seeded at $2 * 10^4$ cells per well in a 12-well plate and cultured in growth medium for 4 days, one day after 100 % confluency was reached. Then the medium was changed to induction medium, stimulating the cells to start differentiation. After 72 h, medium was changed to differentiation medium, which was used until the end of the experiment and changed every 2–3 days.

dCas9-KRAB transfection

CRISPR-Cas9 is a widely used genome editing technology that allows precise site-directed DNA modifications. A single guide RNA (sgRNA) is used to target a specific genomic location for Cas9, which cuts DNA at the specified location. The dead Cas9 (dCas9) used here was a modified

protein, unable to cut DNA. However, the additional feature of a transcription-inactivating Krüppel-associated box (KRAB) domain allows to study the interaction of the targeted genomic site with the gene expression machinery of nearby genes. Thus, the functionality of the targeted region can be studied in a genomic context. Here, the dCas9-KRAB was used to identify whether the regulatory *Lep* enhancer site RS1 affects *Lep* expression.

The plasmid (Figure A.1) was a kind gift from Verónica Yumiceba Corral from the Human Molecular Genomics lab, Institute of Human Genetics, University Clinics Lübeck, Germany, and was amplified in a midi-preparation as described in section 2.3.17. For transfection into 3T3-L1, cells were differentiated as described in "Differentiation and Maintenance" but in 10 mm dishes seeded with $4 * 10^5$ cells. After 10 days of differentiation, cells were transferred to a 12-well plate with antibiotic-free differentiation medium. One day after seeding, cells were transfected using the 3T3-L1 Cell Avalanche® Transfection Reagent. For the transfection solution 300 ng plasmid, 12 µL Opti-MEM and 0.4 µL Transfection Reagent were vigorously mixed, incubated for 15 min at room temperature, and added dropwise to the well. The plates were centrifuged at 300 xg for 5 min. After 4.5 h medium was changed and sgRNA transfected: Solutions for sgRNA transfection were prepared and added as described above and consisted of 50 µL Opti-MEM, 15 pmol sgRNA and 0.4 µL Transfection Reagent. The medium was changed after 4.5 h and cells were incubated for 36 h at 37 °C, 5 % CO_2. A scramble sgRNA without a target in the mouse genome was transfected as a control. The sequences of all sgRNAs are given in Table A.7.

Mechanobiological experiments

I performed the mechanobiological experiments on a custom apparatus during my research stay at Dafna Benayahu's laboratory at the Department of Cell and Developmental Biology, Tel Aviv University, Israel. The apparatus is published in [56, 218]. An image of the apparatus can be found in Figure 2.5a. Two different zones of force were discriminated in the experimental setup: The outer ring area and the ring area. In the here performed analysis, the ring area is described in the results as "stretch" and the outer ring area was not further investigated within the scope of this work. The differentiation protocol was slightly different from the protocol stated in "Differentiation and Maintenance": 3T3-L1 cells were grown to the maximum of passage 5 and maintained in growth medium. Cells were seeded at $1 * 10^4$ cells/cm^2 in a 6-Well BioFlex® culture plate with Collagen I. After reaching 90 % confluency, differentiation was induced by changing growth medium to induction medium. On day two of differentiation, the medium was changed to differentiation medium. The differentiation medium was changed every 3–4 days. For stretch during differentiation, the plate was placed on the apparatus on day 2 of differentiation and only removed on days 9 and 16 of differentiation (days 7 and 14 of stretch) to take microscopic images (compare section 2.2.1 "Microscopy"). Cells were harvested on day 16 of differentiation (Figure 2.5b). The compositions of the media can be found in Table A.3. For the stretch of mature adipocytes, the plate was placed in the apparatus on day 16 of differentiation and the cells were harvested on day 18 (Figure 2.5c). The harvesting method depended on the type of downstream analysis and is described

in further detail in section 2.3.1 and section 2.3.6. 3T3-L1 cells growing simultaneously on a BioFlex® culture plate with Collagen I, but not placed in the stretching apparatus, receiving the same culture medium as the stretched cells, served as a control and were named "flex". To account for differentiation biases between biological replicates, normalization to the control was performed within a biological replicate. Also, statistical analysis was performed differently, the ddCT=mean(dCt(flex)$_{\text{technical replicates}}$)−mean(dCt(stretch)$_{\text{technical replicates}}$) for each biological replicate were used for analysis with Student's t-test.

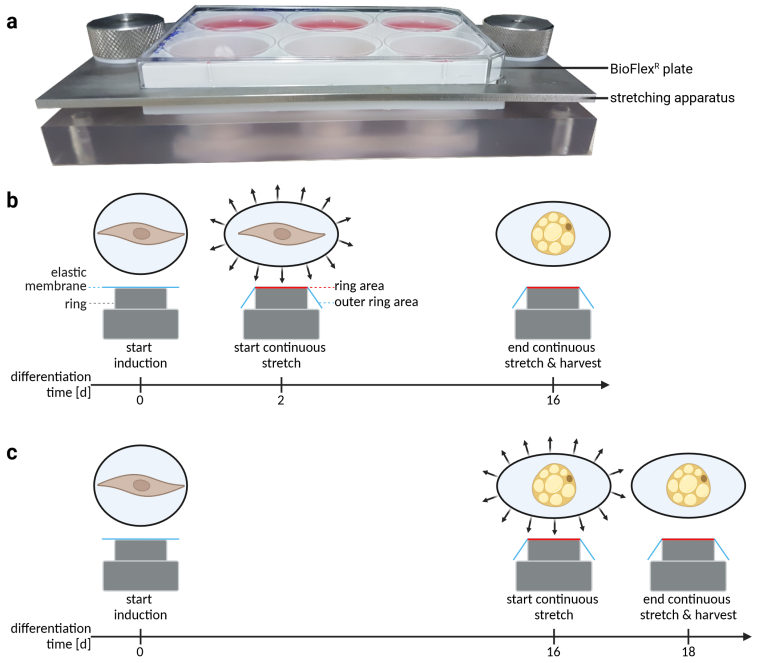

Figure 2.5.: Design of the mechanobiological experiments. a) Picture of the stretching apparatus. Schematic of (b) stretch during differentiation of 3T3-L1 cells and (c) of mature 3T3-L1 adipocytes.

Microscopy

For the evaluation of adipogenesis, the EVOS FL Auto 2 microscope was used with a 4x or 20x magnification and a custom 3D printed mounting plate to enable the analysis of the BioFlex® plates. The 4x images were stitched to calculate the level of adipogenesis with ImageJ. Example images of the unprocessed and processed images are given in Figure A.4.

Palmitate/oleate treatment

3T3-L1 cells were treated with palmitate/oleate to stimulate adipocyte enlargement. On day 10 of differentiation, as described in "Differentiation and Maintenance", the 3T3-L1 adipocytes were switched to medium containing 1:1 palmitate:oleate at $c_{final} = 0.5\,\text{mM}$. Cells treated with 0.75 % bovine serum albumin (BSA) in 25 mM NaOH in DMEM served as a direct control. Palmitate/oleate treatment was repeated with every medium change every 2–3 days.

Work stocks with c_{final} = 5 mM in 7.5 % of palmitate or oleate were prepared as follows: 1.8 g BSA were solved in 18 mL DMEM overnight at 4 °C yielding a 10 % BSA solution. Sodium palmitate was solved at 8.5 mg in 1.5 mL 0.1 M NaOH at 70 °C for a maximum of 10 min. Subsequently, 2.5 mL solved palmitate was added to 7.5 mL 50 °C 10 % BSA, mixing every 500 µL. Sodium oleate was solved at 9.2 mg in 1.5 mL 0.1 M NaOH at 70 °C for a maximum of 10 min. Then 2.5 mL solved palmitate was added to 7.5 mL 50 °C 10 % BSA, mixing with every 500 µL. The palmitate and oleate solved were sterile filtered through a syringe filter and stored at −20 °C.

Forskolin treatment

3T3-L1 cells were differentiated for 14 days as stated in "Differentiation and Maintenance". On day 14, cells were treated with 10 µM forskolin ($c_{workstock}$ = 10 mM in 100 % EtOH) for 6.5 h before harvest. The harvesting method depended on the type of downstream analysis and is further described in section 2.3.1 and section 2.3.6. Cells treated with 0.5 µL EtOH per well were used as a control.

2.2.2. HEK cell culture

HEK293T is a human immortalized kidney cell line. HEK 293T cells were maintained in high glucose medium in a T75 flask and passaged using trypsin when reaching 70 % confluency as described in section 2.2.1 "Differentiation and Maintenance". The medium was the same growth medium as that for 3T3-L1 cells (Table A.2).

Transfection and luciferase assay.

HEK293T cells were used for transfection and subsequent analysis of luciferase activity. The *Lep* enhancer site of interest (RS1, RS2, or RS3) was cloned into a CpG-free plasmid containing a firefly luciferase under the control of a cytomegalovirus (CMV) promoter. The CpG-free plasmid was a kind gift from Prof. Rehli [219]. This plasmid was either methylated or mock-methylated to study the effects of methylation in the *Lep* enhancers on the expression of the luciferase gene, which was indirectly measured by luciferase activity. The creation of the plasmid is described in section 2.3.15–section 2.3.18. HEK293T cells were seeded in growth medium without antibiotics, one day before transfection at $1 * 10^4$ cells per 100 µL per well in a 96-well plate. The cells reached between 70–80 % confluency after 24 h. For transfection, 0.2 µL lipofectamin 2000 and 5 µL Opti-MEM per well were mixed and incubated for 5 min at room temperature. Meanwhile, 100 ng of each plasmid containing the insert of interest and the Renilla-SV40 plasmid (pRL-SV40, Promega, US) were mixed with 2 µL Opti-MEM per well. The Renilla vector was used for transfection normalization. The plasmid solution was added to the lipofectamin-Opti-MEM, mixed, and incubated for 20 min at room temperature. Then 10 µL of the solution per well was added to the cells and the plate was gently shaken. A triplicate of each plasmid and each condition (mock vs methylated) was transfected. For the luciferase assay,

the Dual-Glo® Luciferase Assay system was used and the buffers were prepared according to the manufacturer's instructions. After 24 h of incubation, cells were lyzed by adding the same volume of Dual-Glo®Reagent as cell culture medium and the plate was gently shaken. After at least 10 min of incubation at room temperature shielded from light, the luminescence of the Firefly luciferase activity was measured. Then an equal to the media volume of freshly prepared Dual-Glo®Stop&Glo®Reagent was added, incubated for 10 min at room temperature shielded from light and the luminescence of the Renilla activity measured. For each well individually, the Firefly signal was divided by the Renilla signal for normalization before analyzing the differences between the condition mock vs methylation.

2.3. Molecular Methods

All molecular methods were performed at room temperature if not otherwise stated.

2.3.1. RNA isolation

RNA was extracted using the miRNeasy Kit. For RNA isolation from tissue, 50–100 mg adipose tissue was incised on dry ice and transferred to a tube containing 3–4 cell lysis and 700 µL QIAzol® Lysis Reagent. The tissue was lyzed with a bead mill (cycles=2, a_{pause}=5 s, $time_{cycle}$=20 s, $duration_{homogenization}$=15 s). For cells from cell culture, 700 µL QIAzol® Lysis Reagent was added directly to the cells. For RNA isolation from sorted adipocytes, refer to section 2.3.14. The homogenate was either frozen at −80 °C or immediately processed further: The homogenate was incubated for 5 min at room temperature. 140 µL chloroform was added, the tubes were vigorously shaken for 15 s and incubated for 3 min at room temperature. The samples were centrifuged for 15 min, 12 000 xg at 4 °C. The aqueous phase was transferred to new tubes and mixed with 1.5x volume absolute ethanol for RNA precipitation. RNA was cleaned after manufacturer's instructions on the RNeasy Mini spin columns. An optional DNase digestion was performed: 10 µL DNase I (Qiagen) and 70 µL RDD were mixed by inversion, 80 µL added to the membrane, and incubated for 15 min at room temperature. RNA was eluted in 15–30 µL RNase-free water. RNA was stored at −80 °C.

2.3.2. RNA quantification

RNA was quantified photometrically using the NanoDrop One with 1 µL RNA and the quality was ensured by the build-in software analysis of 260 nm/280 nm absorbance ratio indicating purity of the RNA. DNA contamination could be excluded as a result of previous DNase treatment of the columns during extraction.

2.3.3. Reverse transcription: cDNA synthesis

RNA is unstable as a consequence of its single-stranded nature, an additional OH-group at the ribose, and exposure to environmental RNAses. Therefore, further analysis, such as gene

expression analysis, was based on the synthesis of complementary DNA (cDNA), which is more stable. For the synthesis of cDNA with reverse transcription, three kits were used here due to supply shortages during the COVID pandemic, yielding a similar pool of cDNA. For all kits, all steps except cycling were performed on ice. The mastermix was prepared and added to the diluted RNA. Mastermix and cycles are described in Table 2.2 and Table 2.3. The same kits were used within a specific cohort and comparability was ensured by normalization against the housekeeper gene as described in section 2.3.4. For each cDNA library, two negative controls were used: a no-template control without any RNA and a no-reverse transcriptase control without the addition of the reverse transcriptase.

For human samples, performed by Helen Sievert, 1000 ng RNA was reverse transcribed using SuperScript™IV VILO™according to manufacturer's instruction and published in [216].

Table 2.2.: Composition of the mastermixes per reaction for cDNA synthesis using the PrimeScript™ RT Master Mix, RevertAid cDNA synthesis kit and High Capacity cDNA kit. Up to 1000 ng RNA per reaction were used. RevertAid was used for eWAT of DIO mice, metformin treated mice and weight cycling mice. PrimeScript™ was used for iWAT. High Capacity was used for eWAT of VSG, 10-day intervention with fasting, ob/ob and 3T3 cell culture experiments.

Kit	Reagent	Volume [µL]
RevertAid	Random hexamer primers	0.5
	Oligo(dT)$_{18}$primer	0.5
	H_2O	1
	total RNA	10
	5X Reaction Buffer	4
	RiboLock RNase Inhibitor (20 U/µL)	1
	10 mM dNTP Mix	2
	RevertAid M-MuLV RT (200 U/µL)	1
PrimeScript™	5X PrimeScript RT Master Mix (Perfect Real Time)	4
	H_2O	6
	total RNA	10
High capacity	10X RT Buffer	2
	25X dNTP Mix (100 mM)	0.8
	10X RT Random Primers	2
	MultiScribe™ Reverse Transcriptase	1
	RNase Inhibitor	1
	H_2O	3.2
	total RNA	10

Table 2.3.: Cycles for the cDNA reactions for each kit specifically: PrimeScript™ RT Master Mix, RevertAid cDNA synthesis kit and High Capacity cDNA kit.

RevertAid		PrimeScript™		High capacity	
Temperature [°C]	Time	Temperature [°C]	Time	Temperature [°C]	Time
37	15 min	25	5 min	25	10 min
85	5 s	42	60 min	37	120 min
4	∞	70	5 min	85	5 min
		4	∞	4	∞

2.3.4. Quantitative real-time polymerase chain reaction (qPCR)

PCR is used for the amplification of a specific DNA segment. Oligonucleotide primers, typically 18–25 base pairs in length, are utilized to define the gene segment of interest. This involves a forward primer binding to the complementary strand and a reverse primer binding to the leading strand. DNA must be denatured to allow primer annealing. Subsequently, DNA polymerase elongates the DNA strand from the primers in the 3' to 5' direction, annealing complementary nucleotides to the strand. After three cycles, the DNA segment of interest is initially derived.

In this context, quantitative real-time PCR (qPCR) is employed for gene expression analysis. The primers are specific for the cDNA derived from the mRNA of the gene of interest, as described in section 2.3.3. The even amplification of the PCR product during the exponential phase is quantitatively measured relative to a fluorescence signal. The Ct value obtained is the cycle in which the fluorescence signal becomes greater than the threshold set to distinguish from any background signal. Two systems relying on the same principle were used: The PrimeTime™ system (Integrated DNA Technologies, US) and the TaqMan™ system (ThermoFisher) use a forward and reverse primer along with a specially labeled probe. In the elongation phase, the reverse transcriptase removes the probe's 3' quencher, allowing it to emit light and produce a detectable signal. As different fluorescence dyes can be used for the probe, several genes are detectable within the same reaction, as long as the emission spectra are not overlapping. The qPCR measurement allows quantification of gene expression relative to a stably expressed housekeeping gene. The Hypoxanthine-guanine phosphoribosyltransferase gene (*Hprt*) was used as housekeeper for mouse eWAT and cell culture, the Ribosomal protein lateral stalk subunit P0 gene (*Rplp0*) as housekeeper for mouse iWAT and the ribosomal protein L37a gene *RPL37A* for human. The appropriate housekeepers were identified using the Normfinder algorithm [220]. The qPCR reaction for mouse tissue or cells involved the use of 4 µL cDNA (c_{tissue}=2.5 ng/µL, c_{cells}=5 ng/µL). For the qPCR reaction for human samples with the TaqMan system, 12.5 ng cDNA was used. The composition of the reaction mixtures is detailed in Table 2.4, with a list of primers provided in Table A.8. A standard curve was used to evaluate primer efficiency for each assay and primer pair to ensure proper performance of the assays. Detection and analysis were performed using the Quantstudio™ 5 Real-Time PCR System and the ThermoFisher Scientific Design and Analysis software. For fold changes of samples and cohorts, which were directly compared, the same thresholds were used for the calculation of Ct values. The fold change was analyzed from the Ct values after Pfaffl [221].

Table 2.4.: qPCR reaction mixture using PrimeTime or TaqMan mastermixes.

Volume	Reagent
5 µL	PrimeTime MasterMix or TaqMan Fast Advanced Master Mix
0.5 µL	qPCR assay (20X)
0.5 µL	qPCR assay 2 (20X) or diethylpyrocarbonat-treated H_2O
4 µL	cDNA

2.3.5. RNA sequencing

RNA sequencing was performed by Nathalie Kruse at the Institute of Human Genetics. Total RNA isolated as described in section 2.3.1 was used to prepare a library using the QuantSeq 3'mRNA Seq V2 Library Prep Kit after manufacturer's protocol including the add on PCR. The quality of the library was accessed using the Qubit 1X dsDNA HS Assay Kit after manufacturer's protocol and the Qubit® fluorometer 2.0 as well as the 2100 Bioanalyzer Instrument. The library was quantified using the NEBNext® Library Quant Kit for Illumina® after manufacturer's protocol, with qPCRs performed on the 7300 Real Time PCR System and final calculations performed using the NEBioCalculator®. Sequencing was performed on the NextSeq 2000 system. RNA sequencing data were further processed as described in section 2.4.4.

2.3.6. DNA isolation

DNA was isolated using the QIAmp Fast DNA Tissue Kit or the QIAmp Mini Kit after manufacturer's protocol with the following changes. For tissue lysation, 50–100 mg adipose tissue was incised on dry ice and transferred to a 2 mL screw cap micro tube containing 3–4 cell lysis beads and lysis buffer (for Fast DNA Tissue Kit: 200 µL AVE, 40 µL VXL, 1 µL DX reagent, 20 µL Proteinase K and 4 µL RNase A; for QIAmp Mini Kit: 100 µL ATL). Homogenisation was performed with a bead mill (cycles=2, a_{pause}=5 s, $time_{cycle}$=20 s, $duration_{homogenization}$=15 s). All other steps were performed after manufacturer's instruction for both kits with elution in 30–50 µL ATE (Fast DNA Tissue Kit) or DEPC-treated H_2O (QIAmp Mini Kit).

For DNA isolation of cells from cell culture, only the QIAmp Mini Kit was used. For lysis, cells were washed three times in cold 1xDPBS. Then 200 µL 1xDPBS was added, cells were harvested using a cell scraper, and the suspension was transferred to a reaction tube. Subsequently, 20 µL proteinase K was added, mixed, and 200 µL lysis buffer AL was added. The cells were incubated at 56 °C for 10 min. All other steps were performed after manufacturer's instruction with elution in 50 µL DEPC-treated H_2O. For DNA isolation from isolated and sorted murine adipocytes, refer to section 2.3.13. For DNA isolation from human adipocytes, refer to section 2.3.14.

2.3.7. DNA quantification

DNA was quantified using the Qubit™ spectrophotometer with the Qubit™ dsDNA BR Assay. Qubit™ dsDNA BR Reagent was diluted 1:200 with Qubit™ dsDNA BR Buffer Reaction buffer. Per reaction, 199 µL were transferred to special Qubit™ 0.5 mL PCR tubes and 1 µL DNA was added and incubated for at least 2 min at room temperature in the dark. Measurement was performed using the Qubit™ 4 with built-in software that calculated the amount of DNA in the original tube. Calibration with a standard curve was performed on each measurement day by mixing 190 µL of each with 10 µL of Standard 1 and Standard 2.

2.3.8. Protein isolation

Whole protein isolation

Whole protein isolation from DIO mice adipose tissue was performed by Jan Hendric Britsemmer. The Bio-Plex® Cell lysis kit was used. Lysis buffer was prepared by mixing Factor 1 1:250 and Factor 2 1:500 with Bio-Plex® Cell lysis buffer. 300 µL lysis buffer was added to approximately 50 mg eWAT in a screw cap micro tube containing 3–4 cell lysis beads. Homogenization was performed with a bead mill (cycles=2, a_{pause}=5 s, $time_{cycle}$=20 s, $duration_{homogenization}$=15 s) followed by 15 min incubation at 4 °C. Without transferring any lipids from the top layer, 250 µL of the upper layer was transferred to a new tube, centrifugation was repeated, and 200 µL supernatant was transferred again to a new tube with the final protein sample.

Nuclear protein extraction

For nuclear protein extraction using the Ne-Per Nuclear and Cytoplasmic Extraction Kit, 13-day differentiated 3T3 cells were washed three times with cold DPBS and harvested using a cell scraper. All steps were performed under sterile conditions to minimize contamination. Cells were centrifuged at 6000 xg for 5 min and the supernatant was discarded. The other steps were performed after manufacturer's instructions with the following changes. The pellet was resuspended in 300 µL CER I by vigorous mixing using a vortexer for 15 s. A volume of 165 µL CERII and 150 µL NER was used. Nuclear proteins were stored at −80 °C.

2.3.9. Protein quantification

Proteins were quantified using the Pierce™BCA Protein Assay Kit after manufacturer's protocol. Work reagent was prepared by mixing 1:50 Reagent B with Reagent A. In a 96-well plate, 2 µL sample or standards were pipetted as duplicates. Then 200 µL work reagent was added, mixed and incubated at 37 °C for 30 min. The light signal was measured using the plate reader CLARIOstar Plus at 562 nm. Protein concentrations were calculated from the BSA standard curve included in the kit.

2.3.10. Bisulfite conversion

Bisulfite conversion of DNA coupled to pyrosequencing is used to discriminate methylated and unmethylated cytosines, as introduced in section 1.2.3. For DNA bisulfite conversion, the EpiTect Fast DNA Bisulfite Kit was used after manufacturer's instruction with the following adaptions: Where possible, 1000 ng DNA was used in the reaction in a volume of 20 or 40 µL with 85 µL bisulfite solution and 35 or 15 µL DNA Protect Buffer. Incubation cycles are shown in Table 2.5. Clean-up and desulfonation were performed as stated by the manufacturer with all recommended drying and cleaning steps. In the case of <100 ng input DNA, Carrier-RNA was added to Buffer BL. Bisulfite-converted DNA was eluted in 15–50 µL EB, depending on the

amount of input DNA: The elution volume was calculated in relation to the input DNA to yield a concentration of 20 ng/µL relative to the amount of input DNA.

Table 2.5.: Cycles for bisulfite conversion of genomic DNA

Purpose	time [min]	temperature [°C]
Denaturation	5	95
Incubation	30	60
Denaturation	5	95
Incubation	20	60
Hold	∞	20

2.3.11. Bisulfite polymerase chain reaction

Bisulfite polymerase chain reaction (bisPCR) is used to amplify the region of interest with certain forward and reverse primers for bisulfite-converted DNA as introduced in section 1.2.3. In these steps, the uraciles are converted to thymines. One of the primers contains a 5' biotin tag, so the PCR product can then be used for the pyrosequencing analysis as described in section 2.3.12. The PyroMark PCR kit was used. A 25 µL reaction contained 12.5 µL 2x PyroMark PCR MasterMix, 2.5 µL CoralLoad, 0.2 µM each forward and reverse primer, 10–20 ng bisulfite-converted DNA, and ad water. A general cycle program of the bisPCR can be found in Table 2.6. The size and intensity of the PCR product were evaluated by agarose gel electrophoresis: 1 % agarose was dissolved in 1x TAE (for composition refer to Table A.6) using a microwave. For visualization of DNA on the gel, 1 µL per 10 mL of the SYBR Safe DNA gel stain were added and the gel casted. The samples as well as the GeneRuler 100 bp DNA Ladder were loaded at 4 µL. Horizontal gel electrophoresis was performed in 1x TAE buffer for 20–25 min at 150 V. The gel was visualized on the ChemiDoc™ Touch Imaging System and the image was analyzed using Image Lab.

Table 2.6.: General cycles for bisPCR, parameters described as variable are assay specific and can be found in Table A.9.

time	temperature [°C]	cycles
10 min	95 °C	1
30 s	94 °C	variable
25 s	variable	
25 s	72 °C	
10 min	72 °C	1

The assays for the regulatory enhancer sites of *Lep* were designed using the PyroMark Assay Design 2.0 software and are given in Table A.10. Each assay was optimized for its annealing temperature in the PCR by testing multiple annealing temperatures starting at 5 °C below the lowest melting temperature of the primer pair. The annealing temperature that produced the strongest product in PCR was chosen as assessed by agarose gel electrophoresis and provided in Table A.9.

2.3.12. Pyrosequencing

Pyrosequencing is a method to sequence a defined strand of DNA. The method used here is CpG sequencing which allows nucleotide resolution identification and quantification of DNA methylation as introduced in section 1.2.3. Here, the PyroMark Q48 Autoprep was loaded and used after the machine's and manufacturer's instructions with the PyroMark Q48 advanced CpG Kit and the sequencing primers of the assays (Table A.10). The machine was programmed using the PyroMark Q48 Autoprep software. A well of the disc was loaded with 3 µL magnetic beads and 10 µL (15 µL for RS3 assay of sorted adipocyte samples) bisPCR product. The results of DNA methylation were given in percentage of the observed methylation at the given CpG site discerned by the incorporation of a dTTP or a dCTP. Each well was individually checked for sequencing failures in the PyroMark Q48 Autoprep software and finally methylation data were standardized in Microsoft Excel using a standard curve.

Each pyrosequencing assay was thoroughly implemented to ensure accuracy. The following combinations of primers and buffers were tested to identify any potential signal from primer interactions or (self)priming: biotinylated primer (bio-p) + annealing buffer (AB), bio-p + PCR-product, PCR-product + AB, sequencing primer + bio-p. Any detected signals in these control setups lead to the exclusion of the assay. Additionally, the signal strength generated by the combination of sequencing primer and PCR-product was evaluated to ascertain its suitability against background noise. Furthermore, standard curves were prepared for each assay for better comparability between different experimental runs. These standard curves were constructed by amplifying genomic mouse DNA using whole genome amplification as described in section 2.3.19, eradicating pre-existing methylation and resulting in a 0 % methylated DNA pool. For the creation of a 100 % methylated DNA pool, genomic DNA extracted from eWAT samples were *in vitro* methylated as described in section 2.3.18. The two DNA pools were mixed to produce 0, 25, 50, 75 and 100 % methylated DNA. These samples were pyrosequenced for each assay to produce the standard curve and normalize mouse methylation data across runs (Figure A.2).

2.3.13. Adipocyte size sorting

Size sorting was performed in collaboration with Dr. Sonja Schriever and Andreas Israel at the Helmholtz Center Munich. Adipocytes were isolated from freshly dissected eWAT from mice fed a chow or a 60 % HFD for 10–11 weeks and housed under the same conditions as the mice of the intervention studies (section 2.1.4). The eWAT was minced with razor blades and transferred directly to digestion medium (1x DMEM, 1 mg/mL collagenase, 1% BSA) and incubated at 37 °C, 30 min, 1000 rpm. The solution was sieved through a 250 µm mesh. After centrifugation for 5 min at 500 xg, floating adipocytes were collected and stained with HCS LipidTox™Green neutral lipid colouring for 30 min at room temperature. Adipocytes were identified by emission, size and optical density using the COPAS FP500 and the FlowPilotTM III software with a 488 nm solid state laser. Size sorting gates were defined by the time of flight (TOF) and the extinction of the adipocytes: for chow-fed mice into "small" and "large" and for

HFD-fed mice into "small", "intermediate", and "large" (Table A.13, Table A.14). Adipocyte data of "intermediate" and "large" in HFD were analyzed together. Different size fractions of adipocytes were sorted dropwise at around 10,000 to 40,000 cells per fraction with stable flow into 50 mL falcon tubes. DNA was extracted by Kathrin Huber. Triton-X was added 1:100 to the cell suspension, vigorously mixed for 30 s, rotated for 30 min at 4 °C, again mixed for 30 s and 1 L/10 mL GlycoBlue™was added. The suspension was centrifuged at 4 °C for 15 min, the supernatant discarded and the pellet resuspended. DNA was further isolated with the Quick-DNA™Microprep Plus Kit after manufacturer's protocol. Data for the relative size fraction information were obtained and analyzed per sample from raw data files of the first 20,000 adipocytes measured, but not necessarily sorted, using R Studio.

2.3.14. RNA and DNA isolation from human adipocytes

The AllPrep DNA/RNA/Protein Mini Kit was used to isolate DNA and RNA simultaneously from human adipocytes from control subjects (section 2.1.5) after manufacturer's instructions. RNA was eluted in 14 µL RNase-free H_2O and DNA in 50 µL 70 °C warm EB.

2.3.15. Restriction digestion and ligation of plasmid DNA

To analyze the effect of *Lep* enhancer DNA methylation on expression activity in the luciferase assay (section 2.2.2) the vector was created as follows: The inserts were generated using genomic PCR (gPCR) or ordered as single-stranded oligonucleotides (Integrated DNA Technologies, see Table A.11) and dimerized. The oligonucleotides were designed to include the overlap necessary for ligation, eliminating the need for restriction enzymes. For dimerization of single-stranded oligonucleotides, 100 µM forward and reverse complementary oligonucleotides were mixed, and incubated for 5 min at 95 °C with gradual temperature decrease (−1 °C/min).

The inserts generated in the gPCR contained a recognition motif at the 5' end for the restriction enzyme NcoI and at the 3' end for HindIII with three additional bases for efficient digestion. The gPCR was performed for the RS3 site with primers stated in Table A.11. Details of the reaction can be found in Table 2.7. The size of the PCR product was analyzed by agarose gel electrophoresis as described in section 2.3.11 and purified using the WIZARD® SV Gel and PCR Clean-up system: PCR products were cleaned by column purification on an SV Minicolumn according to the manufacturer's instructions. Gel purification was achieved by running the complete product on an agarose gel, followed by excising the band of interest under UV light and dissolving the gel fragment in 10 µL Membrane Binding Solution per 10 mg gel slice at 60 °C. Cleaning was performed on a SV Minicolumn. DNA was quantified as described in section 2.3.7.

For restriction digestion, 500 ng each CMV-pCpGL plasmid and PCR product were used in a 50 µL reaction containing 5 µL 10X rCutSmart Buffer, 1 µL each NcoI and HindIII and nuclease-free water. The reactions were incubated for 15 min at 37 °C. The enzymes were heat inactivated for 20 min at 80 °C. The restriction digested plasmid and PCR product were purified

Table 2.7.: Details of the genomic PCR for the creation of the insert for the luciferase vector. The reaction contained 1X GoTaq® G2 Green Master Mix, 0.2 µM each forward and reverse primer, and 95 ng genomic mouse eWAT DNA.

Temperature [°C]	Usage	Time [min]	Repetition
95	initial denaturation	2	1
95	denaturation	0.5	35x
65	annealing	0.5	
72	extension	0.25	
72	final extension	5	1

as described above.

The QuickLigation Kit was used for the ligation reaction of plasmids with the inserts. The 50 µL reaction contained 1X Quick ligase reaction buffer, a molar ratio of 1:3 vector to insert, nuclease-free water and 1 µL Quick ligase. The reaction was incubated for 10 min at room temperature and stored at −20 °C.

2.3.16. Cloning

Transformation was used to clone the luciferase vectors with and without insert as well as the dCas9-KRAB plasmid. For the inserts PiR1 OneShot® E.coli and for the dCas9 the OneShot® Top10 E.coli were used. 50 µL bacteria were thawed on ice, either 5 µL ligation reaction from section 2.3.15 or dCas9-KRAB plasmid was added, mixed by gently flicking the tube and incubated for 30 min on ice. Transformation was achieved by heat shock at 42 °C for 30 s, followed by the addition of 250 µL room temperature SOCS medium and incubation for 1 h at 37 °C and 300 rpm. 100 µL bacteria were plated on agar plates containing antibiotic zeocin for the luciferase plasmids and ampicillin for the dCas9 plasmid. Plates were incubated overnight at 37 °C. Single colonies were picked and transferred to 5 mL or 50 mL medium, followed by at least 16 h incubation at 37 °C at 150 rpm. The volumes of the medium depended on the choice of plasmid preparation 5 mL for mini or 50 mL for midi.

2.3.17. Mini and midi plasmid preparation

To purify the plasmids from bacteria, either a mini or midi plasmid preparation was used, depending on the copy number of plasmids per bacterial cell. Bacteria were pelleted for 15 min at 4 °C and 6000 xg. The subsequent steps were performed after manufacturer's instruction. Plasmids prepared with the mini preparation were eluted in 25 µL. Plasmids prepared with midi preparations were eluted in 3 mL followed by an isopropanol precipitation and washing in 70 % ethanol. These plasmids were resuspended in 150 uL 1X TE buffer. The plasmids for the luciferase assay were sent for sequencing at Eurofins GATC, Cologne, Germany, to ensure correct ligation and sequence of the insert.

2.3.18. *In vitro* DNA methylation

Plasmids for the luciferase assay (section 2.2.2), double-stranded oligonucleotides (section 2.3.21) or genomic DNA (section 2.3.12) were *in vitro* methylated. The 20 µL reaction contained 1000 ng plasmid DNA or 25 µM oligonucleotides, 320 µM S-adenosyl methionine, 2 µL NEB buffer 2, nuclease-free water and 1 µL (4 U) M.SssI CpG methyltransferase. The mock reaction serving as control was set up in the same way, but water instead of the methyltransferase was used. The reaction was incubated for 4 h at 37 °C and enzymes were inactivated with an incubation for 20 min at 65 °C. Plasmids and oligonucleotides were purified by drop dialysis through Millipore membrane filters and deionized H_2O.

2.3.19. Whole genome amplification

Whole genome amplification was used to amplify mouse DNA, producing 0 % methylated DNA. This DNA was used to create a standard curve for pyrosequencing (section 2.3.12). The REPLI-g Mini Kit was used after manufacturer's instructions. Briefly, 2.5 µL, 400 ng total mouse DNA of eWAT from the DIO study was used and 2.5 µL D1 buffer was added, mixed and incubated for 3 min at room temperature. Then 5 µL N1 buffer was added, mixed, and briefly centrifuged. A mastermix containing 10 µL DEPC-treated H_2O, 29 µL reaction buffer and 1 µL REPLI-g Mini DNA polymerase was added to the DNA solution and incubated for 16 h at 30 °C, followed by a 3 min at 65 °C inactivation. DNA was purified by drop dialysis via Millipore membrane filters.

2.3.20. ELISA

The enzyme-linked immunosorbent assay (ELISA) is an antibody-based detection method of proteins of interest. The ELISA used here is a direct sandwich ELISA: An antibody-coated microtiter plate is loaded with a mixture of protein and the appropriate antigen-baring substance will bind to its antibody. All unbound substances are washed away. A second, biotinylated monoclonal antibody specific for the antigen is added and binds to the antigen. Lastly, an enzyme-linked streptavidin polymer binds to the biotinylated antibody, and the substrate solution leads to the development of a detectable color signal in direct relation to the amount of antigen bound in the plate.

For the mouse leptin Quantikine ELISA, plasma from chow mice was diluted 1:20, from HFD mice 1:40 or 1:80 with Calibrator Diluent. All steps were performed at room temperature with room temperature reagents. All components were prepared after manufacturer's instructions. All samples, controls, and standards were assayed as duplicates. 50 µL Assay Diluent were added to each well of the microplate, followed by loading 50 µL diluted samples, blank, control or standard and incubated for 2 h on a microplate shaker at 500 rpm. After incubation, the wells were washed 4x with prepared wash buffer using an automated washer. Then 100 µL Mouse/Rat Leptin Conjugate were added per well and incubated for 1 h as described above. The wells were washed 4x as described above and 100 µL Streptavidin-HRP1 was added per well, incubated for 30 min and washed as described above. Then 100 µL Substrate Solution was added and

incubated for 30 min as described above, but protected from light. Finally, 100 µL Stop Solution was added per well and thorough mixing ensured by gently tapping the plate. Absorbance was acquired at 450 nm and 590 nm using the CLARIOstar Plus. The analysis of the result was performed using the Microplate Data Analysis Software as follows: The raw data of the blank was subtracted from the raw data of the wells within the respective absorbance wavelength (450 nm and 590 nm). Then the blank corrected absorbance at 590 nm (optical density) was subtracted from the blank corrected absorbance at 450 nm. A four-parameter logistic regression model of the corrected standards was used to fit a standard curve, which was then used to calculate the concentrations of the samples based on their corrected absorbance.

2.3.21. Mass spectrometry

Liquid-tomography coupled mass spectrometry analysis was performed to identify potential binding proteins of the *Lep* enhancer sites RS1, RS2 and RS3. The Pierce MS-compatible Magnetic IP Kit was used. Oligonucleotides containing a 5'biotin tag (Table A.12) were dimerized as described in section 2.3.15. RS2 and RS3 oligonucleotides and methylated or unmethylated RS1 oligonucleotides (methylation performed as described in section 2.3.18) were incubated with either 200 µg protein extract from eWAT of mice on 12 week HFD or 100 µg nuclear protein extract from 3T3-L1 adipocytes, differentiated for 13 days (section 2.3.8), in IP-MS cell lysis buffer (V_{final} =500 µL overnight at 4 °C). Immunoprecipitation and cleaning of the oligonucleotide-bound proteins were performed after manufacturer's instructions. Liquid chromatography coupled mass spectrometry and primary analysis were performed by Julia Horn and Thorben Sauer in collaboration with Prof. Timo Gemoll: Immunoprecipitated oligonucleotide-protein complexes were lyophilized and redissolved in 0.1 % formic acid in water. The reconstituted complexes were loaded onto C18 EvoTip disposable trap columns. The EvoSep One system with a C18 Performance column (EV1137, 15 cmx150 µm, 1.5 µm) and an extended 15 SPD method (88 min gradient, 220 nL/min) was used to chromatographically separate the complexes. The system was coupled to the hybrid TIMS quadrupole TOF mass spectrometer with a nano-electrospray ion source. The mass spectrometer was run in diaPASEF mode with the settings for scan range, ion mobility, and mass accuracy specified in Table A.15.

2.4. Statistics, visualization and multi-omics analysis

2.4.1. Basic statistics

Data were analyzed and visualized using R Studio or GraphPad PRISM. Differences between two groups were analyzed using a two-tailed Student's t-test. Differences between more than two groups were analyzed using a one-way analysis of variance (ANOVA) and differences in multiple groups over time were analyzed using a two-way ANOVA, in case of the measurement of samples from the same mice over time, two-way repeated measures ANOVA, or, in case mice or values were missing, mixed-effects analysis with post hoc analysis after Holm-Sidak. P-values

< 0.05 were considered significant if not stated otherwise. CpG sites of each *Lep* enhancer site were independently tested. The results of the tests are given in the graphs and in detail in section A.3. DNA methylation data were analyzed for each CpG independently. Data are presented, if not otherwise stated, as mean ± standard deviation of the mean (SD) or as boxplots with min and max indicated. Malperforming samples due to technical difficulties were identified after quality checks in pyrosequencing (low peak height) or in qPCR (high deviation in the replicates) and omitted, if no replication was possible, from the analysis as individual values. Complete subject outliers were identified by outlier testing after "Robust regression followed by Outlier removal" (ROUT) in GraphPad PRISM and omitted from analysis if they were outliers in most or all of the measured parameters. For statistical analysis of gene expression, the ΔCt=($Ct_{\text{target gene}}-Ct_{\text{housekeeper}}$) values were used. Pearson correlation was performed using R Studio and visualized using the corrplot package (v.2023.12.1, [222]) or using GraphPad PRISM. An additional simple linear regression was performed for visual presentation.

2.4.2. Illustrations

The mouse and human *Lep* enhancer sequences were aligned using the msa R package [223] and subsequently illustrated using LaTeX. The schematics and illustrations were created using *BioRender.com*.

2.4.3. Mass spectrometry analysis

Mass spectrometry data, acquired as described in section 2.3.21, were processed using the DIA-NN software [224] with parameters specified in Table A.16. I analyzed the generated protein group list in R Studio: Data were filtered for transcription factors (Riken Mouse transcription factor database, *http://gerg.gsc.riken.jp/TFdb/*, accessed: 12/12/2023). The data for RS2 and RS3 were scanned for their known transcription factors, which were introduced in section 1.1.3 and summarized in Table A.25). Unmethylated and methylated data for RS1 were analyzed for differential abundance of proteins with log2 transformed data using the limma package [225]. Data from mouse adipose tissue proteins and 3T3-L1 proteins were analyzed separately.

2.4.4. RNA-sequencing analysis

RNA sequencing was performed on the extracted RNA from 3T3-L1 under stretching conditions in the mechanobiological experiments described in section 2.3.5. Biological triplicates of each condition were used. The mapping using spliced transcript alignment to a reference (STAR) (version 2.7.11b) [226], trimming adaptor sequences and poly-A tails (cutadapt v3.4), quality assessment (fastQC v0.11.9), gene calling and counting of reads mapping to genomic features using featureCounts for Ubuntu and principal component analysis (PCA) were performed by Dr. Christin Krause. I performed further analysis on the count tables using R Studio. Genes with counts < 30 were excluded from further analysis. The threshold was chosen based on the presence of liver-specific genes that were no longer apparent with the set threshold. The count

table was cleaned from RIKEN genes, which are genes without a proper gene name or known function. For differential expression analysis, I used the limma package relying on general linear modeling. The resulting gene list was further analyzed with a Kyoto Encyclopedia of Genes and Genomes (KEGG) pathway analysis using the pathfindR package (v2.3.0, [227]) to analyze differentially expressed genes enriched in certain pathways using the false discovery rate (FDR) after Benjamini-Hochberg. A FDR< 0.05 was considered significant.

3. Results

In this doctoral thesis, I studied the impact of two epigenetic modifications, namely the DNA methylation in enhancer sites of the *Lep* as well as the long non-coding RNA *lncOb*, on quantitative *Lep* expression within adipocytes and their contribution to uncontrolled expression of *Lep* in obesity. To this end, DNA methylation in the *Lep* enhancer sites was investigated in white adipose tissue with respect to *Lep* expression, tissue specificity, adipocyte size, and reversibility.

Lep enhancer sites with CpG sites as loci, where DNA methylation can potentially occur, were identified through literature research. I focused on sites that were already described to be associated with *Lep* expression. These *Lep* regulatory enhancer sites (RS) are illustrated in Figure 3.1 and a tabular overview of the described transcription factors, the associated studies, and the precise locations of the measured CpGs is given in Table A.25. Two to three CpGs were investigated in each enhancer site, within or near the binding site of transcription factors, if they were known.

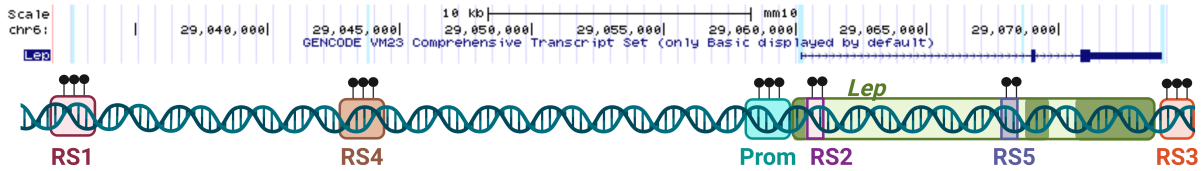

Figure 3.1.: Illustration of *Lep* enhancer sites, where DNA methylation was measured within the scope of this study, in the context of the mouse genome mm10, chromosome 6 (UCSC). RS–*Lep* regulatory enhancer site; Prom–*Lep* promoter region. The figure is part of the submitted manuscript.

First, DNA methylation in these *Lep* enhancer sites was investigated in a mouse model of diet-induced obesity (DIO), where an increase of DNA methylation in the three sites RS1, RS2, and RS3 specific to the adipocytes of epididymal adipose tissue (eWAT) was observed. The specific methylation pattern was also observed in human visceral adipose tissue (VAT). CpG sites in RS4 and RS5 were differentially methylated in inguinal adipose tissue (iWAT), although the differences in DNA methylation were not as pronounced as for eWAT RS. Further research aimed to identify the reason for the change in *Lep* enhancer DNA methylation in eWAT and revealed large hypertrophic adipocytes in obesity as the driver of the higher and apparently reprogrammed DNA methylation pattern in *Lep* enhancers. The impact of *Lep* enhancer sites DNA methylation on gene expression was then functionally studied. Final investigations of *Lep* enhancer DNA methylation sites in eWAT aimed at the dynamics and reversibility of the observed *Lep* enhancer DNA methylation pattern in dietary, pharmacological and surgical weight loss interventions.

Furthermore, an additional epigenetic regulator, the long non-coding RNA *lncOb*, and its effects on *Lep* expression were analyzed in the context of progression and reversibility of obesity. If not stated otherwise, the data are presented as mean ± SD. Some data have already been published or are part of the submitted manuscript in the Journal of Advanced Research, Elsevier, as indicated in the text or figure legends.

3.1. DNA methylation in *Lep* enhancer sites in obesity development and progression

A common model to study obesity and obesity progression is the DIO mouse model, where mice gain weight through feeding, like the here used high-fat diet (HFD) with 60 kcal% fat. These mice become insulin resistant, have high blood glucose levels, and are obese [185]. I used white adipose tissue from male DIO mice to investigate changes of DNA methylation in previously identified *Lep* enhancer sites (Figure 3.1) over the 12 week course of obesity development. An illustration of the study is given in Figure 2.1.

3.1.1. DNA methylation in epididymal adipose tissue of diet-induced obese mice

First, I investigated the DNA methylation in *Lep* enhancer sites in eWAT of DIO mice, as the expansion of eWAT is associated with metabolic unhealthy obesity [50, 51, 228]. In three of the studied *Lep* enhancer sites (RS1, RS2, RS3), DNA methylation increased significantly by up to 20 % during the 12-week progression of obesity compared to age-matched, chow-fed control mice (Figure 3.2a–c), while DNA methylation in RS4 and RS5 did not change after 12 weeks (Figure 3.2d, e). Body weight, fat mass, and circulating leptin levels increased concomitantly (Figure 3.3a–c). *Lep* expression initially increased by 3.15 fold±0.91 with the start of HFD feeding, followed by a slower increase to 2.26 fold±1.18 in week 8 of obesity progression and a final drop to 1.63 fold±0.94 in week 12 (Figure 3.3d).

Along with the initial peak in *Lep* expression, RS1 DNA methylation increased by 5.2 %±3.4 compared to chow in week one, indicating RS1 as an early responder site (Figure 3.2a). Subsequently, DNA methylation gradually increased and reached a 20.6 %±2.5 difference in methylation in week 12. RS2 DNA methylation increased in the fourth week and reached a final difference of 21.7 %±3.9 (Figure 3.2b). From week 7 on, RS3 DNA methylation responded to HFD, with a final methylation difference of 18.5 %±5.0 in week 12 (Figure 3.2c). RS4 DNA methylation was unaltered with the development of obesity (Figure 3.2d). RS5 DNA methylation decreased significantly in weeks 6–8 in CpG1 by a maximum of 13.2 %±3.5 in week 7 caused by a minimal increase in DNA methylation in chow (Figure 3.2e). However, the difference in DNA methylation in RS5 was no longer present in week 12.

DNA methylation in *Lep* enhancer sites correlated mainly positively with *Lep* expression and body weight (Figure 3.4a), supporting the hypothesis that DNA methylation is coupled to *Lep* expression, especially in the early weeks of obesity development in DIO. The correlation plot further illustrates the described differences in responsiveness and timing of the different

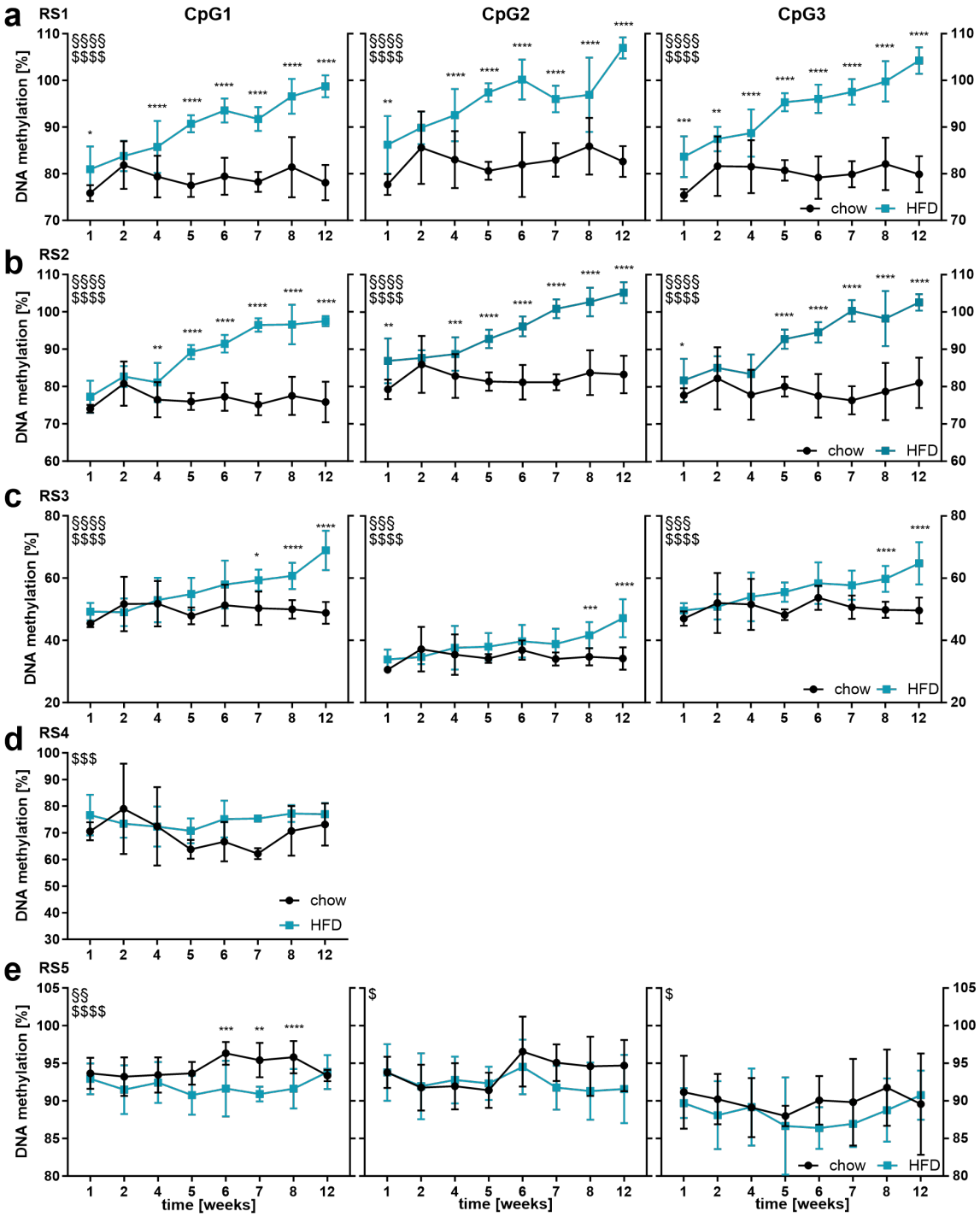

Figure 3.2.: Differential DNA methylation in *Lep* enhancer sites in eWAT of DIO (HFD-fed) mice. Two to three CpG sites were measured per site. Statistical analysis was performed using a two-way ANOVA with post hoc analysis after Holm-Sidak; §§ $p_{interaction} < 0.01$, §§§ $p_{interaction} < 0.001$, §§§§ $p_{interaction} < 0.0001$; \$ $p_{group} < 0.05$, \$\$\$ $p_{group} < 0.001$, \$\$\$\$ $p_{group} < 0.0001$; *$p < 0.05$, **$p < 0.01$, ****$p < 0.0001$; $n = 8$–16/week/group; details of the ANOVA are given in Table A.26. Data are part of the submitted manuscript.

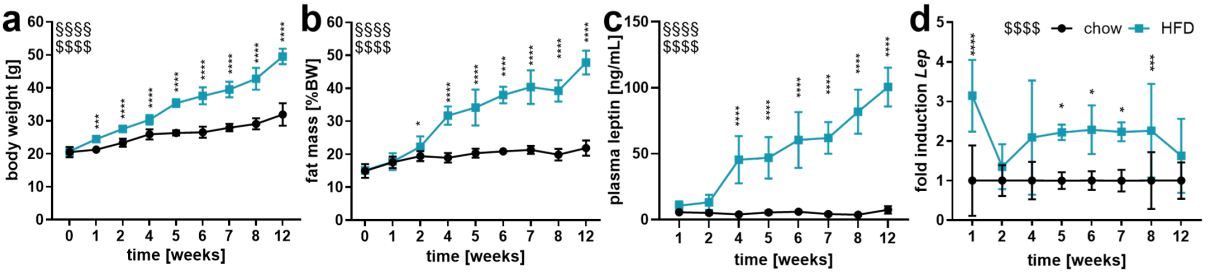

Figure 3.3.: Body weight (a), fat mass (b), circulating leptin levels (c) and eWAT *Lep* expression (d) during obesity progression of DIO (HFD) and chow control mice. Body composition and circulating leptin level measurements were obtained from weight-, feeding- and age-matched mice from the metformin treatment cohort (section 3.4.2) that were treated and housed identically to DIO mice. Data were analyzed using a two-way ANOVA with post hoc analysis after Holm-Sidak and significance shown as §§§§ $p_{interaction} < 0.0001$ and $$$$ $p_{group} < 0.0001$; $^{*}p < 0.05$, $^{**}p < 0.01$, $^{****}p < 0.0001$; weight, *Lep* expression: n = 8–16/week/group; body composition, circulating leptin: n = 4–20/week/group; details of the ANOVA are given in Table A.27. *Lep* expression was normalized to adjacent chow within the week. Body weight data are published in [185] and graphs are part of the submitted manuscript.

Lep enhancer sites in response to the HFD. DNA methylation in the early responder RS1, the intermediate responder RS2 and the late responder RS3 in eWAT were positively correlated with *Lep* expression until weeks 7/8 and with body weight until week 12. Interestingly, in week 12, the *Lep* expression of eWAT was mainly uncoupled from DNA methylation, as well as from body weight (Figure 3.4b). In contrast, RS4 DNA methylation was not continuously correlated with *Lep* expression (only at weeks 2, 5, 7, and 12) and correlated with body weight only at weeks 5–8. RS5 DNA methylation negatively correlated with *Lep* expression at weeks 6 and 7 and with body weight at weeks 6–8, indicating that DNA methylation in RS4 and RS5 was not as involved with *Lep* expression in eWAT as RS1, RS2 and RS3 (Figure 3.4a).

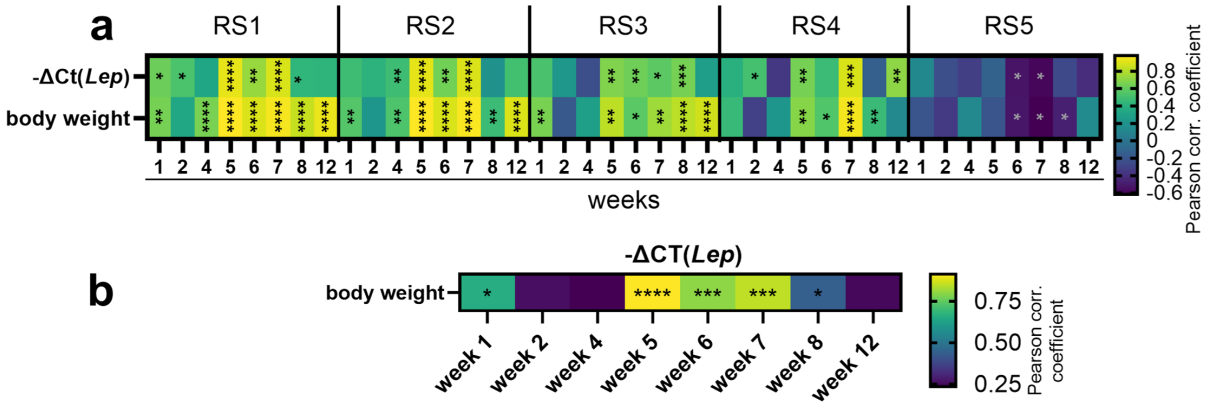

Figure 3.4.: *Lep* enhancer site (RS) DNA methylation in eWAT correlates positively with *Lep* expression and body weight in a time-dependent manner during obesity induction (a). *Lep* expression and body weight stop correlating with obesity progression (b). Pearson correlation analysis was performed with the mean DNA methylation of the 2–3 CpG sites per *Lep* enhancer site per week. For the calculation, the $-\Delta$Ct(*Lep*−*Hprt*) values were taken, representing the *Lep* expression. Significance is shown as $^{*}p < 0.05$, $^{**}p < 0.01$, $^{***}p < 0.001$, $^{****}p < 0.0001$; $n = \frac{15-32}{week}$. Details of the analysis are given in Table A.28 and Table A.29

Adipose tissue consists not only of adipocytes but also of adipose progenitors and immune cells such as macrophages. As eWAT inflammation accompanies obesity, I analyzed the expres-

sion of macrophage-specific genes. In the DIO cohort, the immune cell marker Arginase 1 gene *Arg1* for adipose tissue resident macrophages was not increased, while the immune cell marker for recruited macrophages in adipose tissue Integrin Subunit Alpha X gene *CD11c (Itgax)* [229, 230] increased slightly in week 1 of HFD and then in the progression of obesity from week 8 on (Figure 3.5).

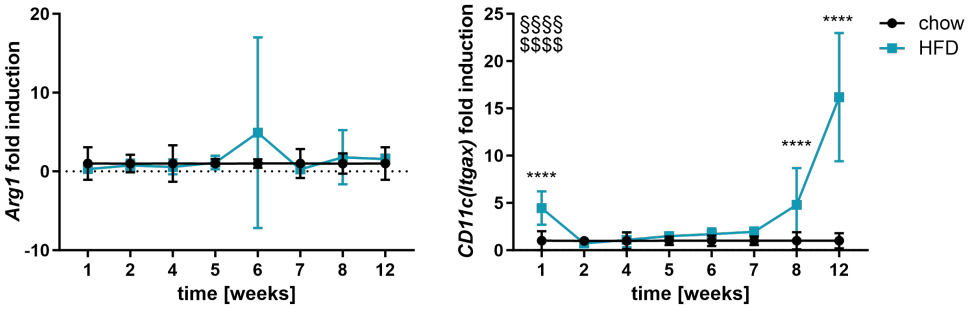

Figure 3.5.: Inflammatory markers during the progression of obesity show an increase in infiltrating macrophages from week 8 of HFD-feeding in eWAT from the DIO mouse model. Data were normalized to adjacent chow within the week. Data were analyzed using a two-way ANOVA with post hoc analysis after Holm-Sidak; §§§§ $p_{interaction} < 0.0001$ and $$$$ $p_{group} < 0.0001$; ****$p < 0.0001$; $n = \frac{7-16}{week}$; details of ANOVA statistics in Table A.30

To verify that the observed change in *Lep* DNA methylation originated from adipocytes and not from infiltrating macrophages or other cell types, DNA methylation in *Lep* enhancer sites RS1, RS2 and RS3—as they showed a specific DNA methylation pattern associated with *Lep* expression in contrast to RS4 and RS5—was measured in isolated adipocytes of mice on HFD for 10–11 weeks and age-matched chow controls. RS1, RS2, and RS3 DNA methylation was higher in isolated adipocytes from DIO mice compared to chow (Figure 3.6a–c), as seen in bulk adipose tissue. Therefore, the difference in DNA methylation observed in eWAT came from adipocytes. To address the importance of DNA methylation for *Lep* expression and to test whether high enhancer methylation is more associated with *Lep* repression or activation, DNA methylation in the *Lep* enhancer sites was measured in the liver, which does not express *Lep*. DNA methylation was not different between DIO mice and chow, and high in RS1 and RS2 (Figure 3.6d–f). These findings support that differential DNA methylation in *Lep* enhancer sites in eWAT is important for *Lep* expression and indicate a repressive effect of DNA methylation, at least for RS1 and RS2.

Furthermore, the increase in DNA methylation is in line with the observations in enzymes involved in the *de novo* methylation process (compare Figure 1.7): *Dnmt3a* expression was elevated in eWAT even after 12 weeks of HFD-feeding, while *Dnmt3b*, *Tet2* and *Tet3* expression did not change between chow and HFD (Figure 3.7). This indicates more *de novo* methylation, and is in accordance with the observed higher DNA methylation in the *Lep* enhancer sites.

3.1.2. *LEP* enhancer DNA methylation in human visceral adipose tissue

To translate the observations of differential DNA methylation in *Lep* enhancers and the association with *Lep* expression from mouse to human, the RS1, RS2, and RS3 sites were aligned

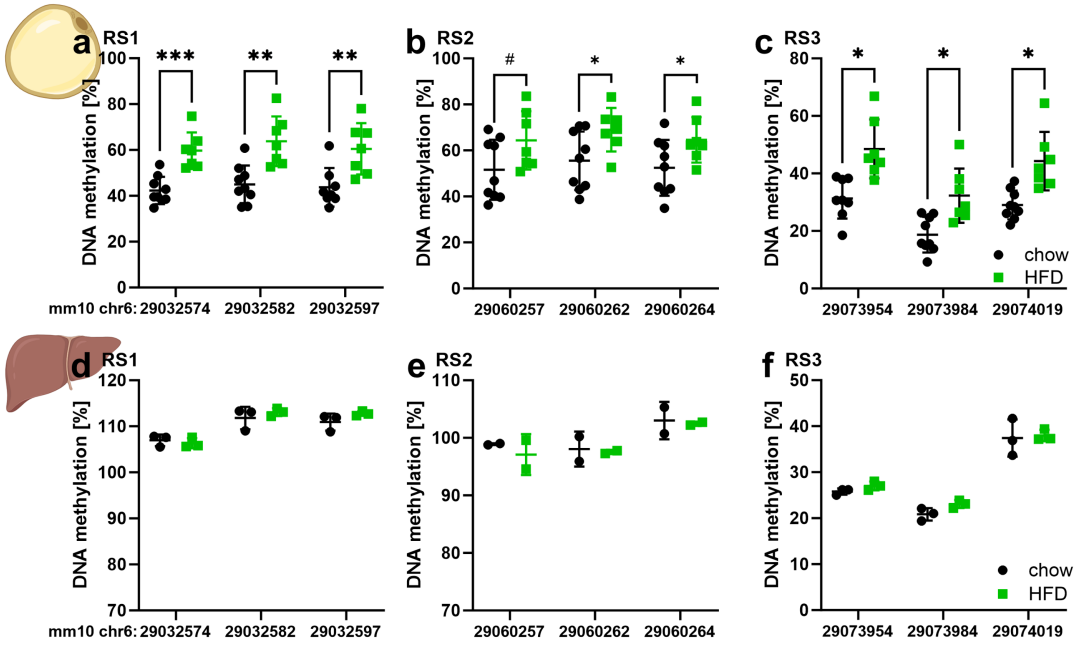

Figure 3.6.: *Lep* enhancer DNA methylation is specific to adipocytes. a–c) *Lep* enhancer DNA methylation was measured in isolated adipocytes of eWAT from mice on HFD for 10–11 weeks and age-matched chow-fed controls. d–f) DNA methylation in RS1, RS2 and RS3 were measured in liver samples of DIO mice (week 12) and age-matched chow-fed controls. Liver DNA was extracted and bisulfite converted by Cathleen Geißler. Data were analyzed using a two-tailed Student's t-test per CpG site; $^*p < 0.05$, $^{**}p < 0.01$, $^{***}p < 0.001$. Graphs a–c are part of the submitted manuscript.

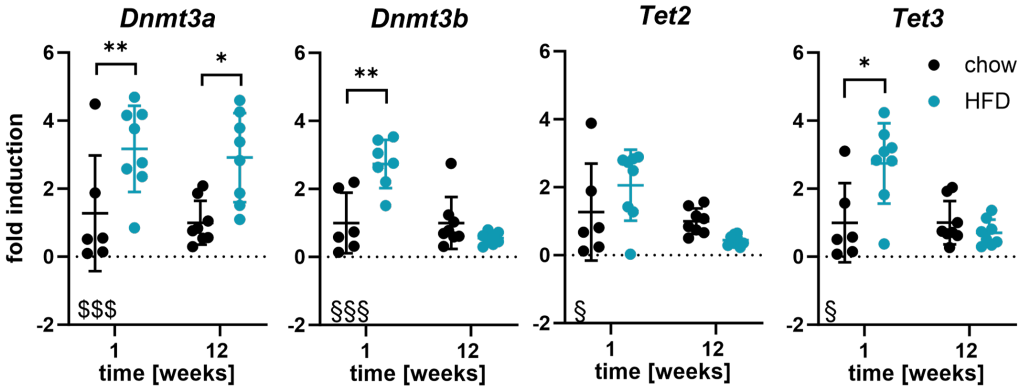

Figure 3.7.: DIO mice show *de novo* methylation signature in eWAT. Expression of enzymes involved in (de)methylation of the DIO study week 1 and week 12 are shown. Fold induction was calculated to adjacent chow control group within each week. Data were analyzed using a two-way ANOVA with post hoc analysis after Holm-Sidak; § $p_{interaction} < 0.05$, §§§ $p_{interaction} < 0.001$, \$\$\$ $p_{group} < 0.001$; $^*p < 0.05$, $^{**}p < 0.01$; details of the ANOVA are given in Table A.30.

to the human genome. RS1 was 75 %, RS2 was 84 % and RS3 was 89 % similar between mouse and human. An illustration of the alignments and the genomic contexts is given in Figure A.3. I compared *LEP* expression and *LEP* enhancer DNA methylation in VAT of obese and isolated VAT adipocytes of non-obese individuals (Figure 3.8a). Despite the small cohort of non-obese subjects, a higher DNA methylation was observed in obesity compared to non-obesity (control), while *LEP* expression was not different between the two groups (Figure 3.8b–e). Furthermore, *LEP* expression and BMI positively correlated with *Lep* enhancer DNA methylation (expression: RS1 CpG1: $r = 0.14$, $p = 0.19$; CpG2: $r = 0.12$, $p = 0.25$, BMI: RS1 CpG2: $r = 0.18$, $p = 0.10$; RS2 CpG2: $r = 0.21$, $p = 0.05$, Figure 3.8f).

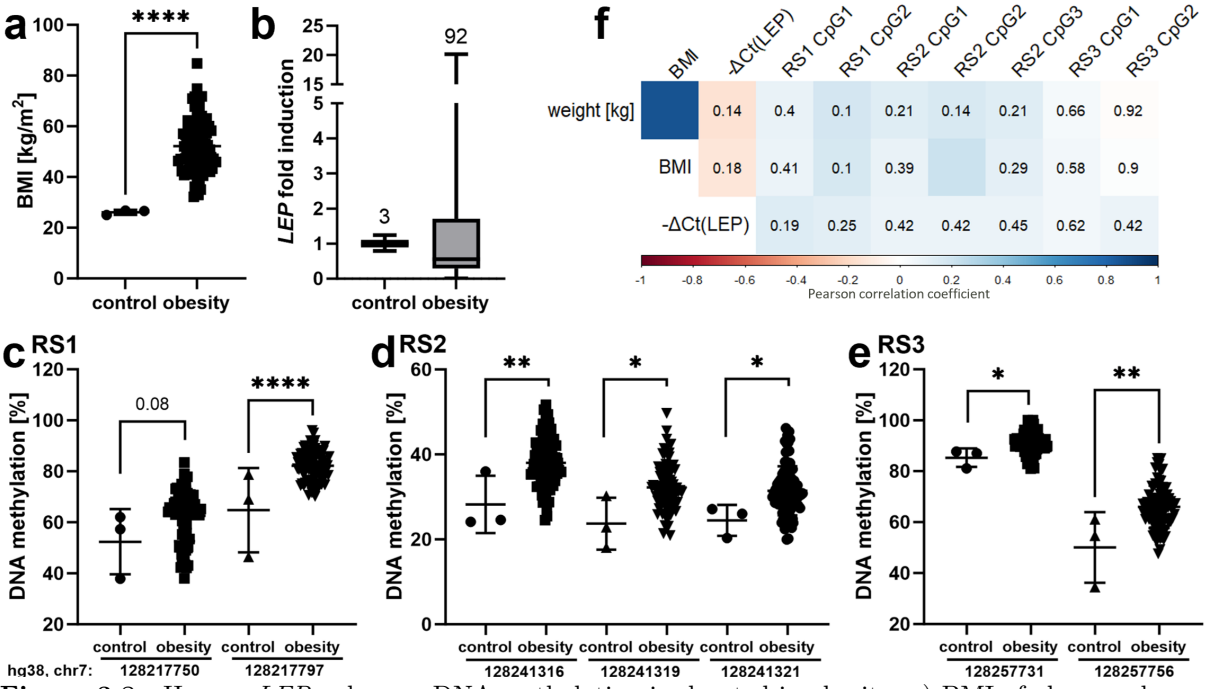

Figure 3.8.: Human *LEP* enhancer DNA methylation is elevated in obesity. a) BMI of obese and non-obese subjects at time of tissue collection. b) *LEP* expression, DNA methylation in *LEP* enhancer sites RS1 (c), RS2 (d) and RS3 (e) translated to human. f) Pearson correlation matrix of DNA methylation, BMI and weight. P-values$\geqslant$0.05 are shown and color indicates the Pearson correlation coefficient (detailed analysis in Table A.32 and Table A.31). Data were analyzed per CpG using a two-tailed Student's t-test; $^{*}p < 0.05$, $^{**}p < 0.01$, $^{****}p < 0.0001$. The figure is part of the submitted manuscript.

3.1.3. DNA methylation in inguinal adipose tissue of diet-induced obese mice

The other major WAT depot in mice is inguinal adipose tissue (iWAT), which corresponds to human subcutaneous adipose tissue and is associated with metabolic homeostasis [231, 232]. Unlike in eWAT, *Lep* expression increased by 12.8 fold±4.8 at week 12 in iWAT compared to control, while *Lep* enhancer DNA methylation in RS1, RS2, and RS3 of iWAT from DIO mice did not change with obesity induction (Figure 3.9a–d). Moreover, the correlation of individual weeks did not indicate any association of methylation and expression, marking RS1–RS3 as specifically methylated *Lep* enhancer sites of the eWAT (Figure 3.9e). However, DNA methylation in RS4 increased by 6.2 %±1.3 in HFD compared to chow after 12 weeks, while the DNA methylation

in intragenic RS5 decreased at CpG1 by 4.1 %±1.7 in iWAT (Figure 3.9f, g), which is supported by the correlation of DNA methylation with *Lep* expression and body weight (Figure 3.9e). In contrast to eWAT, iWAT *Lep* expression correlated strongly and positively with body weight from week 1 of the switch to HFD onward (compare Figure 3.9h and Figure 3.4b). This indicates that an additional factor to the relatively mild changes in DNA methylation in RS4 and RS5 could be driving iWAT *Lep* expression.

Taken together, hypermethylation by 20 % was observed in RS1, RS2, and RS3 during different time points of the progression of obesity, specifically in eWAT. The increase in DNA methylation was also observed in human VAT. The DNA methylation correlated with *Lep* expression until the eighth week of DIO. The RS4 and RS5 showed an iWAT-specific change in DNA methylation. As the observed changes in DNA methylation were tremendously higher in eWAT samples and eWAT is the white adipose tissue associated with metabolic malfunction in the progression of obesity [50, 231, 232], further experiments focused on the eWAT and therefore RS1, RS2, and RS3.

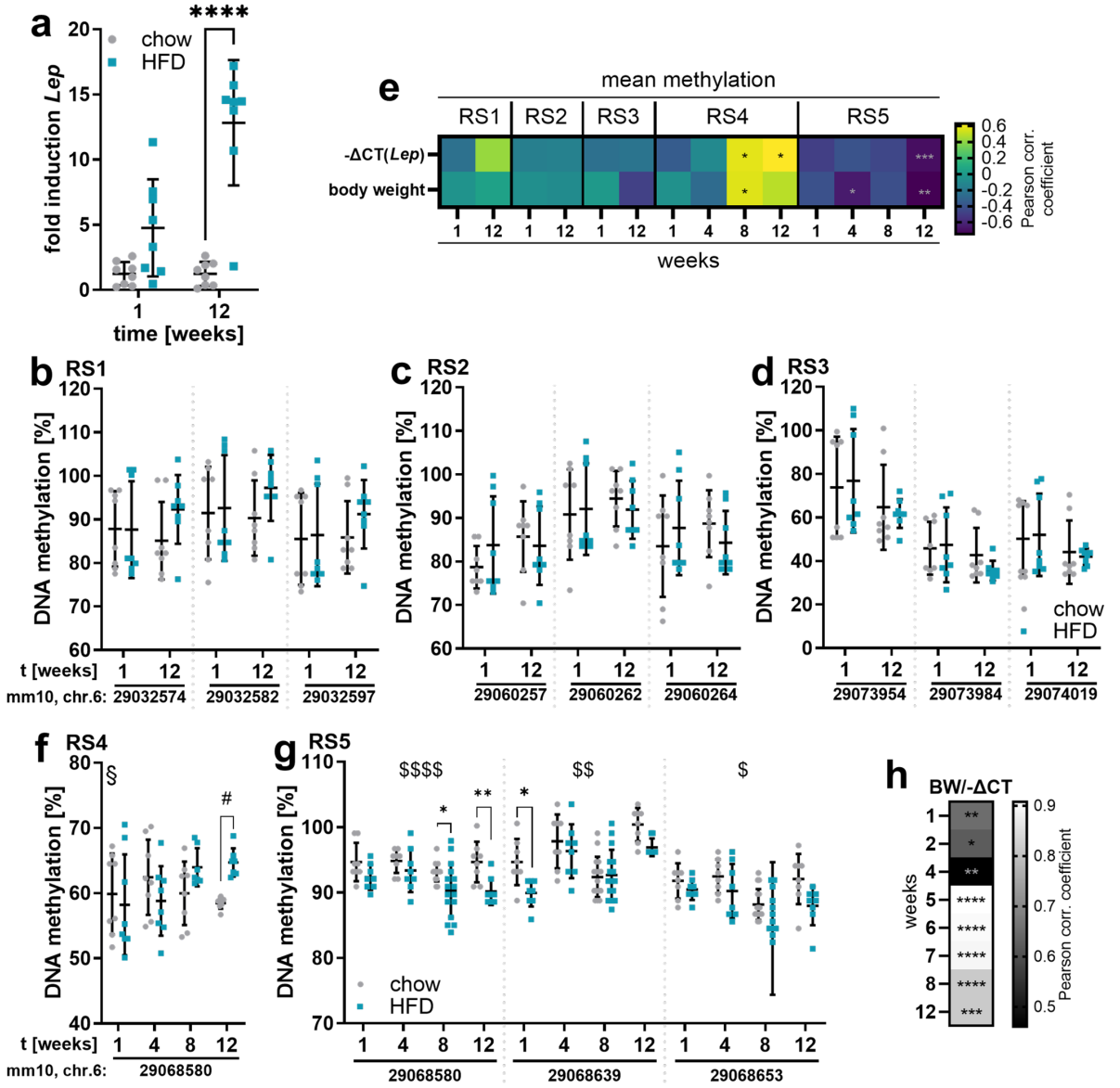

Figure 3.9.: *Lep* enhancer DNA methylation in inguinal white adipose tissue (iWAT) of DIO mice is different to eWAT and shows tissue-specific signatures. a) *Lep* expression normalized to age-matched chow group, b–d) DNA methylation in RS1, RS2, and RS3. e) Pearson correlation plot of *Lep* expression and body weight with the mean DNA methylation in *Lep* enhancer sites per week of the DIO mouse model. f, g) DNA methylation in iWAT-responsive sites RS4 and RS5. Data (a–d, f, g) were analyzed using a two-way ANOVA with post hoc analysis after Holm-Sidak; § $p_{interaction} < 0.05$, \$ $p_{group} < 0.05$, \$\$ $p_{group} < 0.01$, \$\$\$\$ $p_{group} < 0.0001$; #$p < 0.1$, *$p < 0.05$, **$p < 0.01$, ****$p < 0.0001$, details of ANOVA statistics in Table A.33. For the correlation calculation, the $-\Delta\mathrm{Ct}(Lep{-}Rplp0)$ values were taken, representing the *Lep* expression. Pearson correlation analysis was performed with the mean DNA methylation, where $\geqslant 1$ CpG per *Lep* enhancer site. Significance is shown as *$p < 0.05$, **$p < 0.01$, ***$p < 0.001$, ****$p < 0.0001$, details in Table A.35 and Table A.34. Data (a–d, f, g) are part of the submitted manuscript.

3.2. Identification of stimulators of *Lep* enhancer DNA methylation change in eWAT

In the preceding section, the differential DNA methylation in *Lep* enhancer sites correlating with *Lep* expression throughout the progression of obesity and its fat depot-specificity was elucidated. In this section, the underlying factors contributing to the tremendous alterations in DNA methylation in eWAT are addressed.

3.2.1. Central leptin feedback-signaling

To dissect if DNA methylation in obesity is mediated by central leptin feedback signaling, DNA methylation and *Lep* expression were quantified in eWAT of ob/ob mice. As introduced in section 1.1.4, ob/ob mice produce *Lep* mRNA, but no functional leptin protein rendering leptin feedback-signaling non-functional. *Lep* expression in ob/ob mice was higher than in DIO mice, and RS1, RS2, and RS3 DNA methylation was similar to DIO and elevated compared to chow control mice Figure 3.10. Consequently, induction of DNA methylation in *Lep* enhancer sites with increasing fat mass does not require feedback from leptin signaling. Therefore, the stimulus for the DNA methylation change might rather come from within the adipose tissue and the direct surrounding of the adipocytes. In the following, first, mechanobiological cues such as cellular deformation and nuclear stretch, and second, adipocyte cell size were investigated in regard to their effects on *Lep* enhancer DNA methylation and *Lep* expression.

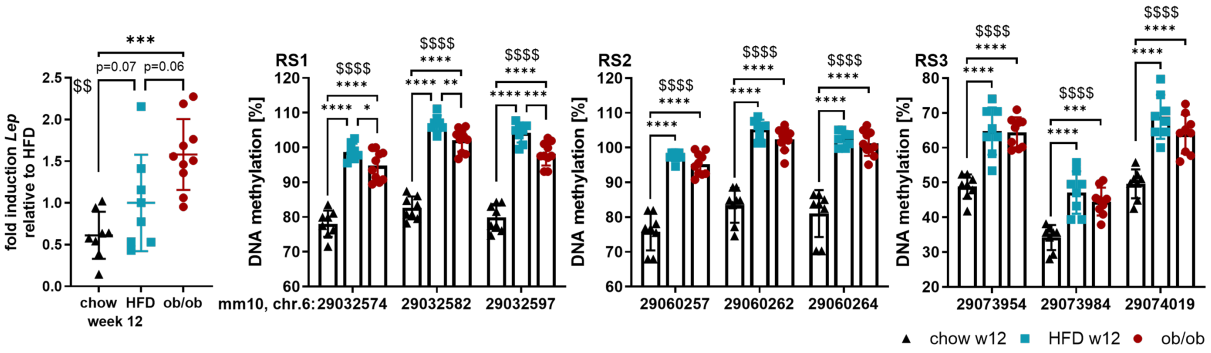

Figure 3.10.: Genetically obese ob/ob mice show a similar *Lep* enhancer DNA methylation signature as chronic obese mice. Data of ob/ob mice is compared to chronically obese mice of week 12 DIO mice and their chow controls. Data were analyzed using a one-way ANOVA with post hoc analysis after Holm-Sidak; \$\$\$\$ $p_{group} < 0.0001$; *$p < 0.05$, **$p < 0.01$, ***$p < 0.001$, ****$p < 0.0001$; details of ANOVA statistics in Table A.36. Data are part of the submitted manuscript.

3.2.2. Mechanobiological cues: cellular deformation and nuclear stretch

In the progression of obesity, adipocytes accumulate more lipids, leading to stiffening of the cell and the surrounding matrix [56]. Stiffness as a mechanobiological alteration can trigger gene expression changes through nuclear deformation [55]. I hypothesized that the nuclear deformation occurring in hypertrophic adipocytes caused by the accumulation of lipids in obesity can trigger the observed change in DNA methylation. To modulate cellular deformation and extracellular

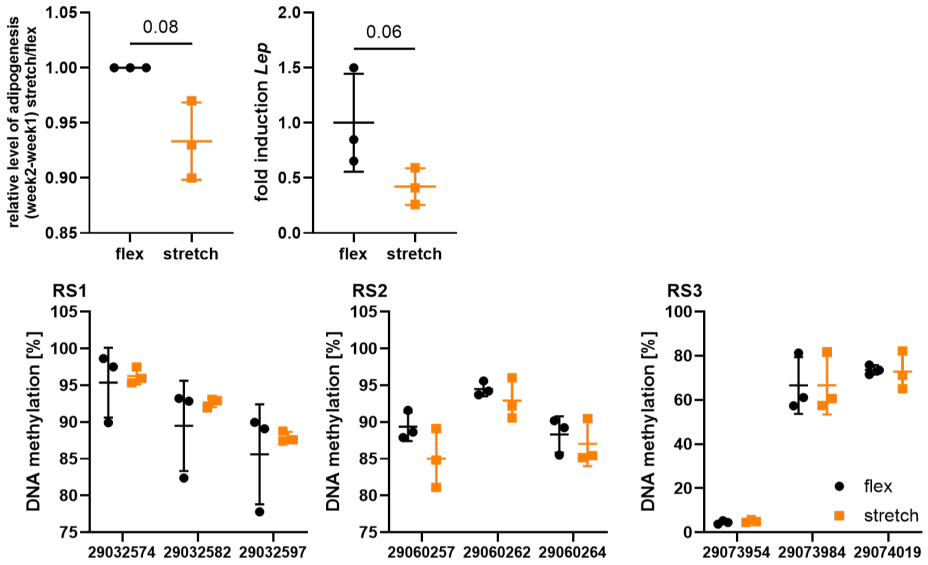

Figure 3.11.: Stretch during 3T3-L1 differentiation to adipocytes does not alter adipogenesis, *Lep* expression or DNA methylation in *Lep* enhancer sites. The level of adipogenesis was determined from stitched microscopic images using ImageJ. Data were analyzed using a two-tailed Student's t-test. P-values < 0.1 are shown.

stiffness mimicking the obese state, a static tensile strain was applied to differentiating and mature 3T3-L1 adipocytes. An illustration of the experimental setup can be found in Figure 2.5. I performed the experiment in collaboration with Nadav Kislev and Prof. Dafna Benayahu at Tel Aviv University, Israel.

3T3-L1 cells were cultured in flexible bottom cell culture plates that were clamped on the stretching apparatus, expanding the flexible bottom and creating tensile strain and a rigid growing surface. The strain ("stretch") applied during the 14 days of differentiation led to a non-significant decrease in adipogenesis ($p = 0.08$) and *Lep* expression ($p = 0.06$), and no changes in DNA methylation compared to the control group without strain ("flex") (Figure 3.11).

However, PCA of RNA-sequencing data indicated a general difference between stretch and flex (Figure 3.12a) with differential gene expression analysis revealing 358 genes that were significantly downregulated ($log2FoldChange < -0.6$, $q < 0.05$, Table A.37) and 453 genes that were significantly upregulated ($log2FoldChange > 0.6$, $q < 0.05$; Table A.38) of a total of 9098 genes (Figure 3.12b). Pathway analysis of differentially regulated genes revealed enrichment in several pathways, including alcoholic liver disease, focal adhesion, inflammation, and regulation of lipolysis in adipocytes (Figure 3.12c). Further examination of these pathways showed that genes associated with alcoholic liver disease in adipocytes, as well as genes associated with lipolysis, were predominantly downregulated in 3T3 cells stretched during differentiation, while genes involved in focal adhesion were upregulated (Figure 3.12d).

A 2-day stretch of 3T3-L1 adipocytes did not alter the level of adipogenesis or DNA methylation in RS1, RS2, and RS3, and non-significantly increased *Lep* expression ($p = 0.067$), which could be explained by the brevity of the stretch (Figure 3.13). PCA of RNA-sequencing data also confirmed that there were no differences between stretch and flex (Figure 3.13). Therefore,

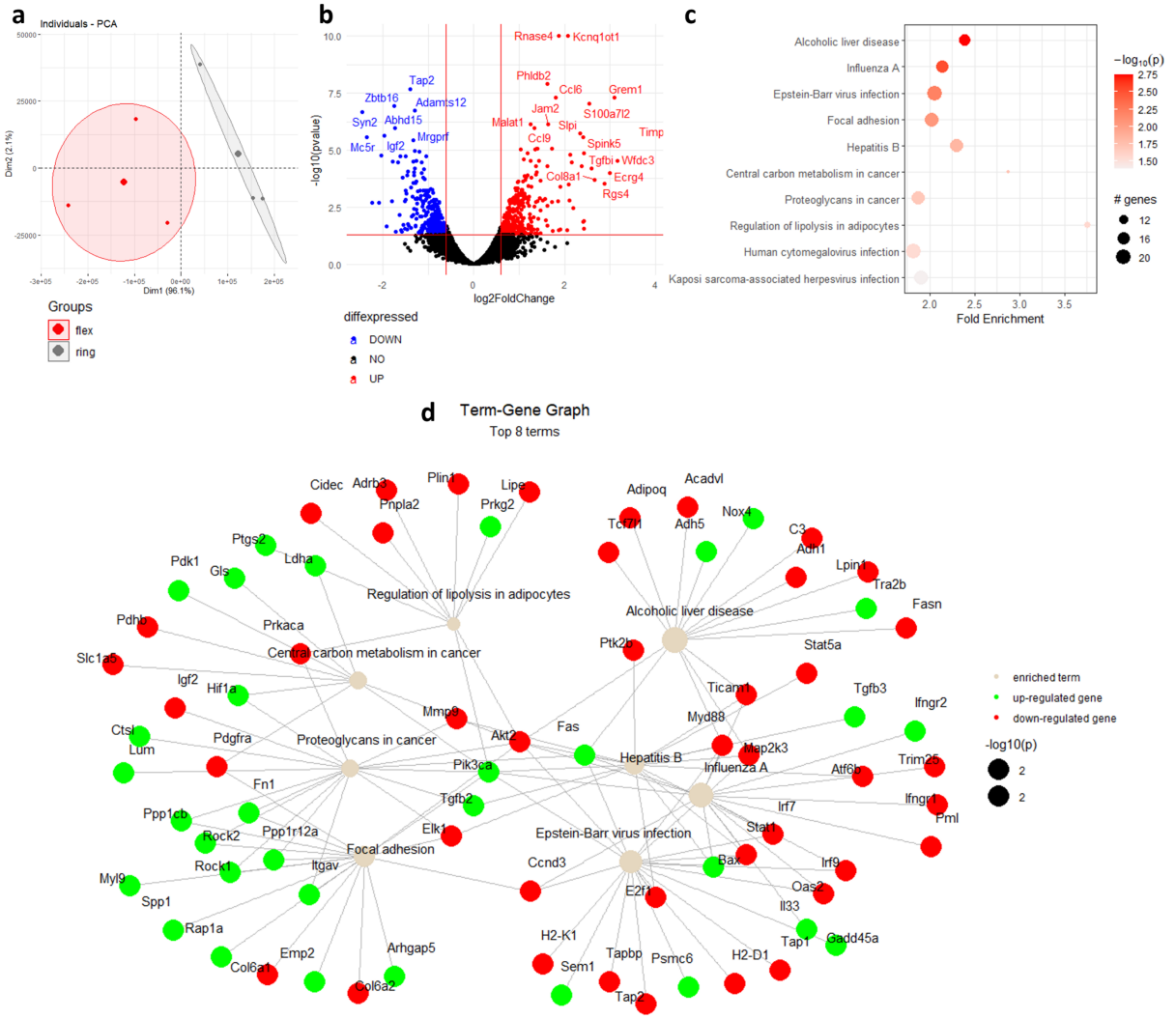

Figure 3.12.: RNA-sequencing results of 3T3-L1 cells stretched during differentiation. a) Principal component analysis (PCA) of RNA-sequencing count data. b) Differential expression of genes of flex (control) vs stretch. c) Top 10 enriched pathways after KEGG-pathway analysis. d) Individual display of genes of the enriched pathways.

no additional analysis was performed.

Overall, *Lep* expression and DNA methylation were not altered with a stretch of differentiating adipocytes or with a 2-day stretch of mature adipocytes. However, stretch during adipocyte differentiation appears to alter important pathways such as lipolysis or focal adhesion.

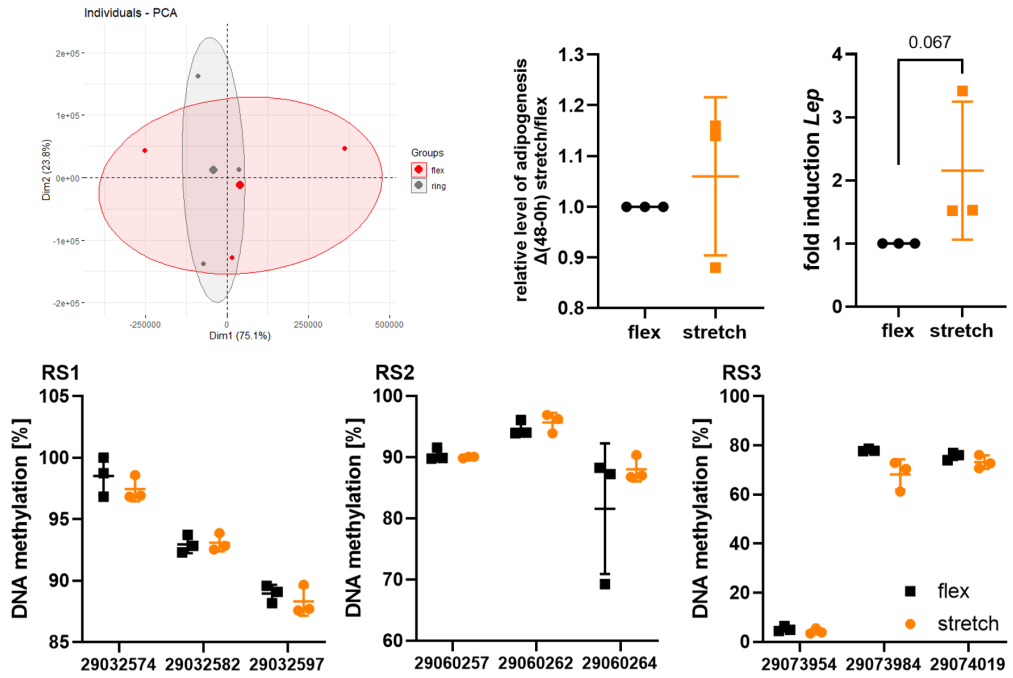

Figure 3.13.: Stretch of 3T3-L1 adipocytes for two days does not alter adipogenesis, as seen in the principal component analysis (PCA) of the RNA-sequencing data, *Lep* expression or DNA methylation in *Lep* enhancer sites. The level of adipogenesis was determined from stitched microscopic images using ImageJ. Data were analyzed using a two-tailed Student's t-test.

3.2.3. Adipocyte size

Another intracellular trigger for *Lep* enhancer DNA methylation change could be the size of adipocytes per se. Hypertrophic expansion of adipocyte size due to fat accumulation and lipid droplet growth is associated with unhealthy adipose tissue expansion [49]–[52] and *Lep* expression is associated with adipocyte size [58]. Therefore, in collaboration with Dr. Sonja Schriever, Prof. Paul Pfluger, and Andreas Israel, I isolated and sorted adipocytes after their sizes at the Research Unit NeuroBiology of Diabetes, Institute for Diabetes and Obesity, Helmholtz Centre Munich. DNA of the size-sorted adipocytes was extracted by Kathrin Huber.

Adipocytes of eWAT from chow and DIO mice were sorted after their sizes, determined by the relative time of flight (TOF), into large (hypertrophic) and small adipocytes (Figure 3.14a). DIO mice had significantly higher body weight ($\Delta = 5.3g \pm 0.7$, $p = 0.001$), resulting in larger epididymal fat pads and more isolated adipocytes per DIO sample (Figure 3.14b). However, frequency-size fraction analysis showed a smaller percentage amount of middle and large than small adipocytes in DIO but not in lean mice, indicating additional hyperplasia in these mice (Figure 3.14c). In lean control mice, RS1, RS2, and RS3 DNA methylation was significantly

higher in small than in large adipocytes (Figure 3.14d–f), which corresponds to a higher expression of *Lep* in large adipocytes [58]. In DIO mice, there was no difference in DNA methylation between small and large adipocytes, suggesting that the *Lep* enhancer DNA methylation pattern is reprogrammed in large adipocytes of eWAT from DIO mice. The higher DNA methylation in large adipocytes explains the pattern of DNA methylation observed before in bulk adipose tissue from DIO mice (Figure 3.2). Furthermore, this could indicate a loss of functional repression of *Lep* expression or a counterregulatory mechanism against elevated *Lep* expression by large adipocytes through RS DNA methylation.

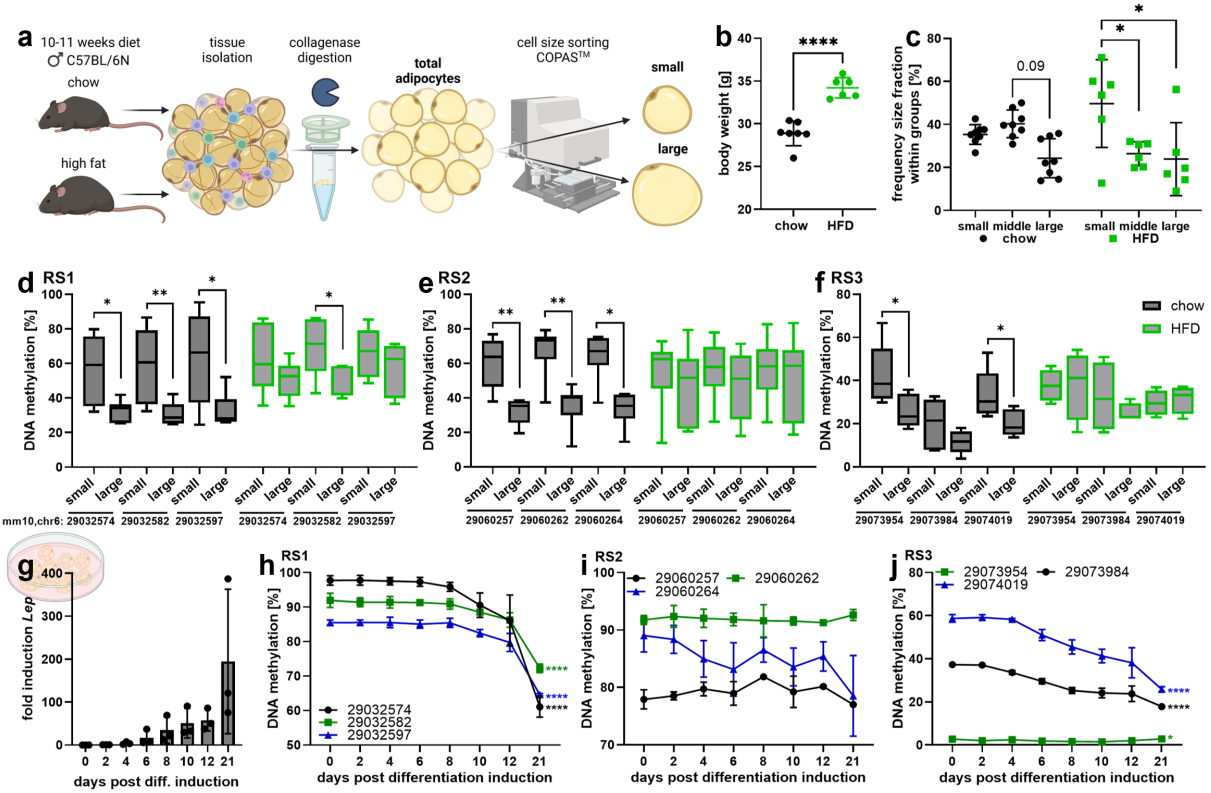

Figure 3.14.: *Lep* enhancer DNA methylation is defined by adipocyte size in lean mice and is reprogrammed in obesity. a) Illustration of the experimental setup of adipocytes sorted from eWAT. b) Body weights of mice at the time of sacrifice. c) Distribution of size fractions (measured in relative units time-of-flight: small: 20.9–198.5, middle: 214.2–365.7, large: 377.5–1020.1) within the chow or HFD group. DNA methylation in *Lep* enhancers RS1 (d), RS2 (e), RS3 (f) in small and large adipocytes from chow and HFD-fed mice. g) *Lep* expression and DNA methylation in RS1 (h), RS2 (i), RS3 (j) during differentiation of 3T3 cells. Since *Lep* expression was minimal in undifferentiated (day 0) 3T3 cells, fold induction was calculated relative to day 2 of differentiation for each biological replicate, accounting for batch differences. Data were analyzed using a two-tailed Student's t-test (b), a two-way ANOVA (c), a two-way repeated measures ANOVA (d, e), a mixed-effect model (f) with post hoc analysis after Holm-Sidak, $*p < 0.05$, $**p < 0.01$, $****p < 0.0001$, $n = 4 - 7$; analysis details of the two-way ANOVA and mixed-effect models are given in Table A.39; and one-way ANOVA (h–j) with $*p_{time} < 0.05$, $****p_{time} < 0.0001$; analysis details are given in Table A.40; $n = 3$. The figure is part of the submitted manuscript.

Measurement of *Lep* expression was not possible in this experiment due to the small amount of cells in a large volume after adipocyte sorting, which led to too little isolated RNA. Therefore, I used 3T3-L1 cells, induced adipocyte differentiation, and tracked the differentiating and in size

growing adipocytes over a 21-day period. DNA methylation in RS1 and RS3 decreased with an increase in *Lep* expression, while the RS2 site and CpG3 of RS3 did not react. However, the observations in RS1 and RS3 are consistent with our findings in isolated adipocytes of eWAT from normal-weight mice. The efforts to stimulate larger adipocytes by fatty acid (palmitate/oleate) treatment, mimicking the hypertrophic adipose tissue expansion, were unsuccessful. No increase in adipocyte size was observed and *Lep* expression and DNA methylation were similar between fatty acid treatment and the related control condition with BSA (Figure A.5). Nevertheless, the treatment with fatty acid and BSA increased DNA methylation compared to treatment-naive 3T3-L1 adipocytes receiving neither fatty acids nor BSA.

Overall, *Lep* DNA enhancer methylation changed with adipocyte size in lean mice, inducing changes in *Lep* expression. In obesity, the size-dependent DNA methylation was reprogrammed. The change in DNA methylation could not be induced with biomechanical alteration during adipogenesis or a 2-day stretch of adipocytes *in vitro*.

3.3. Functional analysis of RS1, RS2 and RS3 DNA methylation

This section focuses on the functional investigation of *Lep* enhancer DNA methylation on gene expression. First, RS1 was validated to be a functional enhancer of the *Lep*. The RS2 and RS3 sites were already thoroughly shown to be enhancer sites for *Lep* expression as introduced in section 1.1.3. Then, a methylation-sensitive luciferase assay was used to directly validate the effects of DNA methylation in each *Lep* enhancer site on gene expression. Finally, transcription factor binding was confirmed for the sites.

3.3.1. Enhancer site RS1 influences *Lep* expression

To validate the enhancer activity for the RS1 site, a dCas9-KRAB system was employed. The dCas9 binds specifically to its target sequence specified by a single guide RNA (sgRNA). In case of enhancer activity of the investigated sequence in the target gene, the enhancer site with the bound d-Cas9-KRAB folds into proximity to the promoter of the target gene and the KRAB domain subsequently silences the expression of the target gene. Three different sgRNAs, binding within the RS1 region, were tested. A scramble sgRNA served as control. sgRS1_1 decreased *Lep* expression, indicating that RS1 is indeed an enhancer site for the *Lep* (Figure 3.15a), although being approx. 27.6 kilobases away from *Lep* (calculated from mm10, UCSC browser). The other sgRNAs did not alter *Lep* expression, which shows the differential potencies of the sgRNAs and underlines the need to test multiple sgRNAs for CRISPR-dCas9 experiments (Figure 3.15b).

3.3.2. DNA methylation influences gene expression

To now discriminate the effects of *Lep* enhancer DNA methylation on gene expression directly, I used a CpG-free firefly luciferase vector, where RS1, RS2, and RS3 were cloned in front of the firefly gene, respectively. The vectors were methylated or mock-methylated and then transfected

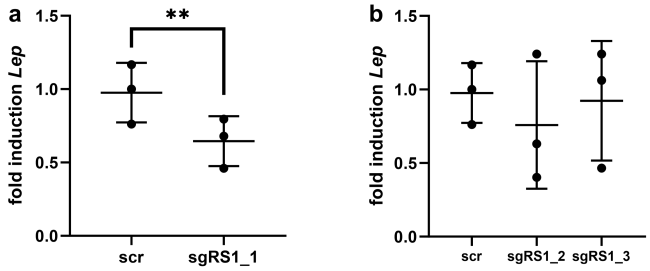

Figure 3.15.: RS1 is an enhancer site of *Lep*. Differentiated 3T3-L1 adipocytes were transfected with a dCas9-KRAB and three different sgRNAs specific for the RS1 sequence. a) *Lep* expression in scramble (scr) vs sgRS1_1 transfected cells. b) *Lep* expression in scr vs unsuitable sgRNAs transfected cells. Statistical analysis was performed on the dCT values using a two-tailed paired Student's t-test between control and sgRNA; $^{**}p < 0.01$. Fold induction was calculated within each biological replicate to account for differentiation differences.

into HEK293T cells (Figure 3.16a). Luciferase activity served as read out for gene expression of the luciferase gene on the vectors and, thereby, as read out for the effect of DNA methylation in the RS on gene expression. Luciferase activity was reduced with DNA methylation in RS1, indicating that DNA methylation in RS1 inhibits transcription (Figure 3.16b). DNA methylation in RS2 or RS3 did not significantly alter luciferase activity (Figure 3.16c, d).

3.3.3. Identification of RS1 binding factors

As DNA methylation in the RS1 site showed significant effects on gene expression, I identified possible methylation-dependent RS1 binding factors. For this purpose, I performed a methylation-specific immunoprecipitation followed by mass spectrometry analysis: Methylated and non-methylated RS1 oligonucleotides were incubated with eWAT proteins or 3T3-L1 adipocyte proteins. The binding proteins were identified using mass spectrometry. The mass spectrometry was performed in collaboration with Prof. Timo Gemoll. In methylated RS1 two methyl-binding proteins were identified: MECP2 ($q = 0.22$, $p = 0.002$ and log2(FoldChange) = 1.61; Figure 3.16e, Table A.41) and MBD2 ($q = 0.11$, $p = 0.001$, log2(FoldChange) = 3.43, Figure 3.16f, Table A.43). These proteins are associated with transcriptional repression and therefore their binding to RS1 is in line with the downregulation of luciferase activity observed in the luciferase assay (Figure 3.16b). Additional proteins enriched in methylated RS1 were Intracellular Antigen 1-restricted T Cell Proteins (TIAR), Ubiquitin Like With PHD And Ring Finger Domains 1 (UHRF1), MAF BZIP Transcription Factors G (MAFG) and K (MAFK) (Figure 3.16e, f).

The transcription factors binding to RS2 and RS3 were identified in previous studies and summarized in Table A.25. In mass spectrometry analysis of the RS2 and RS3 oligonucleotides, binding of the transcription factors Ap-2 Alpha (AP2A) and AP2β-interactor Transcriptional Repressor Protein Ying-Yang 1 (TYY1) to the RS2, and binding of RXRα, PPARγ, NFIa, NFIb, NFIc and NFIx to the RS3 were confirmed (compare section 1.1.3, Table A.45, Table A.46).

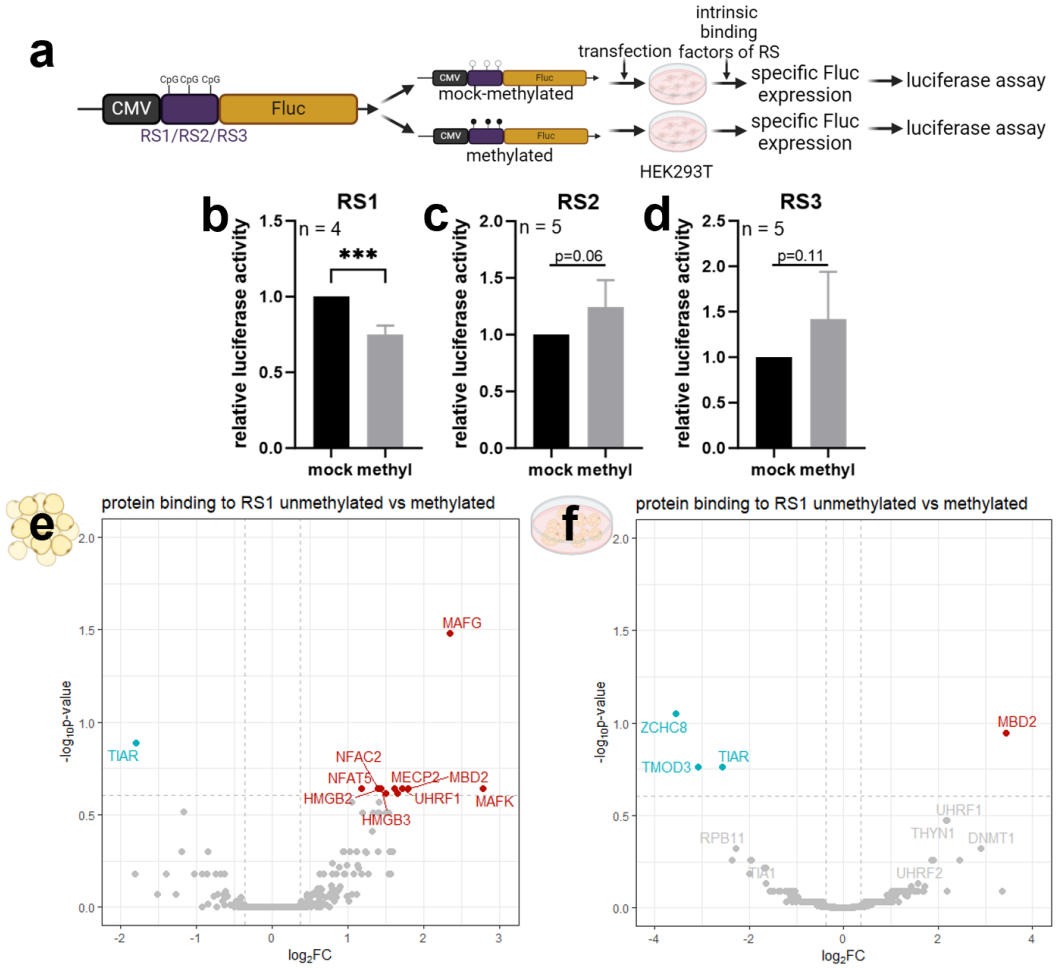

Figure 3.16.: Functional analysis of DNA methylation in RS1, RS2 and RS3 on gene expression. a) Experimental scheme of the luciferase experiment with site of RS1, RS2 or RS3 inserts, indicated in the context of the CpG-free firefly luciferase (FLuc) vector. Luciferase activity of methylated RS1 (b), RS2 (c) and RS3 (d) relative to the mock methylated vector. Data were analyzed using a two-tailed Student's t-test; $***p < 0.001$. Differential binding to methylated vs non-methylated RS1-oligonucleotide by proteins from eWAT (e) or proteins from 3T3 adipocytes (f) identified by mass spectrometry. The figure is adapted from the submitted manuscript.

3.4. Dynamics and reversibility of *Lep* enhancer DNA methylation

Since DNA methylation in the *Lep* enhancer sites RS1, RS2, and RS3 increased with obesity induction and eWAT expansion in diet-induced and in leptin-deficient obesity, the reversibility of the DNA methylation pattern with weight loss was tested. The weight loss approaches included dietary, pharmacological, and surgical interventions. DNA methylation in *Lep* enhancer sites reacted in a time- and intervention-dependent manner.

3.4.1. Dietary interventions

The dietary intervention included a short-term 10-day intervention with an additional overnight fast and a long-term 12-week intervention. The *in vivo* studies and tissue collection were performed by Dr. Sonja Schriever.

In the short-term 10-day intervention, DIO mice were subjected to two dietary interventions: a switch from HFD to chow diet (HC) with *ad libitum* access to food and the switch to chow with additional calorie restriction (CR). An illustration of the study can be found in Figure 2.4a. Age-matched chow or HFD-fed mice served as controls. The 10-day dietary intervention led to a significant reduction in body weight by 12.4 %±2.4 (HC) and 19.5 %±3.0 (CR) (Figure 3.17a, b) with concomitant fat mass loss (Figure 3.17c). However, since their weight remained higher in comparison to the chow group, HC and CR mice were still considered obese (Figure 3.17b). Calorie restriction for 10 days was sufficient to significantly reduce *Lep* expression in eWAT by 0.8 fold±0.2 only in the CR group compared to the HFD group (Figure 3.17d). However, DNA methylation in the early responder site RS1 and intermediate responder site RS2 remained high (Figure 3.17e, f). Interestingly, DNA methylation in the late responder RS3 of the HC and CR group decreased significantly compared to HFD at CpG1 (chr6:29073954) by 8.9 %±2.9 (HC) and by 12.3 %±2.9 (CR), as well as at CpG2 (chr6:29073984) by 12.8 %±3.4 (HC) and 13.6 %±3.4 (CR) (Figure 3.17g). Although no changes were observed in the DNA methylation in RS1 and RS2, DNA methylation at all measured *Lep* enhancer sites correlated positively with body weight, fat mass and plasma leptin levels (Figure 3.17h). In addition, DNA methylation of CpG1 in RS2 and of CpG1 and CpG2 in RS3 correlated positively with *Lep* expression, demonstrating dynamics in the *Lep* enhancer DNA methylation of eWAT already after 10 days of weight loss intervention.

In order to study the impact of hypertrophy on *Lep* enhancer DNA methylation in eWAT in the dietary intervention, a subset of each 10-day intervention group underwent an overnight fast on day 10 to acutely reduce adipocyte size. The overnight fasting led to a significant decrease in body weight for chow (2.54 g±0.61), HFD (2.58 g±0.84), and diet switch (HC, 3.45 g±0.4) mice, but not for calorie restricted mice (CR, 1.42 g±0.58) (Figure 3.18a), likely as they already adapted to restricted access to food. Interestingly, the overnight fast resulted in decreased eWAT *Lep* expression but not yet plasma leptin levels exclusively in chow-fed mice (Figure 3.18b, c). In contrast, the HC group showed no decrease in eWAT *Lep* expression, but a decrease in plasma leptin levels. Together, this suggests acute metabolic inflexibility in eWAT of obese

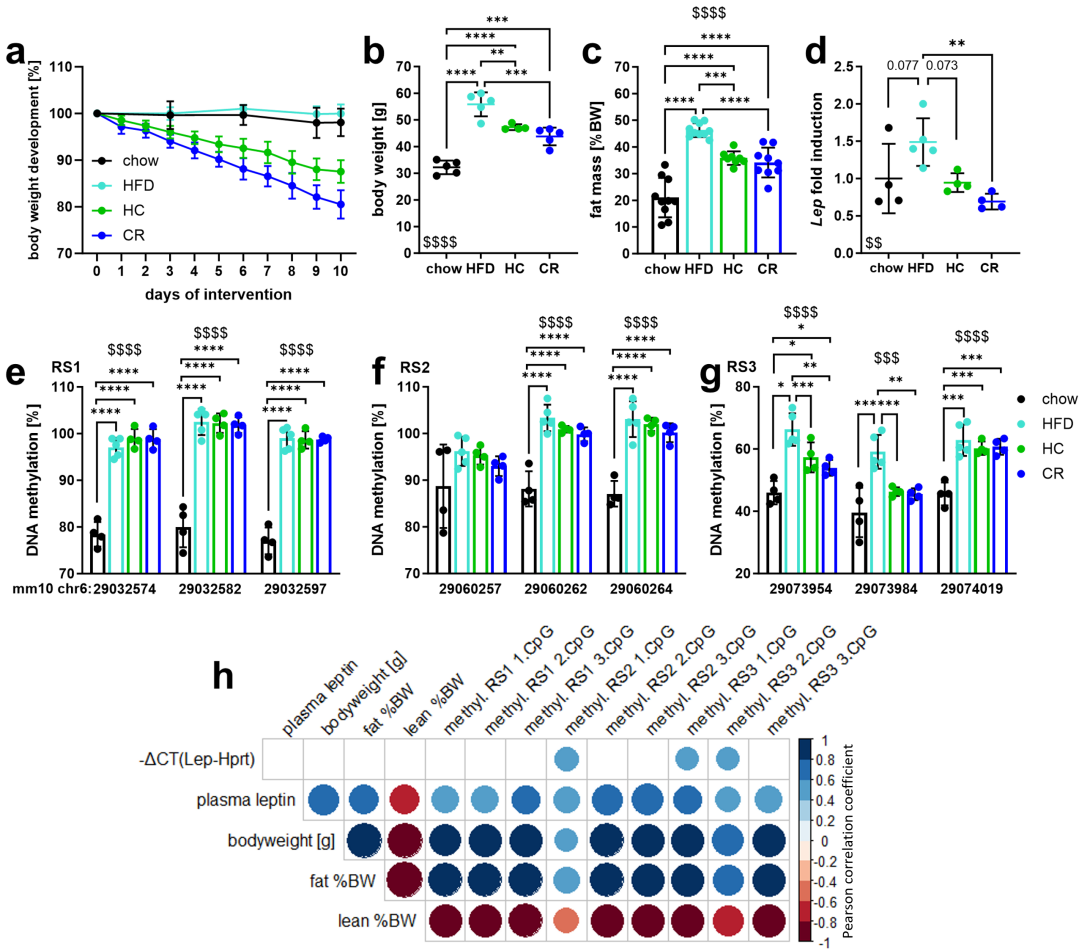

Figure 3.17.: DNA methylation in the late responder RS3 starts to be reversed by a 10-day dietary intervention. a) Development of body weight over time, b) body weight and c) fat mass on the day of sacrifice of mice from the 10-day dietary intervention study: diet switch from HFD to chow (HC), diet switch with additional calorie restriction (CR), HFD- and chow-fed mice. d) *Lep* expression of eWAT from these mice. DNA methylation in RS1 (e), RS2 (f), and RS3 (g) in eWAT. Data were analyzed using a one-way ANOVA with post hoc analysis after Holm-Sidak; \$\$ $p_{group} < 0.01$, \$\$\$ $p_{group} < 0.001$, \$\$\$\$ $p_{group} < 0.0001$, ; $^*p < 0.05$, $^{**}p < 0.01$, $^{***}p < 0.001$, $^{****}p < 0.0001$; analysis details of the ANOVA are given in Table A.47. h) Pearson correlation matrix of *Lep* expression, plasma leptin levels, body weight, fat mass and lean mass. Only correlation with $p < 0.1$ are shown as different sized circles, the larger the circle, the lower the p-value. Detailed results of the correlation analysis can be found in Table A.48 and Table A.49. For the correlation calculation, the $-\Delta$Ct(Lep$-$*Hprt*) values were taken representing the *Lep* expression. Only data from fed (not fasted) mice were considered and are shown here. The graphs are part of the submitted manuscript.

and formerly obese mice. Accordingly, in lean chow mice which were fasted, likely inducing adipocyte shrinkage through lipolysis, DNA methylation in the early responder site RS1 was higher compared to their fed counterparts (Figure 3.18d). This observation is consistent with previous findings of higher DNA methylation levels in small adipocytes compared to large ones in chow-fed mice and in 3T3 cells (section 3.2.3). In obese mice, fasting decreased (HC) or did not alter (HFD, CR) DNA methylation in RS1, RS2, and RS3, underscoring the reprogramming of *Lep* enhancer DNA methylation in obesity (Figure 3.18d, e, f).

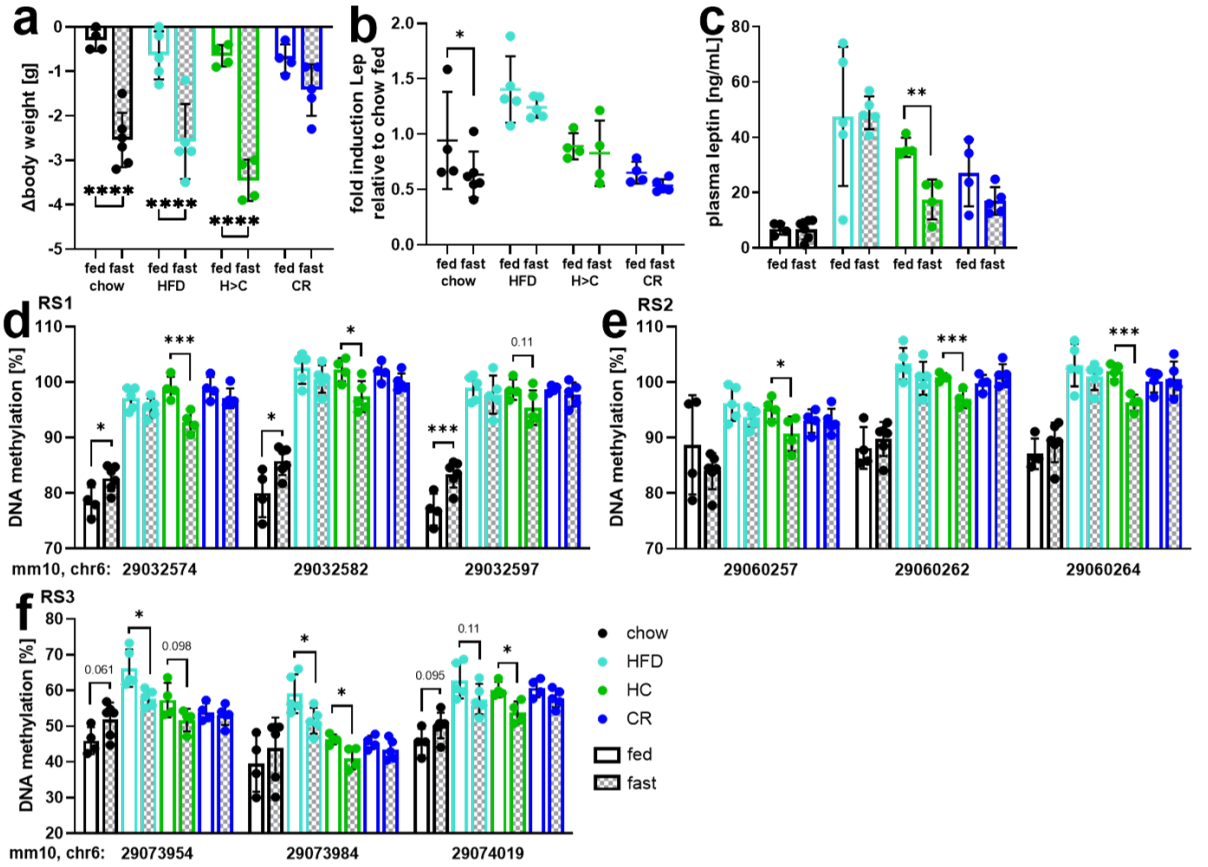

Figure 3.18.: Hypertrophy of adipocytes is responsible for the change in DNA methylation in *Lep* enhancers in eWAT of lean and is reprogrammed in obese mice. 10-day dietary intervention data with additional overnight fast is shown here: diet switch from HFD to chow (HC), diet switch with additional calorie restriction (CR), HFD- and chow-fed mice. a) Body weight reduction, b) *Lep* expression and DNA methylation in RS1 (d), RS2 (e), RS3 (f) with an emphasis on fasting effects within each intervention group in eWAT. Data were analyzed to delineate the fasting/feeding effects within each feeding group with a two-tailed Student's t-test; $*p < 0.05$, $**p < 0.01$, $***p < 0.001$, $****p < 0.0001$. The graphs are part of the submitted manuscript.

To evaluate whether prolonged weight loss exacerbates the effects observed during the 10-day weight loss, *Lep* enhancer DNA methylation was measured in eWAT of mice under a 12-week weight cycling regime [213]. Instead of including a calorie restriction (CR) group, a Yoyo group was introduced, which first lost weight through a 12-week diet switch (HC), before regaining weight through 12-week HFD feeding (Yoyo). An illustration of the study design can be found in Figure 2.4b. The 12 weeks on chow diet led to a decrease in body weight to almost chow

levels in the HC group (Figure 3.19a) together with reduction of *Lep* expression in eWAT (Figure 3.19b). These decreases in *Lep* expression and circulating leptin levels [213] were reversed in the Yoyo group which regained weight. Prolonged weight loss in the HC group, compared to the HFD group, led to a significant decrease in DNA methylation in RS1, RS2, and RS3, with only the DNA methylation in the late responder site RS3 returning to the level of the chow group (Figure 3.19c–e). In particular, the approximately 20 % increase in DNA methylation at the obesity-responsive enhancer sites RS1, RS2, and RS3 was replicated (Figure 3.2 and Figure 3.19c–e). As weight regain in the Yoyo group was associated with elevated DNA methylation in RS1, RS2, and RS3 back to the levels in the HFD group, expansion of adipose tissue in obesity appears to drive *Lep* enhancer DNA methylation.

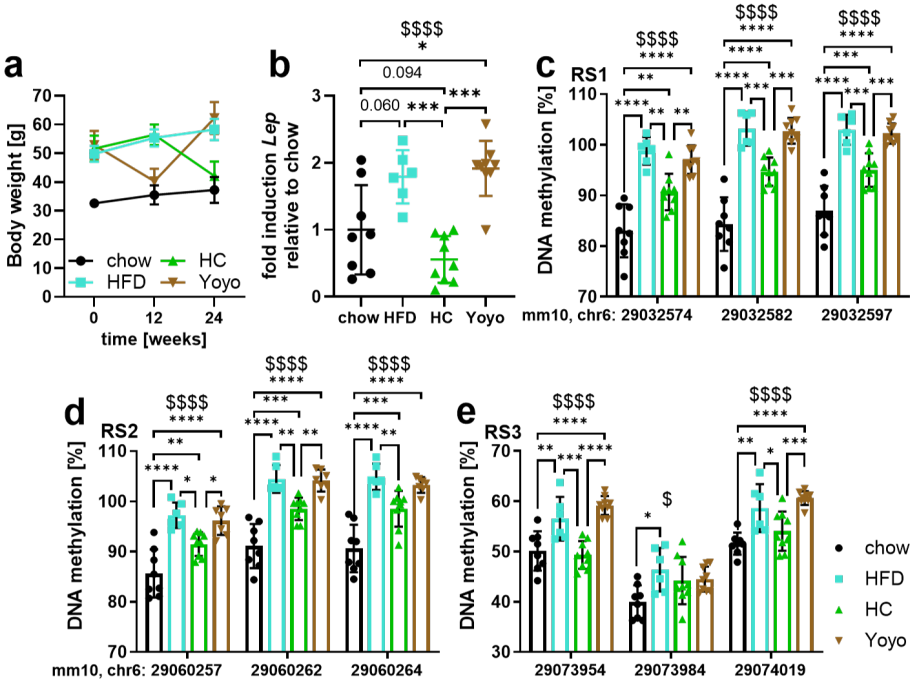

Figure 3.19.: Long-term dietary intervention is necessary but not sufficient to reverse the *Lep* enhancer DNA methylation pattern to the levels of lean mice. Data of mice from the weight cycling study are shown: chow, HFD, diet switch from HFD to chow (HC) and mice which were HC for 12 weeks, then switched back to HFD (Yoyo). a) Body weight during the intervention; data published in [213]. b) *Lep* expression and DNA methylation in RS1 (c), RS2 (d), and RS3 (e) in eWAT. Data were analyzed using a one-way ANOVA with post hoc analysis after Holm-Sidak; \$ $p_{group} < 0.05$, \$\$\$\$ $p_{group} < 0.0001$, ; *$p < 0.05$, **$p < 0.01$, ***$p < 0.001$, ****$p < 0.0001$; analysis details of the ANOVA are given in Table A.50. The graphs are part of the submitted manuscript.

3.4.2. Pharmacological intervention: metformin treatment

Metformin is commonly prescribed as a primary therapy for type 2 diabetes. It is also known to reduce weight in obese individuals with and without type 2 diabetes [233, 234].

Here, DIO mice were treated with metformin orally over the drinking water after 12 weeks of HFD for 2 or 6 weeks with continued HFD-feeding. An illustration of the study can be found in Figure 2.2. As in the previously described DIO cohort (section 3.1.1), mice gained

weight with concomitant increase in fat mass during 18 weeks of HFD-feeding, while additional metformin treatment did not alter weight or body composition (Figure 3.20a, b). However, glucose tolerance improved compared to week 12 ($\Delta AUC_{HFD-HFD+Metf} = -6051 \pm 2717$, Figure 3.20c) with metformin treatment in week 14 (2 weeks of metformin treatment; $\Delta AUC_{HFD-HFD+Metf} = 12537 \pm 3389$, Figure 3.20d) and week 18 (6 weeks of metformin treatment, $\Delta AUC_{HFD-HFD+Metf} = 10619 \pm 2698$, Figure 3.20e) indicating a successful metformin treatment. This was further shown by improvements in liver triglycerides [185].

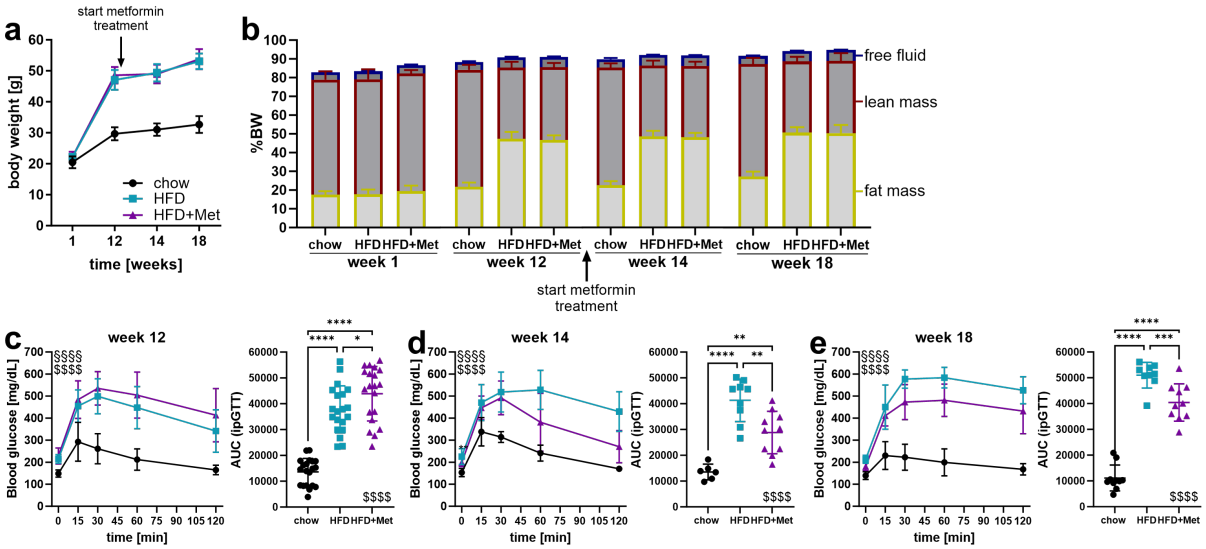

Figure 3.20.: Phenotyping of metformin treated mice. a) Body weight of metformin treated mice and chow- and HFD-fed control mice. b) Body composition of mice in week 12 (before the start of metformin treatment), week 14 (2 weeks of metformin treatment) and week 18 (6 weeks of metformin treatment). Results of ipGTTs as glucose levels and their area under the curve (AUC) in week 12 (c), week 14 (d) and week 18 (e). Data of ipGTTs were analyzed using a two-way repeated measures ANOVA (glucose levels) or one-way ANOVA with post hoc analysis after Holm-Sidak; §§§§ $p_{interaction} < 0.0001$, $$$$ $p_{group} < 0.0001$; $^{*}p < 0.05$, $^{**}p < 0.01$, $^{***}p < 0.001$, $^{****}p < 0.0001$; analysis details of the tests are given in Table A.51; $n = 9$–10/week/group. Body weight data are published in [185].

Interestingly, at week 18, *Lep* levels in eWAT were elevated compared to HFD and chow (Figure 3.21a), probably due to the reduction in *Lep* levels in HFD, as observed in the DIO cohort (Figure 3.3). However, circulating leptin levels remained the same (Figure 3.21b). DNA methylation levels, as shown in Figure 3.21c–e, were not altered with metformin treatment, but for a slight decrease of 4.5 %±2.0 in CpG1 of the late responder RS3 (Figure 3.21e), which cannot be associated with other changes in these mice.

The pharmacological intervention study indicates that metformin administration over a 6-week period failed to alter *Lep* expression. This outcome is not surprising given the concurrent lack of changes in fat mass or body weight.

3.4.3. Surgical intervention

Vertical sleeve gastrectomy (VSG) is a widely used surgical intervention against obesity. In this procedure, the size of the stomach is reduced, leading to a lower calorie intake and a decrease

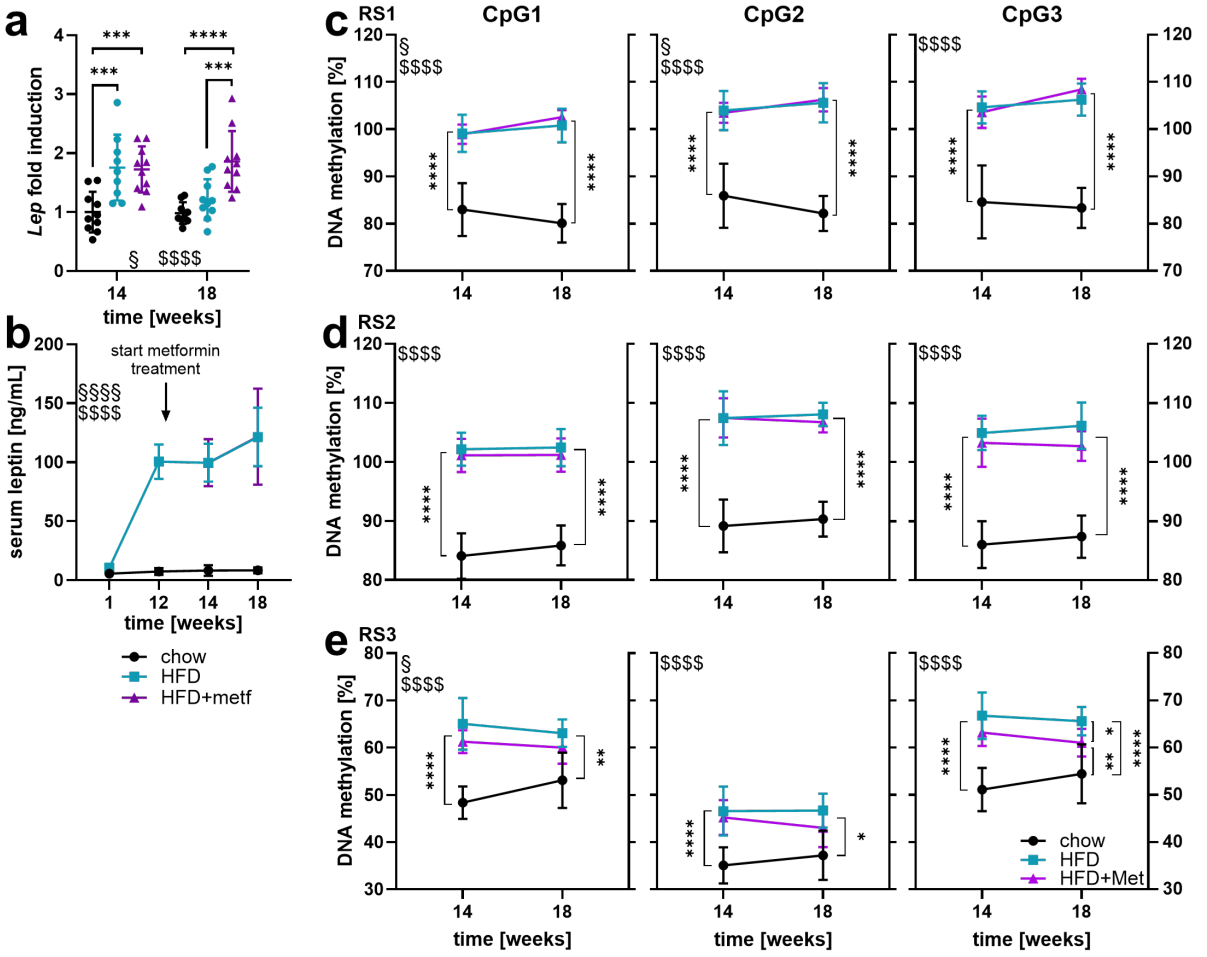

Figure 3.21.: Metformin treatment changes *Lep* expression in eWAT but not circulating leptin or DNA methylation in *Lep* enhancer sites. a) *Lep* fold induction of eWAT and (b) circulating serum leptin levels. DNA methylation in RS1 (c), RS2 (d), and RS3 (e) of eWAT. Data were analyzed using a two-way ANOVA with post hoc analysis after Holm-Sidak; § $p_{interaction} < 0.05$, §§§§ $p_{interaction} < 0.0001$, \$\$\$\$ $p_{group} < 0.0001$; $^{*}p < 0.05$, $^{**}p < 0.01$, $^{***}p < 0.001$, $^{****}p < 0.0001$; analysis details of the ANOVA are given in Table A.51 and Table A.52; $n = 9$–10/week/group.

in appetite. The *in vivo* procedures were performed by Dr. Anne-Marie Neumann [211]. *Lep* expression decreased 9 days after surgery compared to sham mice, but this difference was no longer present after 35 days (Figure 3.22a). The body weight of mice decreased significantly 9 and 35 days after VSG compared to their respective sham controls (Figure 3.22b). Notably, the body weight difference compared to day 0 was more pronounced at 9 days (ΔBW =9.07 g±2.04) than at 35 days post-surgery (ΔBW =2.88 g±4.23, Figure 3.22c), indicating a cessation of weight loss beyond the initial period. This observation aligns with the findings in *Lep* expression. The initial weight loss and the drop in *Lep* expression are mirrored by the *Lep* enhancer DNA methylation at most CpG sites: DNA methylation in the early responder RS1, CpG3 (Figure 3.22d), the intermediate responder RS2 (Figure 3.22e) and late responder RS3 (Figure 3.22f) increased. This is in line with observations of higher methylation in small adipocytes from lean mice (section 3.2.3) and indicated that DNA methylation of adipocytes was sensitive to changes, although VSG mice were still obese. Together with no discernible difference in *Lep* expression between the VSG and sham groups (Figure 3.22b), the difference in DNA methylation in RS1, RS2, and RS3 was no longer evident at day 35 post-surgery (Figure 3.22d–f).

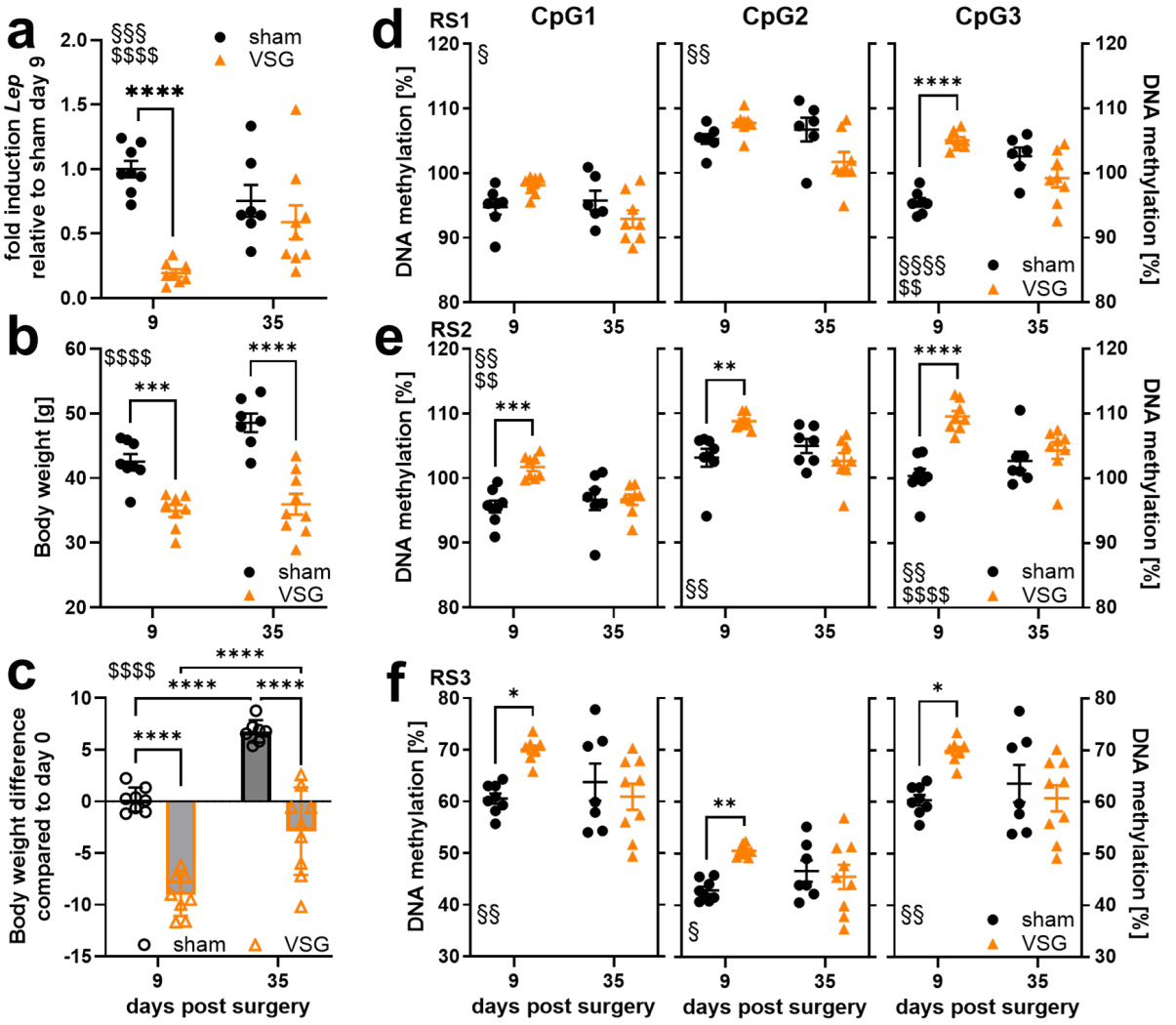

Figure 3.22.: Vertical sleeve gastrectomy is effective to reduce *Lep* expression and alter *Lep* enhancer DNA methylation in eWAT in the short but not long term. a) *Lep* expression, b) body weight and c) body weight difference of mice (day of sacrifice−day of surgery). DNA methylation in RS1 (d), RS2 (e) and RS3 (f). Data were analyzed using a two-way ANOVA with post hoc analysis after Holm-Sidak; § $p_{interaction} < 0.05$, §§ $p_{interaction} < 0.01$, §§§ $p_{interaction} < 0.001$, §§§§ $p_{interaction} < 0.0001$, $$ $p_{surgery} < 0.01$, $$$$ $p_{surgery} < 0.0001$; *$p < 0.05$, **$p < 0.01$, ***$p < 0.001$, ****$p < 0.0001$; analysis details of the ANOVA are given in Table A.53. Body weight data are published in [211].

3.5. Another epigenetic controller of *Lep* expression—The *lncOb*

As introduced in section 1.3 and shown in Figure 1.4, in addition to DNA methylation, long non-coding RNAs are epigenetics, which can influence gene expression. *Lep* expression was quantitatively linked to *lncOb* expression in mature adipocytes [93, 194]. Therefore, I investigated the expression of *lncOb* during the progression of obesity in different fat depots, scrutinized its response in intervention studies, and correlated *lncOb* with *Lep* expression.

Surprisingly, *lncOb* expression decreased after an initial peak during obesity progression in the eWAT of DIO mice compared to the chow controls (Figure 3.23a) and did not correlate with *Lep* expression (Figure 3.23b). *LncOb* correlated negatively with *Lep* expression when taking data from only weeks 1 and 12 into account (Figure 3.23c, d), suggesting a potential uncoupling of *lncOb* from *Lep* expression regulation, as observed in *Lep* enhancer DNA methylation in eWAT. However, in iWAT, the *lncOb* expression correlated positively with *Lep* expression (Figure 3.23e, f). After 18 weeks on HFD with *lncOb* expression remaining minimal and no correlation of *lncOb* and *Lep* expression in eWAT (Figure 3.23g, h), iWAT *lncOb* expression, despite still being high, became uncoupled from *Lep* expression, as indicated by the now negative correlation (Figure 3.23i, j).

Furthermore, investigation of *lncOb* expression in various weight loss interventions revealed that *lncOb* expression remains responsive in obesity, without fully reverting to control expression levels. In the 10-day dietary intervention with additional fasting, *lncOb* expression remained lower in obese (HFD, HC and CR) than in the chow-fed, lean mice (Figure 3.24a; for body weight compare Figure 3.18a). However, unlike *Lep* enhancer DNA methylation, *lncOb* expression was still responsive to fasting in HFD mice and positively correlated with *Lep* expression, indicating responsiveness to fasting in all groups (Figure 3.24b). The 12-week long-term intervention was unable to reverse *lncOb* expression levels to normal (Figure 3.24c). *LncOb* and *Lep* expression correlated negatively, which can be explained by the two obese and low *lncOb* expressing HFD and Yoyo group which shift the correlation in parallel (Figure 3.24d; compare orange/black to blue/turquoise). *LncOb* expression also responded to surgical intervention in the VSG cohort (Figure 3.24e), with a strong positive correlation with *Lep* expression indicating a recoupling of *lncOb* and *Lep* expression in eWAT of VSG mice (Figure 3.24f).

Notably, induction of lipolysis with forskolin in 3T3-L1 adipocytes led to a rapid reduction in *Lep* and *lncOb* expression, suggesting a potential link between lipolysis and *lncOb* regulation in acute nutritional changes such as fasting or acute HFD (week 1 of DIO) (Figure 3.24a, b and Figure 3.25). However, lipolysis was not responsible for the uncoupling of *Lep* expression during DIO progression. In DIO, lipolysis was repressed, indicated by the downregulation of expression of enzymes involved in lipolysis (Figure A.6).

Overall, the *lncOb* data indicate, that it regulates *Lep* expression rather in the iWAT than eWAT, but responds to acute nutritional changes in both depots, likely through lipolysis. Interestingly, the same impaired reversibility was observed as for the DNA methylation pattern in eWAT, pointing toward a general epigenetic reprogramming of adipocytes in obesity.

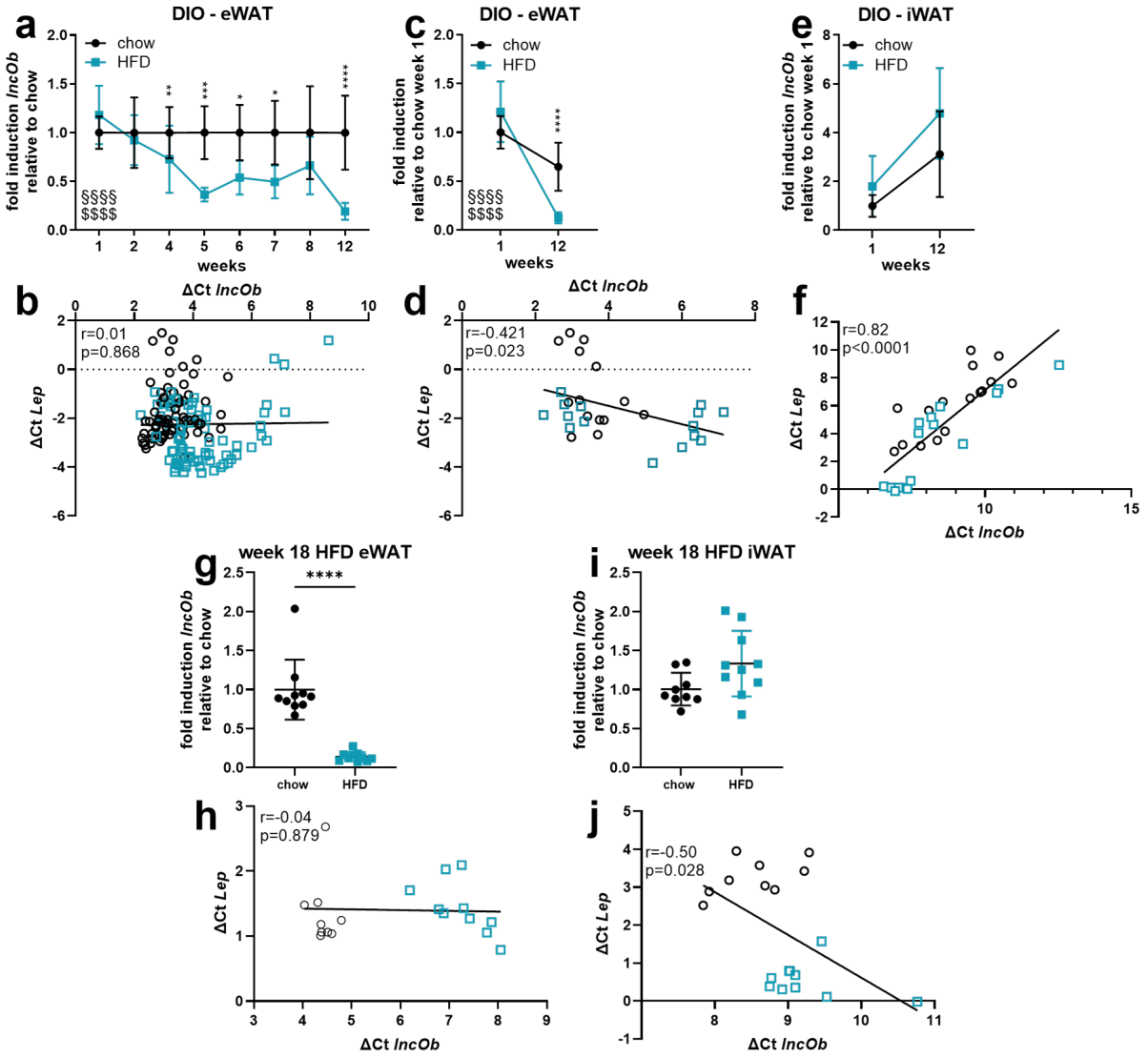

Figure 3.23.: *Lep* expression becomes uncoupled from *lncOb* expression in DIO in eWAT and iWAT. *LncOb* expression (a) over time of DIO and (b) correlation of *lncOb* and *Lep* expression over all time-points in eWAT. *LncOb* expression at the start and endpoints of DIO relative to chow week 1 and adjacent correlation of *lncOb* and *Lep* expression in (c, d) eWAT and (e, f) iWAT. *LncOb* expression and adjacent correlation of *lncOb* and *Lep* expression in prolonged DIO for 18 weeks in (g, h) eWAT and (i, j) iWAT; these data were taken from the chow and HFD group of the mouse cohort of the metformin treatment study. Expression data were analyzed using a two-way ANOVA with post hoc analysis after Holm-Sidak or a two-tailed Student's t-test, §§§§ $p_{interaction} < 0.0001$, $$$$ $p_{group} < 0.0001$; *$p < 0.05$, **$p < 0.01$, ***$p < 0.001$, ****$p < 0.0001$; analysis details of the ANOVA are given in Table A.54. Pearson correlation was performed on the $-\Delta Ct$ values of the gene expressions; r–Pearson correlation coefficient.

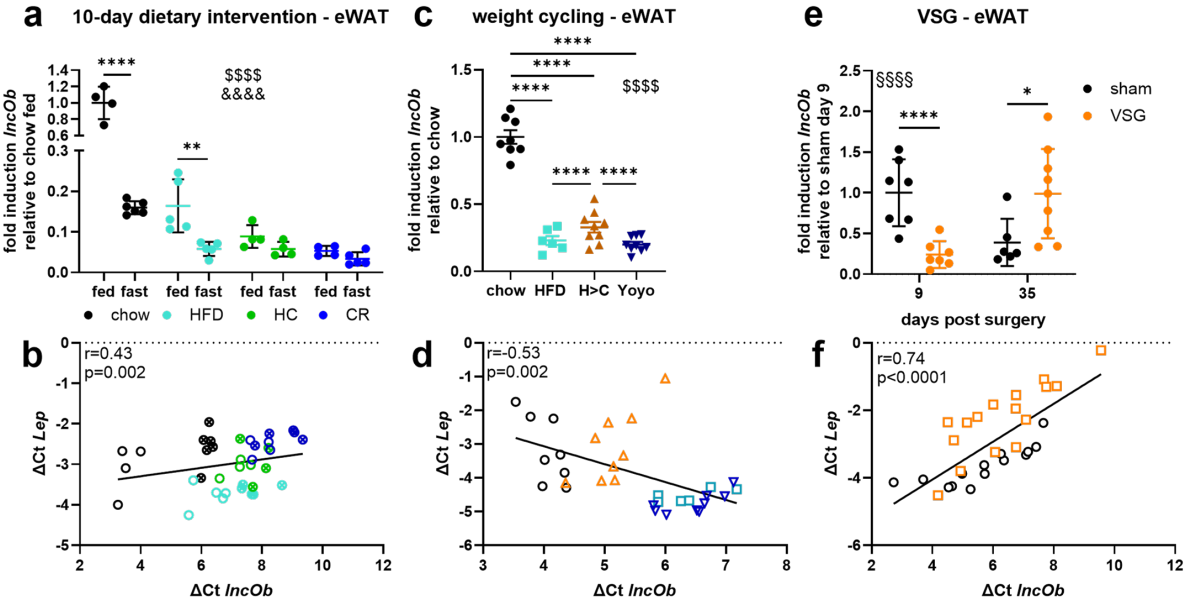

Figure 3.24.: *LncOb* is responsive in obesity and is recoupled to *Lep* expression with VSG but is not reversed to lean control levels with long-term dietary weight loss intervention in eWAT. *LncOb* expression and correlation with *Lep* expression in (a, b) the 10-day dietary intervention with additional overnight fasting, (c, d) the long-term weight-cycling study, and (e, f) VSG. Expression was analyzed using a two-way ANOVA (10-day intervention, VSG) or a one-way ANOVA (weight cycling) with post hoc analysis after Holm-Sidak; §§§§ $p_{interaction} < 0.0001$, $$$$ $p_{group} < 0.0001$; &&&& $p_{feeding/fasting} < 0.0001$, $^{*}p < 0.05$, $^{**}p < 0.01$, $^{****}p < 0.0001$; analysis details of the ANOVA are given in Table A.54. Pearson correlation was performed on the $-\Delta Ct$ values of the gene expressions; r–Pearson correlation coefficient.

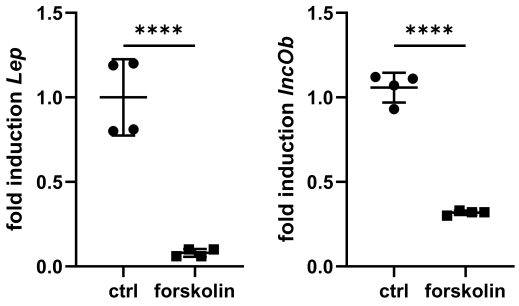

Figure 3.25.: Lipolysis induced by forskolin treatment reduces *lncOb* and *Lep* expression. Differentiated 3T3-L1 adipocytes were treated for 6.5 h with forskolin. Control cells were treated with the forskolin solvent 100 % ethanol. Data were analyzed using a two-tailed Student's t-test, $^{****}p < 0.0001$.

4. Discussion

Obesity, as one of the leading health problems worldwide, is accompanied by severe comorbidities such as cardiovascular disease, type 2 diabetes, and liver diseases [110]. Our hypercaloric environment and sedentary lifestyle promote the development of obesity. Leptin resistance that develops due to high levels of circulating leptin, as introduced in section 1.1.5, worsens the obesity condition. The body has lost its ability to properly react to the anorexigenic effects of leptin. Despite extensive research, the molecular and mechanical cues determining the quantitative expression of leptin within the adipocyte in relation to fat mass in both lean and obese individuals have not yet been fully elucidated. Therefore, I hypothesized that epigenetic modifications, particularly DNA methylation in enhancer regions, play a crucial role in the regulation of quantitative *Lep* expression and enable adipocytes to discern the need for increased *Lep* production. Thereby, epigenetic modifications could contribute to the observed increase in *Lep* expression during the progression of obesity.

This work thoroughly investigated two epigenetic mechanisms of *Lep* regulation using a combination of multiple *in vivo* and *in vitro* approaches, complemented by OMIC studies. I identified novel mechanisms that highlight epigenetic reprogramming in hypertrophic adipocytes in obesity, providing insights into the massive leptin overproduction in obesity. I discovered that the *Lep* enhancer DNA methylation pattern is fat depot-specific. It increased depending on its location in a time-dependent manner during obesity induction and progression in male mice and indeed influenced *Lep* expression. Human data indicated a similar rise in DNA methylation in VAT. The adipocyte size emerged as the key factor in affecting DNA methylation without the need for central leptin feedback signaling: Large, hypertrophic adipocyte DNA methylation became reprogrammed in obesity.

Highlighting the dynamic nature of *Lep* enhancer DNA methylation patterns, the findings reveal reversibility in eWAT after long-term dietary intervention, particularly in RS3, where DNA methylation completely reversed to chow levels. A surgical weight loss intervention with vertical sleeve gastrectomy showed a fast response of DNA methylation to weight reduction. Unexpectedly, the long non-coding RNA *lncOb* was downregulated during obesity progression in a fat depot-specific manner, yet retained responsiveness to fasting in the obese state. Despite this responsiveness, expression levels remained unrecoverable with long-term dietary intervention.

4.1. Adipocyte size drives DNA methylation and becomes reprogrammed in obesity

Adipose tissue expands through two different mechanisms: hyperplasia and hypertrophy. Hypertrophic adipocyte expansion is an acute response to overnutrition in lean mice and humans, where energy is stored in the form of triglycerides in lipid droplets [49, 235]–[237]. In obesity, excessive hypertrophic expansion of adipose tissue, in contrast to newly differentiating adipocytes as in hyperplasia, is associated with metabolic unhealthy obesity [50, 51, 228].

4.1.1. Adipocyte size driven DNA methylation in lean

In the lean state, adipocyte size drives DNA methylation in *Lep* enhancer sites in eWAT. DNA methylation decreased with an increase in *Lep* expression in fed compared to fasted lean, chow-fed mice (Figure 3.18). This decrease in *Lep* enhancer DNA methylation can be explained by the adipocyte size: Acute fasting led to an increase in lipolytic genes and a reduction in adipocyte size in eWAT already after 24 h of fasting [71, 238]. The observation of the adipocyte size driving the DNA methylation is supported by the decrease in DNA methylation in RS1 and RS3 during 3T3-L1 differentiation with a concomitant increase in *Lep* expression (Figure 3.14g–j). The adipocyte sorting data validated the observation further: Small adipocytes from the chow group showed higher methylation in RS1, RS2, and RS3 than large adipocytes. Unfortunately, due to a small number of adipocytes in a large volume after sorting, it was impossible to isolate a sufficient amount of RNA of the size-sorted adipocytes. Therefore, these data lack a direct comparison of size-dependent DNA methylation with *Lep* expression. Nevertheless, the data described above and published data show that with adipocyte volume, also *Lep* expression changes, as *Lep* expression positively correlated with the eWAT volume of lean male mice [239]. Furthermore, adipocyte hypertrophy was associated with hyperleptinemia [240] and in SAT of obese humans, *LEP* expression was higher in large adipocytes [58]. However, *Lep* enhancer DNA methylation was reprogrammed in large adipocytes in obesity as described in the next section.

4.1.2. DNA methylation reprogramming in hypertrophic adipocytes in obesity

Surprisingly, in obese mice, adipocyte size did not alter the DNA methylation in *Lep* enhancer sites in eWAT: The DNA methylation in RS1, RS2, and RS3 of large adipocytes was as high as the DNA methylation in these sites in small adipocytes, in contrast to the reduced DNA methylation observed in large compared to lean adipocytes in lean mice (Figure 3.14). This suggests an epigenetic reprogramming of hypertrophic adipocytes in obesity. The reprogramming of DNA methylation in large adipocytes explains the increase in DNA methylation observed in bulk adipose tissue during diet-induced obesity (DIO) (Figure 3.2): With more hypertrophic adipocytes with high DNA methylation, the overall DNA methylation in *Lep* enhancer sites in the white adipose tissue (WAT) increases compared to its lean counterparts, where hypertrophic adipocytes exhibit a lower DNA methylation pattern. This was further shown by the increase

in *Lep* enhancer DNA methylation of obese mice (diet switch HC, HFD) from the 10-day intervention with additional overnight fasting study (Figure 3.18). The epigenetic reprogramming is underlined by an uncoupling of eWAT volume and *Lep* expression observed in male, HFD-fed and old mice [59], and mirrors either a loss of controlled *Lep* expression or a counterregulatory mechanism of large adipocytes as a response to excessive leptin levels. The observed reprogramming in obesity compared to lean is congruent with the association of hypertrophic expansion of adipose tissue with diminished white adipose tissue plasticity and adipocyte function, thus limiting lipid storage capacity [50, 232, 236, 241]. Additionally, hypertrophic expansion of adipose tissue was associated with metabolic complications, including altered fatty acid metabolism, increased immune reactivity, and mitochondrial dysfunction [242, 243]. The resulting regional hypoxia and fibrosis of adipose tissue further limited the capacity for lipid storage [241, 244, 245].

The origins of the signal for the reprogramming of DNA methylation are unclear. Local hypoxia could contribute to hypermethylation by reducing TET activity. TET activity requires oxygen for its function, thus hypoxia could suppress DNA demethylation, leading to a general higher DNA methylation pattern, as shown in cancer [246, 247]. Mechanobiological cues could also lead to reprogramming of DNA methylation: Adipocytes underwent drastic actin remodeling under HFD feeding, while increasing in size [54], and adipose tissue stiffened with accumulation of lipid droplets in obesity [57]. Stretching of 3T3-L1 cells during differentiation, a model mimicking the obese state, accelerated lipid production, thus increasing the size of lipid droplets [56]. These mechanobiological changes were associated with alterations in DNA methylation. Stiffness of the extracellular matrix led to DNA hypermethylation in mouse embryonic stem cells and embryonic fibroblasts [248]. Nuclear deformation, which can occur through increased lipid droplet size, was coupled with chromatin remodeling, leading to altered gene expression [55]. However, in the experimental setup, within the here presented work, to stretch cells and deform nuclei mimicking the obese state, stretching during adipogenesis of 3T3-L1 cells did not affect *Lep* expression or DNA methylation in *Lep* enhancers despite showing differences in focal adhesion and regulation of lipolysis pathways (Figure 3.12). The difference observed in the focal adhesion and regulation of lipolysis pathways proved that the stretch per se was working. As the stretch was applied during the onset of adipogenesis, where *Lep* is not yet expressed, the timing of the mechanical stretch could be the reason, why it did not significantly influence *Lep* expression in cells during adipogenesis. To determine the relevance of mechanobiological effects on mature adipocytes, the stretch experiment was repeated using differentiated 3T3-L1 adipocytes, without significant results (Figure 3.13). However, the absence of differences between the control and stretched populations in the RNA-seq analysis, as indicated by the PCA (Figure 3.13), suggests that the 48-hour stretch duration could have been insufficient to evoke any differences. Repetition of this experiment with a longer stretch of mature adipocytes and the addition of a single-cell nuclear stretch would be useful in determining whether there is no mechanobiological effect on mature adipocytes. Furthermore, an alternative cell culture system, such as primary adipocytes, should be considered. Since 3T3-L1 adipocytes have multiple lipid

droplets instead of a single unilocular droplet, they do not adequately reflect the *in vivo* state.

Interestingly, the reprogramming of the DNA methylation pattern in hypertrophic adipocytes in obesity can be reversed by bariatric surgery. Weight loss intervention with bariatric surgery has been shown to reduce adipose tissue mass and adipocyte size in SAT and eWAT of humans and rodents, together with increased lipolysis [249]–[253]. In my observations, mice that underwent vertical sleeve gastrectomy (VSG) showed higher DNA methylation with reduced *Lep* expression compared to sham mice 9 days after surgery (Figure 3.22). This observation is consistent with observations in size-sorted adipocytes of lean, healthy mice, where DNA methylation was high in small adipocytes, that likely produced less leptin, as discussed above (Figure 3.14). Thus, adipocytes from VSG mice show the same responsiveness in the DNA methylation pattern as healthy adipocytes in lean. This is further indicated by the 35-day post-surgery time-point: *Lep* expression increased with weight regain, likely leading to an increase in adipocyte size, and DNA methylation decreased compared to the 9-day VSG mice (Figure 3.22). This is consistent with the decrease in DNA methylation in larger adipocytes of lean mice. The recoupling of the DNA methylation pattern to *Lep* expression in VSG is reflected in the recoupled correlation of *lncOb* with *Lep* expression in comparison to other obese mice (Figure 3.24). However, other dietary and pharmacological interventions were unable to completely reverse epigenetic reprogramming, which will be discussed in more detail in section 4.4.

Overall, the results show that the DNA methylation in *Lep* enhancers is driven by adipocyte size in lean mice. The increase in the DNA methylation pattern observed in DIO mice can be attributed to epigenetic reprogramming in hypertrophic adipocytes in obesity, as illustrated in in the summary Figure 4.1. The epigenetic reprogramming is either a counterregulatory mechanism to counteract high *Lep* levels, or mirrors a loss of controlled *Lep* expression leading to overproduction. A normalized epigenetic response is achieved through VSG. Furthermore, reflecting the plasticity of adipocytes, recent advances in single-cell sequencing techniques have revealed heterogeneous populations of adipocytes in human and mouse adipose tissues [254]–[257]. These populations exhibited different gene expression profiles with respect to lipolysis, insulin sensitivity, and adipokine profile. Their appearance depended on their location within adipose tissue and revealed differences in adipocyte size and interaction with neighboring cells [255, 256]. These observations and techniques open another exciting avenue for investigations in regard to spatial single-cell epigenetic analysis integrated with spatial transcriptomic data to provide insights into potential triggers that alter the epigenetic profile of adipocytes.

4.2. Epigenetic regulators as fine-tuners of quantitative *Lep* expression

In this section, the putative mechanisms through which DNA methylation in the different *Lep* enhancer sites modulates *Lep* expression in an obesogenic-dependent manner in eWAT will be discussed and the role of the *lncOb* in *Lep* expression regulation elucidated.

4.2.1. Time-dependent DNA methylation change in obesity induction and progression and potential regulatory pathways

DNA methylation of promoters is often associated with a binary on/off switch of expression, as it mainly makes the promoter inaccessible to the transcription machinery [168, 258]. In contrast, DNA methylation in enhancers regulates transcription in a more nuanced way through protein-DNA binding modulation [168, 258]. This modulation can occur through various mechanisms. These include spatial hindrance caused by DNA methylation that prevents transcription factors from binding to their enhancer site; transcription factors preferentially binding methylated DNA; or recruitment of enzymes that induce chromatin closure, rendering the DNA inaccessible to the transcription machinery.

DNA methylation in the *Lep* promoter was correlated with *Lep* expression in humans and mice, often depending on the nutritional status of the organism, but not as the sole regulator of *Lep* expression (compare section 1.3). Multiple factors have been identified to regulate *Lep* expression. Most of these factors have only been described to influence *Lep* expression in general, while only some studies have investigated how factors confer adipose tissue-specific, quantitative *Lep* expression in response to nutritional changes (compare Figure 1.4). Given the obesity-dependent increase in DNA methylation in *Lep* enhancers, along with the specificity to eWAT and its change occurring at different timepoints during obesity development, the here presented data provide evidence for the epigenetic regulation of *Lep* expression by *Lep* enhancer DNA methylation and *lncOb* as fine-tuners.

RS1 DNA methylation responded earliest, after the first week of HFD, with a concomitant increase in *Lep* expression (Figure 3.2a and Figure 3.4a). Upon RS1 methylation, the methyl-binding proteins MECP2 and MBD2 were identified to bind (Figure 3.16e, f), which are associated with transcriptional repression. These methyl-sensitive proteins recruit components of the repressor complex, including histone deacetylases, leading to chromatin closure [259, 260]. These repressive effects support the diminished luciferase activity observed upon RS1 methylation (Figure 3.16b). Moreover, the enrichment of other transcription factors, including UHRF1, MAFG, MAFK and NRF1, binding to methylated RS1 suggests a concerted effort towards transcriptional repression of *Lep* in the hypermethylated state of RS1 (compare Figure 4.1): UHRF1 was associated with stem cell proliferation and prevention of adipogenesis. The transcription factor recruited DNMT1, thus contributing to the maintenance of DNA methylation [261, 262]. Furthermore, MAFs showed differential binding capacity to methylation [263] and interacted with NRF1. NRF1 is known to negatively regulate adipogenesis through PPARγ repression and support the expansion of healthy adipose tissue [264]–[267]. However, while these studies did not present data on *Lep* expression, another study asserted that an NRF1 knockout had no effect on *Lep* expression without providing supporting data, leaving uncertainty about the mechanistic interpretation [95]. Collectively, these findings suggest that methylation in the early responder RS1 functions as a repressive signal. This is further supported by the observation of high DNA methylation in liver samples, where no *Lep* is expressed (Figure 3.6d). Therefore, the repressive function of RS1 DNA methylation could serve as counterregulation by hypertrophic

adipocytes against the overshooting *Lep* expression observed in obesity, as discussed in section 4.1.1. However, the counterregulatory signal is likely overpowered during the early stages of obesity development, since *Lep* expression in eWAT decreases after 12 weeks and not directly when DNA methylation changes in week 1.

The intermediate responder RS2 contains the binding site for the transcription factor AP2β [89]. Notably, AP2β downregulated *Lep* expression [89], and competition between AP2-protein binding and SP1 binding has been observed [268]. Given the proximity of the SP1 binding site to the RS2 site in the *Lep* locus (compare Figure 1.4), the competition between transcription factors may contribute to the observed repression of *Lep* by AP2β. In the work presented here, the AP2β interactor TYY1, as well as the AP2-family protein AP2α bound to the RS2-oligonucleotide (Table A.45). Previous studies demonstrated that the binding of TYY1 to hypermethylated DNA was inhibited [269], and the AP2 proteins did not bind to hypermethylated promoters [268]. The reduced binding of the repressor to RS2 aligns with the observed increase in *Lep* expression during DIO (Figure 3.2b) and the trend toward increased luciferase activity upon methylation (Figure 3.16c). However, its importance appears to manifest in later stages, as mean methylation correlated with *Lep* expression in weeks 4–7 (Figure 3.4a), and DNA methylation in RS2 did not react in 3T3-L1 cells during differentiation (Figure 3.14i). Consequently, RS2 DNA methylation does not function as a master regulator but likely contributes to the quantitative fine-tuning mechanism of *Lep* expression. Together, these findings suggest that DNA methylation in the intermediate responder RS2 facilitates *Lep* expression at later stages of obesity development and less during differentiation in adipogenesis, as summarized in Figure 4.1. Furthermore, DNA methylation in RS2 could mirror a loss of controlled *Lep* expression in obesity that leads to inhibition of the transcriptional repressor.

The late responder RS3 showed significantly higher DNA methylation after 8 weeks of DIO and correlation with *Lep* expression from week 5 on (Figure 3.2d, e and Figure 3.4a). RS3 contains a non-canonical binding site for PPARγ/RXRα, which together with an unknown cofactor quantitatively regulated *Lep* expression [92]. This aligns with the observation that RS3 DNA methylation responded to dietary interventions after 10 days as the first of the *Lep* enhancer sites. The DNA methylation in RS3 reduced even before *Lep* expression in the diet switch (HC) group, (Figure 3.17d, g). Strikingly, DNA methylation in RS3 was the only methylation site completely reversible after 12 weeks of dietary intervention in the weight-cycling cohort (Figure 3.19e). Apart from PPARγ/RXRα, the NFI proteins were shown to bind in the RS3 site and to be necessary for *Lep* expression [93]. Furthermore, NFI proteins preferentially bound to demethylated sites during neuronal development [270, 271]. These findings indicate that less binding of NFI proteins results in reduced gene expression and a repressive effect of DNA methylation in this case. The precise interplay between DNA methylation and PPARγ/RXRα remains unclear. Previous studies suggested a potential role of PPARγ/RXRα on modulating DNA methylation in the vicinity of its binding sites, while the transcription factor complex bound more to its hypomethylated binding site in the C/EBPα gene [272, 273]. Nevertheless, my data suggest that DNA methylation serves as a modulator of transcription factor binding

within the binding site: CpG1 lies within the NFI binding region and CpG3 lies within the non-canonical binding site of PPARγ/RXRα. However, CpG2 lies between the two without a binding transcription factor. While CpG1 and CpG3 exhibited strong reactivity to HFD-feeding in DIO and in the interventions, CpG2 DNA methylation reacted less to adipocyte size (Figure 3.14f), fasting (Figure 3.18f) and long-term weight cycling (Figure 3.19e). The indicated reduced binding of the transcription factors caused by DNA methylation in RS3 again points to a counterregulatory mechanism of the hypertrophic adipocytes against high leptin levels, as indicated for RS1.

The DNA methylation in RS4 and RS5 reacted to DIO in iWAT, however, less pronounced with an average difference of 5 % methylation compared to the approximately 20 % difference in DNA methylation in RS1, RS2, and RS3 from eWAT. The RS4 site binds NFY and EBF1 and contains a non-canonical binding site for PPARγ/RXRα [92]–[94]. Notably, EBF1 knockout mice showed reduced levels of leptin [274], and EBF1, as well as NFY exhibited a higher binding affinity to hypomethylated sites [275]–[277], indicating that during DIO, reduced EBF1 and NFY binding can lead to decreased expression of *Lep*. Interestingly, the DNA methylation response in RS4 differs from that of RS3, although it contains a binding site for the same transcription factor complex PPARγ/RXRα. This difference in response underscores the fat depot-specific regulation of *Lep* expression mediated by DNA methylation, which is further discussed in section 4.3. No specific transcription factor was associated with the RS5 site. The RS5 site lies within intron 1 of *Lep*. Increased gene body DNA methylation is associated with increased gene expression that potentially suppresses intragenic transcriptional start sites. Therefore, DNA methylation in RS5, as it was downregulated in DIO iWAT compared to chow (Figure 3.9g), could signify a counterregulatory mechanism against increased *Lep* expression in iWAT [157]–[159].

Together, the data presented here indicate that DNA methylation in *Lep* enhancers regulate *Lep* expression as fine-tuners over time instead of being transcriptional on/off switches. The likely mechanism of fine-tuning is the orchestration and modulation of the binding of transcription factors. In this modulation, the location of the enhancer in the gene context and the surrounding transcription factor binding sites, which can modulate the transcription bubble, are important [160]. Further investigations in this regard could include a CRISPR-dCas9 system that recruits DNMT3A through a SunTag, leading to site-specific DNA methylation [278], or a dCas9 coupled to TET1, leading to site-specific DNA demethylation [279]. Targeting the *Lep* enhancer sites and coupling these experiments to chromatin immunoprecipitation (ChIP) experiments could enable the discrimination of time-dependent and direct contributions of DNA methylation in each regulatory enhancer site to *Lep* expression. This could allow for a cell context-specific view on the regulation in contrast to the more artificial luciferase assays used within the here presented work.

4.2.2. *LncOb* expression as additional epigenetic gate-keeper of *Lep* expression

An additional epigenetic factor regulating *Lep* expression is the long non-coding RNA *lncOb*, which is required for quantitative *Lep* expression in adipose tissue [93, 194, 195]. Surprisingly, *lncOb* expression was reduced in eWAT of DIO mice already after 4 weeks of HFD-feeding (Figure 3.23a). This contrasts with the study by Dallner et al. (2019). They reported a higher *lncOb* expression in eWAT and iWAT of DIO compared to chow-fed mice, although with a small sample size of 4 mice showing a high standard deviation [93]. Consistent with my observation (Figure 3.23g, i), Lo et al. (2018) demonstrated that *lncOb* (called lnc-ORIA9 or lncLep in their study) was higher only in iWAT but not eWAT from 16 weeks HFD-fed mice compared to chow-fed mice [194]. Furthermore, they observed a reduction in *lncOb* expression with a concomitant decrease of *Lep* expression in both adipose tissues caused by fasting, indicating that *lncOb* is responsive to the nutritional status. Intriguingly, my data confirmed this responsiveness of *lncOb* to fasting together with a correlation to *Lep* expression of lean and obese mice, despite the general downregulation of *lncOb* in the latter (Figure 3.24a, b). Fasting leads to an acute stimulation of lipolysis [238]. Indeed, the data from forskolin-treated 3T3-L1 adipocytes support that lipolysis could suppress *lncOb* together with *Lep* expression (Figure 3.25). Nevertheless, this mechanism cannot explain the general downregulation observed in DIO, since lipolysis is generally downregulated in obesity. This is indicated by downregulation of key lipolytic genes (Figure A.6). However, the dysregulation of the *lncOb* in DIO is similar to the epigenetic reprogramming of *Lep* enhancer DNA methylation observed in hypertrophic adipocytes in obesity. Furthermore, *lncOb* reversibility to lean levels was impaired (Figure 3.24c, d), which is similar to the impaired reversibility of DNA methylation in RS1 and RS2, further discussed in section 4.4.

Taken together, I could confirm that *lncOb* is an additional and responsive epigenetic gate-keeper for *Lep* expression regulation specific to iWAT. However, *lncOb* is not the sole regulator of quantitative *Lep* expression. The results further highlight that hypertrophic adipocytes are reprogrammed at various epigenetic levels.

4.3. Fat depot-specificity of the epigenetic regulators of *Lep*

The observed *Lep* enhancer DNA methylation patterns were specific for the two major white adipose tissue depots: In eWAT, RS1, RS2, and RS3 responded, while in iWAT, DNA methylation changed only in RS4 and RS5. Interestingly, when RS4 was identified as a site important for quantitative *Lep* expression, adipocyte nuclei of iWAT were used [92]. This is consistent with my observation that RS4 is specifically methylated in iWAT (Figure 3.9e, f). Furthermore, fat depot-specific DNA methylation was observed with higher DNA methylation of *Lep* and *Pparg2* promoters in eWAT but not in iWAT of DIO mice [184]. Additionally, the expression of *Lep* in iWAT exceeded eWAT during the progression of obesity [59], while in lean mice, *Lep* expression was higher in eWAT [58, 239]. Similarly, *LEP* expression was higher in VAT compared to SAT in lean humans [280], but this pattern inversed in obesity [60]–[63]. Therefore, RS1, RS2, and RS3 are the enhancer sites responsible for *Lep* expression regulation in eWAT, while RS4 and

RS5 function in iWAT. This fat-depot specific epigenetic signature is underlined by my observation that *lncOb* is responsible for *Lep* expression only in iWAT but not eWAT, as discussed in section 4.2.2.

Previous studies have demonstrated that eWAT contains more large adipocytes compared to iWAT in DIO mice [235, 281]. This finding is consistent with the observations discussed in section 4.1.1 regarding the influence of adipocyte size on DNA methylation patterns. Thus, it substantiates the fat depot-specific DNA methylation pattern driven by adipocyte size. Furthermore, previous studies associated eWAT/VAT with metabolic unhealthy tissue expansion [50, 51, 228], indicating the differences in function between the two white adipose tissue depots in obesity. Possible contributors to the fat depot-specific association with metabolic impairment could be the VAT and SAT locations, with VAT being closer to the portal vein, thus draining fatty acids, cytokines, and adipokines directly to the liver [282]. Moreover, the distinct metabolic effects of the different fat depots could be attributed to developmental and functional differences, as well as different capacities of plasticity [50, 232]. The difference in plasticity between the two fat depots was shown by eWAT containing more large adipocytes compared to iWAT in DIO mice, as mentioned above [235, 281]. This was also confirmed in humans, where the expandability of larger adipocytes and the overall expandability of SAT were reduced and were associated with a worse glucometabolic profile and lower plasma insulin levels compared to VAT adipocytes [53]. Adipogenesis contributed more to the expansion of eWAT than to iWAT in the later stages of HFD-feeding [49, 235, 237]. As my data confirmed size-dependent changes in *Lep* enhancer DNA methylation in adipocytes, as discussed in section 4.1.1, differential plasticity could explain the observed fat depot-specific changes in DNA methylation. Moreover, this provides a link to the distinct metabolic functions of the two major white adipose tissue depots.

Another factor influencing fat depot-specific DNA methylation could be the varying paracrine and autocrine effects of leptin, which are determined by the abundance of LEPR in the particular depot. However, ob/ob mice, which lack functional leptin and therefore leptin signaling, exhibited the same elevated DNA methylation pattern as DIO mice compared to lean controls Figure 3.10. These findings suggest that leptin signaling in adipose tissue does not influence the DNA methylation dependent regulation of *Lep* expression. Therefore, differential leptin signaling within the depot is unlikely to drive the fat depot-specific *Lep* enhancer DNA methylation. In addition, the availability of transcription factors could add to the differential expression pattern of *Lep* between eWAT and iWAT. As shown in section 1.1.3, various transcription factors are known to regulate *Lep* expression and different transcription and methylation profiles have already been identified between VAT and SAT in healthy, lean women [283].

Overall, the data confirmed that fat depot plasticity is crucial in the distinct epigenetic regulation of *Lep* expression between the two major white adipose tissue depots. This provides a link to their distinct metabolic functions and the overproduction of *Lep* in obesity. Further research should focus specifically on these differences and on the switch in *Lep* regulation between eWAT and iWAT (or VAT and SAT in humans) during the progression of obesity. Additionally, further studies should explore intervention studies, as eWAT has been shown to be more sensitive

to weight reduction than iWAT [238].

4.4. Dynamics of *Lep* enhancer DNA methylation and its counterregulatory mechanism

The above discussions show that the adipocyte size-dependent DNA methylation in *Lep* enhancer sites and additionally *lncOb* contribute to quantitative *Lep* expression as fine-tuners in a fat depot-specific manner. There are two possible functions of the upregulation of DNA methylation in hypertrophic adipocytes in eWAT. The higher DNA methylation observed in obesity either contributes to uncontrolled *Lep* expression, which is suppressed by another factor in the late stages of obesity (week 12 in DIO). Alternatively, DNA methylation acts as a counterregulatory mechanism to prevent overexpression of *Lep*, which is mostly inhibited by another factor during DIO progression (week 1–8 in DIO). However, there is clear evidence for the latter, explainable by the above discussed factors and the impaired dynamics of the observed DNA methylation pattern as discussed in the following.

DNA methylation in *Lep* enhancers was reversible in eWAT after a 10-day dietary intervention (Figure 3.17), and even more so after a prolonged dietary intervention (Figure 3.19). However, of the three responsive enhancer sites in eWAT, only the RS3 site was reversible to healthy, chow levels (Figure 3.19e). Consequently, although changes in DNA methylation are indeed reversible, there appears to be a certain "imprinting" effect on DNA methylation in the RS1 and RS2 sites. DNA methylation at these sites did not return to healthy control levels, even after the long-term intervention (Figure 3.19c–e). This suggests the counterregulatory role of DNA methylation: The switch from HFD to chow eliminates the additional factor that led to leptin overproduction, yet the "imprinted" DNA methylation pattern contributes to a disproportionate reduction in *Lep* expression. This reduction in *Lep* expression was observed in the diet-switch (HC) group after the long-term intervention (Figure 3.19b), supporting the counterregulatory function of DNA methylation. Notably, similar observations have been made in humans, where weight reduction resulted in excessively reduced leptin levels [5, 129, 130]. Due to the reduced anorexigenic effects of leptin, the counterregulatory DNA methylation pattern that reduces *Lep* expression could be responsible for weight regain. Weight regain after weight loss is evolutionary favorable to protect against periods of starvation and maintain weight [130]. Therefore, the rise in *Lep* enhancer DNA methylation suppressing *Lep* expression could act as a compensatory mechanism to counteract the evolutionary unfavorable weight loss. This hypothesis is further supported by observations in VSG mice. VSG mice still exhibited high levels of DNA methylation (Figure 3.22), despite showing a responsive form of the DNA methylation pattern comparable to healthy controls, as discussed in section 4.1.2 . These high levels did not reverse to lean control levels, which could be a reason why the mice regained weight 35 days after VSG.

Metformin, a biguanide compound, is commonly prescribed as a primary therapy for type 2 diabetes [284]. In addition to its primary action on the liver, metformin acts on adipose tissue,

suppressing inflammation, improving insulin sensitivity, and modulating fatty acid metabolism [284]–[287]. Furthermore, it has been proposed that metformin may influence DNA methylation through AMPK-mediated reduction of DNMT1 and by enhancing the activity of S-adenosylhomocystein hydrolase, an inhibitor of DNNMT1 [288]. Treatment of DIO mice with metformin did not successfully reduce weight, fat mass and *Lep* enhancer DNA methylation (Figure 3.20a, b and Figure 3.21c–e). The treatment even led to a slight increase in *Lep* expression (Figure 3.21a), which, however, was not mirrored in the circulating leptin levels (Figure 3.21b). This is in contrast to previous studies reporting weight reduction and concomitant reduction in leptin [285, 289] and even restoration of leptin sensitivity [290]. However, observations of an improvement in liver triglycerides [185] and an improvement in glucose tolerance (Figure 3.20c–e) indicate a successful treatment with metformin in the mouse cohort studied in this thesis. Most likely, the reduction in leptin observed in other studies might have been induced primarily by the reduction in weight and fat mass rather than by the direct effects of metformin on *Lep* enhancer DNA methylation and *Lep* expression.

Overall, the data indicate an impaired reversibility of the epigenetically reprogrammed *Lep* enhancer DNA methylation pattern. They further suggest that the fine-tuning mechanism of DNA methylation is a putative counterregulatory mechanism against overshooting *Lep* expression, at least for the RS1 and RS3 sites (see Figure 4.1). However, this mechanism to remain leptin sensitive is bypassed in obesity.

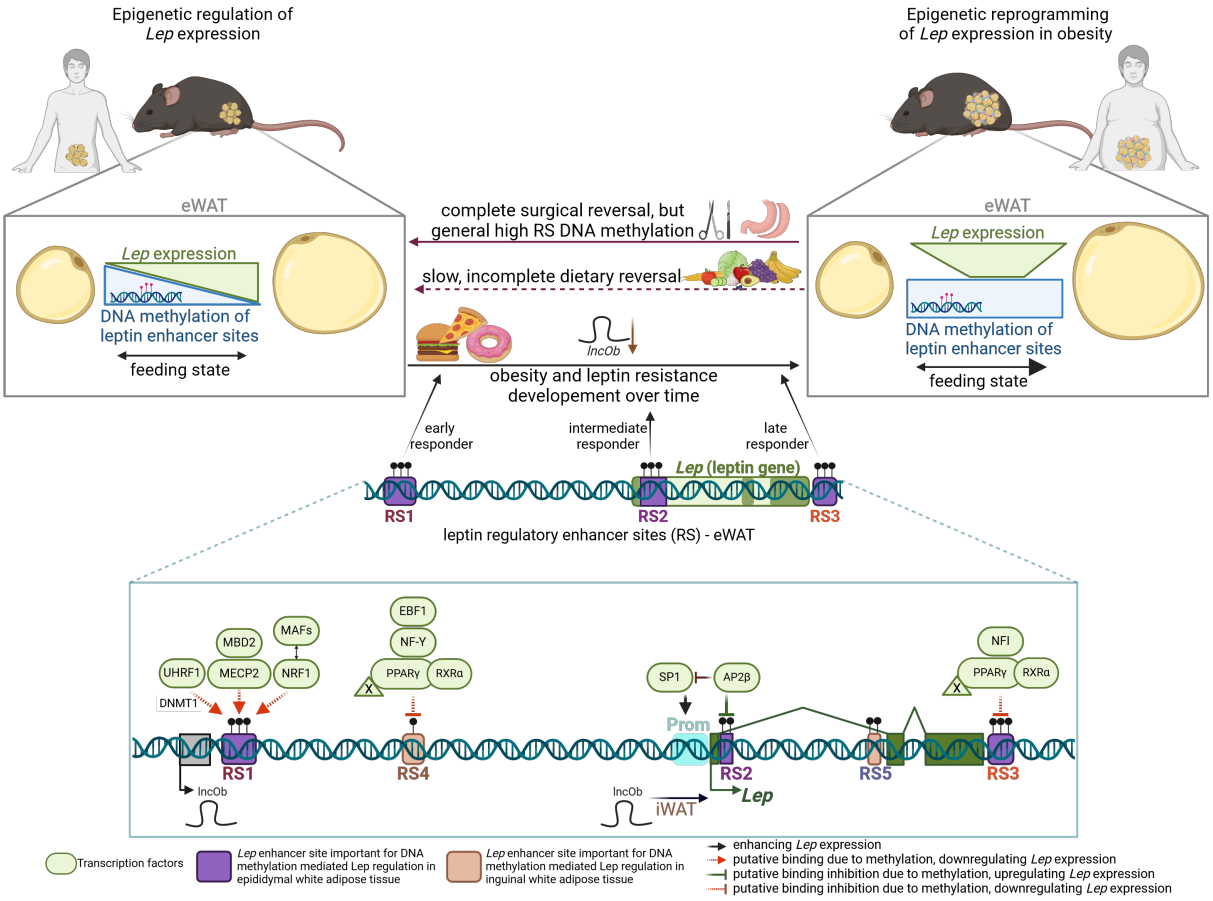

Figure 4.1.: Summary illustration of the key findings of this work in the upper part with suggested mechanisms for the *Lep* enhancer DNA methylation mediated regulation of *Lep* expression as counter-regulation in obesity in the lower part.

4.5. Epigenetic regulation of leptin as therapeutic approach in obesity treatment

With recent approval of the effective weight-lowering dual GIP/GLP-1 agonist for obesity treatment [120], there may be a perception that the urgent need for weight reduction interventions has diminished. However, alongside the prevention of obesity development, the sustainability of weight loss remains a critical concern. Weight regain was observed after discontinuation of these agonists [128], underscoring the importance of sustainable weight loss interventions. Understanding the intricate adipocyte-specific quantitative regulation of *Lep* expression could offer valuable insights in this regard. Leptin cannot exert its anorexigenic effect in obesity due to resistance to leptin. As the data presented here show, leptin is regulated through DNA methylation patterns that counterregulate in part the obesity-induced *Lep* overexpression. As mentioned above, the reduced reversibility of the *Lep* enhancer DNA methylation pattern works as a compensatory mechanism to counteract the evolutionary unfavorable weight loss. Elevating the impaired dynamics of DNA methylation in RS1 and RS3, effectively reversing them to healthy, lean levels, along with restoring *lncOb* expression, could potentially mitigate the negative surge of leptin and prevent weight relapse after weight loss. Previous studies investigating leptin replacement therapy after weight loss observed normalization of energy expenditure and sympathetic nerve tone, indicating the successful restoration of energy homeostasis to healthy, lean levels [291, 292]. In contrast to leptin replacement therapy, targeting *Lep* enhancer DNA methylation, particularly in sites such as RS1 and RS3, could present a novel approach to normalizing leptin levels in VAT. This approach offers a more endogenous and sustainable alternative to external leptin administration. However, further research is required to fully understand the regulation of *LEP* expression in humans (Figure 3.8), as only limited data from lean individuals were available and differences in the human fat depot were not explored within the scope of this work.

Interestingly, leptin levels in obesity were predictive of the outcome of weight-lowering therapies. Individuals with higher leptin levels were less responsive to weight lowering therapy and plasma leptin adjusted for fat mass was negatively correlated with the amount of weight loss [124, 125, 293]. This is consistent with research indicating that decreasing leptin levels through genetic or pharmacological approaches can reverse leptin resistance, ultimately resulting in leptin resensitization in obesity. Leptin resensitization led to a high-fat-diet induced weight gain arrest and even weight reduction, underlining the beneficial effect of reducing leptin levels to overcome leptin resistance [126, 127]. Notably, leptin levels might determine why some individuals respond to dietary or pharmacological weight loss interventions while others do not. Further research on these weight loss responders and non-responders could provide valuable insight into the underlying DNA methylation pattern of *Lep* enhancer sites. The level of *lncOb* might be an additional predictor of the responsiveness to weight loss, as a polymorphism in *lncOb* (rs10487505) was associated with leptin levels [195, 294]. Alteration of the DNA methylation pattern in obesity, particularly at the RS2 site binding the putative inhibitor AP2β, could potentially enable the resensitization to leptin. This approach could even stop the detrimental cycle of increasing leptin

levels, exacerbating leptin resistance in turn leading to further increases in leptin levels by diminishing the anorexigenic response in the brain. Thus, the increase in leptin with concomitant increase in weight and leptin resistance could be limited early in overweight, preventing obesity progression.

Although drugs targeting epigenetics, such as DNMT1 inhibitors, are already available in cancer treatment [295], challenges arise to the application of epigenetic drugs due to concerns about toxicity, likely caused by the lack of specificity [296]. As epigenetics is essential for functions such as cell differentiation, small unspecific effects when targeting DNMTs or TETs could lead to severe disturbances in physiology. In this regard, recent advances in the engineering of dCas9 fusion proteins with KRAB, DNMT3L, or DNMT3A indicated promising site-specific transcriptional repression [297]. Similarly, attaching TET1 to dCas9 demonstrated the potential to reactivate silenced genes in human induced pluripotent stem cells and mouse brain [298]. However, effective delivery of these systems must be tissue-specific and, more importantly, fat depot-specific, requiring a complete understanding of the fine-tuning mechanisms of leptin regulation before considering epigenetic modifications of *Lep* expression as a therapeutic target.

5. Conclusion

This doctoral thesis aimed to elucidate the epigenetic mechanisms that regulate quantitative *Lep* expression in adipocytes in relation to the fat mass. The findings provide two epigenetic mechanisms of *Lep* regulation. The DNA methylation in *Lep* enhancer sites acts as a fine-tuner for *Lep* expression in an obesogenic-dependent manner, likely through the orchestration of transcription factor binding. Furthermore, DNA methylation in *Lep* enhancer sites is regulated by the size of the adipocyte in epididymal adipose tissue in leanness and is reprogrammed in hypertrophic adipocytes in obesity. This reprogramming is a putative counterregulatory mechanism against excessive leptin production and the subsequent development of leptin resistance in obesity, which, however, is bypassed in the development and progression of obesity. The epigenetic regulator *lncOb* is a responsive, although not the sole gatekeeper of quantitative *Lep* expression regulation, with particular importance for *Lep* expression in inguinal white adipose tissue.

The fat depot-specific regulation of *Lep* plays a critical role in the overshooting *Lep* production observed in obesity, with distinct DNA methylation patterns identified at five *Lep* enhancer sites between iWAT and eWAT. Understanding the dynamics of epigenetic reprogramming in hypertrophic adipocytes could pave the way for novel therapeutic strategies that mitigate unregulated leptin levels and avoid the adverse metabolic consequences of leptin resistance. Furthermore, restoring endogenous leptin levels after weight loss intervention as a therapeutic strategy could contribute to the sustainability of weight loss. This doctoral thesis offers the foundation for understanding this complex interaction between adipocyte size, fat depot-specificity, and epigenetic *Lep* expression regulation, revealing how this interplay leads to leptin dysregulation in obesity.

References

[1] Zhang, Y., Proenca, R., Maffei, M., Barone, M., Leopold, L., and Friedman, J. M. (1994). Positional cloning of the mouse obese gene and its human homologue. *Nature*.

[2] Considine, R. V., Sinha, M. K., Heiman, M. L., Kriauciunas, A., Stephens, T. W., Nyce, M. R., et al. (1996). Serum Immunoreactive-Leptin Concentrations in Normal-Weight and Obese Humans. *New England Journal of Medicine* 334.5, pp. 292–295.

[3] Ostlund, R. E., Yang, J. W., Klein, S., and Gingerich, R. (1996). Relation between plasma leptin concentration and body fat, gender, diet, age, and metabolic covariates. *The Journal of Clinical Endocrinology & Metabolism* 81.11, pp. 3909–3913.

[4] Frederich, R. C., Hamann, A., Anderson, S., Löllmann, B., Lowell, B. B., and Flier, J. S. (1995). Leptin levels reflect body lipid content in mice: Evidence for diet-induced resistance to leptin action. *Nature Medicine* 1.12, pp. 1311–1314.

[5] Maffei, M. and Giordano, A. (2022). Leptin, the brain and energy homeostasis: From an apparently simple to a highly complex neuronal system. *Reviews in Endocrine and Metabolic Disorders* 23.1, pp. 87–101.

[6] Cowley, M. A., Smart, J. L., Rubinstein, M., Cerdán, M. G., Diano, S., Horvath, T. L., Cone, R. D., and Low, M. J. (2001). Leptin activates anorexigenic POMC neurons through a neural network in the arcuate nucleus. *Nature* 411.6836, pp. 480–484.

[7] Pinto, S., Roseberry, A. G., Liu, H., Diano, S., Shanabrough, M., Cai, X., Friedman, J. M., and Horvath, T. L. (2004). Rapid Rewiring of Arcuate Nucleus Feeding Circuits by Leptin. *Science* 304.5667, pp. 110–115.

[8] Yang, Y. K., Thompson, D. A., Dickinson, C. J., Wilken, J., Barsh, G. S., Kent, S. B., and Gantz, I. (1999). Characterization of Agouti-related protein binding to melanocortin receptors. *Molecular Endocrinology* 13.1, pp. 148–155.

[9] Park, H. K. and Ahima, R. S. (2015). Physiology of leptin: energy homeostasis, neuroendocrine function and metabolism. *Metabolism* 64.1, pp. 24–34.

[10] Berglund, E. D., Vianna, C. R., Donato, J., Kim, M. H., Chuang, J. C., Lee, C. E., et al. (2012). Direct leptin action on POMC neurons regulates glucose homeostasis and hepatic insulin sensitivity in mice. *The Journal of Clinical Investigation* 122.3, pp. 1000–1009.

[11] Wang, M. Y., Chen, L., Clark, G. O., Lee, Y., Stevens, R. D., Ilkayeva, O. R., et al. (2010). Leptin therapy in insulin-deficient type I diabetes. *Proceedings of the National Academy of Sciences of the United States of America* 107.11, pp. 4813–4819.

[12] Roman, E. A., Reis, D., Romanatto, T., Maimoni, D., Ferreira, E. A., Santos, G. A., Torsoni, A. S., Velloso, L. A., and Torsoni, M. A. (2010). Central leptin action improves skeletal muscle AKT, AMPK, and PGC1α activation by hypothalamic PI3K-dependent mechanism. *Molecular and Cellular Endocrinology* 314.1, pp. 62–69.

[13] Childs, G. V., Odle, A. K., MacNicol, M. C., and MacNicol, A. M. (2021). The Importance of Leptin to Reproduction. *Endocrinology* 162.2, pp. 1–18.

[14] Padilla, S. L., Qiu, J., Nestor, C. C., Zhang, C., Smith, A. W., Whiddon, B. B., Rønnekleiv, O. K., Kelly, M. J., and Palmiter, R. D. (2017). AgRP to Kiss1 neuron signaling links nutritional state and fertility. *Proceedings of the National Academy of Sciences of the United States of America* 114.9, pp. 2413–2418.

[15] Martins, A. D., Moreira, A. C., Sá, R., Monteiro, M. P., Sousa, M., Carvalho, R. A., Silva, B. M., Oliveira, P. F., and Alves, M. G. (2015). Leptin modulates human Sertoli cells acetate production and glycolytic profile: a novel mechanism of obesity-induced male infertility? *Biochimica et Biophysica Acta (BBA) - Molecular Basis of Disease* 1852.9, pp. 1824–1832.

[16] Scarpace, P. J. and Matheny, M. (1998). Leptin induction of UCP1 gene expression is dependent on sympathetic innervation. *American Journal of Physiology - Endocrinology and Metabolism* 275.2 38-2.

[17] Martínez-Sánchez, N. (2020). There and Back Again: Leptin Actions in White Adipose Tissue. *International Journal of Molecular Sciences* 21.17, pp. 1–26.

[18] Koltes, D. A., Spurlock, M. E., and Spurlock, D. M. (2017). Adipose triglyceride lipase protein abundance and translocation to the lipid droplet increase during leptin-induced lipolysis in bovine adipocytes. *Domestic Animal Endocrinology* 61, pp. 62–76.

[19] Zeng, W., Pirzgalska, R. M., Pereira, M. M., Kubasova, N., Barateiro, A., Seixas, E., et al. (2015). Sympathetic Neuro-adipose Connections Mediate Leptin-Driven Lipolysis. *Cell* 163.1, pp. 84–94.

[20] William, W. N., Ceddia, R. B., and Curi, R. (2002). Leptin controls the fate of fatty acids in isolated rat white adipocytes. *Journal of Endocrinology* 175.3, pp. 735–744.

[21] Bai, Y., Zhang, S., Kim, K. S., Lee, J. K., and Kim, K. H. (1996). Obese Gene Expression Alters the Ability of 30A5 Preadipocytes to Respond to Lipogenic Hormones. *Journal of Biological Chemistry* 271.24, pp. 13939–13942.

[22] Wagoner, B., Hausman, D. B., and Harris, R. B. (2006). Direct and indirect effects of leptin on preadipocyte proliferation and differentiation. *American Journal of Physiology - Regulatory Integrative and Comparative Physiology* 290.6, pp. 1557–1564.

[23] Gullicksen, P. S., Hausman, D. B., Dean, R. G., Hartzell, D. L., and Baile, C. A. (2003). Adipose tissue cellularity and apoptosis after intracerebroventricular injections of leptin and 21 days of recovery in rats. *International Journal of Obesity* 27.3, pp. 302–312.

[24] Plum, L., Rother, E., Münzberg, H., Wunderlich, F. T., Morgan, D. A., Hampel, B., et al. (2007). Enhanced Leptin-Stimulated Pi3k Activation in the CNS Promotes White Adipose Tissue Transdifferentiation. *Cell Metabolism* 6.6, pp. 431–445.

[25] Souza-Almeida, G., Palhinha, L., Liechocki, S., Silva Pereira, J. A. da, Reis, P. A., Dib, P. R. B., et al. (2021). Peripheral leptin signaling persists in innate immune cells during diet-induced obesity. *Journal of Leukocyte Biology* 109.6, pp. 1131–1138.

[26] Kiernan, K. and MacIver, N. J. (2021). The Role of the Adipokine Leptin in Immune Cell Function in Health and Disease. *Frontiers in Immunology* 11, p. 622468.

[27] Monteiro, L., Pereira, J. A. d. S., Palhinha, L., and Moraes-Vieira, P. M. M. (2019). Leptin in the regulation of the immunometabolism of adipose tissue-macrophages. *Journal of Leukocyte Biology* 106.3, pp. 703–716.

[28] Tartaglia, L. A., Dembski, M., Weng, X., Deng, N., Culpepper, J., Devos, R., et al. (1995). Identification and Expression Cloning of a Leptin Receptor, OB-R. *Cell* 83, pp. 1263–1271.

[29] Chen, H., Charlat, O., Tartaglia, L. A., Woolf, E. A., Weng, X., Ellis, S. J., et al. (1996). Evidence That the Diabetes Gene Encodes the Leptin Receptor: Identification of a Mutation in the Leptin Receptor Gene in db/db Mice. *Cell* 84.3, pp. 491–495.

[30] Tartaglia, L. A. (1997). The Leptin Receptor. *Journal of Biological Chemistry* 272.10, pp. 6093–6096.

[31] Moreno-Aliaga, M. J., Swarbrick, M. M., Lorente-Cebrián, S., Stanhope, K. L., Havel, P. J., and Martínez, J. A. (2007). Sp1-mediated transcription is involved in the induction of leptin by insulin-stimulated glucose metabolism. *Journal of Molecular Endocrinology* 38.5, pp. 537–546.

[32] Uhlén, M., Fagerberg, L., Hallström, B. M., Lindskog, C., Oksvold, P., Mardinoglu, A., et al. (2015). Tissue-based map of the human proteome. *Science* 347.6220.

[33] Vaisse, C., Halaas, J. L., Horvath, C. M., Dernell, J., Stoffel, M., and Friedman, J. M. (1996). Leptin activation of Stat3 in the hypothalamus of wild–type and ob/ob mice but not db/db mice. *Nature Genetics* 14.1, pp. 95–97.

[34] Münzberg, H., Huo, L., Nillni, E. A., Hollenberg, A. N., and Bjørbæk, C. (2003). Role of Signal Transducer and Activator of Transcription 3 in Regulation of Hypothalamic Proopiomelanocortin Gene Expression by Leptin. *Endocrinology* 144.5, pp. 2121–2131.

[35] Dunn, S. L., Björnholm, M., Bates, S. H., Chen, Z., Seifert, M., and Myers, M. G. (2005). Feedback Inhibition of Leptin Receptor/Jak2 Signaling via Tyr1138 of the Leptin Receptor and Suppressor of Cytokine Signaling 3. *Molecular Endocrinology* 19.4, pp. 925–938.

[36] Bence, K. K., Delibegovic, M., Xue, B., Gorgun, C. Z., Hotamisligil, G. S., Neel, B. G., and Kahn, B. B. (2006). Neuronal PTP1B regulates body weight, adiposity and leptin action. *Nature Medicine* 12.8, pp. 917–924.

[37] Zabolotny, J. M., Bence-Hanulec, K. K., Stricker-Krongrad, A., Haj, F., Wang, Y., Minokoshi, Y., et al. (2002). PTP1B Regulates Leptin Signal Transduction In Vivo. *Developmental Cell* 2.4, pp. 489–495.

[38] Lee, J. Y., Muenzberg, H., Gavrilova, O., Reed, J. A., Berryman, D., Villanueva, E. C., et al. (2008). Loss of Cytokine-STAT5 Signaling in the CNS and Pituitary Gland Alters Energy Balance and Leads to Obesity. *PLOS ONE* 3.2, e1639.

[39] Mütze, J., Roth, J., Gerstberger, R., and Hübschle, T. (2007). Nuclear translocation of the transcription factor STAT5 in the rat brain after systemic leptin administration. *Neuroscience Letters* 417.3, pp. 286–291.

[40] Niswender, K. D., Morton, G. J., Stearns, W. H., Rhodes, C. J., Myers, M. G., and Schwartz, M. W. (2001). Key enzyme in leptin-induced anorexia. *Nature* 413.6858, pp. 794–795.

[41] Schultze, S. M., Hemmings, B. A., Niessen, M., and Tschopp, O. (2012). PI3K/AKT, MAPK and AMPK signalling: protein kinases in glucose homeostasis. *Expert Reviews in Molecular Medicine* 14, e1.

[42] Zhao, A. Z., Huan, J. N., Gupta, S., Pal, R., and Sahu, A. (2002). A phosphatidylinositol 3-kinase–phosphodiesterase 3B–cyclic AMP pathway in hypothalamic action of leptin on feeding. *Nature Neuroscience* 5.8, pp. 727–728.

[43] Ma, W., Fuentes, G., Shi, X., Verma, C., Radda, G. K., and Han, W. (2015). FoxO1 negatively regulates leptin-induced POMC transcription through its direct interaction with STAT3. *Biochemical Journal* 466.2, pp. 291–298.

[44] Minokoshi, Y., Alquier, T., Furukawa, H., Kim, Y. B., Lee, A., Xue, B., et al. (2004). AMP-kinase regulates food intake by responding to hormonal and nutrient signals in the hypothalamus. *Nature* 428.6982, pp. 569–574.

[45] Tanida, M., Yamamoto, N., Shibamoto, T., and Rahmouni, K. (2013). Involvement of Hypothalamic AMP-Activated Protein Kinase in Leptin-Induced Sympathetic Nerve Activation. *PLOS ONE* 8.2, e56660.

[46] Rahmouni, K., Sigmund, C. D., Haynes, W. G., and Mark, A. L. (2009). Hypothalamic ERK Mediates the Anorectic and Thermogenic Sympathetic Effects of Leptin. *Diabetes* 58.3, pp. 536–542.

[47] Sakers, A., De Siqueira, M. K., Seale, P., and Villanueva, C. J. (2022). Adipose-tissue plasticity in health and disease. *Cell* 185.3, pp. 419–446.

[48] Spalding, K. L., Arner, E., Westermark, P. O., Bernard, S., Buchholz, B. A., Bergmann, O., et al. (2008). Dynamics of fat cell turnover in humans. *Nature* 453.7196, pp. 783–787.

[49] Bilal, M., Nawaz, A., Kado, T., Aslam, M. R., Igarashi, Y., Nishimura, A., et al. (2021). Fate of adipocyte progenitors during adipogenesis in mice fed a high-fat diet. *Molecular Metabolism* 54, p. 101328.

[50] Vishvanath, L. and Gupta, R. K. (2019). Contribution of adipogenesis to healthy adipose tissue expansion in obesity. *The Journal of Clinical Investigation* 129.10, pp. 4022–4031.

[51] Ibrahim, M. M. (2010). Subcutaneous and visceral adipose tissue: structural and functional differences. *Obesity Reviews* 11.1, pp. 11–18.

[52] Poret, J. M., Souza-Smith, F., Marcell, S. J., Gaudet, D. A., Tzeng, T. H., Braymer, H. D., Harrison-Bernard, L. M., and Primeaux, S. D. (2018). High fat diet consumption differentially affects adipose tissue inflammation and adipocyte size in obesity-prone and obesity-resistant rats. *International journal of obesity* 42.3, p. 535.

[53] Suárez-Cuenca, J. A., De La Peña-Sosa, G., De La Vega-Moreno, K., Banderas-Lares, D. Z., Salamanca-García, M., Martínez-Hernández, J. E., et al. (2021). Enlarged adipocytes from subcutaneous vs. visceral adipose tissue differentially contribute to metabolic dysfunction and atherogenic risk of patients with obesity. *Scientific Reports* 11.1, p. 1831.

[54] Hansson, B., Morén, B., Fryklund, C., Vliex, L., Wasserstrom, S., Albinsson, S., Berger, K., and Stenkula, K. G. (2019). Adipose cell size changes are associated with a drastic actin remodeling. *Scientific Reports* 9.1, pp. 1–14.

[55] Kalukula, Y., Stephens, A. D., Lammerding, J., and Gabriele, S. (2022). Mechanics and functional consequences of nuclear deformations. *Nature reviews. Molecular cell biology* 23.9, p. 583.

[56] Lustig, M., Gefen, A., and Benayahu, D. (2018). Adipogenesis and lipid production in adipocytes subjected to sustained tensile deformations and elevated glucose concentration: a living cell-scale model system of diabesity. *Biomechanics and Modeling in Mechanobiology* 17.3, pp. 903–913.

[57] Abuhattum, S., Kotzbeck, P., Schlüßler, R., Harger, A., Ariza de Schellenberger, A., Kim, K., et al. (2022). Adipose cells and tissues soften with lipid accumulation while in diabetes adipose tissue stiffens. *Scientific Reports* 12.1, pp. 1–17.

[58] Hagberg, C. E., Li, Q., Kutschke, M., Bhowmick, D., Kiss, E., Shabalina, I. G., et al. (2018). Flow Cytometry of Mouse and Human Adipocytes for the Analysis of Browning and Cellular Heterogeneity. *Cell Reports* 24.10, p. 2746.

[59] Guo, K. Y., Halo, P., Leibel, R. L., and Zhang, Y. (2004). Effects of obesity on the relationship of leptin mRNA expression and adipocyte size in anatomically distinct fat depots in mice. *American Journal of Physiology - Regulatory Integrative and Comparative Physiology* 287.1 56-1, pp. 112–119.

[60] Hube, F., Lietz, U., Igel, M., Jensen, P. B., Tornqvist, H., Joost, H. G., and Hauner, H. (1996). Difference in leptin mRNA levels between omental and subcutaneous abdominal adipose tissue from obese humans. *Hormone and Metabolic Research* 28.12, pp. 690–693.

[61] Russell, C. D., Petersen, R. N., Rao, S. P., Ricci, M. R., Prasad, A., Zhang, Y., Brolin, R. E., and Fried, S. K. (1998). Leptin expression in adipose tissue from obese humans:

Depot-specific regulation by insulin and dexamethasone. *American Journal of Physiology - Endocrinology and Metabolism* 275.3 38-3.

[62] Harmelen, V. V., Reynisdottir, S., Eriksson, P., Thörne, A., Hoffstedt, J., Lönnqvist, F., and Arner, P. (1998). Leptin secretion from subcutaneous and visceral adipose tissue in women. *Diabetes* 47.6, pp. 913–917.

[63] Zhang, Y., Zitsman, J. L., Hou, J., Fennoy, I., Guo, K., Feinberg, J., and Leibel, R. L. (2014). Fat cell size and adipokine expression in relation to gender, depot and metabolic risk factors in morbidly obese adolescents. *Obesity* 22.3, p. 691.

[64] Assinder, S. J. and Boumelhem, B. B. (2021). Oxytocin stimulates lipolysis, prostaglandin E2 synthesis, and leptin secretion in 3T3-L1 adipocytes. *Molecular and Cellular Endocrinology* 534, p. 111381.

[65] Cammisotto, P. G., Gélinas, Y., Deshaies, Y., and Bukowiecki, L. J. (2005). Regulation of leptin secretion from white adipocytes by insulin, glycolytic substrates, and amino acids. *American Journal of Physiology - Endocrinology and Metabolism* 289.1 52-1, pp. 166–171.

[66] Egmond, L. T. van, Meth, E. M., Engström, J., Ilemosoglou, M., Keller, J. A., Vogel, H., and Benedict, C. (2023). Effects of acute sleep loss on leptin, ghrelin, and adiponectin in adults with healthy weight and obesity: A laboratory study. *Obesity* 31.3, pp. 635–641.

[67] Ricci, M. R., Lee, M. J., Russell, C. D., Wang, Y., Sullivan, S., Schneider, S. H., Brolin, R. E., and Fried, S. K. (2005). Isoproterenol decreases leptin release from rat and human adipose tissue through posttranscriptional mechanisms. *American Journal of Physiology - Endocrinology and Metabolism* 288.4 51-4, pp. 798–804.

[68] Chakrabarti, P., Anno, T., Manning, B. D., Luo, Z., and Kandror, K. V. (2008). The Mammalian Target of Rapamycin Complex 1 Regulates Leptin Biosynthesis in Adipocytes at the Level of Translation: The Role of the 5‘-Untranslated Region in the Expression of Leptin Messenger Ribonucleic Acid. *Molecular Endocrinology* 22.10, pp. 2260–2267.

[69] Fried, S. K., Ricci, M. R., Russell, C. D., and Laferrère, B. (2000). Regulation of Leptin Production in Humans. *The Journal of Nutrition* 130.12, 3127S–3131S.

[70] Ricci, M. R., Fried, S. K., and Mittleman, K. D. (2000). Acute cold exposure decreases plasma leptin in women. *Metabolism* 49.4, pp. 421–423.

[71] Trayhurn, P., Duncan, J. S., and Rayner, D. V. (1995). Acute cold-induced suppression of ob (obese) gene expression in white adipose tissue of mice: mediation by the sympathetic system. *Biochemical Journal* 311.3, pp. 729–733.

[72] Caron, A., Lee, S., Elmquist, J. K., and Gautron, L. (2018). Leptin and brain-adipose crosstalks. *Nature Reviews Neuroscience* 19.3, pp. 153–165.

[73] Saladin, R., De Vos, P., Guerre-Millot, M., Leturque, A., Girard, J., Staels, B., and Auwerx, J. (1995). Transient increase in obese gene expression after food intake or insulin administration. *Nature* 377.6549, pp. 527–528.

[74] Marques-Oliveira, G. H., Silva, T. M., Lima, W. G., Valadares, H. M. S., and Chaves, V. E. (2018). Insulin as a hormone regulator of the synthesis and release of leptin by white adipose tissue. *Peptides* 106, pp. 49–58.

[75] Wang, B. and Trayhurn, P. (2006). Acute and prolonged effects of TNF-α on the expression and secretion of inflammation-related adipokines by human adipocytes differentiated in culture. *Pflugers Archiv European Journal of Physiology* 452.4, pp. 418–427.

[76] Trujillo, M. E., Sullivan, S., Harten, I., Schneider, S. H., Greenberg, A. S., and Fried, S. K. (2004). Interleukin-6 Regulates Human Adipose Tissue Lipid Metabolism and Leptin Production in Vitro. *The Journal of Clinical Endocrinology & Metabolism* 89.11, pp. 5577–5582.

[77] Lee, M. J. and Fried, S. K. (2009). Integration of hormonal and nutrient signals that regulate leptin synthesis and secretion. *American Journal of Physiology - Endocrinology and Metabolism* 296.6, E1230.

[78] Murakami, T., Iida, M., and Shima, K. (1995). Dexamethasone Regulates Obese Expression in Isolated Rat Adipocytes. *Biochemical and Biophysical Research Communications* 214.3, pp. 1260–1267.

[79] Lee, M. J., Wang, Y., Ricci, M. R., Sullivan, S., Russell, C. D., and Fried, S. K. (2007). Acute and chronic regulation of leptin synthesis, storage, and secretion by insulin and dexamethasone in human adipose tissue. *American Journal of Physiology - Endocrinology and Metabolism* 292.3, pp. 858–864.

[80] Halleux, C. M., Servais, I., Reul, B. A., Detry, R., and Brichard, S. M. (1998). Multihormonal Control of ob Gene Expression and Leptin Secretion from Cultured Human Visceral Adipose Tissue: Increased Responsiveness to Glucocorticoids in Obesity. *The Journal of Clinical Endocrinology & Metabolism* 83.3, pp. 902–910.

[81] Newcomer, J. W., Selke, G., Melson, A. K., Gross, J., Vogler, G. P., and Dagogo-Jack, S. (1998). Dose-Dependent Cortisol-Induced Increases in Plasma Leptin Concentration in Healthy Humans. *Archives of General Psychiatry* 55.11, pp. 995–1000.

[82] De La Brousse, F. C., Shan, B., and Chen, J. L. (1996). Identification of the promoter of the mouse obese gene. *Proceedings of the National Academy of Sciences of the United States of America* 93.9, p. 4096.

[83] Gong, D. W., Bi, S., Pratley, R. E., and Weintraub, B. D. (1996). Genomic Structure and Promoter Analysis of the Human obese Gene. *Journal of Biological Chemistry* 271.8, pp. 3971–3974.

[84] Mohtar, O., Ozdemir, C., Roy, D., Shantaram, D., Emili, A., and Kandror, K. V. (2019). Egr1 mediates the effect of insulin on leptin transcription in adipocytes. *The Journal of Biological Chemistry* 294.15, p. 5784.

[85] Meriin, A. B., Zaarur, N., Roy, D., and Kandror, K. V. (2022). Egr1 plays a major role in the transcriptional response of white adipocytes to insulin and environmental cues. *Frontiers in Cell and Developmental Biology* 10: 1003030.

[86] He, Y., Chen, H., Quon, M. J., and Reitman, M. (1995). The Mouse obese Gene: Genomic organization, promoter activity, and activation by CAAT / Enhancer-binding protein α. *Journal of Biological Chemistry* 270.48, pp. 28887–28891.

[87] Kim, J. B., Sarraf, P., Wright, M., Yao, K. M., Mueller, E., Solanes, G., Lowell, B. B., and Spiegelman, B. M. (1998). Nutritional and insulin regulation of fatty acid synthetase and leptin gene expression through ADD1/SREBP1. *Journal of Clinical Investigation* 101.1, p. 1.

[88] Mason, M. M., He, Y., Chen, H., Quon, M. J., and Reitman, M. (1998). Regulation of Leptin Promoter Function by Sp1, C/EBP, and a Novel Factor. *Endocrinology* 139.3, pp. 1013–1022.

[89] Fuke, T., Yoshizaki, T., Kondo, M., Morino, K., Obata, T., Ugi, S., Nishio, Y., Maeda, S., Kashiwagi, A., and Maegawa, H. (2010). Transcription factor AP-2B inhibits expression and secretion of leptin, an insulin-sensitizing hormone, in 3T3-L1 adipocytes. *International Journal of Obesity* 34.4, pp. 670–678.

[90] Chen, X. L., Hartzell, D. L., McGraw, R. A., Hausman, G. J., and Dean, R. G. (1999). Analysis of a 762-bp Proximal Leptin Promoter to Drive and Control Regulation of Transgene Expression of Growth Hormone Receptor in Mice. *Biochemical and Biophysical Research Communications* 262.1, pp. 187–192.

[91] Hwang, C. S., Mandrup, S., MacDougald, O. A., Geiman, D. E., and Lane, M. D. (1996). Transcriptional activation of the mouse obese (ob) gene by CCAAT/enhancer binding protein alpha. *Proceedings of the National Academy of Sciences of the United States of America* 93.2, p. 873.

[92] Zhang, Y., Dallner, O. S., Nakadai, T., Fayzikhodjaeva, G., Lu, Y.-H., Lazar, M., Roeder, R., and Friedman, J. (2018). A non-canonical-PPARγ/RXRα-binding sequence regulates leptin expression in response to changes in adipose tissue mass. *Proceedings of the National Academy of Sciences of the USA*, p. 325480.

[93] Dallner, O. S., Marinis, J. M., Lu, Y. H., Birsoy, K., Werner, E., Fayzikhodjaeva, G., et al. (2019). Dysregulation of a long noncoding RNA reduces leptin leading to a leptin-responsive form of obesity. *Nature Medicine* 25.3, pp. 507–516.

[94] Lu, Y. H., Dallner, O. S., Birsoy, K., Fayzikhodjaeva, G., and Friedman, J. M. (2015). Nuclear Factor-Y is an adipogenic factor that regulates leptin gene expression. *Molecular Metabolism* 4.5, pp. 392–405.

[95] Wrann, C. D., Eguchi, J., Bozec, A., Xu, Z., Mikkelsen, T., Gimble, J., Nave, H., Wagner, E. F., Ong, S. E., and Rosen, E. D. (2012). FOSL2 promotes leptin gene expression in human and mouse adipocytes. *The Journal of Clinical Investigation* 122.3, p. 1010.

[96] Hollenberg, A. N., Susulic, V. S., Madura, J. P., Zhang, B., Moller, D. E., Tontonoz, P., Sarraf, P., Spiegelman, B. M., and Lowell, B. B. (1997). Functional Antagonism between CCAAT/Enhancer Binding Protein-α and Peroxisome Proliferator-activated Receptor-γ on the Leptin Promoter. *Journal of Biological Chemistry* 272.8, pp. 5283–5290.

[97] Coleman, D. L. (1978). Obese and diabetes: Two mutant genes causing diabetes-obesity syndromes in mice. *Diabetologia* 14.3, pp. 141–148.

[98] Coleman, D. L. and Hummel, K. P. (1967). Studies with the mutation, diabetes, in the mouse. *Diabetologia* 3.2, pp. 238–248.

[99] Hellman, B. (1965). Studies in obese-hyperglycemic mice. *Annals of the New York Academy of Sciences* 131.1, pp. 541–558.

[100] Suriano, F., Vieira-Silva, S., Falony, G., Roumain, M., Paquot, A., Pelicaen, R., et al. (2021). Novel insights into the genetically obese (ob/ob) and diabetic (db/db) mice: two sides of the same coin. *Microbiome* 9.1, pp. 1–20.

[101] Giesbertz, P., Padberg, I., Rein, D., Ecker, J., Höfle, A. S., Spanier, B., and Daniel, H. (2015). Metabolite profiling in plasma and tissues of ob/ob and db/db mice identifies novel markers of obesity and type 2 diabetes. *Diabetologia* 58.9, pp. 2133–2143.

[102] Farooqi, I. S., Matarese, G., Lord, G. M., Keogh, J. M., Lawrence, E., Agwu, C., et al. (2002). Beneficial effects of leptin on obesity, T cell hyporesponsiveness, and neuroendocrine/metabolic dysfunction of human congenital leptin deficiency. *The Journal of Clinical Investigation* 110.8, p. 1093.

[103] Licinio, J., Caglayan, S., Ozata, M., Yildiz, B. O., De Miranda, P. B., O'Kirwan, F., et al. (2004). Phenotypic effects of leptin replacement on morbid obesity, diabetes mellitus, hypogonadism, and behavior in leptin-deficient adults. *Proceedings of the National Academy of Sciences of the United States of America* 101.13, pp. 4531–4536.

[104] Perakakis, N., Farr, O. M., and Mantzoros, C. S. (2021). Leptin in Leanness and Obesity: JACC State-of-the-Art Review. *Journal of the American College of Cardiology* 77.6, pp. 745–760.

[105] Lee, J. H., Chan, J. L., Sourlas, E., Raptopoulos, V., and Mantzoros, C. S. (2006). Recombinant Methionyl Human Leptin Therapy in Replacement Doses Improves Insulin Resistance and Metabolic Profile in Patients with Lipoatrophy and Metabolic Syndrome Induced by the Highly Active Antiretroviral Therapy. *The Journal of Clinical Endocrinology & Metabolism* 91.7, pp. 2605–2611.

[106] Lif, E., Rioglu, A., Ral, O., Laine, E., Uiz, R., Ndewelt, L. A., et al. (2002). Leptin-Replacement Therapy for Lipodystrophy. *New England Journal of Medicine* 346.8, pp. 570–578.

[107] McDuffie, J. R., Riggs, P. A., Calis, K. A., Freedman, R. J., Oral, E. A., DePaoli, A. M., and Yanovski, J. A. (2004). Effects of Exogenous Leptin on Satiety and Satiation in Patients with Lipodystrophy and Leptin Insufficiency. *The Journal of clinical endocrinology and metabolism* 89.9, p. 4258.

[108] Javor, E. D., Cochran, E. K., Musso, C., Young, J. R., DePaoli, A. M., and Gorden, P. (2005). Long-Term Efficacy of Leptin Replacement in Patients With Generalized Lipodystrophy. *Diabetes* 54.7, pp. 1994–2002.

[109] Brown, R. J., Oral, E. A., Cochran, E., Araújo-Vilar, D., Savage, D. B., Long, A., Fine, G., Salinardi, T., and Gorden, P. (2018). Long-term effectiveness and safety of metreleptin in the treatment of patients with generalized lipodystrophy. *Endocrine* 60.3, pp. 479–489.

[110] World Obesity Federation, World Obesity Atlas 2023 (2023). *https://data.worldobesity.org/publications/?cat=19*.

[111] Halaas, J. L., Boozer, C., Blair-West, J., Fidahusein, N., Denton, D. A., and Friedman, J. M. (1997). Physiological response to long-term peripheral and central leptin infusion in lean and obese mice. *Proceedings of the National Academy of Sciences of the United States of America* 94.16, pp. 8878–8883.

[112] Harrison, L., Schriever, S. C., Feuchtinger, A., Kyriakou, E., Baumann, P., Pfuhlmann, K., Messias, A. C., Walch, A., Tschöp, M. H., and Pfluger, P. T. (2019). Fluorescent blood–brain barrier tracing shows intact leptin transport in obese mice. *International Journal of Obesity* 43.6, p. 1305.

[113] Kleinert, M., Kotzbeck, P., Altendorfer-Kroath, T., Birngruber, T., Tschöp, M. H., and Clemmensen, C. (2018). Time-resolved hypothalamic open flow micro-perfusion reveals normal leptin transport across the blood–brain barrier in leptin resistant mice. *Molecular Metabolism* 13, pp. 77–82.

[114] Balland, E., Dam, J., Langlet, F., Caron, E., Steculorum, S., Messina, A., et al. (2014). Hypothalamic tanycytes are an ERK-gated conduit for leptin into the brain. *Cell Metabolism* 19.2, pp. 293–301.

[115] Prevot, V., Dehouck, B., Sharif, A., Ciofi, P., Giacobini, P., and Clasadonte, J. (2018). The Versatile Tanycyte: A Hypothalamic Integrator of Reproduction and Energy Metabolism. *Endocrine Reviews* 39.3, pp. 333–368.

[116] Martin, R. L., Perez, E., He, Y. J., Dawson, R., and Millard, W. J. (2000). Leptin resistance is associated with hypothalamic leptin receptor mRNA and protein downregulation. *Metabolism: Clinical and Experimental* 49.11, pp. 1479–1484.

[117] Howard, J. K., Cave, B. J., Oksanen, L. J., Tzameli, I., Bjoørbæk, C., and Flier, J. S. (2004). Enhanced leptin sensitivity and attenuation of diet-induced obesity in mice with haploinsufficiency of Socs3. *Nature Medicine* 10.7, pp. 734–738.

[118] Briancon, N., McNay, D. E., Maratos-Flier, E., and Flier, J. S. (2010). Combined Neural Inactivation of Suppressor of Cytokine Signaling-3 and Protein-Tyrosine Phosphatase-1B Reveals Additive, Synergistic, and Factor-Specific Roles in the Regulation of Body Energy Balance. *Diabetes* 59.12, pp. 3074–3084.

[119] Tsou, R. C., Zimmer, D. J., De Jonghe, B. C., and Bence, K. K. (2012). Deficiency of PTP1B in Leptin Receptor-Expressing Neurons Leads to Decreased Body Weight and Adiposity in Mice. *Endocrinology* 153.9, pp. 4227–4237.

[120] Mesquita, Y. L. L. de, Pera Calvi, I., Reis Marques, I., Almeida Cruz, S., Padrao, E. M. H., Carvalho, P. E. d. P., Silva, C. H. A. da, Cardoso, R., Moura, F. A., and Rafalskiy, V. V. (2023). Efficacy and safety of the dual GIP and GLP-1 receptor agonist tirzepatide for weight loss: a meta-analysis of randomized controlled trials. *International Journal of Obesity* 47.10, pp. 883–892.

[121] Heymsfield, S. B., Greenberg, A. S., Fujioka, K., Dixon, R. M., Kushner, R., Hunt, T., et al. (1999). Recombinant Leptin for Weight Loss in Obese and Lean Adults: A Randomized, Controlled, Dose-Escalation Trial. *JAMA* 282.16, pp. 1568–1575.

[122] Müller, T. D., Sullivan, L. M., Habegger, K., Yi, C. X., Kabra, D., Grant, E., et al. (2012). Restoration of leptin responsiveness in diet-induced obese mice using an optimized leptin analog in combination with exendin-4 or FGF21. *Journal of Peptide Science* 18.6, pp. 383–393.

[123] Quarta, C., Sánchez-Garrido, M. A., Tschöp, M. H., and Clemmensen, C. (2016). Renaissance of leptin for obesity therapy. *Diabetologia* 59.5, pp. 920–927.

[124] Kempf, K., Röhling, M., Banzer, W., Braumann, K. M., Halle, M., Schaller, N., et al. (2022). Early and Strong Leptin Reduction Is Predictive for Long-Term Weight Loss during High-Protein, Low-Glycaemic Meal Replacement—A Subanalysis of the Randomised-Controlled ACOORH Trial. *Nutrients* 14.12, p. 2537.

[125] Sen, A., Jen, K. L. C., and Djuric, Z. (2007). Baseline Leptin Levels Predict Change in Leptin Levels During Weight Loss in Obese Breast Cancer Survivors. *The Breast Journal* 13.2, pp. 180–186.

[126] Zhao, S., Li, N., Zhu, Y., Straub, L., Zhang, Z., Wang, M. Y., Zhu, Q., Kusminski, C. M., Elmquist, J. K., and Scherer, P. E. (2020). Partial leptin deficiency confers resistance to diet-induced obesity in mice. *Molecular Metabolism* 37, p. 100995.

[127] Zhao, S., Zhu, Y., Schultz, R. D., Li, N., He, Z., Zhang, Z., et al. (2019). Partial Leptin Reduction as an Insulin Sensitization and Weight Loss Strategy. *Cell Metabolism* 30.4, pp. 706–719.

[128] Aronne, L. J., Sattar, N., Horn, D. B., Bays, H. E., Wharton, S., Lin, W.-Y., et al. (2024). Continued Treatment With Tirzepatide for Maintenance of Weight Reduction in Adults With Obesity: The SURMOUNT-4 Randomized Clinical Trial. *JAMA* 331.1, pp. 38–48.

[129] Filozof, C. M., Murúa, C., Sanchez, M. P., Brailovsky, C., Perman, M., Gonzalez, C. D., and Ravussin, E. (2000). Low Plasma Leptin Concentration and Low Rates of Fat Oxidation in Weight-Stable Post-Obese Subjects. *Obesity Research* 8.3, pp. 205–210.

[130] Sumithran, P., Prendergast, L. A., Delbridge, E., Purcell, K., Shulkes, A., Kriketos, A., and Proietto, J. (2011). Long-Term Persistence of Hormonal Adaptations to Weight Loss. *New England Journal of Medicine* 365.17, pp. 1597–1604.

[131] Tibben, B. M. and Rothbart, S. B. (2023). Mechanisms of DNA Methylation Regulatory Function and Crosstalk with Histone Lysine Methylation. *Journal of Molecular Biology*, p. 168394.

[132] Kouzarides, T. (2007). Chromatin Modifications and Their Function. *Cell* 128.4, pp. 693–705.

[133] Butler, A. A., Webb, W. M., and Lubin, F. D. (2016). Regulatory RNAs and control of epigenetic mechanisms: expectations for cognition and cognitive dysfunction. *Epigenomics* 8.1, p. 135.

[134] Statello, L., Guo, C. J., Chen, L. L., and Huarte, M. (2020). Gene regulation by long non-coding RNAs and its biological functions. *Nature Reviews Molecular Cell Biology* 22.2, pp. 96–118.

[135] Alajem, A., Roth, H., Ratgauzer, S., Bavli, D., Motzik, A., Lahav, S., Peled, I., and Ram, O. (2021). DNA methylation patterns expose variations in enhancer-chromatin modifications during embryonic stem cell differentiation. *PLOS Genetics* 17.4, e1009498.

[136] Kirchner, H., Osler, M. E., Krook, A., and Zierath, J. R. (2013). Epigenetic flexibility in metabolic regulation: Disease cause and prevention? *Trends in Cell Biology* 23.5, pp. 203–209.

[137] Ling, C. and Rönn, T. (2019). Epigenetics in Human Obesity and Type 2 Diabetes. *Cell Metabolism* 29.5, p. 1028.

[138] King, S. E. and Skinner, M. K. (2020). Epigenetic Transgenerational Inheritance of Obesity Susceptibility. *Trends in endocrinology and metabolism: TEM* 31.7, p. 478.

[139] Bannister, A. J. and Kouzarides, T. (2011). Regulation of chromatin by histone modifications. *Cell Research* 21.3, pp. 381–395.

[140] Vakoc, C. R., Sachdeva, M. M., Wang, H., and Blobel, G. A. (2006). Profile of Histone Lysine Methylation across Transcribed Mammalian Chromatin. *Molecular and Cellular Biology* 26.24, p. 9185.

[141] Bartel, D. P. (2009). MicroRNAs: Target Recognition and Regulatory Functions. *Cell* 136.2, pp. 215–233.

[142] Gu, S. and Kay, M. A. (2010). How do miRNAs mediate translational repression? *Silence* 1.1, p. 11.

[143] Yoder, J. A., Soman, N. S., Verdine, G. L., and Bestor, T. H. (1997). DNA (cytosine-5)-methyltransferases in mouse cells and tissues. studies with a mechanism-based probe. *Journal of Molecular Biology* 270.3, pp. 385–395.

[144] Bestor, T. H. (2000). The DNA methyltransferases of mammals. *Human Molecular Genetics* 9.16, pp. 2395–2402.

[145] Okano, M., Xie, S., and Li, E. (1998). Cloning and characterization of a family of novel mammalian DNA (cytosine-5) methyltransferases. *Nature Genetics* 19.3, pp. 219–220.

[146] Hata, K., Okano, M., Lei, H., and Li, E. (2002). Dnmt3L cooperates with the Dnmt3 family of de novo DNA methyltransferases to establish maternal imprints in mice. *Development* 129.8, pp. 1983–1993.

[147] Tahiliani, M., Koh, K. P., Shen, Y., Pastor, W. A., Bandukwala, H., Brudno, Y., et al. (2009). Conversion of 5-Methylcytosine to 5-Hydroxymethylcytosine in Mammalian DNA by MLL Partner TET1. *Science* 324.5929, p. 930.

[148] Chen, Z. X. and Riggs, A. D. (2011). DNA Methylation and Demethylation in Mammals. *The Journal of Biological Chemistry* 286.21, p. 18347.

[149] He, Y. F., Li, B. Z., Li, Z., Liu, P., Wang, Y., Tang, Q., et al. (2011). Tet-Mediated Formation of 5-Carboxylcytosine and Its Excision by TDG in Mammalian DNA. *Science* 333.6047, p. 1303.

[150] Cortellino, S., Xu, J., Sannai, M., Moore, R., Caretti, E., Cigliano, A., et al. (2011). Thymine DNA Glycosylase Is Essential for Active DNA Demethylation by Linked Deamination - Base Excision Repair. *Cell* 146.1, p. 67.

[151] Moore, L. D., Le, T., and Fan, G. (2012). DNA Methylation and Its Basic Function. *Neuropsychopharmacology* 38.1, pp. 23–38.

[152] Saxonov, S., Berg, P., and Brutlag, D. L. (2006). A genome-wide analysis of CpG dinucleotides in the human genome distinguishes two distinct classes of promoters. *Proceedings of the National Academy of Sciences of the United States of America* 103.5, p. 1412.

[153] Shen, H. and Laird, P. W. (2013). Interplay between the Cancer Genome and Epigenome. *Cell* 153.1, pp. 38–55.

[154] Wutz, A., Smrzka, O. W., Schweifer, N., Schellander, K., Wagner, E. F., and Barlow, D. P. (1997). Imprinted expression of the Igf2r gene depends on an intronic CpG island. *Nature* 389.6652, pp. 745–749.

[155] Park, J., Lee, D. H., Ham, S., Oh, J., Noh, J. R., Lee, Y. K., et al. (2022). Targeted erasure of DNA methylation by TET3 drives adipogenic reprogramming and differentiation. *Nature metabolism* 4.7, pp. 918–931.

[156] Kaluscha, S., Domcke, S., Wirbelauer, C., Stadler, M. B., Durdu, S., Burger, L., and Schübeler, D. (2022). Evidence that direct inhibition of transcription factor binding is the prevailing mode of gene and repeat repression by DNA methylation. *Nature Genetics* 54.12, pp. 1895–1906.

[157] Maunakea, A. K., Nagarajan, R. P., Bilenky, M., Ballinger, T. J., Dsouza, C., Fouse, S. D., et al. (2010). Conserved Role of Intragenic DNA Methylation in Regulating Alternative Promoters. *Nature* 466.7303, p. 253.

[158] Jjingo, D., Conley, A. B., Yi, S. V., Lunyak, V. V., and King Jordan, I. (2012). On the presence and role of human gene-body DNA methylation. *Oncotarget* 3.4, p. 462.

[159] Shayevitch, R., Askayo, D., Keydar, I., and Ast, G. (2018). The importance of DNA methylation of exons on alternative splicing. *RNA* 24.10, pp. 1351–1362.

[160] Panigrahi, A. and O'Malley, B. W. (2021). Mechanisms of enhancer action: the known and the unknown. *Genome Biology* 22.1, pp. 1–30.

[161] Thurman, R. E., Rynes, E., Humbert, R., Vierstra, J., Maurano, M. T., Haugen, E., et al. (2012). The accessible chromatin landscape of the human genome. *Nature* 489.7414, p. 75.

[162] Héberlé, É. and Bardet, A. F. (2019). Sensitivity of transcription factors to DNA methylation. *Essays in Biochemistry* 63.6, p. 727.

[163] Fleischer, T., Tekpli, X., Mathelier, A., Wang, S., Nebdal, D., Dhakal, H. P., et al. (2017). DNA methylation at enhancers identifies distinct breast cancer lineages. *Nature Communications* 8.1, pp. 1–14.

[164] Kirchner, H., Sinha, I., Gao, H., Ruby, M. A., Schönke, M., Lindvall, J. M., et al. (2016). Altered DNA methylation of glycolytic and lipogenic genes in liver from obese and type 2 diabetic patients. *Molecular Metabolism* 5.3, pp. 171–183.

[165] Spruijt, C. G., Gnerlich, F., Smits, A. H., Pfaffeneder, T., Jansen, P. W., Bauer, C., et al. (2013). Dynamic readers for 5-(Hydroxy)methylcytosine and its oxidized derivatives. *Cell* 152.5, pp. 1146–1159.

[166] Hu, S., Wan, J., Su, Y., Song, Q., Zeng, Y., Nguyen, H. N., et al. (2013). DNA methylation presents distinct binding sites for human transcription factors. *eLife* 2.2, p. 726.

[167] Domcke, S., Bardet, A. F., Adrian Ginno, P., Hartl, D., Burger, L., and Schübeler, D. (2015). Competition between DNA methylation and transcription factors determines binding of NRF1. *Nature* 528.7583, pp. 575–579.

[168] Yin, Y., Morgunova, E., Jolma, A., Kaasinen, E., Sahu, B., Khund-Sayeed, S., et al. (2017). Impact of cytosine methylation on DNA binding specificities of human transcription factors. *Science* 356.6337.

[169] Kreibich, E. and Krebs, A. R. (2023). Relevance of DNA methylation at enhancers for the acquisition of cell identities. *FEBS Letters* 597.14, pp. 1805–1817.

[170] Kreibich, E., Kleinendorst, R., Barzaghi, G., Kaspar, S., and Krebs, A. R. (2023). Single-molecule footprinting identifies context-dependent regulation of enhancers by DNA methylation. *Molecular Cell* 83.5, pp. 787–802.

[171] Kribelbauer, J. F., Laptenko, O., Chen, S., Martini, G. D., Freed-Pastor, W. A., Prives, C., Mann, R. S., and Bussemaker, H. J. (2017). Quantitative analysis of the DNA methylation sensitivity of transcription factor complexes. *Cell reports* 19.11, p. 2383.

[172] Du, Q., Luu, P. L., Stirzaker, C., and Clark, S. J. (2015). Methyl-CpG-binding domain proteins: Readers of the epigenome. *Epigenomics* 7.6, pp. 1051–1073.

[173] Hendrich, B. and Bird, A. (1998). Identification and Characterization of a Family of Mammalian Methyl-CpG Binding Proteins. *Molecular and Cellular Biology* 18.11, p. 6538.

[174] Rasmussen, K. D. and Helin, K. (2016). Role of TET enzymes in DNA methylation, development, and cancer. *Genes & Development* 30.7, p. 733.

[175] Li, S. and Tollefsbol, T. O. (2021). DNA methylation methods: global DNA methylation and methylomic analyses. *Methods* 187, p. 28.

[176] Tost, J. and Gut, I. G. (2007). DNA methylation analysis by pyrosequencing. *Nature Protocols* 2.9, pp. 2265–2275.

[177] Mahmoud, A. M. (2022). An Overview of Epigenetics in Obesity: The Role of Lifestyle and Therapeutic Interventions. *International Journal of Molecular Sciences* 23.3.

[178] Manikkam, M., Tracey, R., Guerrero-Bosagna, C., and Skinner, M. K. (2013). Plastics Derived Endocrine Disruptors (BPA, DEHP and DBP) Induce Epigenetic Transgenerational Inheritance of Obesity, Reproductive Disease and Sperm Epimutations. *PLoS ONE* 8.1, p. 55387.

[179] Barrès, R., Yan, J., Egan, B., Treebak, J. T., Rasmussen, M., Fritz, T., Caidahl, K., Krook, A., O'Gorman, D. J., and Zierath, J. R. (2012). Acute Exercise Remodels Promoter Methylation in Human Skeletal Muscle. *Cell Metabolism* 15.3, pp. 405–411.

[180] Rönn, T., Volkov, P., Davegårdh, C., Dayeh, T., Hall, E., Olsson, A. H., et al. (2013). A Six Months Exercise Intervention Influences the Genome-wide DNA Methylation Pattern in Human Adipose Tissue. *PLoS Genetics* 9.6.

[181] Fabre, O., Ingerslev, L. R., Garde, C., Donkin, I., Simar, D., and Barrès, R. (2018). Exercise training alters the genomic response to acute exercise in human adipose tissue. *Epigenomics* 10.8, pp. 1033–1050.

[182] Cedernaes, J., Schönke, M., Westholm, J. O., Mi, J., Chibalin, A., Voisin, S., et al. (2018). Acute sleep loss results in tissue-specific alterations in genome-wide DNA methylation state and metabolic fuel utilization in humans. *Science Advances* 4.8.

[183] Britsemmer, J. H., Krause, C., Taege, N., Geißler, C., Lopez-Alcantara, N., Schmidtke, L., et al. (2023). Fatty Acid Induced Hypermethylation in the Slc2a4 Gene in Visceral

Adipose Tissue Is Associated to Insulin-Resistance and Obesity. *International Journal of Molecular Sciences* 24.7.

[184] Zwamborn, R. A., Slieker, R. C., Mulder, P. C., Zoetemelk, I., Verschuren, L., Suchiman, H. E. D., et al. (2017). Prolonged high-fat diet induces gradual and fat depot-specific DNA methylation changes in adult mice. *Scientific Reports* 7.1, pp. 1–9.

[185] Geißler, C., Krause, C., Neumann, A. M., Britsemmer, J. H., Taege, N., Grohs, M., et al. (2022). Dietary induction of obesity and insulin resistance is associated with changes in Fgf21 DNA methylation in liver of mice. *The Journal of Nutritional Biochemistry* 100, p. 108907.

[186] Rosqvist, F., Iggman, D., Kullberg, J., Cedernaes, J., Johansson, H. E., Larsson, A., et al. (2014). Overfeeding Polyunsaturated and Saturated Fat Causes Distinct Effects on Liver and Visceral Fat Accumulation in Humans. *Diabetes* 63.7, pp. 2356–2368.

[187] Wheatley, K. E., Nogueira, L. M., Perkins, S. N., and Hursting, S. D. (2011). Differential Effects of Calorie Restriction and Exercise on the Adipose Transcriptome in Diet-Induced Obese Mice. *Journal of Obesity* 2011, p. 13.

[188] Lecoutre, S., Oger, F., Pourpe, C., Butruille, L., Marousez, L., Dickes-Coopman, A., et al. (2017). Maternal obesity programs increased leptin gene expression in rat male offspring via epigenetic modifications in a depot-specific manner. *Molecular Metabolism* 6.8, pp. 922–930.

[189] Zhang, Q., Ramlee, M. K., Brunmeir, R., Villanueva, C. J., Halperin, D., and Xu, F. (2012). Dynamic and distinct histone modifications modulate the expression of key adipogenesis regulatory genes. *Cell Cycle* 11.23, p. 4310.

[190] Mikula, M., Majewska, A., Ledwon, J. K., Dzwonek, A., and Ostrowski, J. (2014). Obesity increases histone H3 lysine 9 and 18 acetylation at Tnfa and Ccl2 genes in mouse liver. *International Journal of Molecular Medicine* 34.6, pp. 1647–1654.

[191] Jean-François, L., Derghal, A., and Mounien, L. (2019). MicroRNAs in Obesity and Related Metabolic Disorders. *Cells* 8.8.

[192] Sun, J., Ruan, Y., Wang, M., Chen, R., Yu, N., Sun, L., Liu, T., and Chen, H. (2016). Differentially expressed circulating LncRNAs and mRNA identified by microarray analysis in obese patients. *Scientific Reports* 6.

[193] Liu, Y., Ji, Y., Li, M., Wang, M., Yi, X., Yin, C., Wang, S., Zhang, M., Zhao, Z., and Xiao, Y. (2018a). Integrated analysis of long noncoding RNA and mRNA expression profile in children with obesity by microarray analysis. *Scientific Reports* 8.1.

[194] Lo, K. A., Huang, S., Walet, A. C. E., Zhang, Z. C., Leow, M. K. S., Liu, M., and Sun, L. (2018). Adipocyte long-Noncoding RNA transcriptome analysis of obese mice identified lnc-Leptin, which regulates leptin. *Diabetes* 67.6, pp. 1045–1056.

[195] Manco, M., Crudele, A., Mosca, A., Caccamo, R., Braghini, M. R., De Vito, R., Alterio, A., Pizzolante, F., De Peppo, F., and Alisi, A. (2022). LncOb rs10487505 variant is associated with leptin levels in pediatric non-alcoholic fatty liver disease. *Pediatric Research* 92.6, pp. 1737–1743.

[196] Kuroda, A., Rauch, T. A., Todorov, I., Ku, H. T., Al-Abdullah, I. H., Kandeel, F., Mullen, Y., Pfeifer, G. P., and Ferreri, K. (2009). Insulin Gene Expression Is Regulated by DNA Methylation. *PLOS ONE* 4.9, e6953.

[197] Krause, C., Sievert, H., Geißler, C., Grohs, M., El Gammal, A. T., Wolter, S., et al. (2019). Critical evaluation of the DNA-methylation markers ABCG1 and SREBF1 for Type 2 diabetes stratification. *Epigenomics* 11.8, pp. 885–897.

[198] Dahlman, I., Sinha, I., Gao, H., Brodin, D., Thorell, A., Rydén, M., et al. (2015). The fat cell epigenetic signature in post-obese women is characterized by global hypomethylation and differential DNA methylation of adipogenesis genes. *International Journal of Obesity* 39.6, pp. 910–919.

[199] Keller, M., Hopp, L., Liu, X., Wohland, T., Rohde, K., Cancello, R., et al. (2017). Genome-wide DNA promoter methylation and transcriptome analysis in human adipose tissue unravels novel candidate genes for obesity. *Molecular Metabolism* 6.1, pp. 86–100.

[200] Marchi, M., Lisi, S., Curcio, M., Barbuti, S., Piaggi, P., Ceccarini, G., et al. (2011). Human leptin tissue distribution, but not weight loss-dependent change in expression, is associated with methylation of its promoter. *Epigenetics* 6.10, pp. 1198–1206.

[201] Wilhelm, J., Birkenstock, A., Buchholz, V., Müller, A., Aly, S. A., Gruner-Labitzke, K., et al. (2021). Promoter Methylation of LEP and LEPR before and after Bariatric Surgery: A Cross-Sectional Study. *Obesity Facts* 14.1, p. 93.

[202] Wieting, J., Jahn, K., Buchholz, V., Lichtinghagen, R., Deest-Gaubatz, S., Bleich, S., Eberlein, C. K., Deest, M., and Frieling, H. (2022). Alteration of serum leptin and LEP/LEPR promoter methylation in Prader-Willi syndrome. *Psychoneuroendocrinology* 143, p. 105857.

[203] Milagro, F. I., Campión, J., García-Díaz, D. F., Goyenechea, E., Paternain, L., and Martínez, J. A. (2009). High fat diet-induced obesity modifies the methylation pattern of leptin promoter in rats. *Journal of Physiology and Biochemistry* 65.1, pp. 1–9.

[204] Melzner, I., Scott, V., Dorsch, K., Fischer, P., Wabitsch, M., Brüderlein, S., Hasel, C., and Möller, P. (2002). Leptin Gene Expression in Human Preadipocytes Is Switched on by Maturation-induced Demethylation of Distinct CpGs in Its Proximal Promoter. *Journal of Biological Chemistry* 277.47, pp. 45420–45427.

[205] Kuroda, M., Tominaga, A., Nakagawa, K., Nishiguchi, M., Sebe, M., Miyatake, Y., et al. (2016). DNA Methylation Suppresses Leptin Gene in 3T3-L1 Adipocytes. *PLoS ONE* 11.8.

[206] Kubota, Y., Nagano, H., Kosaka, K., Ogata, H., Nakayama, A., Yokoyama, M., et al. (2021). Epigenetic modifications underlie the differential adipogenic potential of preadipo-

cytes derived from human subcutaneous fat tissue. *American Journal of Physiology - Cell Physiology* 321.3, pp. C596–C606.

[207] Fan, C., Liu, X., Shen, W., Deckelbaum, R. J., and Qi, K. (2011). The Regulation of Leptin, Leptin Receptor and Pro-opiomelanocortin Expression by N-3 PUFAs in Diet-Induced Obese Mice Is Not Related to the Methylation of Their Promoters. *Nutrition & Metabolism* 8, p. 31.

[208] Shen, W., Wang, C., Xia, L., Fan, C., Dong, H., Deckelbaum, R. J., and Qi, K. (2014). Epigenetic modification of the leptin promoter in diet-induced obese mice and the effects of N-3 polyunsaturated fatty acids. *Scientific Reports* 4.1, pp. 1–8.

[209] Cordero, P., Campion, J., Milagro, F. I., Goyenechea, E., Steemburgo, T., Javierre, B. M., and Martinez, J. A. (2011). Leptin and TNF-alpha promoter methylation levels measured by MSP could predict the response to a low-calorie diet. *Journal of Physiology and Biochemistry* 67.3, pp. 463–470.

[210] Geißler, C. (2020). Resistance is futile-A collective of epigenetically reprogrammed genes leads to diet-induced hepatic insulin resistance. PhD thesis. University of Lübeck.

[211] Neumann, A.-M. (2021). Remodelling of the circadian network by bariatric surgery in mice. PhD thesis. University of Lübeck.

[212] Neumann, A. M., Geißler, C., Pilorz, V., Olejniczak, I., Lewis, A. G., Seeley, R. J., Shomroni, O., Salinas-Riester, G., Kirchner, H., and Oster, H. (2021). Restructuring of the male mice peripheral circadian network after bariatric surgery. *Journal of Endocrinology* 250.2, pp. 67–79.

[213] Krause, C., Britsemmer, J. H., Bernecker, M., Molenaar, A., Taege, N., Geißler, C., et al. (2023). Liver microRNA transcriptome reveals miR-182 as link between type 2 diabetes and fatty liver disease in obesity. *eLife* 12.

[214] Krause, C. (2020). Gene expression in Liver is Altered by DNA methylation and miRNAs inObese Subjects. PhD thesis. University of Lübeck.

[215] Krause, C., Geißler, C., Tackenberg, H., El Gammal, A. T., Wolter, S., Spranger, J., Mann, O., Lehnert, H., and Kirchner, H. (2020). Multi-layered epigenetic regulation of IRS2 expression in the liver of obese individuals with type 2 diabetes. *Diabetologia* 63.10, pp. 2182–2193.

[216] Sievert, H., Krause, C., Geiβler, C., Grohs, M., El-Gammal, A. T., Wolter, S., Mann, O., Lehnert, H., and Kirchner, H. (2021). Epigenetic Downregulation of FASN in Visceral Adipose Tissue of Insulin Resistant Subjects. *Experimental and Clinical Endocrinology and Diabetes* 129.9, pp. 674–682.

[217] Brandes, J., Zobel, I., Rohmann, N., Schlicht, K., Geisler, C., Hartmann, K., et al. (2022). Dipeptidylpeptidase (DPP)-4 inhibitor therapy increases circulating levels of anti - infla-

mmatory soluble frizzle receptor protein (sFRP)-5 which is decreased in severe COVID-19 disease. *Scientific Reports* 12.1, pp. 1–9.

[218] Shoham, N., Gottlieb, R., Sharabani-Yosef, O., Zaretsky, U., Benayahu, D., and Gefen, A. (2012). Static mechanical stretching accelerates lipid production in 3T3-L1 adipocytes by activating the MEK signaling pathway. *American Journal of Physiology - Cell Physiology* 302.2, pp. 429–441.

[219] Klug, M. and Rehli, M. (2006). Functional Analysis of Promoter CPG-Methylation using a CpG-Free Luciferase Reporter Vector. *Epigenetics* 1.3, pp. 127–130.

[220] Andersen, C. L., Jensen, J. L., and Ørntoft, T. F. (2004). Normalization of Real-Time Quantitative Reverse Transcription-PCR Data: A Model-Based Variance Estimation Approach to Identify Genes Suited for Normalization, Applied to Bladder and Colon Cancer Data Sets. *Cancer Research* 64.15, pp. 5245–5250.

[221] Pfaffl, M. W. (2001). A new mathematical model for relative quantification in real-time RT–PCR. *Nucleic Acids Research* 29.9, e45.

[222] Taiyun Wei and Viliam Simko (2021). R package corrplot: Visualization of a Correlation Matrix.

[223] Bodenhofer, U., Bonatesta, E., Horejš-Kainrath, C., and Hochreiter, S. (2015). msa: an R package for multiple sequence alignment. *Bioinformatics* 31.24, pp. 3997–3999.

[224] Demichev, V., Messner, C. B., Vernardis, S. I., Lilley, K. S., and Ralser, M. (2019). DIA-NN: neural networks and interference correction enable deep proteome coverage in high throughput. *Nature Methods* 17.1, pp. 41–44.

[225] Ritchie, M. E., Phipson, B., Wu, D., Hu, Y., Law, C. W., Shi, W., and Smyth, G. K. (2015). limma powers differential expression analyses for RNA-sequencing and microarray studies. *Nucleic Acids Research* 43.7, e47–e47.

[226] Dobin, A., Davis, C. A., Schlesinger, F., Drenkow, J., Zaleski, C., Jha, S., Batut, P., Chaisson, M., and Gingeras, T. R. (2013). STAR: ultrafast universal RNA-seq aligner. *Bioinformatics* 29.1, p. 15.

[227] Ulgen, E., Ozisik, O., and Sezerman, O. U. (2019). PathfindR: An R package for comprehensive identification of enriched pathways in omics data through active subnetworks. *Frontiers in Genetics* 10.

[228] Pischon, T., Boeing, H., Hoffmann, K., Bergmann, M., Schulze, M., Overvad, K., et al. (2008). General and Abdominal Adiposity and Risk of Death in Europe. *New England Journal of Medicine* 359.20, pp. 2105–2120.

[229] Russo, L. and Lumeng, C. N. (2018). Properties and functions of adipose tissue macrophages in obesity. *Immunology* 155.4, pp. 407–417.

[230] Morris, D. L., Singer, K., and Lumeng, C. N. (2011). Adipose tissue macrophages: phenotypic plasticity and diversity in lean and obese states. *Current Opinion in Clinical Nutrition and Metabolic Care* 14.4, pp. 341–346.

[231] Foster, M. T., Softic, S., Caldwell, J., Kohli, R., DeKloet, A. D., and Seeley, R. J. (2013). Subcutaneous adipose tissue transplantation in diet-induced obese mice attenuates metabolic dysregulation while removal exacerbates it. *Physiological Reports* 1.2, p. 15.

[232] Tran, T. T., Yamamoto, Y., Gesta, S., and Kahn, C. R. (2008). Beneficial Effects of Subcutaneous Fat Transplantation on Metabolism. *Cell metabolism* 7.5, p. 410.

[233] Seifarth, C., Schehler, B., and Schneider, H. J. (2013). Effectiveness of metformin on weight loss in non-diabetic individuals with obesity. *Experimental and Clinical Endocrinology and Diabetes* 121.1, pp. 27–31.

[234] Matsui, Y., Hirasawa, Y., Sugiura, T., Toyoshi, T., Kyuki, K., and Ito, M. (2010). Metformin reduces body weight gain and improves glucose intolerance in high-fat diet-fed C57BL/6J Mice. *Biological and Pharmaceutical Bulletin* 33.6, pp. 963–970.

[235] Fryklund, C., Neuhaus, M., Morén, B., Borreguero-Muñoz, A., Lundmark, R., and Stenkula, K. G. (2022). Expansion of the Inguinal Adipose Tissue Depot Correlates With Systemic Insulin Resistance in C57BL/6J Mice. *Frontiers in Cell and Developmental Biology* 10, p. 942374.

[236] Li, Q. and Spalding, K. L. (2022). The regulation of adipocyte growth in white adipose tissue. *Frontiers in Cell and Developmental Biology* 10, p. 2253.

[237] Wang, Q. A., Tao, C., Gupta, R. K., and Scherer, P. E. (2013). Tracking adipogenesis during white adipose tissue development, expansion and regeneration. *Nature Medicine* 19.10, pp. 1338–1344.

[238] Tang, H. N., Tang, C. Y., Man, X. F., Tan, S. W., Guo, Y., Tang, J., Zhou, C. L., and Zhou, H. D. (2017). Plasticity of adipose tissue in response to fasting and refeeding in male mice. *Nutrition & Metabolism* 14.1.

[239] Zhang, Y., Guo, K. Y., Diaz, P. A., Heo, M., and Leibel, R. L. (2002). Determinants of leptin gene expression in fat depots of lean mice. *American Journal of Physiology - Regulatory Integrative and Comparative Physiology* 282.1 51-1.

[240] Couillard, C., Mauriège, P., Imbeault, P., Prud'homme, D., Nadeau, A., Tremblay, A., Bouchard, C., and Després, J. P. (2000). Hyperleptinemia is more closely associated with adipose cell hypertrophy than with adipose tissue hyperplasia. *International Journal of Obesity* 24.6, pp. 782–788.

[241] Marcelin, G., Silveira, A. L. M., Martins, L. B., Ferreira, A. V., and Clément, K. (2019). Deciphering the cellular interplays underlying obesity-induced adipose tissue fibrosis. *The Journal of Clinical Investigation* 129.10, p. 4032.

[242] Jernås, M., Palming, J., Sjöholm, K., Jennische, E., Svensson, P.-A., Gabrielsson, B. G., et al. (2006). Separation of human adipocytes by size: hypertrophic fat cells display distinct gene expression. *The FASEB Journal* 20.9, pp. 1540–1542.

[243] Honecker, J., Ruschke, S., Seeliger, C., Laber, S., Strobel, S., Pröll, P., et al. (2022). Transcriptome and fatty-acid signatures of adipocyte hypertrophy and its non-invasive MR-based characterization in human adipose tissue. *EBioMedicine* 79.

[244] Hosogai, N., Fukuhara, A., Oshima, K., Miyata, Y., Tanaka, S., Segawa, K., et al. (2007). Adipose Tissue Hypoxia in Obesity and Its Impact on Adipocytokine Dysregulation. *Diabetes* 56.4, pp. 901–911.

[245] Lawler, H. M., Underkofler, C. M., Kern, P. A., Erickson, C., Bredbeck, B., and Rasouli, N. (2016). Adipose Tissue Hypoxia, Inflammation, and Fibrosis in Obese Insulin-Sensitive and Obese Insulin-Resistant Subjects. *The Journal of Clinical Endocrinology and Metabolism* 101.4, p. 1422.

[246] Thienpont, B., Steinbacher, J., Zhao, H., D'Anna, F., Kuchnio, A., Ploumakis, A., et al. (2016). Tumor hypoxia causes DNA hypermethylation by reducing TET activity. *Nature* 537.7618, p. 63.

[247] Humphries, S., Bond, D. R., Germon, Z. P., Keely, S., Enjeti, A. K., Dun, M. D., and Lee, H. J. (2023). Crosstalk between DNA methylation and hypoxia in acute myeloid leukaemia. *Clinical Epigenetics* 15.1.

[248] Zhao, X. B., Chen, Y. P., Tan, M., Zhao, L., Zhai, Y. Y., Sun, Y. L., Gong, Y., Feng, X. Q., Du, J., and Fan, Y. B. (2021). Extracellular Matrix Stiffness Regulates DNA Methylation by PKCα-Dependent Nuclear Transport of DNMT3L. *Advanced Healthcare Materials* 10.16.

[249] Cummings, B. P., Strader, A. D., Stanhope, K. L., Graham, J. L., Lee, J., Raybould, H. E., Baskin, D. G., and Havel, P. J. (2010). Ileal Interposition Surgery Improves Glucose and Lipid Metabolism and Delays Diabetes Onset in the UCD-T2DM Rat. *Gastroenterology* 138.7, p. 2437.

[250] Galanakis, C. G., Daskalakis, M., Manios, A., Xyda, A., Karantanas, A. H., and Melissas, J. (2015). Computed Tomography-Based Assessment of Abdominal Adiposity Changes and Their Impact on Metabolic Alterations Following Bariatric Surgery. *World Journal of Surgery* 39.2, pp. 417–423.

[251] Stefanidis, A., Lee, C., Greaves, E., Montgomery, M., Arnold, M., Newn, S., et al. (2022). Mechanisms underlying the efficacy of a rodent model of vertical sleeve gastrectomy — a focus on energy expenditure. *bioRxiv*.

[252] Méndez-Giménez, L., Becerril, S., Moncada, R., Valentí, V., Ramírez, B., Lancha, A., et al. (2015). Sleeve Gastrectomy Reduces Hepatic Steatosis by Improving the Coordinated Reg-

ulation of Aquaglyceroporins in Adipose Tissue and Liver in Obese Rats. *Obesity Surgery* 25.9, pp. 1723–1734.

[253] Jahansouz, C., Xu, H., Hertzel, A. V., Kizy, S., Steen, K. A., Foncea, R., et al. (2018). Partitioning of Adipose Lipid Metabolism by Altered Expression and Function of PPAR Isoforms After Bariatric Surgery. *International journal of obesity* 42.2, p. 139.

[254] Emont, M. P., Jacobs, C., Essene, A. L., Pant, D., Tenen, D., Colleluori, G., et al. (2022). A single-cell atlas of human and mouse white adipose tissue. *Nature* 603.7903, pp. 926–933.

[255] Massier, L., Jalkanen, J., Elmastas, M., Zhong, J., Wang, T., Nono Nankam, P. A., et al. (2023). An integrated single cell and spatial transcriptomic map of human white adipose tissue. *Nature Communications* 14.1, pp. 1–19.

[256] Bäckdahl, J., Franzén, L., Massier, L., Li, Q., Jalkanen, J., Gao, H., et al. (2021). Spatial mapping reveals human adipocyte subpopulations with distinct sensitivities to insulin. *Cell Metabolism* 33.9, pp. 1869–1882.

[257] Sárvári, A. K., Van Hauwaert, E. L., Markussen, L. K., Gammelmark, E., Marcher, A. B., Ebbesen, M. F., Nielsen, R., Brewer, J. R., Madsen, J. G. S., and Mandrup, S. (2021). Plasticity of Epididymal Adipose Tissue in Response to Diet-Induced Obesity at Single-Nucleus Resolution. *Cell Metabolism* 33.2, pp. 437–453.

[258] Zhu, H., Wang, G., and Qian, J. (2016). Transcription factors as readers and effectors of DNA methylation. *Nature Reviews Genetics* 17.9, pp. 551–565.

[259] Nan, X., Ng, H. H., Johnson, C. A., Laherty, C. D., Turner, B. M., Eisenman, R. N., and Bird, A. (1998). Transcriptional repression by the methyl-CpG-binding protein MeCP2 involves a histone deacetylase complex. *Nature* 393.6683, pp. 386–389.

[260] Ng, H. H., Zhang, Y., Hendrich, B., Johnson, C. A., Turner, B. M., Erdjument-Bromage, H., Tempst, P., Reinberg, D., and Bird, A. (1999). MBD2 is a transcriptional repressor belonging to the MeCP1 histone deacetylase complex. *Nature Genetics* 23.1, pp. 58–61.

[261] Chen, K., Guo, Z., Luo, Y., Yuan, J., and Mo, Z. (2019). UHRF1 Promotes Proliferation of Human Adipose-Derived Stem Cells and Suppresses Adipogenesis via Inhibiting Peroxisome Proliferator-Activated Receptor γ. *BioMed Research Internation* 2019.

[262] Liu, X., Gao, Q., Li, P., Zhao, Q., Zhang, J., Li, J., Koseki, H., and Wong, J. (2013). UHRF1 targets DNMT1 for DNA methylation through cooperative binding of hemi-methylated DNA and methylated H3K9. *Nature Communications* 4.1, pp. 1–13.

[263] Lin, Q. X. X., Sian, S., An, O., Thieffry, D., Jha, S., and Benoukraf, T. (2019). MethMotif: an integrative cell specific database of transcription factor binding motifs coupled with DNA methylation profiles. *Nucleic Acids Research* 47, p. D145.

[264] Itoh, K., Igarashi, K., Hayashi, N., Nishizawa, M., and Yamamoto, M. (1995). Cloning and characterization of a novel erythroid cell-derived CNC family transcription factor

heterodimerizing with the small Maf family proteins. *Molecular and Cellular Biology* 15.8, p. 4184.

[265] Johnsen, Ø., Murphy, P., Prydz, H., and Kolstø, A. B. (1998). Interaction of the CNC-bZIP factor TCF11/LCR-F1/Nrf1 with MafG: binding-site selection and regulation of transcription. *Nucleic Acids Research* 26.2, p. 512.

[266] Hou, Y., Liu, Z., Zuo, Z., Gao, T., Fu, J., Wang, H., et al. (2018). Adipocyte-specific deficiency of Nfe2l1 disrupts plasticity of white adipose tissues and metabolic homeostasis in mice. *Biochemical and Biophysical Research Communications* 503.1, pp. 264–270.

[267] Ren, S., Bian, Y., Hou, Y., Wang, Z., Zuo, Z., Liu, Z., et al. (2021). The roles of NFE2L1 in adipocytes: Structural and mechanistic insight from cell and mouse models. *Redox Biology* 44, p. 102015.

[268] Jin, C., Luo, Y., Liang, Z., Li, X., Kołat, D., Zhao, L., and Xiong, W. (2023). Crucial role of the transcription factors family activator protein 2 in cancer: current clue and views. *Journal of Translational Medicine* 21.1, pp. 1–21.

[269] Fang, S., Li, J., Xiao, Y., Lee, M., Guo, L., Han, W., et al. (2019). Tet inactivation disrupts YY1 binding and long-range chromatin interactions during embryonic heart development. *Nature Communications* 10.1, pp. 1–18.

[270] Fang, Y., Ji, Z., Zhou, W., Abante, J., Koldobskiy, M. A., Ji, H., and Feinberg, A. P. (2023). DNA methylation entropy is associated with DNA sequence features and developmental epigenetic divergence. *Nucleic Acids Research* 51.5, pp. 2046–2065.

[271] Sanosaka, T., Imamura, T., Hamazaki, N., Chai, M. C., Igarashi, K., Ideta-Otsuka, M., et al. (2017). DNA Methylome Analysis Identifies Transcription Factor-Based Epigenomic Signatures of Multilineage Competence in Neural Stem/Progenitor Cells. *Cell Reports* 20.12, pp. 2992–3003.

[272] Zhao, Q. H., Wang, S. G., Liu, S. X., Li, J. P., Zhang, Y. X., Sun, Z. Y., Fan, Q. M., and Tian, J. W. (2013). PPARγ forms a bridge between DNA methylation and histone acetylation at the C/EBPα gene promoter to regulate the balance between osteogenesis and adipogenesis of bone marrow stromal cells. *The FEBS Journal* 280.22, pp. 5801–5814.

[273] Fujiki, K., Shinoda, A., Kano, F., Sato, R., Shirahige, K., and Murata, M. (2013). PPARγ-induced PARylation promotes local DNA demethylation by production of 5 - hydroxymethylcytosine. *Nature Communications* 4.1, pp. 1–8.

[274] Fretz, J. A., Nelson, T., Xi, Y., Adams, D. J., Rosen, C. J., and Horowitz, M. C. (2010). Altered Metabolism and Lipodystrophy in the Early B-Cell Factor 1-Deficient Mouse. *Endocrinology* 151.4, pp. 1611–1621.

[275] Roy, R., Ramamoorthy, S., Shapiro, B. D., Grosschedl, R., Ferrucci, L., and Sen Correspondence, R. (2021). DNA methylation signatures reveal that distinct combinations of tran-

scription factors specify human immune cell epigenetic identity. *Immunity* 54, pp. 2465–2480.

[276] Fernandez-Jimenez, N., Sklias, A., Ecsedi, S., Cahais, V., Degli-Esposti, D., Jay, A., Ancey, P. B., Woo, H. D., Hernandez-Vargas, H., and Herceg, Z. (2017). Lowly methylated region analysis identifies EBF1 as a potential epigenetic modifier in breast cancer. *Epigenetics* 12.11, p. 964.

[277] Cusack, M., King, H. W., Spingardi, P., Kessler, B. M., Klose, R. J., and Kriaucionis, S. (2020). Distinct contributions of DNA methylation and histone acetylation to the genomic occupancy of transcription factors. *Genome Research* 30.10, pp. 1393–1406.

[278] Huang, Y. H., Su, J., Lei, Y., Brunetti, L., Gundry, M. C., Zhang, X., Jeong, M., Li, W., and Goodell, M. A. (2017). DNA epigenome editing using CRISPR-Cas SunTag-directed DNMT3A. *Genome Biology* 18.1, pp. 1–11.

[279] Choudhury, S. R., Cui, Y., Lubecka, K., Stefanska, B., and Irudayaraj, J. (2016). CRISPR-dCas9 mediated TET1 targeting for selective DNA demethylation at BRCA1 promoter. *Oncotarget* 7.29, p. 46545.

[280] Collares, R. V. A., Salgado, W., Da Cunha Tirapelli, D. P., and Dos Santos, J. S. (2014). The Expression of LEP, LEPR, IGF1 and IL10 in Obesity and the Relationship with microRNAs. *PLoS ONE* 9.4.

[281] Parlee, S. D., Lentz, S. I., Mori, H., and MacDougald, O. A. (2014). Quantifying Size and Number of Adipocytes in Adipose Tissue. *Methods in enzymology* 537, p. 93.

[282] Rytka, J. M., Wueest, S., Schoenle, E. J., and Konrad, D. (2011). The Portal Theory Supported by Venous Drainage–Selective Fat Transplantation. *Diabetes* 60.1, p. 56.

[283] Bradford, S. T., Nair, S. S., Statham, A. L., Dijk, S. J. van, Peters, T. J., Anwar, F., et al. (2019). Methylome and transcriptome maps of human visceral and subcutaneous adipocytes reveal key epigenetic differences at developmental genes. *Scientific Reports* 9.1, pp. 1–13.

[284] Marshall, S. M. (2017). 60 years of metformin use: a glance at the past and a look to the future. *Diabetologia* 60.9, pp. 1561–1565.

[285] Yuan, T., Li, J., Zhao, W. G., Sun, W., Liu, S. N., Liu, Q., Fu, Y., and Shen, Z. F. (2019). Effects of metformin on metabolism of white and brown adipose tissue in obese C57BL/6J mice. *Diabetology and Metabolic Syndrome* 11.1, pp. 1–10.

[286] Tajima, K., Nakamura, A., Shirakawa, J., Togashi, Y., Orime, K., Sato, K., et al. (2013). Metformin prevents liver tumorigenesis induced by high-fat diet in C57Bl/6 mice. *American Journal of Physiology - Endocrinology and Metabolism* 305.8, pp. 987–998.

[287] Luo, T., Nocon, A., Fry, J., Sherban, A., Rui, X., Jiang, B., et al. (2016). AMPK activation by metformin suppresses abnormal extracellular matrix remodeling in adipose tissue and ameliorates insulin resistance in obesity. *Diabetes* 65.8, pp. 2295–2310.

[288] Bridgeman, S. C., Ellison, G. C., Melton, P. E., Newsholme, P., and Mamotte, C. D. S. (2018). Epigenetic effects of metformin: From molecular mechanisms to clinical implications. *Diabetes, Obesity and Metabolism* 20.7, pp. 1553–1562.

[289] Guo, W. R., Liu, J., Cheng, L. D., Liu, Z. Y., Zheng, X. B., Liang, H., and Xu, F. (2021). Metformin Alleviates Steatohepatitis in Diet-Induced Obese Mice in a SIRT1-Dependent Way. *Frontiers in Pharmacology* 12.

[290] Kim, Y.-W., Kim, J.-Y., Park, Y.-H., Park, S.-Y., Won, K.-C., Choi, K.-H., Huh, J.-Y., and Moon, K.-H. (2006). Metformin Restores Leptin Sensitivity in High-Fat–Fed Obese Rats With Leptin Resistance. *Diabetes* 55.3, pp. 716–724.

[291] Rosenbaum, M., Murphy, E. M., Heymsfield, S. B., Matthews, D. E., and Leibel, R. L. (2002). Low Dose Leptin Administration Reverses Effects of Sustained Weight-Reduction on Energy Expenditure and Circulating Concentrations of Thyroid Hormones. *The Journal of Clinical Endocrinology & Metabolism* 87.5, pp. 2391–2394.

[292] Rosenbaum, M., Goldsmith, R., Bloomfield, D., Magnano, A., Weimer, L., Heymsfield, S., Gallagher, D., Mayer, L., Murphy, E., and Leibel, R. L. (2005). Low-dose leptin reverses skeletal muscle, autonomic, and neuroendocrine adaptations to maintenance of reduced weight. *Journal of Clinical Investigation* 115.12, p. 3579.

[293] Verdich, C., Toubro, S., Buemann, B., Holst, J. J., Bülow, J., Simonsen, L., et al. (2001). Leptin Levels Are Associated with Fat Oxidation and Dietary-Induced Weight Loss in Obesity. *Obesity Research* 9.8, pp. 452–461.

[294] Umano, G. R., Cirillo, G., Sanchez, G., Rondinelli, G., Foderini, M. V., Ferrara, S., et al. (2023). The lncOb rs10487505 polymorphism impairs insulin sensitivity and glucose tolerance in children and adolescents with obesity. *Obesity* 31.9, pp. 2359–2364.

[295] Farani, M. R., Sarlak, M., Gholami, A., Azaraian, M., Binabaj, M. M., Kakavandi, S., Tambuwala, M. M., Taheriazam, A., Hashemi, M., and Ghasemi, S. (2023). Epigenetic drugs as new emerging therapeutics: What is the scale‘s orientation of application and challenges? *Pathology - Research and Practice* 248, p. 154688.

[296] Feehley, T., O‘Donnell, C. W., Mendlein, J., Karande, M., and McCauley, T. (2023). Drugging the epigenome in the age of precision medicine. *Clinical Epigenetics* 15.1, pp. 1–13.

[297] Amabile, A., Migliara, A., Capasso, P., Biffi, M., Cittaro, D., Naldini, L., and Lombardo, A. (2016). Inheritable Silencing of Endogenous Genes by Hit-and-Run Targeted Epigenetic Editing. *Cell* 167.1, pp. 219–232.

[298] Liu, X. S., Wu, H., Krzisch, M., Wu, X., Graef, J., Muffat, J., et al. (2018b). Rescue of Fragile X Syndrome Neurons by DNA Methylation Editing of the FMR1 Gene. *Cell* 172.5, pp. 979–992.

[299] Schindelin, J., Arganda-Carreras, I., Frise, E., Kaynig, V., Longair, M., Pietzsch, T., et al. (2012). Fiji: an open-source platform for biological-image analysis. *Nature Methods* 9.7, pp. 676–682.

A. Appendix

A.1. Materials

A.1.1. Buffers, media & solutions

Table A.1.: Antiproteolytic cocktail composition. All chemicals were vigorously mixed, aliquoted and stored at −20 °C for a maximum of 5 weeks.

Chemical	quantity
Heparin	40 µL
1.8 % NaCl	1 mL
anti-proteolytic cocktail	1 tablet

Table A.2.: Media for HEK293T and 3T3L1 cells cultured and differentiated in Lübeck. Components used are stated in Table A.4.

medium	component	concentration
Growth medium (GM)	DMEM w.4.5 g/L glucose, GlutaMAX™, sodium-pyruvate (#31966021)	1X
	FBS	10 %
	penicillin-streptomycin	1 %
Initiation medium	GM	
	dexamethasone	0.25 µM
	3-isobutyl-methylxanthine	0.5 µM
	insulin	1 µg/mL
Differentiation medium	GM	
	insulin	1 µg/mL

Table A.6.: 50 X TAE-buffer as stock; 1:50 diluted in VE-H_2O for usage.

quantity	chemical
242 g	tris(Trizma base)
57.1 mL	glacial acetic acid
100 mL	0.5 M EDTA (pH 8)
ad 1000 mL	VE-water

Table A.3.: Media for 3T3L1 cells cultured and differentiated in Tel Aviv. Components used are stated in Table A.5.

medium	component	concentration
Growth medium (GM)	DMEM w 4.5 g/L glucose	1X
	FBS	10 %
	L-glutamine	1 %
	penicillin-streptomycin	0.1 %
	HEPES	0.5 %
Inititation medium	GM	
	dexamethasone	1 µM
	3-isobutyl−methylxanthine	400 µM
	insulin	100 IU/mL
Differentiation medium	GM	
	insulin	100 IU/mL

Table A.4.: Buffers and media used in Germany

buffer/medium	manufacturer
DPBS w/o calcium w/o magnesium	gibco, Life Technologies GmbH
DMEM (1x) w.GlutaMAX, 4.5 g/L glucose (31966021)	gibco, Life Technologies, Carlsbad, US
Fast Media Amp (Lysogency Broth) LB liquid medium	InvivoGen, San Diego, US
Fast Media Amp Agar solid medium	InvivoGen, San Diego, US
Fast Media Zeo (Terrific Broth) TB liquid medium	InvivoGen, San Diego, US
Fast Media Zeo Agar solid medium	InvivoGen, San Diego, US
Fetal Bovine Serum (FBS), heat-inactivated One Shot	gibco, Life Technologies, Carlsbad, US
Opti-MEM™	gibco, Life Technologies, Carlsbad, US
Penicillin/Streptomycin	gibco, Life Technologies, Carlsbad, US
S.O.C. medium	Invitrogen, Carlsbad, US
TE Buffer (20X) pH 7.5	Promega GmbH, Wisconsin, US

Table A.5.: Buffers used in Israel

Buffers/media	manufacturer
4-(2-hydroxyethyl)−1-piperazineethanesulfonic acid (HEPES), 0.5 %	Sigma Aldrich, St. Louis, US
insulin	Sigma Aldrich, St. Louis, US
L-glutamine	Biological Industries, Kibbutz Beit-Haemek, Israel
Penicillin-streptomycin	Sigma Aldrich, St. Louis, US
DMEM (1x), 4.5 g/L glucose	Biological Industries, Kibbutz Beit-Haemek, Israel

A.1.2. Oligonucleotides

Table A.7.: sgRNA sequence against RS1 for CRISPR-Cas, ordered from ThermoFisher Scientific.

name	sequence
sgRNA1_RS1	ACCGCUGUGGGAAAAACCGC
sgRNA2_RS1	GCAUGUUAGGACACCGCUGU
sgRNA3_RS1	AGCAUGUUAGGACACCGCUG
sgRNA_scramble_ms	GCUUAGUUACGCGUGGACGA

Table A.8.: qPCR assays mouse (Mm., PrimeTime assays, Integrated DNA Technologies, US) and human (Hs, TaqMan Assays, ThermoFisher Scientific, US).

Gene	IDT assay ID or sequence	Fluorophore
Lep	Mm.PT.58.13515402	FAM
Hprt	Mm.PT.39a.22214828	Cy5
Rplp0	Mm.PT.58.43894205	Cy5
lncOb	5'CTAGGCCCACATTCCTGATAC; 5'GACTTTGCCTTCTTGGTTCTTG; 5'-/56-FAM/AGGACCAAG/ZEN/ACCACCAAGCCAATC/3IABkFQ	FAM
Arg1	Mm.PT.39a.22214843	Cy5
CD11c/Itgax	Mm.PT.58.42516719	Cy5
Adrb1	Mm.PT.58.41132658.g	FAM
Lipe	Mm.PT.58.30708147	FAM
Pnpla2	Mm.PT.56a.13424398.g	FAM
Dnmt3b	Mm.PT.58.30251490	Cy5
Tet3	Mm.PT.58.11954119	Cy5
Tet2	Mm.PT.58.30089849	FAM
Dnmt3a	Mm.PT.58.6249586	FAM
LEP	HS00174877_m1	Fam
RPL37A	Hs01102345_m1	VIC

Table A.9.: Assay specific annealing temperatures and cycles for bsPCR. The variable parameters are stated in this table. Oligonucleotides were ordered from Integrated DNA Technologies, US. "hu" indicates human assay, "ms" indicates mouse assays

Assay	cycles	annealing temperature [°C]
ms-RS1	40	49.5
ms-RS2	40	57.3
ms-RS3	40	54.7
ms-RS5	40	54.1
ms-RS4	45	51
hu-RS1	45	52.9
hu-RS2	45	56
hu-RS3	42	52.9

Table A.10.: Pyrosequencing assays. Rev-/Fwd-primers were used for the PCR, S-primers for sequencing. Biotinylated primers are indicated by "-bio" in the primer name. "ms" indicates mouse assays, "hu" indicates human assays. Oligonucleotides were ordered from Integrated DNA Technologies, US. fwd-forward, rev-reverse, S-sequencing

Assay	direction	Sequence	PCR product size [bp]	strand
ms-RS1	fwd	GGGTAGTTGAAATAATTAGTTAGT	130	upper
	rev	CCTCAAAACTACTCCAAACATACA		
	S	AATTGGTGGTTTTGGTATTA		
ms-RS2	fwd	AGAGGGGTAGGTAGGTATGGA	159	upper
	rev	TCCACATAACCTCCTTCTTACCTCAATTT		
	S	AGTTGTAAGGTAAGGTT		
ms-RS3	fwd	TGGTTTTGGGTTTAGGGTAAT	175	lower
	rev	CCTCCACCCTTTATCTTCTACCTCCTATT		
	S	GGGTTTAGGGTAATTTTT		
ms-RS4	fwd	TTTTGTTTTTTGTTGTTTGGTTTTGTTATG	275	upper
	rev	CCCAACACAACTTCTTACTTCTACT		
	S	TGAAGTTTTTAAAGATTTGAATT		
ms-RS5	fwd	GAGTGGTTATGTGGTATATTTGTAGTT	153	upper
	rev	CCTAAAAATCATAAACCCAAACTTATC		
	S	GTGGTATATTTGTAGTTAGGT		
hu-RS1	fwd	GTAGTAGGGGTATTATTATAGGATTATATTGA	267	lower
	rev	ACAAAATATTCTTCCAATCAATTCTTTAAC		
	S	TTGAAGAAGTATTGGTTAAGAAG		
hu-RS3	fwd	GGGAGAGTTGTTTGTGTGTGA	198	upper
	rev	AATATATACTTCCTATACCTCCCTACA		
	S	GGTTTTTATTTATTATTGGGG		
hu-RS2	fwd	AGAGGGGAGGGTAGGTATGG	240	upper
	rev	TCCCCAACTCCCCATAACCTTCTATC		
	S	GGTTGTAAGGTAAGGTTT		

Table A.11.: Oligonucleotides for luciferase assay, sequences shown 5′→ 3′. PCR of RS3 fragment created a 178 bp fragment and was digested with restriction enzymes before vector ligation. Oligonucleotides were ordered from Integrated DNA Technologies, US.

Method	Enhancer site	oligo	sequence
gPCR	RS3	Fwd	CATAAGCTTCTGTTGTGGAGGGGCTTTTG
		Rev	AGTCCATGGCTTCTTGCCTGGCCCTGG
duplexed	RS2	Fwd	AGCTTGCTCCAGCAGCTGCAAGGTAAGGCCCGGGGCGCGCTACTTTCTCCTCC
		Rev	CATGGGAGGAGAAAGTAGCGCGCCCCGGGCCTTACCTTGCAGCTGCTGGAGCA
duplexed	RS1	Fwd	AGCTTTCTGGCATCATCGTGACCAGCGGTTTTTCCCACAGCGGTGTCCTAACAC
		Rev	CATGGTGTTAGGACACCGCTGTGGGAAAAACCGCTGGTCACGATGATGCCAGAA

Table A.12.: Oligonucleotides for mass spectrometry analysis, sequences shown 5′→ 3′. The label "-bio" indicates the biotinylated strand. Oligonucleotides were ordered from Integrated DNA Technologies, US.

Enhancer site	sequence
RS3-fwd-bio	TGTGACAGGGCAAGGCCTGGCTGGCGTCCAGCCATCACCAGGGTCAG
	CCCCACCCGGGCTTGGCCACAGCCAGCTACCAGTTATTCAGGCGAAAGGATTA
RS3-rev	TAATCCTTTCGCCTGAATAACTGGTAGCTGGCTGTGGCCAAGCCCGGGT
	GGGGCTGACCCTGGTGATGGCTGGACGCCAGCCAGGCCTTGCCCTGTCACA
RS2-fwd-bio	TGCTCCAGCAGCTGCAAGGTAAGGCCCGGGGCGCGCTACTTTCTCCTCC
RS2-rev	CATGGGAGGAGAAAGTAGCGCGCCCCGGGCCTTACCTTGCAGCTGCTGGAGCA
RS1-fwd-bio	TTCTGGCATCATCGTGACCAGCGGTTTTTCCCACAGCGGTGTCCTAACAC
RS1-rev	CATGGTGTTAGGACACCGCTGTGGGAAAAACCGCTGGTCACGATGATGCCAGAA

A.1.3. Machine settings

Table A.13.: Gating settings of COPAS FP500 for chow and/or HFD if indicated

red+ (red PH, green PH)	(523,64); (473,30); (560,8); (998,1); (1001,111); (642,100)
green+, chow (red PH, green PH)	(147,231); (180,92); (299,100); (456,143); (667,214); (704,251); (450,250)
green+, HFD (red PH, green PH)	(147,231); (118,80); (295,92); (456,143); (667,214); (704,251); (450,250)
unstained, chow (red PH; green PH)	(94,66); (118,1); (402,21); (487,76); (294,86)
unstained, HFD (red PH, green PH)	(92,59); (118,1); (402,21); (487,76); (103,60)
large, chow (TOF)	214.2–1024.0
large, HFD (TOF)	377.5–1020.1
intermediate, HFD (TOF)	214.2–365.7
small (TOF)	20.9–198.5

TOF = time of flight, PH=peak height

Table A.14.: General settings of COPAS FP500 during adipocyte size sorting

FlowCell	500 micron	
Scan Rate	2500 K	
Focal point 1	Trigger channel	thresholds: T=5000 T1=5000 T2=2000
	Extinction	N1=300 N2=300 Dip=0 Pre-pad=0 Post-pad=0
Focal point 2	Trigger channel	thresholds: T=2000 T1=5000 T2=2000
	Extinction	N1=300 N2=300 Dip=0 Pre-pad=0 Post-pad=0
Minimum time of flight	60	
Channels set-up	Extinction	gains=2.0pmt volts=0
	Green	gains=1.3pmt volts=350
	Yellow	gains=1.0pmt volts=300
	Red	gains=1.5pmt volts=450
Pressure		2.000
		variable
		2.500
		3.000
		0.000
Drop width	6.0	
Sort Delay	9.0	
Coincidence mode	Enrichment	
Laser	Sapphire488	Power = 50
Buffer	1x PBS with 0.5 % BSA	

Table A.15.: Specific settings for scan range, ion mobility, and mass accuracy of mass spectrometry in diaPASEF mode with estimated cycle time of 1.8 s

Scan range	positive ion polarity	100-1700 m/z
TIMS setting	ion mobility range	0.6-1.6 1/K0
	ramp time	100 ms
	accumulation time	100 ms
	ramp rate	9.43 Hz
MS/MS setting	mass range	400 – 1201.0 Da
	mobility range	0.6-1.6 1/K0
fixed dia-PASEF window	width	26.0 Da
	mass overlap	1.0 Da
	mobility overlap	0.0 1/K0
mass steps	32	
mobility window/cycle	1.0	

Table A.16.: Specific settings for analysis with DIA-NN software (v1.8.1) using the human UniprotKB/swiss-prot database (downloaded on 12/22/2021) for deep learning based *in silico* spectral library generation.

LC mode	high precision
RT-dependent cross normalization	enabled
Library generation	smart profiling
neural network classifier	single pass mode
Mass & MS1 accuracy	10.0
scan window	0
Match between runs	enabled
protease setting	trypsin/P
missed cleavage acceptance	1.0
max no. of variable modifications	0.0
N-terminal methionine excision	enabled (fixed modification)
cysteine carbamidomethylation	enabled (fixed modification)
peptide length range	7-30
precursor charge range	2-4
precursor m/z range	100-1700
fragment ion m/z range	400-1201
'pg_matrix' (protein groups) output filter	1% FDR

A.1.4. Consumables, chemicals, kits, cells, enzymes, bacteria and diets used

Table A.17.: Consumables used in the experiments with manufacturers

Consumable	manufacturer
ACCU-CHECK Aviva blood glucose test stripes	Roche Diabetes Care GmbH, Mannheim, Germany
Adhesive PCR seal: MicroAmp™optical adhesive film	Applied Biosystems, Foster City, US
Aluminium foil (0.03 mm x 300 mm x 100 m), Labsolute	Th.Geyer GmbH& Co. KG, Renningen, Germany
Bio Flex® 6-well culture plates BF-3001C Collagen I	Flexcell® Inc., Burlington, US
Biosphere Filter tips 1000, 300, 200, 100, 20, 10, 2.5 µL	Sarstedt AG & Co.KG, Nümbrecht, Germany
C18 EvoTip disposable trap columns	EvoSep Biosystems. Odense, Denmark
C18 Performance column (EV1137)	EvoSep Biosystems. Odense, Denmark
Cell culture flask T50, T75, standard, ventilated cap	Sarstedt AG & Co.KG, Nümbrecht, Germany
Cell culture plates: 6-well, 12-well, 96-well; TC-plates standard	Sarstedt AG & Co.KG, Nümbrecht, Germany
Cell lysis beads: Bulk Beads 1.4 mm Zirconium oxide beads	Precellys, Bertin Technologies, France
Cell scaper	Sarstedt AG & Co.KG, Nümbrecht, Germany
Cellulose swabs	Meditrade GmbH, Kiefersfelden, Germany
Combitips advanced/Plus Biopur R 0.1, 0.2, 0.5, 2.5, 5.0, and 10 mL	Eppendorf SE, Hamburg, Germany
EDTA coated tubes, Microvette® CB 300	Sarstedt AG & Co.KG, Nümbrecht, Germany
Falcon tubes 10 mL, 50 mL	Sarstedt AG & Co.KG, Nümbrecht, Germany
Microplate, 96-well, F, transparent	Sarstedt AG & Co.KG, Nümbrecht, Germany
Microplate, 96-well, PS, F bottom, transparent	Greiner Bio-One, Kremsmünster, Austria
Microtubes PCR-PT for tissue disruption, 2 mL	Sarstedt AG & Co.KG, Nümbrecht, Germany
Millipore membrane filters 0.1 µM	Merck KGaA, Darmstadt, Germany
Pasteur pipettes	Th.Geyer GmbH& Co. KG, Renningen, Germany
PCR plates, HP, 0.2 mL	Th.Geyer GmbH& Co. KG, Renningen, Germany
PCR stripes, Multiply-µStrip 0.2 µL	Sarstedt AG & Co.KG, Nümbrecht, Germany
Petri dish w/ cams, 100 mm	Sarstedt AG & Co.KG, Nümbrecht, Germany
Plating spatula	Sarstedt AG & Co.KG, Nümbrecht, Germany
PyroMark Q48 Absorber Strips	QIAGEN GmbH, Venlo, Netherlands
PyroMark Q48 advancedCpG Reagents	QIAGEN GmbH, Venlo, Netherlands
PyroMark Q48 Discs	QIAGEN GmbH, Venlo, Netherlands
PyroMark Q48 Magnetic Beads	QIAGEN GmbH, Venlo, Netherlands
Qubit Assay tubes, 0.5-mL	Life Technologies, Carlsbad, US
Reactiontubes for oligos: Microtubes, low binding, 1.5 mL, 2 mL	Sarstedt AG & Co.KG, Nümbrecht, Germany
Reactiontubes: SafeSeal 5 mL, 2 mL, 1.5 mL	Sarstedt AG & Co.KG, Nümbrecht, Germany
Scalpel, disposable	Feather Safety Razor Co.Ltd, Osaka, Japan
Serological pipettes 25 mL, 10 mL, 5 mL, 2.5 mL, 1 mL	Sarstedt AG & Co.KG, Nümbrecht, Germany
syringe filter, Filtropur S 0.2 µM	Sarstedt AG & Co.KG, Nümbrecht, Germany
Syringes 1 ml and 20 ml	Becton Dickinson, Franklin Lakes, US
Syringes, insulin 0.5 ml	Becton Dickinson, Franklin Lakes, US

Table A.18.: Cells and Bacteria

Cell line/ Bacteria	manufacturer
3T3-L1	American Type Culture Collection, Manassas, US
HEK293T	American Type Culture Collection, Manassas, US
PiR1 OneShot® E.coli	Thermo Fisher Scientific Inc., Waltham, US
E.coli OneShot® Top10	Thermo Fisher Scientific Inc., Waltham, US

Table A.19.: Enzymes

enzyme	manufacturer
collagenase type II	Sigma Aldrich, St. Louis, US
HindIII-HF	New England Biolabs, Ipswich, US
M.SssI CpG methyltransferase	New England Biolabs, Ipswich, US
NcoI-HF	New England Biolabs, Ipswich, US
Proteinase K	QIAGEN GmbH, Venlo, Netherlands
Pyrophosphatase inorganic (0.1 U/µl) 10 U	Life Technologies, Carlsbad, US
RNase A	QIAGEN GmbH, Venlo, Netherlands

Table A.22.: Kits used with manufacturers

Kit	manufacturer
AllPrep DNA/RNA/Protein Mini Kit	QIAGEN GmbH, Venlo, Netherlands
Bio-Plex® Cell lysis Kit	Bio-Rad Laboratories Inc., Hercules, US
Dual-Glo® Luciferase Assay system	Promega GmbH, Wisconsin, US
EpiTect Fast DNA Bisulfite Kit	QIAGEN GmbH, Venlo, Netherlands
Fast DNA Tissue Kit	QIAGEN GmbH, Venlo, Netherlands
Fast Sort Universal SYBR Green Master Mix	Roche Applied Science, Penzberg, Germany
Fast start advanced Master Mix for TaqMan	Thermo Fisher Scientific Inc., Waltham, US
High Capacity cDNA Reverse Kit	Life Technologies, Carlsbad, US
miRNeasy Mini Kit	QIAGEN GmbH, Venlo, Netherlands
NEBNext® Library Quantt Kit for Illumina®	New England Biolabs, Ipswich, US
Ne-Per Nuclear and Cytoplasmatic Extraction Kit	Thermo Fisher Scientific Inc., Waltham, US
PCR Add-on Kit	Lexogen GmbH, Vienna, Austria
Pierce MS-compatible Magnetic IP Kit	Thermo Fisher Scientific Inc., Waltham, US
Pierce™BCA Protein Assay Kits	Thermo Fisher Scientific Inc., Waltham, US
Plasmid Midi Kit	QIAGEN GmbH, Venlo, Netherlands
Plasmid Mini Kit	QIAGEN GmbH, Venlo, Netherlands
PrimeScript™RT Master Mix (Perfect Real Time)	Takara Bio Inc., Aomori, Japan
PrimeTime™Mastermix	Integrated DNA Technologies, Coralville, US
PyroMark PCR Kit	QIAGEN GmbH, Venlo, Netherlands
PyroMark Q48 advanced CpG Reagents	QIAGEN GmbH, Venlo, Netherlands
QIAamp DNA Mini Kit	QIAGEN GmbH, Venlo, Netherlands
QIAamp Fast DNA Tissue Kit	QIAGEN GmbH, Venlo, Netherlands
QIAprep spin Miniprep Kit	QIAGEN GmbH, Venlo, Netherlands
Quantikine ELISA ms/rat leptin	R/&D Systems, Minnesota, US
QuantSeq 3' mRNA-Seq V2 Library Prep Kit FWD with UDI	Lexogen GmbH, Vienna, Austria
Qubit dsDNA BR Assay	Thermo Fisher Scientific Inc., Waltham, US
Qubit dsDNA HS Assay	Thermo Fisher Scientific Inc., Waltham, US
Quick Ligation Kit	New England Biolabs, Ipswich, US
Quick-DNA™Microprep Plus Kit	Zymo research GmbH, Freiburg, Germany
REPLI-g Mini Kit	QIAGEN GmbH, Venlo, Netherlands
RevertAid cDNA synthesis Kit	Thermo Fisher Scientific Inc., US
RNase-Free DNase Set	QIAGEN GmbH, Venlo, Netherlands
SuperScript™IV VILO™	Thermo Fisher Scientific Inc., Waltham, US
WIZARD® SV Gel and PCR Clean-up system	Promega GmbH, Wisconsin, US

Table A.20.: Chemicals used with manufacturers

Chemical	manufacturer
1,1−Dimethylbiguanide hydrochloride, D150959-5G.	Sigma Aldrich, St. Louis, US
3-Isobutyl−1-methylxanthin	Sigma Aldrich, St. Louis, US
3T3-L1 Cell Avalanche™ Transfection Reagent	EZ Biosystems, College Park, US
Acetic acid	Merck KGaA, Darmstadt, Germany
Agarose Broad Range	Carl Roth, Karlsruhe, Germany
BC isotone saline solution, 0.9 %	Berlin-Chemie AG, Berlin, Germany
Bovine serum albumin (BSA)	Sigma Aldrich, St. Louis, US
chloroform	Carl Roth, Karlsruhe, Germany
cOmplete™, Mini, EDTA-free Protease-Inhibitor-Cocktail	Roche Applied Science, Penzberg, Germany
DEPC treated water	Life Technologies, Carlsbad, US
Dexamethasone	Sigma Aldrich, St. Louis, US
Dimethyl sulfoxide (DMSO)	AppliChem GmbH, Darmstadt, Germany
DNA Away	Thermo Fisher Scientific Inc., Waltham, US
EDTA solution, pH 8.0	AppliChem GmbH, Darmstadt, Germany
Ethanol 70 %, denatured	Carl Roth, Karlsruhe, Germany
Ethanol 99.8 %, denatured	Carl Roth, Karlsruhe, Germany
Ethanol 99.8 %, pure	Carl Roth, Karlsruhe, Germany
Forskolin, CAY11018	Biomol GmbH, Hamburg, Germany
GeneRuler 100 bp DNA Ladder	Life Technologies, Carlsbad, US
GlycoBlue™	Thermo Fisher Scientific Inc., Waltham, US
GoTaq G2 Green Master Mix	Promega GmbH, Wisconsin, US
HCS LipidTox™Green neutral lipid colouring	Thermo Fisher Scientific Inc., Waltham, US
Heparin	ratiopharm GmbH, Ulm, Germany
IBMX BioUltra 99% 100mg	Th.Geyer GmbH& Co. KG, Renningen, Germany
insulin: Humalog 100 IE/mL	Eli Lilly and Company, Indianapolis, US
Isoflurane, IsoFlo®	Zoetis, Belgium
Isopropanol, pure	Thermo Fisher Scientific Inc., Waltham, US
Lipofectamin 2000	Life Technologies, Carlsbad, US
PrimeTime® Gene Expression Master Mix	Integrated DNA Technologies, Coralville, US
QIAzol Lysis Reagent	QIAGEN GmbH, Venlo, Netherlands
RNase Inhibitor	Life Technologies, Carlsbad, US
RNase ZAP	Th.Geyer GmbH& Co. KG, Renningen, Germany
Sodium chloride (NaCl), pure, solid	AppliChem GmbH, Darmstadt, Germany
Sodium oleate, O7501	Sigma Aldrich, St. Louis, US
Sodium palmitate, P9767	Sigma Aldrich, St. Louis, US
SuperScript™IV VILO™	Thermo Fisher Scientific Inc., Waltham, US
SYBR™Safe DNA Gel Stain	Thermo Fisher Scientific Inc., Waltham, US
TaqMan Fast Advanced Master Mix	Thermo Fisher Scientific Inc., Waltham, US
Tris-HCl	Carl Roth, Karlsruhe, Germany
Triton-X	Sigma Aldrich, St. Louis, US
Trizma Base, 2-Amino-2-(hydroxymethyl)-1,3-propanediol	Sigma Aldrich, St. Louis, US
Trypan Blue Solution, 0.4 %	Sigma Aldrich, St. Louis, US
trypsin TrypLE Exp.Enzyme (1X) no phenol red	Life Technologies, Carlsbad, US

Table A.21.: Diets

Diet	ID	manufacturer
60 % HFD	D12492i	Research Diets, New Brunswick, US
Liquid diet (LiD), Nutricia Fortimel Compact vanilla flavor, 2.4 kcal/mL		Danone, Paris, France
60 % HFD	E15742	Ssniff, Germany
chow diet	1314	Altromin, Germany
58 % HFD	D12331	Research Diets, New Brunswick, US

A.1.5. Hard- and Software

Table A.23.: Hardware.

Hardware	Manufacturer
2100 Bioanalyzer Instrument	Agilent Technologies, Inc., Santa Cruz, US
7300 Real Time PCR System	Applied Biosystems, Foster City, US
Autoclave, CX-65	Systec GmbH & Co. KG, Osnabrück, Germany
Cell culture clean bench	Thermo Fisher Scientific Inc., Waltham, US
Centrifuge 5425	Eppendorf SE, Hamburg, Germany
Centrifuge 5430R	Eppendorf SE, Hamburg, Germany
ChemiDoc™Touch Imaging System	Bio-Rad Laboratories Inc., Hercules, US
COPAS FP500 flow cytometer	Union Biometrica, Holliston, US
EVOS FL Auto-2 Microscope	Invitrogen, Waltham, MA, USA
EvoSep One system	EvoSep Biosystems. Odense, Denmark
Fisherbrand Bead Mill 24 Homogenizer	Fisher Scientific, Schwerte, Germany
Fixed-angle rotor FA-45-48-11	Eppendorf SE, Hamburg, Germany
Fixed-angled rotor F-35-6-30	Eppendorf SE, Hamburg, Germany
Flake ice maker	Ziegra Eismaschinen GmbH, Isernhagen, Germany
Glucometer Accu-Check	Roche Diabetes Care GmbH, Mannheim, Germany
Hybrid TIMS quadrupole TOF mass spectrometer (Bruker timsTOF Flex HT)	Thermo Fisher Scientic, Waltham, US
Incubator Hood TH 30	Edmund Bühler GmbH, Bodelshausen, Germany
Incubator with CO_2 CellXpert	Eppendorf SE, Hamburg, Germany
Incubator with CO_2 Hera cell 150	Thermo Fisher Scientic, Waltham, US
Light microscope Axiovert 40	CFL Zeiss, Jena, Germany
Magnetic rack, DiaMag02	diagenode, Belgium
Magnetic stirrer, MR 2002	Heidolph Instruments, Schwabach, Germany
Mastercycler Nexus Gradient	Eppendorf SE, Hamburg, Germany
Mastercycler Nexus X2 eco	Eppendorf SE, Hamburg, Germany
Microplate reader CLARIOstar Plus	BMG Labtech, Ortenberg, DE
Microwave	Siemens, Munich, Germany
Mini centrifuges	VWR, US; Sarstedt, Germany
Minispec LF110	Bruker, Massachusetts, US
Multichannel pipette, 10 µL, 300 µL	Eppendorf SE, Hamburg, Germany
Multifuge 35A Heraeus	Fisher Scientific, Schwerte, Germany

Continued on next page

Table A.23 – continued from previous page

Hardware	**Manufacturer**
Multistep pipette Multipette E3	Eppendorf SE, Hamburg, Germany
Multistep pipette Pipetman P20M, 2–20 µL	Gilson, Lewis Center, US
NanoDrop One spectrophotometer	Thermo Fisher Scientic, Waltham, US
Neubauer counting chamber	VWR, Radnor, US
NextSeq 2000 System	Illumina, San Diego, US
PCR Workstation	VWR, Radnor, US
PerfectBlueTM gel system, Mini L (12 x 14 cm) Peqlab	VWR, Radnor, US
PerfectBlueTM gel system, Mini S (7 x 8 cm) Peqlab	VWR, Radnor, US
pH meter PB-11	Sartorius AG, Göttingen, Germany
Pipettes, 2.5, 10, 20, 100, 200, 300, 1000 µL	Eppendorf SE, Hamburg, Germany
Pipetus Akku	Hirschmann, Neckartenzlingen, Germany
Plate shaker Titramax 100	Heidolph Instruments, Schwabach, Germany
Power supply PowerPac™Basic	Bio-Rad Laboratories Inc., Hercules, US
Precision scale, 440-47N	KERN & SOHN GmbH, Balingen, DE
Precision scale, Atilon Acculab	Sartorius AG, Göttingen, Germany
Precision scale, PCB 1000-1	KERN & SOHN GmbH, Balingen, DE
Precision scale, PT 1200	Sartorius AG, Göttingen, Germany
Precision scale, SE 203 LR	VWR, Radnor, US
PyroMark Q48 Autoprep pyrosequencer Quenzy and cartridges	QIAGEN GmbH, Venlo, Netherlands
QuantStudio 5 Real-Time PCR System	Applied Biosystems, Foster City, US
Qubit™ 4 Fluorometer	Thermo Fisher Scientic, Waltham, US
Qubit™fluorometer 2.0	Thermo Fisher Scientic, Waltham, US
Surgical instruments	Fine Science Tools, Heidelberg, Germany
Swing-bucket rotor Rotor A-2-MTP	Eppendorf SE, Hamburg, Germany
Swivel roller mixer RS-TR 5	Phoenix Instrument GmbH, Garbsen, Germany
ThermoMixer C	Eppendorf SE, Hamburg, Germany
Veiti Thermal cycler	Applied Biosystems, Foster City, US
Vortex mixer 7-2020	neoLab Migge, Heidelberg, Germany
Vortex mixer, mini	Greiner Bio-One, Kremsmünster, Austria
Water bath Grant OLS 200	Grant Instruments, Cambridge, UK
Wellwash 4 Mk 2, Labsystems	Fisher Scientific, Schwerte, Germany

Table A.24.: Software

software	manufacturer/citation	version
Biorender.com	biorender	
Design and Analysis software	Thermo Fisher Scientic, Waltham, US	2.6.0.0
DIA-NN software	[224]	
FlowPilot™III software	Union Biometrica, Holliston, US	
Image Lab	Bio-Rad Laboratories Inc., Hercules, US	6.0.1.34
ImageJ - Fiji	[299]	
Microplate Data Analysis Software (MARS)	BMG Labtech, Ortenberg, Germany	3.01
Microsoft Office 365	Microsoft	2402
Minispec Plus NF	Bruker, Massachusetts, US	
Opus	Bruker, Massachusetts, US	7
Overleaf.com	overleaf	
PRISM	GraphPad Software, Inc, US	10.0.0
PyroMark Assay Design 2.0	QIAGEN GmbH, Venlo, Netherlands	2.0.2.5
PyroMark Q48 Autoprep	QIAGEN GmbH, Venlo, Netherlands	2.4.2
R Studio	Posit PBC	2023.09.1+494
SPECTROstar Nano	BMG Labtech, Ortenberg, Germany	2.1
ThermoFisher Cloud	Thermo Fisher Scientic, Waltham, US	

A.2. Supplementary figures

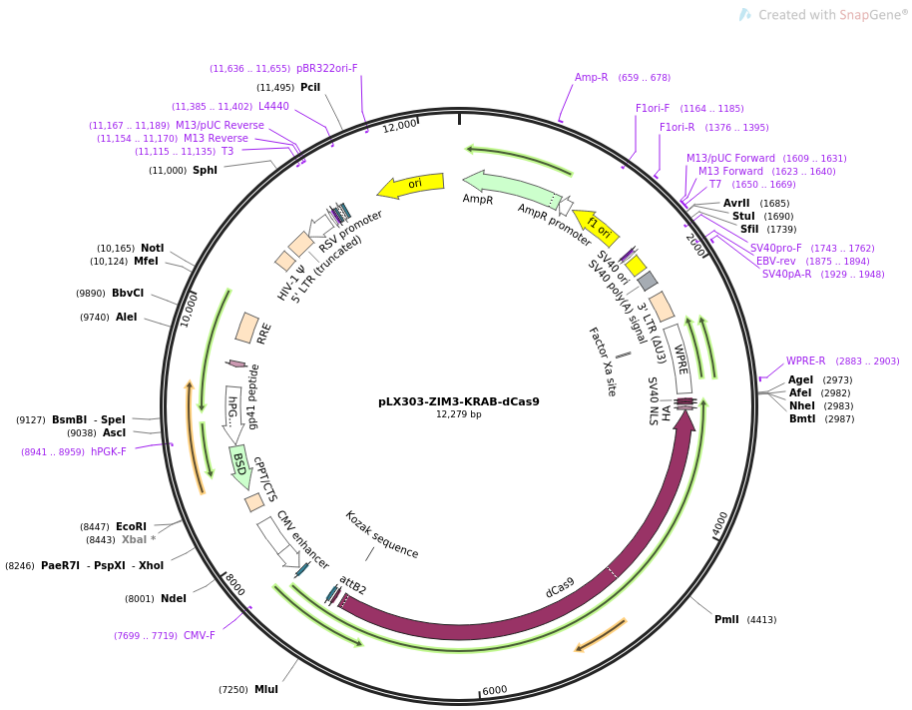

Figure A.1.: Scheme of pLX303-ZIM3-KRAB-dCas9 plasmid from Addgene. Image from https://www.addgene.org/154472/#tab-snapgene-352468.

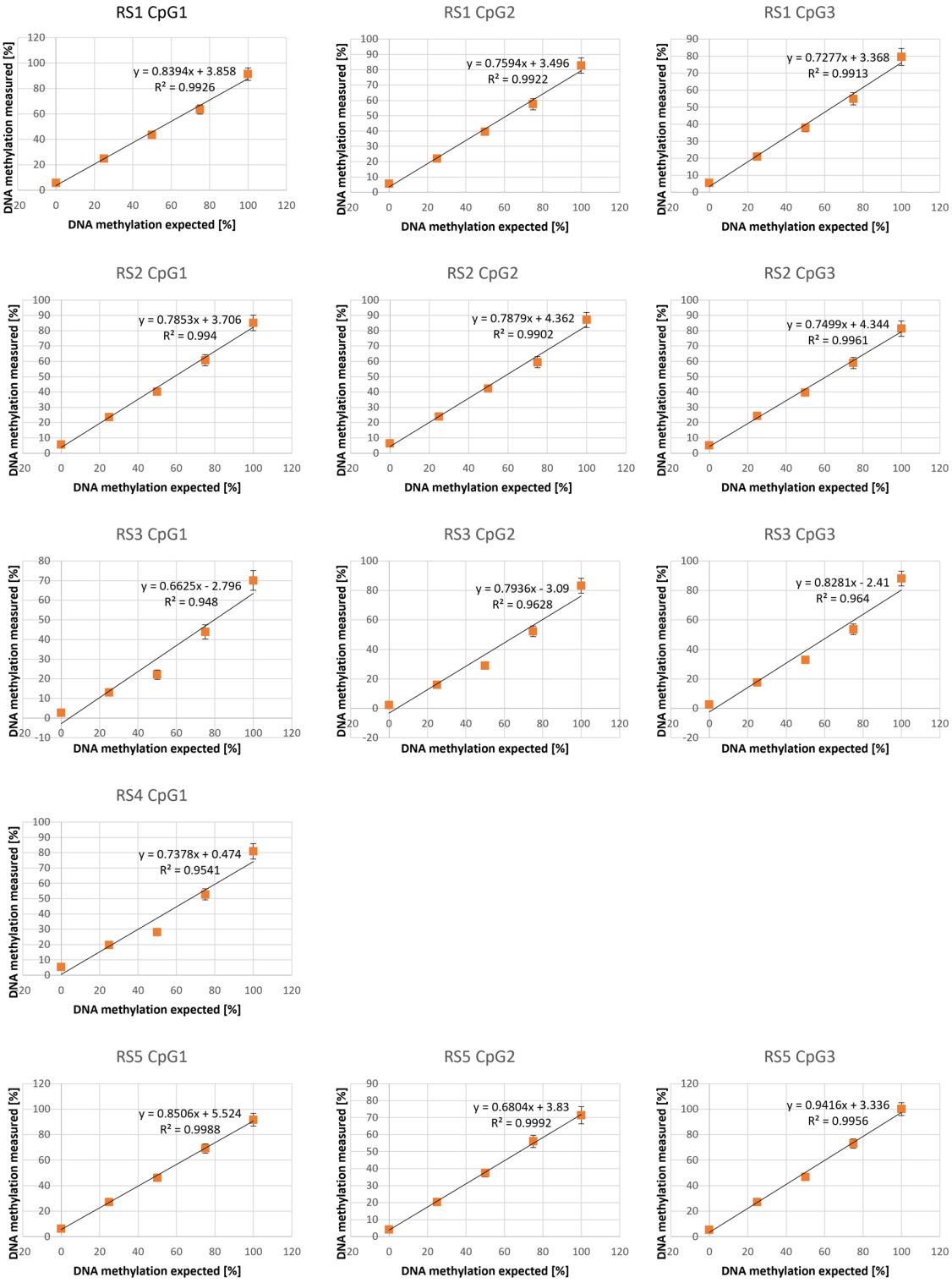

Figure A.2.: Standardcurves of the *Lep* enhancer sites RS1, RS2, RS3, RS4 and RS5 assays, established with 0, 25, 50, 75, 100 % artificially methylated mouse DNA.

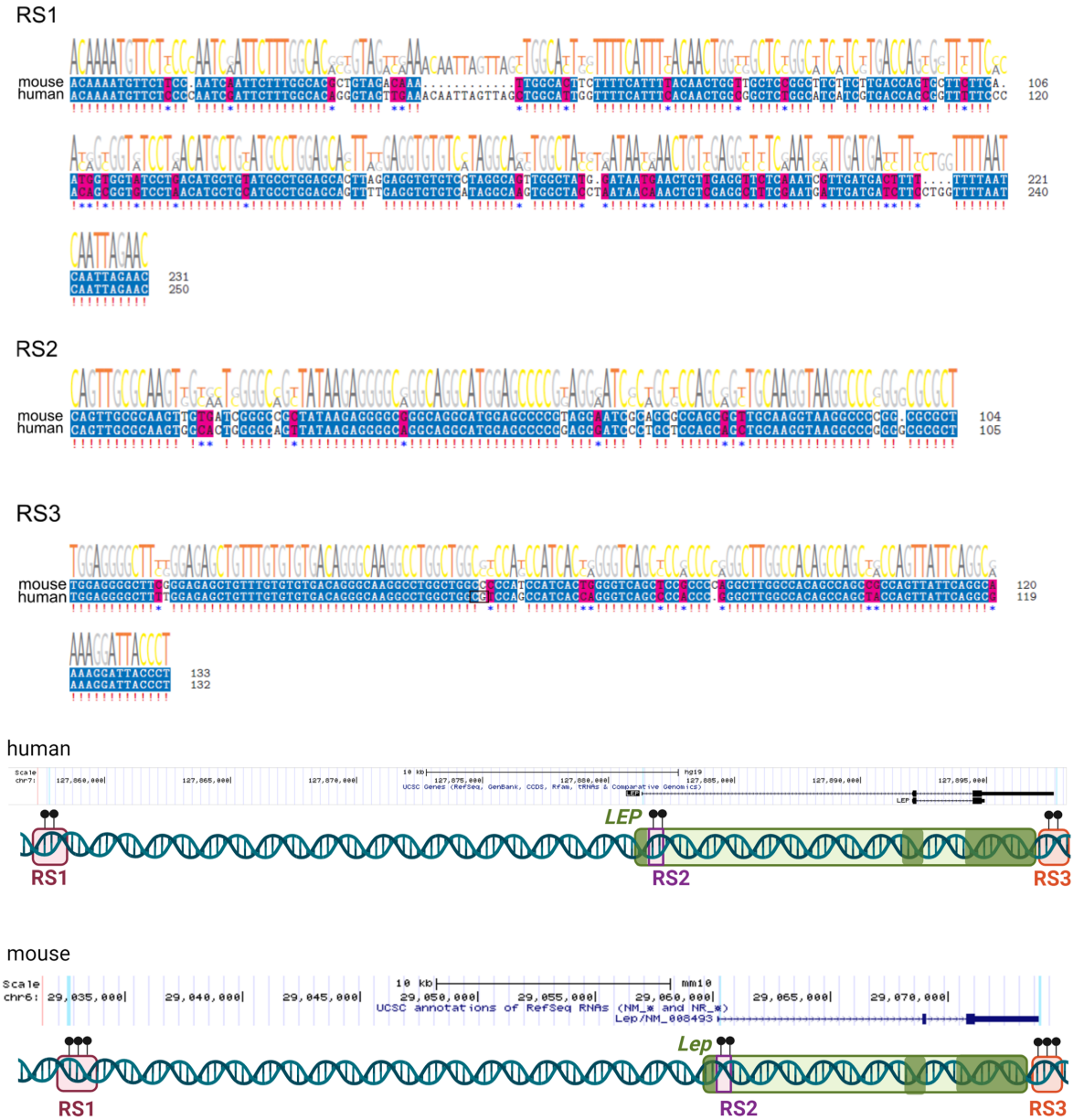

Figure A.3.: Illustration of the alignment between mouse and human and schematic presentation of the *Lep* enhancer regulatory sites (RS) in the human and mouse genomic context. The figure is part of the submitted manuscript.

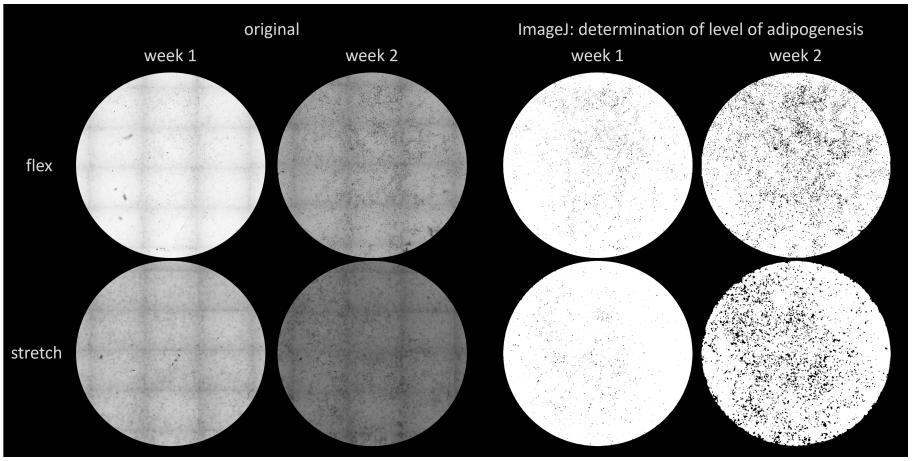

Figure A.4.: Example of microscopic images for analysis of level of adipogenesis. 4X images of 3T3-cell cultures were stitched and analyzed using ImageJ. Weeks post induction of differentiation are indicated under stretch and flex conditions.

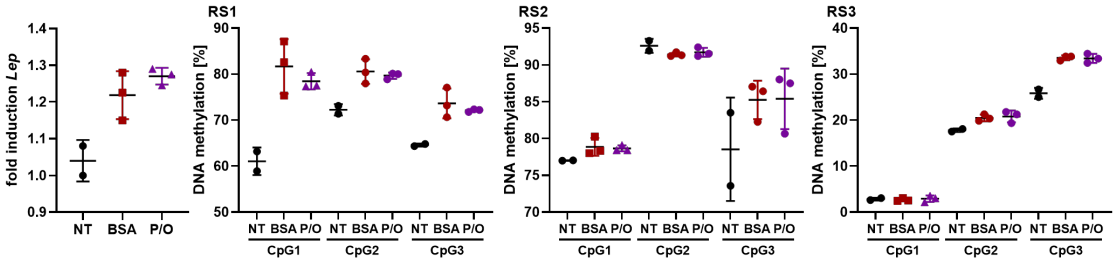

Figure A.5.: 3T3-adipocytes with naive treatment (NT), BSA as control and palmitate/oleate (P/O) treatment.

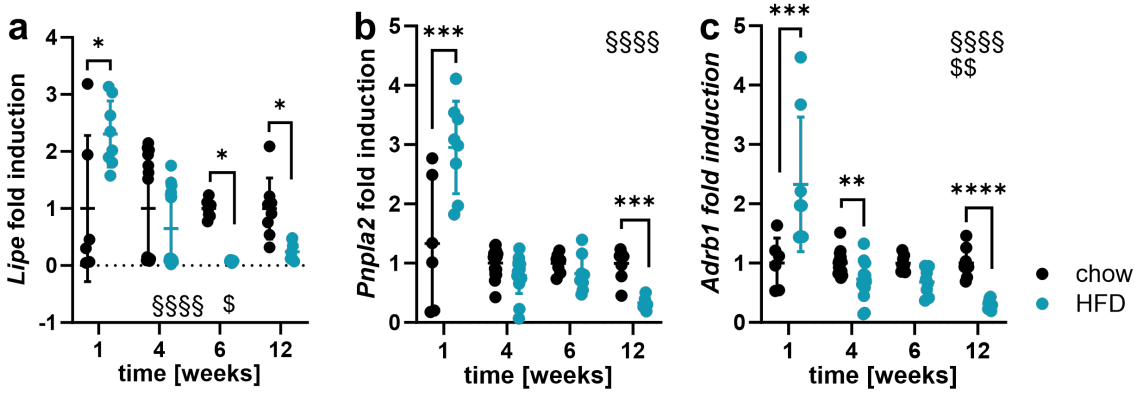

Figure A.6.: Genes of key enzymes of lipolysis in eWAT of DIO mice. Data were analyzed using a two-way ANOVA with post hoc analysis after Holm-Sidak; §§§§ $p_{interaction} < 0.0001$, $$ $p_{group} < 0.01$, $^{*}p < 0.05$, $^{**}p < 0.01$, $^{***}p < 0.001$, $^{****}p < 0.0001$, details of ANOVA statistics in Table A.30. *Lipe*–Lipase E gene; *Pnpla2*–Patatin Like Phospholipase Domain Containing 2 gene, *Adrb1*–β1-adrenergic receptor gene

A.3. Statistical analysis & supplementary tables

Table A.25.: *Lep* regulatory enhancer site and individual CpG location, assignment to their literature and putative transcriptional regulator binding.

Regulatory enhancer site	genomic location (mm10, chr6)	genomic location of CpGs	putative transcriptional regulators	Reference
RS1	29032562 – 29032609	CpG1: 29032574	unknown	[188]
		CpG2: 29032582		
		CpG3: 29032597		
RS2	29060232 – 29060278	CpG1: 29060257	AP2β	[89]
		CpG2: 29060262		
		CpG3: 29060264		
RS3	29073886 – 29074080	CpG1: 29073954	PPARγ/RXRα, NFIa-c, NFIx	[92, 93]
		CpG2: 29073984		
		CpG3: 29074019		
RS4	29068580 – 29068654	CpG : 29043801	PPARγ/RXRα, EBF1, NFY	[92–94]
RS5	29068580 – 29068654	CpG1: 29068580	unknown	[188]
		CpG2: 29068639		
		CpG3: 29068653		

Table A.26.: Details of statistical analysis of 2-way ANOVA of DIO *Lep* enhancer sites (RS) in eWAT, F–F-statistic; DF–degrees of freedom

Enhancer site	CpG	Tested factor	F(DFn. DFd)	p-value	Enhancer site	CpG	Tested factor	F(DFn. DFd)	p-value
RS1	CpG1	time*diet	F (7. 143) = 10.15	<0.0001	RS4	CpG1	time*diet	F (7. 137) = 1.926	0.0699
		time	F (7. 143) = 14.08	<0.0001			time	F (7. 137) = 2.224	0.0358
		diet	F (1. 143) = 265.0	<0.0001			diet	F (1. 137) = 12.34	0.0006
	CpG2	time*diet	F (7. 143) = 5.912	<0.0001	RS5	CpG1	time*diet	F (7. 143) = 3.191	0.0036
		time	F (7. 143) = 8.217	<0.0001			time	F (7. 143) = 1.271	0.2688
		diet	F (1. 143) = 220.5	<0.0001			diet	F (1. 143) = 37.73	<0.0001
	CpG3	time*diet	F (7. 143) = 10.82	<0.0001		CpG2	time*diet	F (7. 142) = 1.598	0.1407
		time	F (7. 143) = 16.13	<0.0001			time	F (7. 142) = 2.051	0.0528
		diet	F (1. 143) = 390.1	<0.0001			diet	F (1. 142) = 4.617	0.0333
RS2	CpG1	time*diet	F (7. 142) = 18.72	<0.0001		CpG3	time*diet	F (7. 143) = 0.6799	0.6888
		time	F (7. 142) = 19.24	<0.0001			time	F (7. 143) = 1.133	0.346
		diet	F (1. 142) = 321.1	<0.0001			diet	F (1. 143) = 5.017	0.0266
	CpG2	time*diet	F (7. 142) = 12.70	<0.0001					
		time	F (7. 142) = 14.53	<0.0001					
		diet	F (1. 142) = 289.7	<0.0001					
	CpG3	time*diet	F (7. 142) = 10.64	<0.0001					
		time	F (7. 142) = 11.02	<0.0001					
		diet	F (1. 142) = 208.0	<0.0001					
RS3	CpG1	time*diet	F (7. 134) = 6.386	<0.0001					
		time	F (7. 134) = 6.287	<0.0001					
		diet	F (1. 134) = 50.54	<0.0001					
	CpG2	time*diet	F (7. 143) = 3.826	0.0008					
		time	F (7. 143) = 4.503	0.0001					
		diet	F (1. 143) = 30.39	<0.0001					
	CpG3	time*diet	F (7. 143) = 3.944	0.0006					
		time	F (7. 143) = 4.462	0.0002					
		diet	F (1. 143) = 43.07	<0.0001					

Table A.27.: Details of statistical analysis of 2-way ANOVA of DIO phenotype results; F–F-statistic; DF–degrees of freedom

Parameter	Tested factors	F(DFn. DFd)	p-value
body weight	Interaction	F (8. 221) = 78.05	<0.0001
	Time	F (8. 221) = 406.1	<0.0001
	Diet	F (1. 221) = 975.6	<0.0001
fat mass %BW	Interaction	F (7. 184) = 186.8	<0.0001
	Time	F (3.356. 88.21) = 386.8	<0.0001
	Diet	F (1. 38) = 200.8	<0.0001
plasma leptin	Interaction	F (7. 76) = 22.36	<0.0001
	Time	F (7. 76) = 22.98	<0.0001
	Diet	F (1. 76) = 420.7	<0.0001
Lep	Interaction	F (7. 134) = 1.487	0.1769
	Time	F (7. 134) = 16.53	<0.0001
	Diet	F (1. 134) = 60.54	<0.0001

Table A.28.: DIO study: r-values Pearson correlation for each indicated week for epididymal adipose tissue

week		weight	-ΔCT(Lep)	RS1_mean	RS2_mean	RS3_mean	RS4_CpG1	RS5_mean
1	weight	1	0.657102	0.644407	0.550781	0.654105	0.455191	-0.20126
	-ΔCT(Lep)	0.657102	1	0.618422	0.4818	0.518538	0.391421	0.125975
2	weight	1	0.258582	0.327788	0.218315	-0.18282	-0.31799	-0.3533
	-ΔCT(Lep)	0.258582	1	0.521767	0.404205	0.226212	0.504069	-0.24007
4	weight	1	0.235077	0.651904	0.527237	0.272671	0.219556	0.132699
	-ΔCT(Lep)	0.235077	1	0.323984	0.479713	-0.24002	-0.36191	-0.32467
5	weight	1	0.913853	0.973321	0.975861	0.817022	0.688354	-0.20555
	-ΔCT(Lep)	0.913853	1	0.917285	0.910228	0.673108	0.642599	-0.12259
6	weight	1	0.798564	0.888023	0.882364	0.567281	0.541631	-0.53071
	-ΔCT(Lep)	0.798564	1	0.728519	0.634281	0.625796	0.466651	-0.54122
7	weight	1	0.847922	0.954338	0.964342	0.744999	0.948501	-0.61677
	-ΔCT(Lep)	0.847922	1	0.884724	0.886874	0.57464	0.884028	-0.59611
8	weight	1	0.434822	0.839958	0.468782	0.815477	0.461168	-0.4809
	-ΔCT(Lep)	0.434822	1	0.422862	0.180799	0.644348	-0.14747	-0.27142
12	weight	1	0.246584	0.926785	0.88962	0.862254	0.130211	0.140203
	-ΔCT(Lep)	0.246584	1	0.414928	0.497115	0.265678	0.705325	-0.42161

Table A.29.: DIO study: p-values Pearson correlation for each indicated week for epididymal adipose tissue

week		weight	-ΔCT(Lep)	RS1_mean	RS2_mean	RS3_mean	RS4_CpG1	RS5_mean
1	weight		0.0147	0.00705	0.02703	0.00598	0.07645	0.45480
	-ΔCT(Lep)	0.01467541		0.02426	0.09548	0.06944	0.18596	0.68175
2	weight		0.3335	0.21520	0.41662	0.49796	0.23004	0.17949
	-ΔCT(Lep)	0.3335394		0.03817	0.12047	0.39954	0.04649	0.37048
4	weight		0.2196	0.00005	0.00193	0.13108	0.24371	0.46906
	-ΔCT(Lep)	0.21962117		0.08643	0.00845	0.20980	0.06360	0.08573
5	weight		0.0000	0.00000	0.00000	0.00011	0.00320	0.44504
	-ΔCT(Lep)	7.5003E-07		0.00000	0.00000	0.00427	0.00726	0.65106
6	weight		0.0002	0.00000	0.00001	0.02192	0.03023	0.03443
	-ΔCT(Lep)	0.00020792		0.00137	0.00832	0.00951	0.06843	0.03038
7	weight		0.0001	0.00000	0.00000	0.00144	0.00000	0.01432
	-ΔCT(Lep)	0.00012764		0.00003	0.00002	0.03160	0.00030	0.02446
8	weight		0.0184	0.00000	0.00680	0.00000	0.00902	0.00533
	-ΔCT(Lep)	0.01841209		0.02229	0.34795	0.00016	0.45394	0.15437
12	weight		0.3572	0.00000	0.00000	0.00002	0.63077	0.60453
	-ΔCT(Lep)	0.3572303		0.11002	0.05010	0.31996	0.00227	0.10384

Table A.30.: Details of statistical analysis of 2-way ANOVA of DIO qPCR results; dCT values against housekeeper *Hprt* were used for expression testing, F–F-statistic; DF–degrees of freedom

gene	Tested factors	F (DFn. DFd)	p-value	gene	Tested factors	F (DFn. DFd)	p-value
Dnmt3a	Interaction	F (1. 28) = 1.390	0.2483	*Arg1*	Interaction	F (7. 135) = 0.9843	0.4454
	Time	F (1. 28) = 7.565	0.0103		Time	F (7. 135) = 5.444	<0.0001
	Diet	F (1. 28) = 19.24	0.0001		Diet	F (1. 135) = 0.4710	0.4937
Dnmt3b	Interaction	F (1. 25) = 14.27	0.0009	*Lipe*	Interaction	F (3. 70) = 9.966	<0.0001
	Time	F (1. 25) = 0.2066	0.6534		Time	F (3. 70) = 0.8281	0.4828
	Diet	F (1. 25) = 3.107	0.0902		Diet	F (1. 70) = 7.002	0.01
Tet2	Interaction	F (1. 28) = 5.507	0.0262	*Pnpla2*	Interaction	F (3. 70) = 12.70	<0.0001
	Time	F (1. 28) = 0.4499	0.5079		Time	F (3. 70) = 3.713	0.0154
	Diet	F (1. 28) = 0.05979	0.8086		Diet	F (1. 70) = 0.7101	0.4023
Tet3	Interaction	F (1. 26) = 7.666	0.0102	*Adrb1*	Interaction	F (3. 67) = 16.37	<0.0001
	Time	F (1. 26) = 0.007601	0.9312		Time	F (3. 67) = 11.10	<0.0001
	Diet	F (1. 26) = 2.481	0.1273		Diet	F (1. 67) = 10.17	0.0022
Itgax	Interaction	F (7. 135) = 12.66	<0.0001				
	Time	F (7. 135) = 24.33	<0.0001				
	Diet	F (1. 135) = 77.51	<0.0001				

Table A.31.: Human correlation, Pearson correlation coefficient r

	weight [kg]	BMI	-dCt_LEP	RS1_CpG1	RS1_CpG2	RS2_CpG1	RS2_CpG2	RS2_CpG3	RS3_CpG1	RS3_CpG2
weight [kg]	1.00	0.87	-0.16	0.09	0.18	0.14	0.16	0.14	0.05	-0.01
BMI	0.87	1.00	-0.14	0.09	0.18	0.09	0.21	0.11	0.06	0.01
-dCt_LEP	-0.16	-0.14	1.00	0.14	0.12	0.09	0.09	0.08	0.05	0.08
RS1_CpG1	0.09	0.09	0.14	1.00	0.45	0.14	0.32	0.30	-0.23	0.15
RS1_CpG2	0.18	0.18	0.12	0.45	1.00	0.27	0.20	0.20	0.18	0.31
RS2_CpG1	0.14	0.09	0.09	0.14	0.27	1.00	0.50	0.65	0.14	0.41
RS2_CpG2	0.16	0.21	0.09	0.32	0.20	0.50	1.00	0.62	-0.06	0.35
RS2_CpG3	0.14	0.11	0.08	0.30	0.20	0.65	0.62	1.00	0.04	0.32
RS3_CpG1	0.05	0.06	0.05	-0.23	0.18	0.14	-0.06	0.04	1.00	0.44
RS3_CpG2	-0.01	0.01	0.08	0.15	0.31	0.41	0.35	0.32	0.44	1.00

Table A.32.: Human correlation, Pearson correlation p-values

	weight [kg]	BMI	-dCt_LEP	RS1_CpG1	RS1_CpG2	RS2_CpG1	RS2_CpG2	RS2_CpG3	RS3_CpG1	RS3_CpG2
weight [kg]		0.00	0.14	0.40	0.10	0.21	0.14	0.21	0.66	0.92
BMI	0.00		0.18	0.41	0.10	0.39	0.05	0.29	0.58	0.90
-dCt_LEP	0.14	0.18		0.19	0.25	0.42	0.42	0.45	0.62	0.42
RS1_CpG1	0.40	0.41	0.19		0.00	0.19	0.00	0.01	0.03	0.15
RS1_CpG2	0.10	0.10	0.25	0.00		0.01	0.07	0.07	0.09	0.00
RS2_CpG1	0.21	0.39	0.42	0.19	0.01		0.00	0.00	0.20	0.00
RS2_CpG2	0.14	0.05	0.42	0.00	0.07	0.00		0.00	0.56	0.00
RS2_CpG3	0.21	0.29	0.45	0.01	0.07	0.00	0.00		0.74	0.00
RS3_CpG1	0.66	0.58	0.62	0.03	0.09	0.20	0.56	0.74		0.00
RS3_CpG2	0.92	0.90	0.42	0.15	0.00	0.00	0.00	0.00	0.00	

Table A.33.: Details of statistical analysis of 2-way ANOVA of DIO *Lep* enhancer sites (RS) in iWAT, dCT values against housekeeper *Rplp0* were used for expression testing, F–F-statistic; DF–degrees of freedom

Enhancer site	CpG	Tested Factors	F(DFn. DFd)	p-value	Enhancer site	CpG	Tested Factors	F(DFn. DFd)	p-value
RS1	CpG1	time*diet	F (1. 28) = 1.282	0.2672	RS4		time*diet	F (3. 54) = 3.277	0.0278
		time	F (1. 28) = 0.08816	0.7687			time	F (3. 54) = 1.043	0.3809
		diet	F (1. 28) = 1.155	0.2917			diet	F (1. 54) = 0.9174	0.3424
	CpG2	time*diet	F (1. 28) = 0.6773	0.4175	RS5	CpG1	time*diet	F (3. 72) = 0.8383	0.4773
		time	F (1. 28) = 0.2452	0.6243			time	F (3. 72) = 3.152	0.03
		diet	F (1. 28) = 1.324	0.2596			diet	F (1. 72) = 18.02	<0.0001
	CpG3	time*diet	F (1. 28) = 0.4185	0.523		CpG2	time*diet	F (3. 72) = 2.515	0.0651
		time	F (1. 28) = 0.5547	0.4626			time	F (3. 72) = 18.03	<0.0001
		diet	F (1. 28) = 0.8045	0.3774			diet	F (1. 72) = 9.460	0.003
RS2	CpG1	time*diet	F (1. 28) = 1.398	0.2469		CpG3	time*diet	F (3. 72) = 0.2564	0.8566
		time	F (1. 28) = 1.275	0.2684			time	F (3. 72) = 4.789	0.0042
		diet	F (1. 28) = 0.2457	0.624			diet	F (1. 72) = 5.213	0.0254
	CpG2	time*diet	F (1. 28) = 0.3831	0.541	*Lep*		F (1, 26) = 5.130	0.0321	
		time	F (1. 28) = 0.3205	0.5758	expression		F (1, 26) = 59.43	<0.0001	
		diet	F (1. 28) = 0.04540	0.8328			F (1, 26) = 24.71	<0.0001	
	CpG3	time*diet	F (1. 28) = 1.596	0.2169					
		time	F (1. 28) = 0.07193	0.7905					
		diet	F (1. 28) = 0.0005782	0.981					
RS3	CpG1	time*diet	F (1. 28) = 0.1808	0.6739					
		time	F (1. 28) = 3.004	0.094					
		diet	F (1. 28) = 0.0002078	0.9886					
	CpG2	time*diet	F (1. 28) = 0.9681	0.3336					
		time	F (1. 28) = 2.908	0.0992					
		diet	F (1. 28) = 0.3920	0.5363					
	CpG3	time*diet	F (1. 28) = 0.1411	0.7101					
		time	F (1. 28) = 2.344	0.137					
		diet	F (1. 28) = 0.0008137	0.9774					

Table A.34.: DIO study: r-values Pearson correlation for each indicated week for inguinal adipose tissue

week		weight	-ΔCT(Lep)	RS1_mean	RS2_mean	RS3_mean	RS4_CpG1	RS5_mean
1	weight	1	-0.071987319	-0.0136531	-0.044855914	-0.4137535	-0.0616107	0.65002759
	-ΔCT(Lep)	0.65002759	-0.164715573	-0.2524385	-0.246314885	-0.4971479	-0.3576737	1
2	weight	1				-0.2787614		0.62028416
	-ΔCT(Lep)	0.62028416				-0.3218777		1
4	weight	1				-0.6576529	-0.275944	0.46063405
	-ΔCT(Lep)	0.46063405				-0.4004824	-0.1031742	1
5	weight	1						0.90748601
	-ΔCT(Lep)	0.90748601						1
6	weight	1						0.89767133
	-ΔCT(Lep)	0.89767133						1
7	weight	1						0.89005383
	-ΔCT(Lep)	0.89005383						1
8	weight	1	0.57967496			-0.4235951	0.56110317	0.81309981
	-ΔCT(Lep)	0.81309981	0.562817528			-0.4588446	0.56897873	1
12	weight	1	-0.096016493	-0.4866335	0.033634678	-0.749842	0.48143297	0.81336227
	-ΔCT(Lep)	0.81336227	-0.156186002	-0.2253537	0.413636887	-0.7047694	0.6263362	1

Table A.35.: DIO study: p-values Pearson correlation for each indicated week for inguinal adipose tissue

week		weight	-ΔCT(Lep)	RS1_mean	RS2_mean	RS3_mean	RS4_CpG1	RS5_mean
1	weight		0.87387906	0.79876324	0.96148307	0.82068317	0.11113209	0.00641271
	-ΔCT(Lep)	0.0064	0.37617787	0.55745418	0.36403826	0.1737828	0.05008597	
2	weight						0.29579019	0.01036179
	-ΔCT(Lep)	0.0104					0.2240782	
4	weight					0.30090139	0.00562515	0.00797606
	-ΔCT(Lep)	0.0080				0.7037695	0.12425408	
5	weight							1.2143E-06
	-ΔCT(Lep)	0.0000						
6	weight							2.3944E-06
	-ΔCT(Lep)	0.0000						
7	weight							8.8031E-06
	-ΔCT(Lep)	0.0000						
8	weight			0.00063184		0.02373708	0.10205046	2.7251E-08
	-ΔCT(Lep)	0.0000		0.00120484		0.02143852	0.07382057	
12	weight		0.90158516	0.72354107	0.05593756	0.05901163	0.00082302	0.00012712
	-ΔCT(Lep)	0.0001	0.11124301	0.5635139	0.401375	0.00943381	0.00229846	

Table A.36.: Details of statistical analysis of one-way ANOVA of ob/ob mice, each CpG individual; dCT values against housekeeper *Hprt* were used for expression testing, F–F-statistic; DF–degrees of freedom

Enhancer Site/Gene	CpG	F(DFn. DFd)	p-value
Lep expression		F (2. 23) = 9.244	0.0011
RS1	CpG1	F (2. 23) = 74.58	<0.0001
	CpG2	F (2. 23) = 147.5	<0.0001
	CpG3	F (2. 23) = 115.5	<0.0001
RS2	CpG1	F (2. 23) = 86.57	<0.0001
	CpG2	F (2. 23) = 83.02	<0.0001
	CpG3	F (2. 23) = 58.95	<0.0001
RS3	CpG1	F (2. 22) = 26.50	<0.0001
	CpG2	F (2. 22) = 17.45	<0.0001
	CpG3	F (2. 22) = 27.33	<0.0001

Table A.37.: Stretch during 3T3 differentiation: first 50 differentially downregulated genes.

geneID	logFC	logCPM	LR	PValue	adj.P.Val
Tap2	-1.39378	7.087545	46.53232	9.01E-12	2.05E-08
Zbtb16	-1.74456	5.984871	41.83139	9.95E-11	1.13E-07
Adamts12	-1.29827	5.703009	40.6261	1.84E-10	1.86E-07
Syn2	-2.45457	6.257265	40.19869	2.29E-10	2.09E-07
Abhd15	-1.72923	5.303444	36.49756	1.53E-09	1.07E-06
Igf2	-1.96306	6.250479	34.63636	3.97E-09	2.26E-06
Mc5r	-2.35389	3.690164	34.03585	5.41E-09	2.73E-06
Mrgprf	-1.32588	5.528844	33.22507	8.21E-09	3.8E-06
Nectin2	-1.30203	5.607857	30.68725	3.03E-08	1.06E-05
Farsa	-1.18681	7.55392	30.49652	3.34E-08	1.13E-05
Clec3b	-2.032	8.333514	29.36155	6.01E-08	1.76E-05
Bcat2	-1.50255	5.901373	29.22127	6.46E-08	1.84E-05
Rhob	-1.04793	7.048098	29.14445	6.72E-08	1.85E-05
Chst1	-1.61217	5.581295	29.06268	7.01E-08	1.88E-05
Rgma	-1.2548	5.618645	28.01619	1.2E-07	2.88E-05
Zfp41	-1.78823	3.596088	27.7181	1.4E-07	3.19E-05
Pim3	-1.32164	7.627988	27.65621	1.45E-07	3.22E-05
Pnpla2	-1.66611	9.674888	27.48065	1.59E-07	3.33E-05
Dlc1	-1.13603	8.40264	27.45438	1.61E-07	3.33E-05
Rnf157	-1.29575	4.495802	26.00109	3.41E-07	6.47E-05
Irf1	-1.08919	6.921066	25.83541	3.72E-07	6.77E-05
Atp1a2	-1.45177	6.289141	25.38037	4.71E-07	8.4E-05
Mcam	-1.31126	5.431786	25.16883	5.25E-07	9.19E-05
Gtpbp1	-1.14068	5.490048	24.82766	6.27E-07	0.000104
Abca2	-1.31305	5.435931	24.35176	8.03E-07	0.000128
Cldn15	-1.46026	7.303267	24.22821	8.56E-07	0.000132
Ksr1	-1.11224	5.261657	23.75647	1.09E-06	0.000158
Glul	-1.56859	8.816345	23.75047	1.1E-06	0.000158
Cluh	-1.07942	7.979601	23.36417	1.34E-06	0.000188
Slc2a10	-1.26127	4.758802	22.842	1.76E-06	0.000229
Dgat2	-1.32589	7.396538	22.42267	2.19E-06	0.000269
Cebpa	-1.27929	7.159001	22.32377	2.3E-06	0.000279
Rassf2	-1.37204	5.421481	21.25546	4.02E-06	0.000451
R3hdm4	-0.94705	6.922484	21.01202	4.56E-06	0.000494
Smarcd2	-0.91735	6.588822	20.77829	5.16E-06	0.000546
Lgals3bp	-1.10709	9.025465	20.60547	5.64E-06	0.000573

Continued on next page

Table A.37 – continued from previous page

geneID	logFC	logCPM	LR	PValue	adj.P.Val
H2-K1	-1.01693	10.30264	20.59865	5.66E-06	0.000573
Lpin1	-1.05975	6.42763	20.57422	5.74E-06	0.000574
Lipe	-1.48873	9.23201	20.40106	6.28E-06	0.000608
Fus	-1.18054	10.22028	20.36787	6.39E-06	0.000612
Phldb1	-0.9997	5.860296	20.23266	6.86E-06	0.000644
Fndc10	-1.23396	4.969365	20.23146	6.86E-06	0.000644
Akt2	-1.04207	6.808515	20.04447	7.57E-06	0.000695
Ptpa	-0.90088	7.328958	19.87397	8.27E-06	0.000753
Plin1	-1.47328	7.374605	19.73516	8.89E-06	0.000786
Spag7	-1.00974	7.167001	19.3872	1.07E-05	0.000922
Fasn	-1.08098	8.517693	19.31768	1.11E-05	0.000932
Spry4	-1.15418	4.328834	19.09217	1.25E-05	0.00103
Cidec	-1.34158	9.413705	18.97907	1.32E-05	0.001074
Abcd1	-0.97332	5.752937	18.87256	1.4E-05	0.001106

Table A.38.: Stretch during 3T3 differentiation: first 50 differentially upregulated genes.

geneID	logFC	logCPM	LR	PValue	adj.P.Val
Kcnq1ot1	2.076889	6.431163	59.05461	1.53E-14	9.51E-11
Rnase4	1.873626	8.111427	58.44422	2.09E-14	9.51E-11
Phldb2	1.614908	6.632333	48.02931	4.2E-12	1.27E-08
Grem1	3.091711	4.050289	44.16953	3.01E-11	5.09E-08
Ccl6	1.805514	6.379733	43.95769	3.36E-11	5.09E-08
S100a7l2	2.546386	4.511897	42.54707	6.9E-11	8.97E-08
Jam2	1.645903	4.275493	37.51748	9.06E-10	7.44E-07
Malat1	1.254258	12.47005	37.36126	9.82E-10	7.44E-07
Ccl9	1.330917	5.494694	36.32115	1.67E-09	1.09E-06
Slpi	2.342351	4.465984	35.1453	3.06E-09	1.86E-06
Spink5	2.406358	4.149581	34.24097	4.87E-09	2.61E-06
Timp3	4.269511	4.881919	33.18883	8.36E-09	3.8E-06
Aspn	1.389643	9.605494	31.4414	2.06E-08	8.72E-06
Tmsb4x	1.3989	9.632391	31.39188	2.11E-08	8.72E-06
Nexn	1.720485	4.268593	31.28919	2.22E-08	8.79E-06
Hif1a	1.031545	7.071384	31.09503	2.46E-08	8.99E-06
Dzip3	1.34599	5.217686	31.08455	2.47E-08	8.99E-06
Ttc14	1.189019	5.394931	30.07531	4.16E-08	1.35E-05

Continued on next page

Table A.38 – continued from previous page

geneID	**logFC**	**logCPM**	**LR**	**PValue**	**adj.P.Val**
Gm5886	2.429563	8.126666	29.92276	4.5E-08	1.41E-05
Nox4	2.128784	3.343403	29.57383	5.38E-08	1.63E-05
Ankrd12	1.104194	7.578097	28.37863	9.98E-08	2.59E-05
Cd9	1.252292	6.40818	28.04678	1.18E-07	2.88E-05
Wfdc3	3.170996	3.580888	28.04271	1.19E-07	2.88E-05
Pdgfrl	1.43791	6.90807	27.96926	1.23E-07	2.88E-05
Sorbs2	2.155561	3.888773	27.46613	1.6E-07	3.33E-05
Tgfbi	2.380545	4.031774	26.66514	2.42E-07	4.89E-05
Bdnf	1.625627	5.531146	26.56955	2.54E-07	4.97E-05
Ccn5	1.377187	4.899657	26.55078	2.57E-07	4.97E-05
Mgp	2.59586	9.117778	25.95324	3.5E-07	6.49E-05
Ctla2a	1.384739	5.319292	25.02531	5.66E-07	9.71E-05
Ecrg4	2.993169	3.202989	24.93686	5.92E-07	9.98E-05
Ogn	1.365205	7.378799	24.53117	7.31E-07	0.000119
Ccdc88a	1.192618	7.039832	24.22993	8.55E-07	0.000132
Fam162a	1.110867	7.130902	24.13158	9E-07	0.000136
Cop1	1.145488	5.116807	23.825	1.06E-06	0.000157
Prpf39	1.272986	5.491943	23.67675	1.14E-06	0.000162
Col8a1	2.65254	6.810672	23.25395	1.42E-06	0.000196
Ccdc34	1.131137	6.499099	23.09132	1.54E-06	0.00021
Fn1	1.477983	10.16434	22.94417	1.67E-06	0.000223
Arid4b	0.984427	6.748328	22.83614	1.76E-06	0.000229
Paxbp1	1.087353	4.951213	22.81453	1.78E-06	0.000229
Ppig	0.981053	7.663535	22.73919	1.86E-06	0.000234
Akap9	0.960938	6.479251	22.49189	2.11E-06	0.000263
Rgs4	2.880195	2.486969	22.19151	2.47E-06	0.000295
Gas5	2.096137	6.421263	21.96216	2.78E-06	0.000329
Col12a1	1.206284	5.512387	21.61706	3.33E-06	0.000388
Ctsk	1.912003	5.398023	21.52318	3.5E-06	0.000403
Ppef1	1.273925	5.571947	21.42707	3.68E-06	0.000418
Samd4	0.967558	5.617537	21.1876	4.16E-06	0.000462
Naa50	0.910487	6.958706	21.14099	4.27E-06	0.000468

Table A.39.: Details of statistical analysis of 2-way repeated measures ANOVA or mixed effects analysis of sorted adipocytes; F–F-statistic; DF–degrees of freedom

Enhancer site / Parameter	CpG	Tested factors	F(DFn. DFd)	p-value	Enhancer site / Parameter	CpG	Tested factors	F(DFn. DFd)	p-value
RS1	CpG1	Fraction x Feeding	F (1. 11) = 0.8517	0.3759	RS3	CpG1	Fraction	F (1. 7) = 3.638	0.0981
		Fraction	F (1. 11) = 14.79	0.0027			Feeding	F (1. 8) = 0.4454	0.5233
		Feeding	F (1. 11) = 2.779	0.1237			Fraction x Feeding	F (1. 7) = 4.191	0.0799
		Mouse	F (11. 11) = 1.448	0.2749		CpG2	Fraction	F (1. 15) = 2.861	0.1114
	CpG2	Fraction x Feeding	F (1. 11) = 0.4040	0.538			Feeding	F (1. 15) = 7.318	0.0163
		Fraction	F (1. 11) = 25.40	0.0004			Fraction x Feeding	F (1. 15) = 0.004505	0.9474
		Feeding	F (1. 11) = 4.106	0.0677		CpG3	Fraction	F (1. 7) = 8.642	0.0217
		Mouse	F (11. 11) = 1.755	0.1825			Feeding	F (1. 8) = 0.2456	0.6335
	CpG3	Fraction x Feeding	F (1. 11) = 1.499	0.2463			Fraction x Feeding	F (1. 7) = 4.061	0.0837
		Fraction	F (1. 11) = 13.62	0.0036	Adipocyte		Fraction x Diet	F (2. 24) = 3.511	0.046
		Feeding	F (1. 11) = 2.245	0.1622	proportions		Fraction	F (2. 24) = 5.965	0.0079
		Mouse	F (11. 11) = 1.596	0.2254			Diet	F (1. 12) = 1.714	0.2149
RS2	CpG1	Fraction x Feeding	F (1. 11) = 2.660	0.1312			Mouse	F (12. 24) = 2.133e-006	>0.9999
		Fraction	F (1. 11) = 13.74	0.0035					
		Feeding	F (1. 11) = 0.1370	0.7183					
		Mouse	F (11. 11) = 1.918	0.1475					
	CpG2	Fraction x Feeding	F (1. 11) = 2.547	0.1388					
		Fraction	F (1. 11) = 11.64	0.0058					
		Feeding	F (1. 11) = 0.004136	0.9499					
		Mouse	F (11. 11) = 1.029	0.4814					
	CpG3	Fraction x Feeding	F (1. 11) = 2.617	0.134					
		Fraction	F (1. 11) = 7.687	0.0181					
		Feeding	F (1. 11) = 0.4418	0.52					
		Mouse	F (11. 11) = 0.7857	0.6519					

Table A.40.: Details of statistical analysis of one-way ANOVA of 3T3-timeline; F–F-statistic; DF–degrees of freedom

Enhancer site	CpG	F(DFn. DFd)	p-value
RS1	CpG1	F (7. 15) = 32.82	<0.0001
	CpG2	F (7. 15) = 40.84	<0.0001
	CpG3	F (7. 15) = 57.49	<0.0001
RS2	CpG1	F (7. 14) = 2.408	0.0766
	CpG2	F (7. 14) = 0.1837	0.9844
	CpG3	F (7. 14) = 2.124	0.1092
RS3	CpG1	F (7. 8) = 4.946	0.0194
	CpG2	F (7. 15) = 43.53	<0.0001
	CpG3	F (7. 15) = 32.31	<0.0001

Table A.41.: Mass-spectrometry results of the top differential expressed mouse epididymal adipose tissue proteins binding to methylated vs unmethylated RS1 with raw count data given in Table A.42.

protein	logFC	AveExpr	t	P.Value	adj.P.Val	B	Protein.Group
MAFG	2.34150954	0.29324388	6.46497672	9.63E-05	0.0330172	1.69065183	O54790
TIAR	-1.8066637	0.44933035	-4.8979754	0.00075268	0.12908453	-0.1265916	P70318
MAFK	2.78053385	-2.3837781	4.27711281	0.00242283	0.22771926	-1.1462677	Q61827
MECP2	1.61136247	3.54078603	4.0134364	0.00280117	0.22771926	-1.3367206	Q9Z2D6
NFAC2	1.38755639	0.87914336	3.90425821	0.00331952	0.22771926	-1.4947156	Q60591
HMGB2	1.42058486	1.69680225	3.4644928	0.00667861	0.22907626	-2.1472589	P30681
HMGB3	1.4356109	-0.1741929	3.7535768	0.00420678	0.22907626	-1.7155356	O54879
MBD2	1.79504026	0.88372441	3.58677349	0.00658931	0.22907626	-2.0643651	Q9Z2E1
NFAT5	1.17963225	-1.1281401	3.63473044	0.00508112	0.22907626	-1.8918166	Q9WV30
UHRF1	1.71062041	0.61970199	3.53870753	0.00592587	0.22907626	-2.0354994	Q8VDF2
HMGA2	1.64659492	-0.1883841	3.36466283	0.00785143	0.24336375	-2.2984819	P52927
NFAC3	1.49825763	-1.8143392	3.31489164	0.00851418	0.24336375	-2.3742235	P97305
ARGI1	1.40894099	1.10821236	3.25505446	0.01090095	0.27148137	-2.5304361	Q61176
UHRF2	1.05207423	0.57517283	3.15403025	0.01108087	0.27148137	-2.6203695	Q7TMI3
TM109	-1.1715955	-0.3006607	-3.0377245	0.01342411	0.3069646	-2.7993558	Q3UBX0
DEK	1.32390781	1.06300752	2.84913149	0.01835645	0.31061096	-3.0906346	Q7TNV0
NFAC1	1.18881252	1.68749996	2.8646457	0.01788867	0.31061096	-3.0666491	O88942
NFKB1	1.404028	-0.6654837	2.83000134	0.0189504	0.31061096	-3.1202115	P25799
SP110	1.3896585	0.97207387	2.89723919	0.019017	0.31061096	-3.0460566	Q8BVK9
TAOK2	1.53162694	-1.2486948	2.92963626	0.01605722	0.31061096	-2.9661994	Q6ZQ29
TAOK3	1.49841098	1.12982214	2.92454559	0.01619352	0.31061096	-2.9740652	Q8BYC6
TAOK1	1.31712009	1.29692996	2.66323731	0.02502659	0.39018732	-3.3778613	Q5F2E8
NOL12	1.38623802	0.08960285	2.48651493	0.03361836	0.50135206	-3.649633	Q8BG17
CCNT1	0.94877323	-2.6760477	2.31561369	0.04783409	0.50373478	-3.8933086	Q9QWV9
CEBPA	1.02129667	2.00318874	2.31006661	0.04511309	0.50373478	-3.9181879	P53566
HMGA1	1.58498871	4.05929906	2.43856525	0.03641923	0.50373478	-3.7229582	P17095
MTA2	1.54848337	0.99510745	2.32395084	0.04408315	0.50373478	-3.8971965	Q9R190
RFX5	1.10906139	0.56937052	2.30629891	0.04539663	0.50373478	-3.9238795	Q9JL61
SP100	1.02330598	0.44445367	2.29038208	0.04661382	0.50373478	-3.9479006	O35892
SQSTM	-1.2009054	-1.6206254	-2.3664175	0.04411809	0.50373478	-3.8197703	Q64337
TF7L1	0.92704046	-0.5510309	2.2669464	0.04846428	0.50373478	-3.9831983	Q9Z1J1
TMEDA	-0.8471909	1.00278484	-2.306083	0.04541293	0.50373478	-3.9242056	Q9D1D4
TR150	1.22527853	1.35142174	2.36362075	0.04126594	0.50373478	-3.8370737	Q569Z6
PRRX1	1.23360702	-0.4870057	2.24464043	0.05029205	0.507358	-4.0167129	P63013

Table A.42.: Mass-spectrometry results raw count data of the top differential expressed mouse epididymal adipose tissue proteins binding to methylated vs unmethylated RS1. S–sample, Sme–methylated sample

protein	First.Protein.Description	S_1	S_2	S_3	S_4	Sme_1	Sme_2	Sme_3
MAFG	Transcription factor MafG	2662.58	1220.63	1114.45	4202.58	8560.72	19133.8	16260.6
TIAR	Nucleolysin TIAR	8941.93	4745	5461.75	13998.5	2744.88	2985.15	3252.73
MAFK	Transcription factor MafK	#NV	65.6339	310.648	633.126	921.24	4072.95	3025.32
MECP2	Methyl-CpG-binding protein 2	19835.5	15638.8	27065.7	35125.4	44937.9	170049	125398
NFAC2	Nuclear factor of activated T-cells, cytoplasmic 2	4990.7	2373.16	2525.81	8023.36	7412.97	21149.3	18492.3
HMGB2	High mobility group protein B2	8145.01	2969.26	5033.6	18295.4	13691.3	35365.7	34097
HMGB3	High mobility group protein B3	2593.37	944.059	1561.74	3196.18	3613.72	8675.63	10953.8
MBD2	Methyl-CpG-binding domain protein 2	#NV	2462.97	1431.18	9111.23	6890.63	19356.9	27278
NFAT5	Nuclear factor of activated T-cells 5	1127.7	734.717	862.496	1646.13	2141.62	4081.29	3987.33
UHRF1	E3 ubiquitin-protein ligase UHRF1	2136.93	2123.27	4693.1	3740.02	9793.02	21953.7	11541.8
HMGA2	High mobility group protein HMGI-C	1493.87	1178.32	1013.19	5127.08	2482.25	10940.1	15776.7
NFAC3	Nuclear factor of activated T-cells, cytoplasmic 3	783.998	316.319	290.775	1666.65	1267.65	2278.86	4228.95
ARGI1	Arginase-1	#NV	2147.39	3565.98	9993.43	12624.5	15945.4	19295.2
UHRF2	E3 ubiquitin-protein ligase UHRF2	3227.93	2742.26	3205.93	5424.6	6664.53	12964.8	11970.3
TM109	Transmembrane protein 109	4184.28	2114.02	2230.65	9663.01	1706.39	3138.91	2224.84
DEK	Protein DEK	2771.75	3234.96	2964.17	16216.6	9593.55	16223.1	25314.3
NFAC1	Nuclear factor of activated T-cells, cytoplasmic 1	10535.6	3555.92	5626.32	13562.2	9788.2	38870.2	32315.9
NFKB1	Nuclear factor NF-kappa-B p105 subunit	665.961	945.689	1196.7	4311.68	2136.34	7753.21	7189.36
SP110	Sp110 nuclear body protein	#NV	1978.61	2778.99	10698.4	6249.27	17833.4	25738.5
TAOK2	Serine/threonine-protein kinase TAO2	363.339	692.518	809.884	2719.94	1906.47	3652.62	5917.84
TAOK3	Serine/threonine-protein kinase TAO3	4330.25	2356.29	2420.83	17067.9	7016.23	22530	35237.6
TAOK1	Serine/threonine-protein kinase TAO1	5814.73	2839.79	2702.85	18621.8	8485.7	19699.4	38026.7
NOL12	Nucleolar protein 12	1865.83	2764.95	1702.4	3066.22	7824.57	4217.89	16983.1
CCNT1	Cyclin-T1	#NV	319.877	197.589	746.995	594.525	1031.85	1500.37
CEBPA	CCAAT/enhancer-binding protein alpha	12205	5532.42	10754.2	11526.8	13380.7	53540.2	27116
HMGA1	High mobility group protein HMG-I/HMG-Y	23527.3	19051.3	24492.3	116714	29616.6	272378	338395
MTA2	Metastasis-associated protein MTA2	1443.43	3834.09	2761.35	17891.8	5623.23	23573.1	33701.5
RFX5	DNA-binding protein Rfx5	1933.68	2428.3	4424.57	6813.99	4061.15	17437.5	15441
SP100	Nuclear autoantigen Sp-100	2020.19	3511.43	1997.79	7822.99	4289.42	10665.6	16647.9
SQSTM	Sequestosome-1	#NV	2066.86	757.288	2531.1	897.988	1086.19	906.303
TF7L1	Transcription factor 7-like 1	2887.16	847.486	1210.22	2656.6	2458.19	5064.21	6885.35
TMEDA	Transmembrane emp24 domain-containing protein 10	9716.77	5828.23	7698.33	11038.6	5269.68	7518.84	6649.04
TR150	Thyroid hormone receptor-associated protein 3	2860.71	8306.38	3316.85	13679.1	9783.91	33362.4	19555.8
PRRX1	Paired mesoderm homeobox protein 1	1994.12	892.058	1196.19	3067.18	1252.86	12174.5	9241.11

Table A.43.: Mass-spectrometry results of the top differential expressed 3T3-adipocyte proteins binding to methylated vs unmethylated RS1 with raw count data shown in Table A.44.

protein	logFC	AveExpr	t	P.Value	adj.P.Val	B	Protein.Group
ZCHC8	-3.5494384	-0.0570201	-5.1648043	0.00020688	0.08937206	0.92242444	Q9CYA6
MBD2	3.42837203	1.59734315	4.75965221	0.0005236	0.11309836	0.09412843	Q9Z2E1
TIAR	-2.5753094	0.7676786	-4.1117167	0.00132935	0.17277454	-0.7583559	P70318
TMOD3	-3.0861378	0.92466847	-4.0107982	0.00159976	0.17277454	-0.9273127	Q9JHJ0
THYN1	2.16300807	1.84000428	3.45768601	0.00448339	0.3353933	-1.8695002	Q91YJ3
UHRF1	2.1877812	3.21163231	3.43736154	0.00465824	0.3353933	-1.9044825	Q8VDF2
DNMT1	2.89512065	0.12537363	3.19069789	0.00816711	0.47710006	-2.3557342	P13864
RPB11	-2.2916691	-0.9543639	-3.1474736	0.00883519	0.47710006	-2.4263577	O08740
COE1	-2.376272	2.05134019	-2.7759103	0.01624577	0.54878794	-3.0415983	Q07802
PRRX1	2.45894285	1.21417212	2.72781038	0.01778479	0.54878794	-3.1233011	P63013
TEFM	1.85978054	3.61036189	2.83435194	0.01455147	0.54878794	-2.9419997	Q5SSK3
TIA1	-1.9695791	-1.3050583	-2.835046	0.01453244	0.54878794	-2.9408149	P52912
TLN1	1.90503516	-1.6041328	2.75542878	0.0168844	0.54878794	-3.0764202	P26039
UHRF2	1.87407641	1.41225031	2.84686193	0.01421212	0.54878794	-2.9206374	Q7TMI3
RPAB5	-1.9515174	1.11484837	-2.685639	0.0192513	0.55443731	-3.1947071	P62876
CARF	-1.6543389	-0.0487655	-2.5681048	0.02399101	0.60965382	-3.3924178	Q8BI72
PP1RA	-1.6829704	0.17074651	-2.5783187	0.02353763	0.60965382	-3.3753204	Q80W00
BAZ1B	-2.0029251	2.72545268	-2.526105	0.02736906	0.65685735	-3.4359608	Q9Z277
RPB3	-1.6428419	0.421514	-2.3766743	0.03423016	0.73937146	-3.7092919	P97760
T2EB	1.57387605	-1.6701332	2.38826313	0.0335059	0.73937146	-3.6903228	Q9D902
FOXP4	1.72332386	-1.1516707	2.33348518	0.03870662	0.76005724	-3.7411129	Q9DBY0
TFB1M	1.42933431	-0.5117064	2.31357377	0.03844414	0.76005724	-3.8120279	Q8JZM0

Table A.44.: Mass-spectrometry results raw count data of the top differential expressed mouse 3T3-adipocyte proteins binding to methylated vs unmethylated RS1. S–sample, Sme–methylated sample

protein	First.Protein.Description	S_1	S_2	S_3	Sme_1	Sme_2
ZCHC8	Zinc finger CCHC domain-containing protein 8	8527.11	12058.5	16045.9	1143.61	1079.92
MBD2	Methyl-CpG-binding domain protein 2	#NV	3766.85	3756.52	28287.2	89193.5
TIAR	Nucleolysin TIAR	15427.4	14952.4	17674.3	2372.28	3672.08
TMOD3	Tropomodulin-3	12211.8	21314.1	33205.1	3511.68	2016.28
THYN1	Thymocyte nuclear protein 1	11896.7	8073.8	7666.5	26746.3	74142.9
UHRF1	E3 ubiquitin-protein ligase UHRF1	22137.3	20210.7	27935.1	106386	127409
DNMT1	DNA (cytosine-5)-methyltransferase 1	#NV	2112.05	1260	4558.29	49703
RPB11	DNA-directed RNA polymerase II subunit RPB11	#NV	3261.75	6651.76	685.969	2029.71
COE1	Transcription factor COE1	13007.3	55366	69227.4	7409.53	8222.96
PRRX1	Paired mesoderm homeobox protein 1	8897.23	8190.21	2150.14	9215.03	115598
TEFM	Transcription elongation factor, mitochondrial	60528.3	17218.2	36098.1	120847	148396
TIA1	Nucleolysin TIA-1	2264.57	3506.18	4167.22	953.049	854.796
TLN1	Talin-1	839.183	1428.33	590.527	2652.72	5091.85
UHRF2	E3 ubiquitin-protein ligase UHRF2	6342.74	7102.88	8540.09	29929.3	28795.9
RPAB5	DNA-directed RNA polymerases I, II, and III subunit RPABC5	9662.43	19388.6	26662.6	4578.34	5172.77
CARF	CDKN2A-interacting protein	6196.63	8311.24	6737.74	1802.54	3352.22
PP1RA	Serine/threonine-protein phosphatase 1 regulatory subunit 10	9873.21	4775.21	11897.8	2682.67	2981.72
BAZ1B	Tyrosine-protein kinase BAZ1B	#NV	35988	81054.9	7105.64	39312.1
RPB3	DNA-directed RNA polymerase II subunit RPB3	6522.48	11368	12325.1	1952.51	5996.72
T2EB	General transcription factor IIE subunit 2	712.635	993.069	1148.42	1947.97	4804.21
FOXP4	Forkhead box protein P4	#NV	648.651	1573.81	3785.28	4523.59
TFB1M	Dimethyladenosine transferase 1, mitochondrial	2987.61	1909.95	1786.4	4665.38	8862.29

Table A.45.: Filtered mass-spectrometry DIA-NN-results of proteins known to bind to RS2.

Protein.Group	protein	Genes	First.Protein.Description	RS2.3T31	RS2.3T32	RS2.adipo1	RS2.adipo2
Q00899	TYY1	Yy1	Transcriptional repressor protein YY1	9389.27	6833.89	4782.75	2783.68
P34056	AP2A	Tfap2a	Transcription factor AP-2-alpha	68195	67381.5	NA	NA

Table A.46.: Filtered mass-spectrometry DIA-NN-results of proteins known to bind to RS3.

Protein.Group	protein	Genes	First.Protein.Description	RS3.3T31	RS3.3T32	RS3.adipo1	RS3.adipo2
P28700	RXRA	Rxra	Retinoic acid receptor RXR-alpha	5735.16	7982.97	NA	484.001
P37238	PPARG	Pparg	Peroxisome proliferator-activated receptor gamma	942.517	1064.64	NA	NA
P70353	NFYC	Nfyc	Nuclear transcription factor Y subunit gamma	917.175	1261.65	NA	NA
P70257	NFIX	Nfix	Nuclear factor 1 X-type	3233650	5001810	112259	47034.3
P97863	NFIB	Nfib	Nuclear factor 1 B-type	1422660	2320990	44535.7	19557.6
Q02780	NFIA	Nfia	Nuclear factor 1 A-type	461014	423032	24599.4	11735.6
P70255	NFIC	Nfic	Nuclear factor 1 C-type	581387	1023810	29612.6	14022.2

Table A.47.: Details of statistical analysis of one-way ANOVA of 10-day intervention study, just fed results; for *Lep* expression dCT values against housekeeper *Hprt* were used for expression testing, F–F-statistic; DF–degrees of freedom

Enhancer Site/Parameter	CpG	F(DFn. DFd)	p-value
Lep expression		F (3. 13) = 7.684	0.0033
body weight (day 10)		F (3. 15) = 46.30	<0.0001
Fat mass		F (3. 33) = 41.96	<0.0001
RS1	CpG1	F (3. 13) = 82.31	<0.0001
	CpG2	F (3. 13) = 58.89	<0.0001
	CpG3	F (3. 13) = 108.4	<0.0001
RS2	CpG1	F (3. 13) = 2.024	0.1603
	CpG2	F (3. 13) = 29.99	<0.0001
	CpG3	F (3. 13) = 29.79	<0.0001
RS3	CpG1	F (3. 13) = 17.12	<0.0001
	CpG2	F (3. 13) = 12.45	0.0004
	CpG3	F (3. 13) = 19.17	<0.0001

Table A.48.: 10 day intervention, fed correlation, Pearson correlation coefficient r

		-ΔCT (Lep-Hprt)	plasma leptin	body weight [g]	fat %BW	lean %BW	methyl. RS1 1.CpG	methyl. RS1 2.CpG	methyl. RS1 3.CpG	methyl. RS2 1.CpG	methyl. RS2 2.CpG	methyl. RS2 3.CpG	methyl. RS3 1.CpG	methyl. RS3 2.CpG	methyl. RS3 3.CpG
-ΔCT(Lep-Hprt)		1.00	0.34	0.33	0.36	-0.37	0.00	0.09	0.10	0.45	0.17	0.13	0.42	0.42	0.09
plasma leptin		0.34	1.00	0.73	0.70	-0.70	0.60	0.59	0.62	0.52	0.71	0.77	0.61	0.49	0.57
bodyweight [g]		0.33	0.73	1.00	0.94	-0.94	0.80	0.84	0.84	0.44	0.89	0.85	0.85	0.76	0.83
fat %BW		0.36	0.70	0.94	1.00	-1.00	0.86	0.88	0.90	0.54	0.87	0.84	0.84	0.71	0.85
lean %BW		-0.37	-0.70	-0.94	-1.00	1.00	-0.83	-0.85	-0.87	-0.51	-0.85	-0.82	-0.84	-0.74	-0.84
methyl. 1.CpG	RS1	0.00	0.60	0.80	0.86	-0.83	1.00	0.98	0.98	0.45	0.92	0.92	0.67	0.49	0.92
methyl. 2.CpG	RS1	0.09	0.59	0.84	0.88	-0.85	0.98	1.00	0.99	0.44	0.93	0.90	0.72	0.54	0.92
methyl. 3.CpG	RS1	0.10	0.62	0.84	0.90	-0.87	0.98	0.99	1.00	0.52	0.91	0.90	0.73	0.55	0.91
methyl. 1.CpG	RS2	0.45	0.52	0.44	0.54	-0.51	0.45	0.44	0.52	1.00	0.40	0.51	0.49	0.45	0.40
methyl. 2.CpG	RS2	0.17	0.71	0.89	0.87	-0.85	0.92	0.93	0.91	0.40	1.00	0.97	0.82	0.69	0.96
methyl. 3.CpG	RS2	0.13	0.77	0.85	0.84	-0.82	0.92	0.90	0.90	0.51	0.97	1.00	0.76	0.63	0.92
methyl. 1.CpG	RS3	0.42	0.61	0.85	0.84	-0.84	0.67	0.72	0.73	0.49	0.82	0.76	1.00	0.92	0.84
methyl. 2.CpG	RS3	0.42	0.49	0.76	0.71	-0.74	0.49	0.54	0.55	0.45	0.69	0.63	0.92	1.00	0.72
methyl. 3.CpG	RS3	0.09	0.57	0.83	0.85	-0.84	0.92	0.92	0.91	0.40	0.96	0.92	0.84	0.72	1.00

Table A.49.: 10 day intervention, fed correlation, Pearson correlation, p-values

		-ΔCT (Lep-Hprt)	plasma leptin	body weight [g]	fat %BW	lean %BW	methyl. RS1 1.CpG	methyl. RS1 2.CpG	methyl. RS1 3.CpG	methyl. RS2 1.CpG	methyl. RS2 2.CpG	methyl. RS2 3.CpG	methyl. RS3 1.CpG	methyl. RS3 2.CpG	methyl. RS3 3.CpG
-ΔCT(Lep-Hprt)			0.18	0.20	0.15	0.15	1.00	0.72	0.70	0.07	0.52	0.63	0.09	0.09	0.74
plasma leptin		0.18		0.00	0.00	0.00	0.01	0.01	0.01	0.03	0.00	0.00	0.01	0.04	0.02
bodyweight [g]		0.20	0.00		0.00	0.00	0.00	0.00	0.00	0.08	0.00	0.00	0.00	0.00	0.00
fat %BW		0.15	0.00	0.00		0.00	0.00	0.00	0.00	0.03	0.00	0.00	0.00	0.00	0.00
lean %BW		0.15	0.00	0.00	0.00		0.00	0.00	0.00	0.04	0.00	0.00	0.00	0.00	0.00
methyl. 1.CpG	RS1	1.00	0.01	0.00	0.00	0.00		0.00	0.00	0.07	0.00	0.00	0.00	0.04	0.00
methyl. 2.CpG	RS1	0.72	0.01	0.00	0.00	0.00	0.00		0.00	0.07	0.00	0.00	0.00	0.03	0.00
methyl. 3.CpG	RS1	0.70	0.01	0.00	0.00	0.00	0.00	0.00		0.03	0.00	0.00	0.00	0.02	0.00
methyl. 1.CpG	RS2	0.07	0.03	0.08	0.03	0.04	0.07	0.07	0.03		0.11	0.04	0.05	0.07	0.11
methyl. 2.CpG	RS2	0.52	0.00	0.00	0.00	0.00	0.00	0.00	0.00	0.11		0.00	0.00	0.00	0.00
methyl. 3.CpG	RS2	0.63	0.00	0.00	0.00	0.00	0.00	0.00	0.00	0.04	0.00		0.00	0.01	0.00
methyl. 1.CpG	RS3	0.09	0.01	0.00	0.00	0.00	0.00	0.00	0.00	0.05	0.00	0.00		0.00	0.00
methyl. 2.CpG	RS3	0.09	0.04	0.00	0.00	0.00	0.04	0.03	0.02	0.07	0.00	0.01	0.00		0.00
methyl. 3.CpG	RS3	0.74	0.02	0.00	0.00	0.00	0.00	0.00	0.00	0.11	0.00	0.00	0.00	0.00	

Table A.50.: Details of statistical analysis of one-way ANOVA of weight cycling study; dCT values against housekeeper *Hprt* were used for expression testing, F–F-statistic; DF–degrees of freedom

Enhancer site	CpG	F(DFn. DFd)	p-value
RS1	CpG1	F (3. 28) = 27.49	<0.0001
	CpG2	F (3. 28) = 46.66	<0.0001
	CpG3	F (3. 28) = 36.69	<0.0001
RS2	CpG1	F (3. 26) = 18.47	<0.0001
	CpG2	F (3. 26) = 30.81	<0.0001
	CpG3	F (3. 26) = 25.34	<0.0001
RS3	CpG1	F (3. 27) = 20.10	<0.0001
	CpG2	F (3. 27) = 4.362	0.0125
	CpG3	F (3. 27) = 14.43	<0.0001
Lep expression		F (3. 28) = 11.26	<0.0001

Table A.51.: Details of statistical analysis of 2-way ANOVA and one-way ANOVA of metformin treatment study phenotype and ipGTT results; dCT values against housekeeper *Hprt* were used for expression testing, F–F-statistic; DF–degrees of freedom

week	Tested factors	F(DFn. DFd)	p-value	Parameter / week	Tested factors	F(DFn. DFd)	p-value
w12	Treatment x time	F (8. 228) = 16.76	<0.0001	Body	Interaction	F (6. 198) = 77.92	<0.0001
	Time	F (3.109. 177.2) = 218.7	<0.0001	weight	Time	F (3. 198) = 1146	<0.0001
	Treatment	F (2. 57) = 71.81	<0.0001		treatment	F (2. 198) = 775.2	<0.0001
	Subject	F (57. 228) = 7.324	<0.0001	serum	time	F (3. 76) = 17.23	<0.0001
	AUC	F (2. 57) = 69.42	<0.0001	leptin	treatment	F (2. 76) = 105.3	<0.0001
w14	Treatment x time	F (8. 88) = 5.712	<0.0001	*Lep*	Interaction	F (2. 52) = 3.528	0.0366
	Time	F (3.345. 73.59) = 71.35	<0.0001	expression	time	F (1. 52) = 1.448	0.2344
	Treatment	F (2. 22) = 27.57	<0.0001		treatment	F (2. 52) = 19.92	<0.0001
	Subject	F (22. 88) = 3.354	<0.0001				
	AUC	F (2. 22) = 25.72	<0.0001				
w18	Treatment x time	F (8. 104) = 17.67	<0.0001				
	Time	F (2.864. 74.47) = 115.8	<0.0001				
	Treatment	F (2. 26) = 122.8	<0.0001				
	Subject	F (26. 104) = 3.180	<0.0001				
	AUC	F (2. 26) = 119.5	<0.0001				

Table A.52.: Details of statistical analysis of 2-way ANOVA of metformin treatment study, F–F-statistic; DF–degrees of freedom

Enhancer Site	CpG	Tested factors	F(DFn. DFd)	p-value	Enhancer Site	CpG	Tested factors	F(DFn. DFd)	p-value
RS1	CpG1	Interaction	F (2. 53) = 4.064	0.0228	RS3	CpG1	Interaction	F (2. 50) = 3.710	0.0314
		Time	F (1. 53) = 0.6915	0.4094			Time	F (1. 50) = 0.2136	0.6459
		Diet	F (2. 53) = 170.9	<0.0001			Diet	F (2. 50) = 52.29	<0.0001
	CpG2	Interaction	F (2. 52) = 3.452	0.0391		CpG2	Interaction	F (2. 49) = 1.209	0.3073
		Time	F (1. 52) = 0.04273	0.837			Time	F (1. 49) = 8.534e-005	0.9927
		Diet	F (2. 52) = 162.2	<0.0001			Diet	F (2. 49) = 29.93	<0.0001
	CpG3	Interaction	F (2. 53) = 2.369	0.1034		CpG3	Interaction	F (2. 48) = 2.158	0.1266
		Time	F (1. 53) = 2.291	0.1361			Time	F (1. 48) = 0.0002186	0.9883
		Diet	F (2. 53) = 159.7	<0.0001			Diet	F (2. 48) = 47.08	<0.0001
RS2	CpG1	Interaction	F (2. 52) = 0.4181	0.6605					
		Time	F (1. 52) = 0.7412	0.3932					
		Diet	F (2. 52) = 181.0	<0.0001					
	CpG2	Interaction	F (2. 52) = 0.4199	0.6593					
		Time	F (1. 52) = 0.1689	0.6828					
		Diet	F (2. 52) = 183.0	<0.0001					
	CpG3	Interaction	F (2. 52) = 0.4450	0.6432					
		Time	F (1. 52) = 0.5115	0.4777					
		Diet	F (2. 52) = 158.5	<0.0001					

Table A.53.: Details of statistical analysis of 2-way ANOVA of VSG; dCT values for *Lep* expression against housekeeper *Hprt* were used for expression testing, F–F-statistic; DF–degrees of freedom

Enhancer Site	CpG	Tested factors	F(DFn. DFd)	p-value	Parameter	Tested factors	F(DFn. DFd)	p-value
RS1	CpG1	interaction	F (1. 25) = 7.164	0.0129	*Lep*	interaction	F (1. 28) = 18.87	0.0002
		time	F (1. 25) = 3.319	0.0805	expression	time	F (1. 28) = 4.572	0.0414
		surgery	F (1. 25) = 0.05975	0.8089		surgery	F (1. 28) = 41.41	<0.0001
	CpG2	interaction	F (1. 25) = 9.128	0.0057	body	interaction	F (1. 28) = 3.472	0.0729
		time	F (1. 25) = 3.375	0.0781	weight	time	F (1. 28) = 6.994	0.0133
		surgery	F (1. 25) = 1.080	0.3087		surgery	F (1. 28) = 58.07	<0.0001
	CpG3	interaction	F (1. 25) = 38.02	<0.0001	body	interaction	F (1. 28) = 0.05214	0.821
		time	F (1. 25) = 0.3461	0.5616	weight	time	F (1. 28) = 48.12	<0.0001
		surgery	F (1. 25) = 8.633	0.007	differences	surgery	F (1. 28) = 105.5	<0.0001
RS2	CpG1	interaction	F (1. 27) = 8.999	0.0057				
		time	F (1. 27) = 3.893	0.0588				
		surgery	F (1. 27) = 9.041	0.0056				
	CpG2	interaction	F (1. 27) = 13.38	0.0011				
		time	F (1. 27) = 3.960	0.0568				
		surgery	F (1. 27) = 2.311	0.14				
	CpG3	interaction	F (1. 27) = 10.60	0.003				
		time	F (1. 27) = 1.583	0.219				
		surgery	F (1. 27) = 21.51	<0.0001				
RS3	CpG1	interaction	F (1. 28) = 7.708	0.0097				
		time	F (1. 28) = 1.779	0.193				
		surgery	F (1. 28) = 2.239	0.1458				
	CpG2	interaction	F (1. 28) = 7.021	0.0131				
		time	F (1. 28) = 0.1531	0.6985				
		surgery	F (1. 28) = 3.875	0.059				
	CpG3	interaction	F (1. 28) = 7.702	0.0097				
		time	F (1. 28) = 1.773	0.1938				
		surgery	F (1. 28) = 2.230	0.1465				

Table A.54.: Details of statistical analysis of one-way and 2-way ANOVA of *lncOb* results; dCT values against housekeeper *Hprt* (eWAT) and against *Rplp0* (iWAT) were used for expression testing, F–F-statistic; DF–degrees of freedom

Cohort	Tested Factor	F(DFn. DFd)	p-value
DIO eWat		F (7. 135) = 5.649	<0.0001
		F (7. 135) = 15.15	<0.0001
		F (1. 135) = 65.05	<0.0001
DIO iWat		F (1. 28) = 0.1240	0.7274
		F (1. 28) = 16.76	0.0003
		F (1. 28) = 2.183	0.1507
eWAT week 18		F (2. 27) = 86.32	<0.0001
iwat week 18		F (2. 26) = 5.053	0.014
VSG		F (1. 25) = 31.66	<0.0001
		F (1. 25) = 0.02481	0.8761
		F (1. 25) = 3.468	0.0744
weight cycling		F (3. 28) = 54.47	<0.0001
10-day intervention	Interaction	F (4. 40) = 1.951	0.1208
	feeding	F (1. 40) = 40.89	<0.0001
	diet	F (4. 40) = 46.05	<0.0001

List of Figures

List of Tables

Acknowledgements

I am utterly grateful to the many individuals who have accompanied me on the stormy adventure of my PhD. First and foremost, I would like to express my heartfelt gratitude to my doctoral advisor Prof. Dr. Henriette Kirchner for her exceptional support, guidance, and mentorship throughout this endeavor. Her expertise, skills, humanity, and demeanor were instrumental in shaping the direction of this work and will always serve as an inspiration to me. Additionally, I extend my thanks to Prof. Olaf Jöhren for his support and stimulating questions as the co-supervisor. I am grateful to Dr. Zouhair Aherrahrou for his tireless mentorship, constructive suggestions, and ideas.

My boundless gratitude goes out to Dr. Sonja Schriever, who consistently provided invaluable insights from outside the institute and encouraged me to aim higher, while also helping me maintain patience in the face of initial inexplicable data. I would also like to thank her for her exceptional collaboration, providing mouse samples from her extensive and time-consuming studies, which she graciously shared.

Furthermore, I would like to express my gratitude to the RTG 1957 *Adipocyte Brain Crosstalk* funded by the DFG for funding this project, particularly to Prof. Henrik Oster as spokesperson and Chaoqun Jiang for her organizational support. I would like to thank the members of the RTG for the scientific exchange despite the adverse circumstances of the pandemic.

Also, this work was made possible with the support of the lab members, former lab members and students of Epi(c)genetics and Metabolism, Jan Britsemmer, Dr. Christin Krause, Alison Naujack, Tessa Kazubeck, Martina Grohs, Sina Junge and Helen Sievert. Thanks to Christin, for showing me the bioinformatic side and helping me loose my fear to try this out, and for your valuable input to my work. Special thanks to Jan and Sarah for their friendship, support, staying sane together, regular exchange, and coffee breaks, or strawberry picking.

I am thankful to Prof. Dafna Benayahu for her input and support during my research stay in Israel, as well as Nadav and Nachum for being amazing lab partners and demonstrating an active and stimulating scientific and political exchange on-site, as well as to Roza, Shelly, Roza, Razel, Jordan and Marièlle for making my time in Israel truly enjoyable.

I would also like to express my gratitude to all those who contributed to this work in various ways, namely Andreas Israel and Katrin Huber for their support with adipocyte sorting and DNA extraction, Dr. Cathleen Geißler and Anne-Marie Neumann for conducting *in vivo* studies and sharing fat tissue; Prof. Timo Gemoll, Julia Horn and Thorben Sauer for their support with mass spectrometry performance and analysis; Nathalie Kruse for her assistance with RNA-seq and Verónica Yumiceba for sharing the plasmid and her knowledge on CRISPR-Cas9. I am

grateful to Dr. med Oliver Mann and Dr. med. Stefan Wolter for providing human VAT and to Prof. Matthias Laudes and Dr. Katharina Heitmann for providing VAT adipocyte samples.

Finally, I am forever grateful to my family and extended family. Mama, Papa, Yanis, Tim, Susan, Delia, Clara and Zaky, your endless love, support, encouraging presence, unwavering encouragement, and understanding have been and will always be a cherished treasure for me. Thanks to multiple people proofreading parts of this work and finding the grammatical-, illustration- and complicated sentences-hiders, namely Pia, Anni, Tim, Susan, Jule, Christin, Yanis, Mama and Papa, thanks for helping me making this work better! And to all my friends, the rugby team, and the wonderful community here in Lübeck and beyond, without whom this time would not have been what it has become. Thank you!